Experimental Investigation of the Time- and Rate-dependent Behaviour of Unsaturated Clays



Department of Civil Engineering

Meghdad Bagheri

(B.Sc., M.Sc.)

Thesis submitted to the University of Nottingham for the degree of Doctor of Philosophy

February 2018

Declaration

I hereby declare that except where specific reference is made to the work of others, the contents of this dissertation are original and have not been submitted in whole or in part for consideration for any other degree or qualification in this, or any other university. This dissertation is my own work and contains nothing which is the outcome of work done in collaboration with others, except as specified in the text and Acknowledgements.

Meghdad Bagheri

February 2018

List of Publications

Journal Papers

Bagheri, M., Rezania, M. and Mousavi Nezhad, M. (2018). Cavitation in high-capacity tensiometers: effect of water reservoir surface roughness. *Geotechnical Research*, 5(2): 81-95. DOI: 10.1680/jgere.17.00016

Rezania, M., Bagheri, M., Mousavi Nezhad, M. and Sivasithamparam, N. (2017). Creep analysis of an earth embankment on soft soil deposit with and without PVD improvement. *Geotextiles and Geomembranes*, 45(5): 537-547. DOI: 10.1016/j.geotexmem.2017.07.004.

Conference Papers and Presentations

Bagheri, M., Rezania, M. and Mousavi Nezhad, M. (2017). One-dimensional creep of unsaturated soft soils. 3rd annual InterPore UK Chapter conference and 1st Monash-Warwick PREFRAC workshop, Warwick, UK.

Pagano, A., Tarantino, A., Bagheri, M., Rezania, M. and Sentenac, P. (2016). An experimental investigation of the independent effect of suction and degree of saturation on very small-strain stiffness of unsaturated sand. *In*: E3S Web of Conferences. 3rd European Conference on Unsaturated Soils, Paris, France, 9, [14015]. DOI: 10.1051/e3sconf/20160914015.

Bagheri, M., Rezania, M. and Mousavi Nezhad, M. (2016). On long-term direct measurement of suction in soft cohesive soils. 2nd annual InterPore UK Chapter conference, Loughborough, UK.

Bagheri, M., Rezania, M. and Mousavi Nezhad, M. (2015). An experimental study of the initial volumetric strain rate effect on the creep behaviour of reconstituted clays. IOP Conference Series: Earth and Environmental Science, 26, 012034. DOI:10.1088/1755-1315/26/1/012034.

Bagheri, M. (2013). CO_2 sequestration in unsaturated superficial soils. Infrastructure and Environment Scotland 1st Postgraduate Conference, Edinburgh, UK.

Acknowledgements

The work presented in this thesis was carried out through collaboration between University of Nottingham and University of Warwick. The financial support provided by the Department of Civil Engineering of the University of Nottingham is gratefully acknowledged.

Firstly, I would like to thank my primary supervisor, Dr Mohammad Rezania, for his sincere encouragement and thoughtful guidance. I have been honoured to work with him since my MSc studies at the University of Strathclyde. His continuous presence and support has been precious in the past 8 years. I share the success of this research work with him. Thanks are also given to Dr Alec Marshall and Dr Nick Thom for their support of this project as my secondary supervisors.

I would like also to express my gratitude to Dr Mohad Mousavi-Nezhad of the University of Warwick for her kind support for development of the state-of-the-art experimental testing systems. I am also grateful to Prof Alessandro Tarantino of the University of Strathclyde and Dr Sina Saremi Yarahmadi of Loughborough University for valuable advices in the design of the new HCT.

Special thanks are given to the engineering technicians at the University of Warwick, especially Mr Graeme Thacker, for their useful suggestions and unrivalled skills in the design and manufacturing of the novel testing equipment presented.

Finally, I would like to express my greatest gratitude to my mother and my wife who have encouraged and supported me. This thesis is dedicated to them.

Abstract

With the aim to achieve a better understanding of the time- and rate-dependent behaviour of unsaturated clays, particularly stiff natural clays, a critical review of the literature and a program of laboratory testing were carried out as part of this research. With emphasis on examining the effect of suction on viscous response, mainly primary and secondary consolidation (creep), stress-relaxation, and rate-dependency, a series of conventional multi-stage loading (MSL) oedometer tests, long-term single-stage loading (SSL) oedometer tests, and advanced constant-rate-of-strain (CRS) oedometer tests were carried out on natural and corresponding reconstituted specimens of a stiff clay namely, London Clay, retrieved from a site in the Isle of Sheppey, UK. The results obtained provide a significant contribution to the existing database and address important knowledge gaps highlighted from the literature review. The experimental studies performed included;

a) An investigation of the effect of water reservoir surface roughness on the cavitation mechanism and performance of a newly designed high-capacity tensiometer (HCT), with regard maximum sustainable suction (s_{max}) and maximum duration of measurements (t_{max}).
b) An examination of the influence of soil suction on the primary and secondary consolidation of natural and reconstituted London Clay from a set of MSL and SSL oedometer tests.
c) Characterisation of the stress-relaxation behaviour of the reconstituted London Clay subjected to suction and strain-rate variations from a set of CRS oedometer tests in an in-house designed suction-monitored cell.
d) An examination of the coupled effects of suction and strain-rate on one-dimensional (1D) stress–strain response of reconstituted London Clay.

Based on the experimental findings, the validity of the empirical relationships proposed in the literature for correlating time- and rate-dependency coefficients was examined and necessary modifications were proposed. The main experimental findings can be outlined as:

- The mechanism of cavitation in tensiometers is indeed influenced by the surface roughness of the water reservoir. The new approach for expanding the range

and duration of suction measurements for a newly designed HCT, based on hydrophilic coating of the reservoir walls, sounds promising.

- The compression index (C_c) and creep index ($C_{\alpha e}$) and the ratio $\alpha = C_{\alpha e}/C_c$ for Sheppey London Clay are stress- and suction-dependent. The hypothesis of constant α for natural clays, as suggested by Mesri et al. (1994), is therefore rejected.
- The volumetric creep deformations of unsaturated stiff clays appear to be relatively simply modelled by a creep law based on a power function.
- A coupled effect of suction and strain-rate on 1D compression response was identified. At a constant suction, the higher the strain-rate, the higher the apparent preconsolidation pressure (σ'_p). Similarly, at a constant strain-rate, the higher the suction, the higher the σ'_p.
- The values of relaxation coefficient (R_α) differ in saturated and unsaturated states. However, a clear relationship between R_α and suction was not found. The $R_\alpha = C_{\alpha e}/C_c$ relationship, suggested by Yin et al. (2014) for saturated soft clays, appears, with an approximation, to be valid for the unsaturated stiff London Clay in the range of applied vertical stresses and soil suctions in this study.
- The process of stress-relaxation in unsaturated clays is highly influenced by factors such as soil suction, pre-relaxation strain, stress, and strain-rate.

Keywords: Unsaturated soils, Suction, Tensiometer, Creep, Stress-relaxation, Strain-rate

Table of Contents

CHAPTER 1: INTRODUCTION **1**

1.1 Problem Statement 1
1.2 Aim and Objectives 1
1.3 Research Methodology 2
1.4 Layout of the Thesis 3

CHAPTER 2: LITERATURE REVIEW **5**

2.1 Introduction 5
2.2 Structural Properties of Natural Clays 6
2.2.1 Mineralogy 6
2.2.2 Fabric Anisotropy and Inter-particle Bonding 7
2.3 Unsaturated Soils 8
2.3.1 Soil Suction 9
2.3.2 Capillarity 10
2.3.3 Contact Angle 12
2.3.4 Adsorption 13
2.3.5 Water Menisci and Contractile Skin 14
2.3.6 State Variables 17
2.3.7 Soil Water Retention Curve 20
2.3.8 Suction Measurement and Control Techniques 25
2.3.8.1 Axis-Translation 26
2.3.8.2 Thermal Conductivity Sensors 27
2.4 Primary and Secondary Consolidation in Saturated vs. Unsaturated Clays 28
2.4.1 Primary Consolidation in Saturated Clays 28
2.4.2 Primary Consolidation in Unsaturated Clays 35
2.4.3 Secondary Consolidation in Saturated Soft Soils 38
2.4.3.1 Creep Hypotheses 42
2.4.3.2 Creep Phases 43
2.4.3.3 Creep Index 44
2.4.3.4 Factors Affecting Creep Index 46
Effect of Soil Structure 46
Effect of Consolidation Pressure 46
Effect of Temperature 48
2.4.3.5 The Concept of Isochrones or Time Lines 50
2.4.4 Secondary Consolidation in Unsaturated Clays 51
2.4.4.1 Creep in Oedometric Conditions 52
2.4.4.2 Creep in Triaxial Conditions 55
2.4.4.3 Unsaturated Creep Models 56
2.5 Rate-dependency in Saturated vs. Unsaturated Clays 60

2.5.1 Strain-Rate Effects on Oedometric Behaviour of Saturated Clays 60
2.5.1.1 CRS Oedometer Test 60
2.5.1.2 Determination of Appropriate Strain-Rate for CRS Tests 61
2.5.1.3 Strain-Rate Effects on Compression Behaviour 64
2.5.1.4 The Concept of Isotach or Strain-Rate Lines 68
2.5.2 Strain-Rate Effects on Oedometric Behaviour of Unsaturated Clays 69
2.6 Stress-Relaxation in Saturated vs. Unsaturated Clays 72
2.6.1 Stress-Relaxation in Saturated Clays 72
2.6.1.1 Stress-Relaxation in Oedometric Conditions 74
2.6.1.2 Empirical Approaches for Formulation of Stress-Relaxation 76
2.6.2 Stress-Relaxation in Unsaturated Clays 77
2.7 Concluding Remarks 78
CHAPTER 3: SOIL SAMPLING & BASIC CHARACTERISATION 81
3.1 Introduction 81
3.2 Samples Quality and Sampling Techniques 82
3.2.1 Effect of Sampling Method on Soil Suction Measurement 85
3.3 Sampling Programme 86
3.3.1 The London Clay Formation 86
3.3.2 Geological History and Physical Properties of the Sheppey Member 89
3.3.3 Sampling Site 90
3.3.4 Sampling Procedure 91
3.3.5 Transportation and Storage 94
3.4 Types of Specimens for Laboratory Testing 95
3.4.1 Undisturbed Specimens 95
3.4.2 Reconstituted Specimens 96
3.4.3 Compacted Specimens 97
3.5 Preparation of Testing Specimens 98
3.5.1 Undisturbed Specimens 98
3.5.2 Reconstituted Specimens 99
3.6 Properties of the Sheppey London Clay 101
3.6.1 Index properties 101
3.6.2 Macro-fabric 103
3.6.3 Microstructure 104
3.6.4 Mechanical Properties 108
3.6.5 SWRC 109
3.7 Concluding Remarks 110
CHAPTER 4: A NEW HIGH-CAPACITY TENSIOMETER 112
4.1 Introduction 112
4.2 Background of HCTs 112
4.3 Water in Tension and Cavitation 115

4.3.1 Effect of the Size and Properties of the Water Reservoir 118
4.3.2 Effect of the Size and Properties of the Ceramic Filter 119
4.3.3 Effect of Saturation and Pre-conditioning Procedures 120
4.3.3.1 Pressurisation Magnitude 123
4.3.3.2 Pressurisation Duration 123
4.3.3.3 Saturation Check 124
4.4 Suction Measurements 125
4.5 Calibration Methods 126
4.6 Application for SWRC Development 127
4.7 The New HCT 128
4.7.1 Design 128
4.7.1.1 Body, Diaphragm, and Water Reservoir 129
Strain-gauging 130
Porous Ceramic 132
4.7.2 Minimising Diaphragm's Surface Roughness 133
4.7.2.1 Electro Discharge Machining 134
4.7.2.2 SiC Abrasive Paper 134
4.7.2.3 Diamond Paste Abrasive 135
4.7.2.4 Coating Diaphragms with Hydrophilic Materials 136
Anti-fog Agent 137
Triton X-100 Surfactant 137
Titanium Dioxide (TiO_2) 138
4.8 Surface Roughness Analysis 138
4.8.1 Surface Metrology 138
4.8.2 Microscopic Inspection 140
4.8.3 Contact Angle 142
4.9 Experimental Program for Evaluation of the New HCTs' Performance 146
4.9.1 Saturation 146
4.9.2 Calibration 148
4.9.3 Determination of Maximum Sustainable Suction s_{max} 149
4.9.4 Response to Sudden Pressure Changes 151
4.9.5 Evaluation of Long-term Stability of Measurements and t_{max} 153
4.9.5.1 Constant Suction Tests 154
4.9.5.2 Increasing Suction Tests 159
4.10 Using the Developed HCTs for SWRC Development 160
4.10.1 Experimental Setup and Measurement Procedure 161
4.10.2 Continuous Drying Tests 162
4.10.3 Continuous Drying Tests with Controlled Evaporation-Rate 164
4.10.4 Discussion of the Results 165
4.11 Mathematical Extrapolation of SWRC 168
4.11.1 The Fredlund and Xing (1994) Equation 169

4.11.1 Curve-fitting the Experimental Data 171
4.12 Concluding Remarks 175
CHAPTER 5: TIME-DEPENDENCY IN UNSATURATED CONDITIONS **178**
5.1 Introduction 178
5.2 Tests Nomenclature 178
5.3 Theoretical Framework 179
5.3.1 Determination of Void ratio 179
5.3.2 Determination of Effective Stress 180
5.3.3 Determination of Compression and Consolidation Parameters 181
5.4 Saturated MSL Oedometer Tests 181
5.4.1 Test Procedure and Apparatus 181
5.4.2 Test Results 184
5.4.2.1 Stress-Dependency of the Slope of Compression Curve 187
5.4.2.2 Stress-Dependency of the Secondary Consolidation Index ($C_{\alpha e}$) 190
5.4.2.3 $C_{\alpha e}/C_c$ Ratio 193
5.5 Unsaturated MSL Oedometer Tests 196
5.5.1 Test Procedure and Apparatus 196
5.5.2 Test Results 198
5.5.2.1 Suction-Dependency of the Slope of Compression Curve 202
5.5.2.2 Suction-Dependency of the Secondary Consolidation Index ($C_{\alpha e}$) 204
5.5.2.3 $C_{\alpha e}/C_c$ Ratio 205
5.6 Dry MSL Oedometer Tests 206
5.6.1 Test Procedure and Apparatus 206
5.6.2 Test Results 207
5.6.2.1 Stress-Dependency of the Slope of Compression Curve 208
5.6.2.2 Stress-Dependency of the Secondary Consolidation Index ($C_{\alpha e}$) 209
5.6.2.3 $C_{\alpha e}/C_c$ Ratio 210
5.7 MSL Tests Remarks 211
5.8 Saturated SSL Oedometer Creep Tests 212
5.8.1 Test Procedure 212
5.8.2 Test Results 213
5.9 Unsaturated SSL Oedometer Tests 216
5.9.1 Test Procedure 216
5.9.2 Test Results 217
5.10 Dry SSL Oedometer Tests 221
5.10.1 Test Procedure 221
5.10.2 Test Results 222
5.11 A Creep Law 223

5.12 Concluding Remarks 225

CHAPTER 6: RATE-DEPENDENCY IN UNSATURATED CONDITIONS 228

6.1 Introduction 228
6.2 Background of Multi-functional CRS Oedometer Cells 228
6.3 The New CRS Oedometer Cell 230
6.3.1 Calibrations 234
6.3.1.1 Inner Wall Friction 234
6.3.1.2 Transducers 235
6.4 Theoretical Framework 235
6.4.1 Determination of Effective Stress and Void Ratio 235
6.4.2 Determination of Compression and Stress-Relaxation Parameters 236
6.5 Experimental Program for CRS Tests 236
6.6 CRS Tests Nomenclature 238
6.7 Single-Staged Compression–Relaxation Tests 238
6.7.1 Test Procedure 238
6.7.2 Test Results 239
6.7.2.1 MSL Oedometer Tests vs. CRS Tests 241
6.7.2.2 Effect of Suction and Strain-Rate on Stress-Relaxation Process 243
6.8 Multi-Staged Compression–Relaxation Tests 247
6.8.1 Test Procedure 247
6.8.2 Test Results 248
6.9 Concluding Remarks 252

CHAPTER 7: CONCLUSIONS AND RECOMMENDATIONS 254

7.1 Conclusions 254
7.1.1 Experimental Developments 255
7.1.1.1 The New HCT 255
7.1.1.2 The New Suction- and Temperature-Controlled CRS Oedometer 256
7.1.2 1D Primary and Secondary Consolidation in Unsaturated Conditions 257
7.13 1D Rate-Dependent Response in Unsaturated Conditions 258
7.1.4 1D Stress-Relaxation Response in Unsaturated Conditions 259
7.2 Recommendations for Future Works 260

REFERENCES 262

List of Figures

2.1	Fabric of clays	8
2.2	Idealised structure of unsaturated soils (after Raveendiraraj 2009)	9
2.3	Concept of capillary rise: (a) intermolecular forces in a liquid-gas system; (b) capillary mechanism; (c) pressures and surface tension acting on a two-dimensional surface (after Fredlund and Rahardjo, 1993)	11
2.4	Concept of contact angle: (a) wetting surface; (b) non-wetting surface; (c) tilted surface	12
2.5	Schematic representation of the adsorbed and diffuse double layers in clays	14
2.6	Schematic representation of menisci shape at the particle contact of idealised spherical grains: (a) concave menisci; (b) tensile pressure inside the concave meniscus; (c) convex menisci; (d) compressive pressure inside the convex meniscus – T is the tangential component of intergranular force due to the external stress, Nσ is the normal component of the intergranular force due to external stress, and Ns is the intergranular force due to suction	15
2.7	The forces diagram of two idealised spherical soil particles in contact (Raveendiraraj, 2009)	16
2.8	Typical water retention curve for non-deformable soils: (a) in $S_r - s$ plane; (b) in $w - s$ plane	20
2.9	The ink bottle effect: (a) capillary drainage; (b) capillary rise (after Laloui, 2010)	22
2.10	Scanning curves from the main drying and wetting curves; 1- crossing, 2- converging, 3- returning (after Tompsett et al., 2005)	23
2.11	Schematic SWRC-w with λ/λ_p different from $G_s w_{AEV}$ along with the proposed graphical method to obtain parameters: (a) NC soils; (b) OC soils with $\sigma'_p < s_{AEV}$ (Pasha et al., 2016)	24
2.12	Axis-translation technique: (a) atmospheric conditions; (b) axis-translation (Marinho et al., 2008)	26
2.13	Schematic diagram of a thermal conductivity sensor (Leong et al., 2012)	28
2.14	Schematic compression curve for natural soft clays (after Mataic, 2016)	30
2.15	Normalised compression curves for Yangtze River Delta clays: (a) reconstituted samples; (b) undisturbed samples (Sun et al., 2014)	31
2.16	Time-settlement graphs for flocculated and dispersed kaolinite samples subjected to 1D consolidation tests under a pressure range of 10–20 kPa (re-drawn from Pillai et al., 2012)	32
2.17	Schematic compression curves for natural and reconstituted overconsolidated stiff clays (Stallebrass et al., 2007)	33
2.18	Oedometer test results on intact and reconstituted London Clay from T5: (a) in terms of void ratio; (b) in terms of void index [Gasparre et al. (2007) in Hight et al., (2007)]	33

2.19	(a) Expansibility of London Clay at T5 from oedometer swelling tests; (b) water content profile (Hight et al., 2003)	34
2.20	Oedometer tests on unsaturated compacted London Clay: (a) compression curves at different suctions (Monroy et al., 2008); (b) normal compression and swelling indices (Monroy et al., 2008); (c) soil water retention curve (re-drawn after Monroy, 2005)	36
2.21	Compression curves from oedometer tests with controlled suction on a high porosity silty clay (Benatti et al., 2010)	37
2.22	Compression curves from oedometer tests on kaolin clay with controlled suction and temperature (Haghighi, 2011)	38
2.23	Schematic view of the structure of a clayey soil (after Le et al., 2012)	39
2.24	Flow path through intra-particle pores for different particle arrangements (after Bayesteh and Mirghasemi, 2015)	40
2.25	Creep hypotheses A and B (after Ladd et al., 1977)	43
2.26	Definition of creep stages in triaxial creep tests: (a) $\varepsilon - t$ plane; (b) log $\dot{\varepsilon}$ – log t plane (after Augustesen et al., 2004)	44
2.27	Estimation of creep index from conventional consolidation tests	46
2.28	Variation of $C_{\alpha e}$ with consolidation pressure for undisturbed and remoulded specimens: (a) Leda clay (re-drawn after Mesri and Godlewski, 1977); (b) Vanttila Clay (re-drawn after Yin et al., 2011)	47
2.29	Variation of creep strain with logarithm of time for various clays and under various stress states (Mitchell et al., 1997)	49
2.30	Variation of logarithm of creep strain rate with logarithm of time for London Clay under various deviator states levels in drained triaxial creep tests (Mitchell et al., 1997)	50
2.31	Illustration of the time lines concept (Mataic, 2016)	51
2.32	Plastic deformations during cyclic wetting and drying tests on Boom Clay in oedometric conditions (re-drawn after Alonso et al., 1995)	52
2.33	Variation of C_{α} with suction and applied vertical stress for undisturbed (top) and remoulded (bottom) volcanic ashy soils (Bilotta et al., 2008) – numbers in brackets indicate applied vertical stresses in kPa. Symbols are also given in parentheses: [1]=36.9 (□), [2]=87.9 (◊), [3]=160.4 (Δ), [4]=298.1 (<*>), [5]=599.9 (○), [6]=1193.1 (-), [7]=2379.6 (+).	53
2.34	Oedometer creep tests on Lixhe chalk; effect of stress level and suction on the creep coefficient (Priol et al., 2007)	54
2.35	Oedometer creep tests on Estreux chalk; effect of stress level and suction on the creep coefficient (De Gennaro et al., 2005)	55
2.36	Triaxial creep tests under different matric suctions (re-drawn after Zou et al., 2013)	56
2.37	Numerical modelling of creep phase for unsaturated chalk samples at s = 200 kPa (Collin et al., 2008)	57
2.38	Aging effects on 1D stress–strain behaviour (Leroueil et al., 1996)	64
2.39	Effect of strain-rate on preconsolidation pressure from CRS oedometer test results on Batiscan Clay (Leroueil et al., 1985)	65

2.40	CRS oedometer test results on Hong Kong marine clay (Cheng and Yin, 2005)	65
2.41	Effect of strain-rate on the effective stress–strain curve and u_{exc} (Jarad, 2016)	67
2.42	Effect of strain-rate on σ'_p from 1D compression tests on NC and slightly OC soft clays (Soga and Mitchell, 1996)	67
2.43	The Isotach concept from SRS oedometer test results on Batiscan Clay (Leroueil et al., 1985)	69
2.44	Effect of strain-rate in CW-CRS tests on aeolian loess (Muñoz-castelblanco et al., 2011)	70
2.45	Results of unsaturated CRS tests on reconstituted kaolin clay at different strain-rates (Wijaya et al., 2014)	71
2.46	Relaxation test (A→B): (a) stress-strain relationship; (b) strain history; (c) stress history	73
2.47	Results of stress-relaxation tests on reconstituted illite (re-drawn after Yin and Graham, 1989) and Berthierville Clay (re-drawn after Kim and Leroueil, 2001)	75
3.1	Quality analysis of undisturbed samples taken by different sampling methods – The numbers in the brackets correspond to the number of the soil layer (re-drawn from Sun et al., 2014)	83
3.2	Sketch map of the London Clay formation outcrop (Bouch, 2006)	87
3.3	Selenite crystals in London Clay sample from Isle of Sheppey	87
3.4	Divisions of London Clay formation (King, 1981)	88
3.5	Lithological units in London Clay (from Hight et al., 2003)	89
3.6	Geological formations in Isle of Sheppey (Young, 2014)	90
3.7	Site map provided by SW Attwood from Ordnance Survey National Geographic Database, 2014	91
3.8	Block sampling procedure	93
3.9	Transportation and storage of block samples: (a) loading samples to the excavator's bucket; (b) securing samples on the pallets at ground level; (c) accommodating samples in the transit van; (d) storage in a temperature- and humidity-controlled room	94
3.10	Perspex consolidometers: (a) schematic diagram; (b) photo	99
3.11	Preparation of reconstituted samples: (a) cylindrical soil cake removed from the consolidometer; (b) approximately equal size cut pieces for oedometer and CRS specimens	100
3.12	Hydraulic and mechanical paths associated with consolidation and drying (re-drawn from Tarantino et al., 2011)	101
3.13	Particle size distribution (PSD) curve for Sheppey London Clay	102
3.14	Fissured pattern at shallow depth at New Hook Farm reservoir site	103
3.15	ESEM micrographs showing the coarser-grained particles imbedded in the clay matrix at magnification of: (a) 1250x; (b) 2500x	105

3.16	ESEM micrograph: (a) soil fabric; (b) schematic diagram of particles and domains arrangements and presence of large pores in flocculated soil fabric	105
3.17	Clay particles and domains around a pyrite particle: (a) ESEM micrograph; (b) schematic diagram	105
3.18	ESEM micrographs showing the progressive drying of the clay sample	106
3.19	The X-Ray spectra acquired from different points on the same sample	107
3.20	SWRC-S_r for London Clay (Dineen, 1997)	109
3.21	SWRC-w for compacted London Clay over drying path (data points from Monroy, 2005 and Mavroulidou et al., 2013)	110
4.1	Schematic diagram of the working mechanism of a tensiometer: (a) before contact with unsaturated soil; (b) after contact with unsaturated soil	114
4.2	SEM micrographs of a Soil Moisture Corp. ceramic disc at magnifications of: (a) 2000x; (b) 5000x	119
4.3	Effect of pre-pressurisation and cycles of cavitation and pressurisation on cavitation in tensiometers: (a) no pressurisation of water (cavitation occurs); (b) pressurisation of water (cavitation does not occur); (c) a cycle of cavitation and pressurisation (after Take 2003)	122
4.4	Schematic diagram of the tensiometer and its components	129
4.5	(a) Linear strain gauge; (b) Internal circuit diagram (Micro-measurements 2010)	130
4.6	Instrument resolution	132
4.7	Installation of strain gauge: (a) bonding; (b) wiring	132
4.8	Diamond paste polishing method: (a) preparation of the paste with different grades; (b) polishing in milling machine	135
4.9	Effect of liquid advancing contact angle on air entrapment in a crevice: (a) less hydrophobic surface, low liquid contact angle and less entrapped air; (b) more hydrophobic surface, high liquid contact angle and more entrapped air (after Jones et al. 1999)	136
4.10	Surface texture parameters	139
4.11	The Bruker contour GT-K profiler	139
4.12	3D surface metrology diagrams: (a) FM sample; (b) SP polished sample; (c) DP polished sample; (d) AF coated sample; (e) Triton coated sample; (f) TiO_2 coated sample	141
4.13	Microscopic view of the finished surfaces: (a) FM; (b) SP polished; (c) DP polished; (d) AF coated; (e) Triton coated; (f) TiO_2 coated samples	142
4.14	Definition of contact angles: (a) an ideal surface (higher contact angle); (b) a rough surface (lower contact angle) – θ_a and θ_r are advancing and receding contact angles respectively	142
4.15	(a) Wettability of a rough surface (higher θ); (b) enhanced wettability by coating the rough surface with a hydrophilic material (lower θ)	143
4.16	Contact angle hysteresis on an AF coated sample $\theta_a = 45^o$ and $\theta_r = 35^o$	144
4.17	The DataPhysics OCA 20 contact angle measurement apparatus	145

4.18	Measured contact angles: (a) FM sample; (b) SP polished sample; (c) DP polished sample; (d) AF coated sample; (e) Triton coated sample; (f) TiO_2 coated sample	145
4.19	Saturation chamber: (a) schematic diagram; (b) photo	147
4.20	Residual pressure equilibrium by the end of saturation course	148
4.21	Calibration curve for WT4	149
4.22	Free evaporation tests: (a) HCTs with mechanically polished diaphragms; (b) HCTs with hydrophilic coated diaphragms – values in brackets indicate the s_{max}	151
4.23	Cyclic evaporation tests – values in the brackets indicate s_{max}	153
4.24	New oedometer cell for testing unsaturated soil specimens: (a) schematic diagram; (b) photo	154
4.25	Long-term performance of the HCTs during constant suction tests: (a) mechanically polished diaphragms under ~600 kPa suction; (b) hydrophilic coated diaphragms under ~600 kPa suction; (c) mechanically polished diaphragms under ~1000 kPa suction; (d) hydrophilic coated diaphragms under ~1000 kPa suction – Values in brackets indicate the t_{max}	157
4.26	Free evaporation tests on HCTs with hydrophilic coated diaphragms after long-term consolidation tests – values in brackets indicate the s_{max}	158
4.27	Long-term performance of the HCTs during increasing suction tests – Values in brackets indicate s_{max} and t_{max} respectively	160
4.28	Schematic diagram of the experimental setup for SWRC measurement	162
4.29	Variation of water content with time during CD tests	162
4.30	SWRCs form continuous drying tests: (a) CD1; (b) CD2; (c) CD3	163
4.31	SWRC from continuous drying tests with evaporation rate control: (a) CD1(er); (b) CD2(er)	165
4.32	SWRC envelopes: (a) CD tests; (b) CD(er) tests; (c) comparison of the envelopes	167
4.33	Assessment of the HCTs performance during SWRC measurements: (a) s_{AEV} values in CD and CD(er) tests; (b) s_{max} values from FE, CD, and CD(er) tests	168
4.34	Definitions of the parameters of Fredlund and Xing equation in SWRC-*w* space	170
4.35	A best-fit curve to the experimental data obtained from WT8 in CD2(er) test	172
4.36	Best-fit curves to the experimental data obtained from: (a) CD1 test; (b) CD2 test; (c) CD3 test; (d) CD1(er) test; (e) CD2(er) test	173
4.37	Comparison of the best-fit curves from CD and CD(er) tests	174
5.1	Nomenclature of the MSL oedometer tests	179
5.2	Nomenclature of the SSL oedometer creep tests	179
5.3	Conventional oedometer apparatuses at the University of Nottingham	183
5.4	Compression curves for intact Sheppey London Clay	184

5.5	Comparison of the compression curves for intact Sheppey London Clay and natural London Clay from Unit C of Heathrow T5 site	185
5.6	Compression curves for reconstituted Sheppey London Clay	186
5.7	Comparison of the compression curves for reconstituted Sheppey London Clay and reconstituted London Clay from Unit C of Heathrow T5 site	186
5.8	Compression curves for low-quality undisturbed Sheppey London Clay	187
5.9	Comparison of the compression curves for saturated intact, reconstituted, and low-quality undisturbed Sheppey London Clay	187
5.10	Stress-dependency of the slope of compression curve for intact Sheppey London Clay	188
5.11	Stress-dependency of the slope of compression curve for reconstituted Sheppey London Clay	189
5.12	Comparison of the stress-dependency of the slope of compression curve for intact, reconstituted, and low-quality undisturbed Sheppey London Clay	190
5.13	Stress-dependency of the secondary consolidation index ($C_{\alpha e}$) for intact Sheppey London Clay	191
5.14	Stress-dependency of the secondary consolidation index ($C_{\alpha e}$) for reconstituted Sheppey London Clay	192
5.15	Comparison of the stress dependency of $C_{\alpha e}$ for intact, reconstituted, and low-quality undisturbed Sheppey London Clay	192
5.16	Stress-dependency of the α ratio for intact Sheppey London Clay	194
5.17	Stress-dependency of the α ratio for reconstituted Sheppey London Clay	194
5.18	Comparison of the stress-dependency of the α ratio for reconstituted and intact Sheppey London Clay	195
5.19	Comparison of the stress-dependency of the α ratio for intact, reconstituted, and low quality undisturbed Sheppey London Clay	196
5.20	Compression curves for unsaturated reconstituted Sheppey London Clay	199
5.21	Variation of preconsolidation pressure with suction	200
5.22	Monitoring suction changes during step loading oedometer tests	201
5.23	Change in pore-water pressure with each load increment	202
5.24	Suction- and stress-dependency of the slope of compression curve	204
5.25	Variation of C_c and C_s with suction	204
5.26	Suction- and stress-dependency of the $C_{\alpha e}$ for unsaturated reconstituted Sheppey London Clay	205
5.27	Suction- and stress-dependency of the α ratio for unsaturated reconstituted Sheppey London Clay	206
5.28	Compression curves for oven-dried Sheppey London Clay	208
5.29	Oedometer compression tests of saturated reconstituted and oven-dried Sheppey London Clay	209

5.30	Stress-dependency of the slope of compression curve for dry Sheppey London Clay	209
5.31	Stress-dependency of $C_{\alpha e}$ for dry Sheppey London Clay	210
5.32	Stress dependency of the α ratio for dry Sheppey London Clay	210
5.33	SSL oedometer creep tests on saturated Sheppey London Clay: (a) intact specimens; (b) reconstituted specimens	214
5.34	Comparison of intact and reconstituted specimens behaviour during SSL oedometer creep tests at different stress levels	215
5.35	Effect of creep history during oedometer creep tests on saturated intact Sheppey London Clay	216
5.36	Effect of suction during creep tests at different stress levels of: (a) 178 kPa; (b) 222 kPa; (c) 355 kPa; (d) 444 kPa; (e) 666 kPa	218
5.37	Effect of stress level during creep tests on specimens with constant suctions of: (a) 326 kPa; (b) 433 kPa; (c) 513 kPa; (d) 1405 kPa; (e) 1907 kPa	219
5.38	Monitoring suction changes during loading stage of SSL oedometer tests	220
5.39	Monitoring suction changes during creep stage of SSL oedometer tests	221
5.40	SSL oedometer creep tests on dry Sheppey London Clay	222
5.41	Comparison of SSL oedometer creep tests on dry and saturated reconstituted specimens	223
5.42	Variation of α_i with vertical stress and water content	225
6.1	Schematic diagram of the CRS cell structure and components	232
6.2	CRS system setup and components	234
6.3	Nomenclature of the CRS oedometer tests	238
6.4	CRS compression curves for reconstituted Sheppey London Clay at different suction levels and strain rates of: (a) 4.8×10^{-7} s^{-1}; (b) 2.4×10^{-6} s^{-1}	241
6.5	Comparison of compression curves obtained from CRS and MSL tests on specimens with initial water contents of: (a) 43%; (b) 39%; (c) 26%	242
6.6	Variation of σ'_p with suction for fast, slow, and oedometric strain-rates	243
6.7	Stress-relaxation and associated pore-water pressure dissipation in 1D CRS oedometer tests on reconstituted Sheppey London Clay at: (a) 4.8×10^{-7} s^{-1}; (b) 2.4×10^{-6} s^{-1}	245
6.8	Stress-relaxation phases	246
6.9	Effect of strain-rate on the stress-relaxation response	246
6.10	Variation of relaxation coefficient (R_α) with suction	247
6.11	Variation of σ_v and Δu with time during multi-staged CRS tests: (a) MCRSru33-A; (b) MCRSru33-B	249
6.12	Relaxation of stresses with time at different pre-relaxation strain levels in semi-log scale	250
6.13	Relaxation of stresses with time at different pre-relaxation strain levels in log-log scale	251

6.14 Variation of R_α with pre-relaxation strain level and pre-relation strain-rate 252

List of Tables

2.1	Methods of suction measurement and/or control	25
2.2	Correlations for determination of compression indices	35
2.3	Mechanisms of creep (Le et al., 2012)	41
2.4	Volumetric creep strain-rate values observed in conventional oedometer tests	44
2.5	Soil categories based on the values of C_α/C_c (Mesri et al., 1994)	48
2.6	Strain-rate values used for CRS testing on clays	63
3.1	Quality classes of soil samples for laboratory testing (BS-EN-1997:2, 2007)	84
3.2	Physical properties of Sheppey London Clay samples as reported by CET Structures Ltd	103
3.3	Average chemical composition (% by weight) of Sheppey London Clay	108
3.4	Geotechnical parameters of reconstituted Sheppey London Clay	108
4.1	Properties of the developed HCTs	116
4.2	Examples of surface texture parameters obtained from 3D topography analysis on treated AISI 304 stainless steel samples	139
4.3	Properties of the WTs	146
4.4	Long-term suction measurement tests	155
4.5	Results of the CD tests	164
4.6	Results of the CD(er) tests	164
4.7	Input parameters for Fredlund and Xing equation	171
4.8	Improvements achieved by the new HCT	176
5.1	Loading – unloading pattern for MSL tests on saturated specimens	183
5.2	Details of MSL tests on unsaturated specimens	198
5.3	Loading – unloading pattern for MSL tests on dry specimens	207
5.4	Stress ranges for maximum C_c, $C_{\alpha e}$, and α parameters	212
5.5	Details of saturated SSL oedometer tests	213
5.6	Details of unsaturated SSL oedometer tests	217
5.7	Details of dry SSL oedometer tests	221
5.8	Regression coefficients for SSL oedometer tests	224
6.1	Details of the compression stage of the SS-CRS tests	239
6.2	Characterisation parameters for stress-relaxation stage of the SS-CRS tests	244
6.3	Details of MCRS tests	247
6.4	Characterisation parameters for stress-relaxation stage of the MS-CRS tests	248

List of Notations

Roman Symbols

a	material constant in Zhu and Yin (2014) model
b	material constant in Zhu and Yin (2014) model
c_u	undrained shear strength (kPa)
c_v	consolidation coefficient
d	diameter of the capillary tube (m)
e	void ratio
e^*_{100}	void ratio corresponding to σ'_v = 100 kPa
e^*_{1000}	void ratio corresponding to σ'_v = 1000 kPa
e_0	initial void ratio (Chapter 5)
e_f	final void ratio
e_i	initial void ratio (Chapter 2)
e_p	void ratio 24 hours after the end of loading in SSL tests
e_w	water ratio
k_0	coefficient of lateral earth pressure at rest
k_v	coefficient of vertical permeability (ms^{-1})
m	model constant in Yin et al. (2010) model
m	slope of the line in log $\dot{\varepsilon}$ – log t space
m'	material constant in Leroueil et al. (1985) model
m'_c	slope of compression curve in e – log σ_v space for unsaturated conditions
$m_0{}^T$	initial total mass of specimen (kg)
m_c	slope of compression curve in e – log σ'_v space for saturated conditions
m_s	mass of solids (kg)
m_v	coefficient of volume compressibility
m_w	mass of water (kg)
n	porosity
p	confining stress (kPa - Chapter 2)
p'	mean effective stress (kPa)
p'_0	mean effective stress equal to initial suction generated in soil sample upon unloading (kPa)
p'_c	mean effective stress corresponding to the maximum value of the vertical stress (kPa - Chapter 3)
p_a	atmospheric pressure (kPa)
q	deviator stress (kPa)
q_f	drained shear strength (kPa)
q_{peak}	maximum deviator stress (kPa)
r_1	principal radius of meniscus curvature in the air side (m)
r_2	principal radius of meniscus curvature in the water side (m)
s	soil suction (kPa)
s^*	modified suction (kPa)
s'	model parameter in Fredlund and Xing (1994) model

s_0	initial suction (kPa)
s_{AEV}	suction at air-entry value (kPa)
s_{eq}	equilibrium suction (kPa)
s_i	suction at inflection point in SWRC-*w* space (kPa)
s_k	initial suction corresponding to the triaxial stress state at which the sample neither swells nor consolidates (kPa)
s_{max}	HCT's maximum sustainable suction (kPa)
s_p	intersection of the tangent line to the inflection point with the horizontal axis in SWRC-*w* space (kPa)
s_r	residual soil suction (kPa)
s_t	slope of the tangent line at inflection point in SWRC-*w*
t	time (h)
t_0	reference time in Yin and Graham (1989) model (h)
t_1	time at the beginning of creep stage in Lai et al. (2010) model (h)
t_d	HCT's diaphragm thickness (mm)
t_i	reference time corresponding to EOP (h)
t_{ie}	equivalent time (h)
t_{max}	HCT's maximum measurement duration (min)
t_R	period of stress-relaxation (h)
u_a	pore-air pressure (kPa)
u_{exc}	excess pore-water pressure (kPa)
u_w	pore-water pressure (kPa)
u_{wm}	meniscus pressure (kPa)
w	gravimetric water content
$w(s)$	gravimetric water content at any given suction
w_0	initial gravimetric water content
w_f	final gravimetric water content
w_i	water content at inflection point in SWRC-*w* space
w_L	liquid limit
w_P	plastic limit
w_{sat}	saturated gravimetric water content
y	material constant in Zhu and Yu (2014) model (page 59)
Δe	change in void ratio
Δm_w	evaporated mass of water (g)
Δu_w	change in pore-water pressure (kPa)
A	strain rate at $D_r = 0$ and $t = t_1$ in Lai et al. (2010) model (s^{-1} – page 58)
A	material constant in Zhu and Yu (2014) model (page 59)
A	material constant in Leroueil et al. (1985) model (page 66)
A	model constant in Yin et al. (2010) model (page 76)
A_0	initial area of the specimen (m^2)
A_s	excess pore-water ratio corresponding to the removal of the deviatoric stress (kPa)
B	model parameter in Lai et al. (2010) model

C_c	compression index in $e - \log \sigma'_v$ space
C_r	reloading index in $e - \log \sigma'_v$ space
C_s	swelling index in $e - \log \sigma'_v$ space
C_α	creep index
$C_{\alpha e}$	creep index with respect to e
$C_{\alpha \varepsilon}$	creep index with respect to ε
D_r	stress intensity
D_R	modified stress intensity
E	elasticity modulus (MPa) (Chapter 4)
E_{max}	elastic stiffness modulus (MPa)
E_u	undrained elastic stiffness modulus (MPa)
G_s	specific gravity
H	thickness of the consolidating soil layer (m)
H_0	initial height of specimen (mm)
I_p	plasticity index
I_v	index for normalisation of the compression curves
L	unit length (m)
L_e	effective hydraulic flow path (m)
N_s	intergranular force due to suction (N)
N_σ	normal component of the intergranular force due to external stress (N)
P	applied pressure (kPa)
R	radius of the air-water interface curvature (mm)
R_0	HCT's diaphragm radius (mm)
R^2	coefficient of determination in regression
R_a	arithmetic average deviation from the mean line (μm)
R_i	radius of idealised spherical particles (mm)
R_p	maximum peak of roughness (μm)
R_q	root mean square value of roughness
R_t	maximum peak-to-valley height (μm)
R_v	maximum valley of roughness (μm)
R_α	coefficient of stress-relaxation
S	sensitivity parameter
S_r	degree of saturation
S_r^e	effective degree of saturation
S_t	strength sensitivity
T	air-water surface tension (kPa)
T_σ	tangential component of inter-granular force due to the external stress (N)
V_{exc}	excitation voltage (V)
V_{out}	full scale output voltage (V)
V_s	volume of solids (m^3)
V_T	total volume (m^3)
V_v	volume of voids (m^3)

V_w	volume of water (m^3)
ΔN	additional inter-particle force produced by the meniscus water (N)
ΔV	volume change (m^3)

Greek Symbols

$\dot{\varepsilon}^e$	elastic strain-rate (s^{-1})
$\dot{\varepsilon}^p$	visco-plastic strain-rate (s^{-1})
$\dot{\varepsilon}^t$	total strain-rate (s^{-1})
$\dot{\varepsilon}_v$	vertical strain-rate (s^{-1})
$\dot{\varepsilon}_v^c$	volumetric creep strain-rate (s^{-1})
$\dot{\varepsilon}_v^r$	reference volumetric strain-rate (s^{-1})
$\dot{\varepsilon}$	strain-rate (s^{-1})
ε_{v0}^{ep}	elastoplastic strain
α	represents the ratio $C_{\alpha e}/C_c$
α_i	creep coefficient (Chapter 5)
β	rate-dependency coefficient (Chapter 2)
β	represents the ratio e_i/e_p (Chapter 5)
β^c	model parameter in Oldecop and Alonso (2002) model
β_{DR}	model parameter in Lai et al. (2010) model
δ	slope of the graph of ln $\dot{\varepsilon}$ – D_r in Lai et al. (2010) model
δ_{ij}	Kronecker's delta
$\Delta\varepsilon^e$	change in elastic strain
$\Delta\sigma$	relaxed stress (kPa)
$\Delta\sigma_v$	change in applied vertical stress (kPa)
ε	strain
ε_a	axial strain
ε^e	elastic strain
$\varepsilon_f^{\ v}$	final volumetric strain
ε_R	radial strain (Chapter 4)
ε_R	pre-relaxation strain (Chapter 6)
ε_{R0}	radial strain at the periphery of the HCT's diaphragm
ε_{Rc}	radial strain at the centre of the HCT's diaphragm
ε_T	tangential strain
ε_{T0}	tangential strain at the periphery of the HCT's diaphragm
ε_{Tc}	tangential strain at the centre of the HCT's diaphragm
ε_v	vertical strain (Chapter 2)
ε_v	volumetric strain (Chapter 5)
$\varepsilon_v^{\ c}$	creep strain
η	model parameter in Alonso et al. (2005) model
θ	contact angle (º – page 11)
θ	volumetric water content (page 20)
θ_a	advancing contact angle (º)
θ_r	receding contact angle (º)
κ	swelling index in e – ln p' plane

κ_0	reloading index in e – ln p' plane
λ	compression index in e – ln p' plane
λ'	model parameter equal to (1 – m) in Lai et al. (2010) model
λ_i	intrinsic compression index in e – ln p' plane
μ	creep index in Oldecop and Alonso (2002) model
ν	Poisson's ratio
ξ	residual stress ratio
π	osmotic suction (kPa)
ρ_w	density of water (kg/m^3)
σ^*_{ij}	effective stress tensor (Alsonso et al., 2010)
σ'_{ij}	Bishop's effective stress (kPa)
σ'_{pCRS}	σ'_p obtained from CRS tests (kPa)
σ'_{pMSL}	σ'_p obtained from MSL tests (kPa)
σ_0	pre-relaxation total vertical stress (kPa)
σ_3	confining pressure (kPa – Chapter 2)
σ'_3	net confining pressure (kPa)
σ_{ij}	total stress tensor
σ'_p	apparent preconsolidation pressure (kPa)
$\sigma'_{pi}{}^r$	initial value of the current reference stress corresponding to the start of stress-relaxation (kPa)
σ_s	residual total vertical stress (kPa)
σ_v	applied vertical total stress (kPa)
σ'_v	vertical effective stress (kPa)
σ'_{v0}	initial effective stress (kPa)
σ'_{vc}	maximum vertical effective stress (kPa)
σ'_{vi}	initial vertical effective stress (kPa)
σ_{vm}	maximum applied vertical stress (kPa)
σ_{vnet}	net normal vertical stress (kPa)
τ	tortuosity
ϕ'	effective angle of friction (º)
χ	Bishop's effective stress parameter
ψ	total suction (kPa)

Acronyms / Abbreviations

1D	one-dimensional
3D	three-dimensional
AEV	air-entry value
AF	anti-fog agents
BBM	Barcelona Basic Model
BGS	British Geological Survey
CD	continuous drying test
CD(er)	continuous drying test with controlled evaporation
CG	constant gradient of pore-water pressure
CL	constant loading test

CPT	cone penetration test
CRL	constant-rate-of-loading
CRS	constant-rate-of-strain
CS-CRS	constant matric suction CRS test
CW-CRS	constant water content CRS test
DDL	diffuse double layer
DP	diamond paste
EDM	electro discharge machining
EOP	end of primary consolidation
ESEM	environmental scanning electron microscope
FM	face-milling
HCT	high-capacity tensiometer
ICL	intrinsic compression line
IL	incremental loading
LC	London Clay
LPT	linear potentiometric transducer
LVDT	linear vertical displacement transducer
MSL	multi-staged loading
NC	normally consolidated
NCL	normal compression line
NI	national instruments
OC	overconsolidated
OCR	overconsolidation ratio
PPR	pore-water pressure ratio
PPR_{max}	maximum pore-water pressure ratio
PSD	particle (pore) size distribution
PWPT	pore-water pressure transducer
RH	relative humidity
SCL	sedimentary compression line
SiC	silicon carbide
SRS	step-wise change in strain-rate test
SSL	single-staged loading
SWRC	soil water retention curve
TCS	thermal conductivity sensors
THM	thermo-hydro-mechanical
WT	Warwick tensiometer
XRD	x-ray diffraction

CHAPTER 1: INTRODUCTION

1.1 Problem Statement

Climate interacts with natural slopes and shallow-depth soil deposits and causes changes in their hydro-mechanical properties and state variables mainly in terms of their pore-water pressure, volume change, and shear strength parameters. These deposits are typically encountered above the phreatic table and hence are partially water-saturated. Moreover, it is well known that the mechanical behaviour of soils, in particular natural clays, is highly influenced by time and rate effects (Fodil et al., 1997, Tanaka, 2005, Degago et al., 2013, Bagheri et al., 2015). Clays typically present low permeability and shear strength, as well as a tendency to undergo continuous compression with time (creep), even after excess pore pressures have substantially dissipated.

The effect of strain-rate on the mechanical response of clays is highlighted in staged construction of geo-structures where each stage of the construction plan alters the rate of soil straining in the ground. Moreover, the construction plans often involve stages of constant total strain in the soil body during which the deviatoric stress decreases continuously with time at a very slow rate (stress relaxation).

Little is currently known about the creep and relaxation responses of unsaturated clays, in particular stiff clays such as London Clay. With the aim to improve the current understanding of the viscous response of clays in unsaturated conditions, this research project was conducted through collaboration between University of Nottingham and University of Warwick. A better understanding of these behavioural aspects will have implications on development of design and maintenance strategies for geo-structures exposed to climate variations.

1.2 Aim and Objectives

The present work aims at filling the gap in knowledge of viscous processes, mainly creep, stress relaxation, and rate-dependency, in unsaturated clays through critical review of literature and a program of laboratory testing involving state-of-the-art

innovations and improvements in design of advanced laboratory testing equipment and conducting a set of conventional and advanced experiments on natural and corresponding reconstituted samples of London Clay. The main objectives of the research work are outlined as:

a) To develop advanced laboratory equipment capable of testing clays under controlled strain-rates and suctions in ranges of practical interest.
b) To examine the effect of soil suction on primary and secondary consolidation (creep) of intact and reconstituted London Clay in oedometric conditions.
c) To investigate the effect of soil suction on one-dimensional stress-relaxation behaviour of reconstituted London Clay.
d) To investigate the coupled effects of suction and strain-rate on one-dimensional (1D) and three-dimensional (3D) stress–strain response of reconstituted London Clay.
e) To examine the validity of the empirical relationships proposed in the literature for correlating time- and rate-dependency coefficients in saturated (soft) clays, and their applicability for unsaturated (stiff) clays.

1.3 Research Methodology

Through a comprehensive programme of laboratory soil element tests, carried out using conventional and advanced testing equipment, the phenomena associated with viscosity and partial saturation were characterised and their separate and coupled influences on the monotonic behaviour of clays were investigated in detail. Aspects of viscous behaviour including creep, stress-relaxation, and strain-rate-dependency in saturated and unsaturated states were examined. Generally the viscous phenomena have been investigated at a macroscopic scale in the laboratory soil element tests. Characterisation of the micro-mechanisms associated with the observed macroscopic behaviour lay outside the scope of this research.

In order to monitor the evolutions of pore-water pressure, especially in negative ranges, during the long-term creep and relaxation tests, a total of 12 high-capacity tensiometers (HCTs) with improved long-term performance were designed and constructed. Three unsaturated oedometer cells incorporating two HCTs on their loading caps were designed and manufactured making it possible to measure suction changes during MSL

and SSL oedometer tests on unsaturated specimens. To expand the investigation, an advanced suction- and temperature-controlled CRS oedometer cell capable of controlling and monitoring soil suctions up to 1.5 MPa was also developed and calibrated. This new cell made it possible to investigate the coupled effects of strain-rate, suction and temperature on the compression and relaxation responses of the specimens (although investigation of the temperature effects was outside the scope of this research program). The experimental program followed in this research is outlined as;

a) Conventional MSL oedometer tests on saturated and unsaturated specimens.
b) Long-term SSL oedometer creep tests on saturated and unsaturated specimens.
c) CRS oedometer tests at different strain-rates and water contents (suctions) involving stages of stress-relaxation.

All experiments were conducted over a range of 43 – 15% initial water contents corresponding to suctions of 0 – 21000 kPa.

1.4 Layout of the Thesis

This thesis consists of seven chapters in total. Chapter 1 provides an introduction to the conducted research program. The remaining chapters form the structure of the thesis as follows:

Chapter 2 presents a detailed review of the literature with regards to the observed time- and rate-dependent behaviour of clays with emphasis on the reported experimental studies. The main focus is on the effect of suction on primary consolidation, creep, stress-relaxation and rate-dependent behaviours of clays.

In Chapter 3 the selection of testing material and the procedures followed for retrieving undisturbed block samples of London Clay from the field are explained. The geological characteristics of the chosen material including its origin, mineralogy, macro-fabric, and micro-fabric, along with the geotechnical properties including pore-size distribution, index and mechanical properties are briefly discussed. Moreover, the procedures for preparation of the test specimens from undisturbed and reconstituted samples are explained.

Chapter 4 concentrates on the direct measurement of soil suction using HCTs. First a synthesis of recent research on HCTs with the focus on technological improvements in terms of design characteristics, calibration, and preconditioning of the sensors is provided. A new approach is then proposed to expand the range and duration of suction measurements for a newly designed HCT. The procedures employed for design, fabrication, saturation, and calibration of the new tensiometers are addressed in detail. Furthermore, the performance of the developed HCTs is examined based on a series of experiments carried out on a number of unsaturated clay specimens. Finally, the procedure to obtain the soil water retention curve (SWRC) using the developed HCTs is presented and new recommendations to obtain reliable measurements are given.

Chapter 5 presents the outcome of a detailed experimental study on the primary and secondary consolidation of natural and reconstituted London Clay, as observed under both fully saturated and unsaturated states in general oedometric testing conditions. The influence of suction on the time-dependent stress–strain behaviour is examined. The results obtained are used to examine the validity of the relationships proposed in the literature for correlating compression and creep indices. The applicability of these relationships for unsaturated conditions is also discussed.

Chapter 6 presents an experimental investigation into the coupled effects of suction and strain-rate on stress–strain and viscous behaviour of clays. The design procedure and distinctive features of a new suction- and temperature-controlled CRS oedometer cell are provided. The coupled effect of suction and strain-rate on the stress–strain response of reconstituted London Clay is examined in CRS compression/relaxation tests. On the basis of the observed behaviour, the validity of the relationships proposed in the literature for correlating relaxation and consolidation coefficients is examined. Moreover, the applicability of these relationships for unsaturated conditions is also discussed, and necessary modifications are proposed.

Finally, Chapter 7 presents a summary of the main experimental developments and findings from the research work along with the recommendations for future research.

CHAPTER 2: LITERATURE REVIEW

2.1 Introduction

This chapter gives a review of the published literature concerning the time-dependent behaviour of unsaturated clays, in particular natural stiff clays. The time-dependent behaviour of clays is usually divided into viscous and aging/thixotropic effects. However, studying the aging and thixotropic effects lies outside the scope of this research, thus the focus will be on viscous effects which groups together the phenomena of creep, stress-relaxation, and strain-rate effects (Augustesen et al., 2004, Sorensen, 2006). In this work, primary consolidation is also considered as a time-dependent behaviour, as it is now generally accepted that creep strains also take place during the course of excess pore-water pressure dissipation (Degago, 2011). Furthermore, this chapter aims at reviewing the reported experimental work on the viscous behaviour of clays and therefore disregards the numerical analysis and constitutive modelling aspects, though, when necessary, some examples of numerical modelling are given to better describe particular concepts. Moreover, although the main focus of this research is to characterise the viscous behaviour of stiff clays such as London Clay, a supplementary review of soft clay behaviour relative to this study is provided. The viscous behaviour of chalks, granular soils, and rocks is outside the scope of this research, however, some examples of the viscous behaviour of these geo-materials are included where these help to illustrate the influence of suction on general viscous behaviour.

In section 2.2, the structural properties of clays such as mineralogy, fabric anisotropy, and inter-particle bonding are explained. These factors have direct influence on clays' viscous response. The concepts of soil suction, effective stress, and water retention behaviour in unsaturated soils, as well as the current suction measurement techniques are reviewed in section 2.3. In section 2.4, a comparative review of the viscous properties of clays under saturated and unsaturated conditions, with focus on primary and secondary consolidation (creep), is presented. The effect of suction on rate-dependent behaviour of clays under oedometric conditions is reviewed in section 2.5. The phenomenon of stress-relaxation and the empirical approaches for its formulation are explained in section 2.6. Finally, in section 2.7, concluding remarks and gaps of knowledge in time- and rate-dependent response of unsaturated clays are outlined.

2.2 Structural Properties of Natural Clays

It is well known nowadays that the properties of undisturbed natural clays differ from their reconstituted or remoulded properties. Mechanical behaviour of reconstituted clays, termed "intrinsic properties", is independent of the natural states, and mainly stems from the clay mineralogy, whereas, the mechanical behaviour of undisturbed clays, in addition to their inherent (intrinsic) properties, is dependent on their naturally or manually induced *in-situ* properties, known as "structure". Burland (1990) defined the term "structure" as a combination of "fabric" and "bonding", the former being the geometrical arrangement of soil particles and pore space, and the latter being the inter-particle contact forces. An undisturbed (intact) soil is often referred to as being in a structured or metastable state, whereas a reconstituted or remoulded soil is often referred to as being in a non-structured or destructured state (Sorensen, 2006). The effect of soil structure on the engineering behaviour has been shown to be as significant as porosity and stress history (Leroueil and Vaughan, 1990). Hence, in this section the mineralogy and geological features of natural clays developed during depositional and post-depositional processes are briefly discussed.

2.2.1 Mineralogy

Clay minerals are typically groups of crystalline particles of less than 2μm size whose formation has basically resulted from chemical weathering of a parent rock. Silicon-oxygen tetrahedrons and aluminium-hydroxyl octahedrons form the basic structural units of clay minerals. Combinations of the tetrahedral units form an electrically negatively charged sheet structure called "silica", whereas, combinations of the octahedral units form an electrically neutral sheet structure called "gibbsite". Accumulation of the layered structures of chemically bonded silica and gibbsite sheets forms the clay mineral particles. Kaolinite, Illite, and Montmorillonite are the main clay minerals. The negatively charged mineral surfaces due to the presence of silica sheets attract water molecules in the pore space, and hence, influence the mineral's plasticity. Clay minerals are also often found in "plate-like" shapes having a high specific surface. This property substantially enhances the influence of surface forces on these types of soil and causes an increase in their compressibility. Clay minerals are usually found as aggregated units known as domains. Aggregation of the domains form clusters which are consequently aggregated to create naked eye visible peds (McGinty, 2006).

2.2.2 Fabric Anisotropy and Inter-particle Bonding

Deposition of natural clays is the result of a series of environmental processes involving weathering, transportation, geological sedimentation, and chemical reactions with water chemistry. The weathered clay particles are transported and deposited in layers in the beds of the rivers, lakes, and off-shore basins. The physical properties of the sediments such as shape, size, and particle arrangement are therefore influenced by the combination of these processes. These sedimentary deposits in their *in-situ* (intact) conditions are referred to as being in a structured or metastable state. The structural properties of natural sedimentary soils are classified into sedimentation structure and post-sedimentation structure. As stated by Yu and Axelsson (1994), during deposition, orientation of the plate-shaped clay particles is normally such that their long axes are normal to the direction of the major principal stresses (vertical direction) in the ground. The resulting compression pressure of overburden material forms layers of horizontally oriented particles during sedimentation. As a result, horizontally identical properties emerge for each clay layer (an exception to this is the sensitive clays). The fact that the material properties are identical in horizontal directions but different in the vertical direction is referred to as "cross-anisotropy". This type of naturally induced fabric anisotropy is also called "initial anisotropy" and is attributed to the geological history of the clay deposits. Fabric anisotropy can influence the mechanical behaviour of clays (Mesri and Olson, 1971, Wheeler et al., 2003b, Karstunen and Koskinen, 2008). Post-depositional engineering works and subsequent plastic straining change the internal structure of the clay and develop another type of fabric anisotropy in clay material which is called "plastic strain-induced anisotropy".

The depositional and post-depositional processes, and water chemistry (among other phenomena) result in different arrangements of clay particles. The two distinct clay fabric arrangements are "flocculation" and "dispersion" with the former presenting a random arrangement of particles, and the latter presenting a parallel particle arrangement. The flocculated fabric is also found in the forms of "cardhouse" fabric resulting from an arrangement of single particles, or "bookhouse" fabric resulting from an arrangement of domains (Figure 2.1).

In addition to development and evolution of soil fabric during sedimentation, clay deposits gain more strength and resistance to yielding from development of inter-

particle bonds during the post-deposition period. These natural bonds emanate from mineral and pore-water composition, cementation and thixotropic hardening, weathering, leaching, and mechanical unloading and reloading, and play a significant role in the mechanical response of clays (Leroueil et al., 1996, Karstunen et al., 2005).

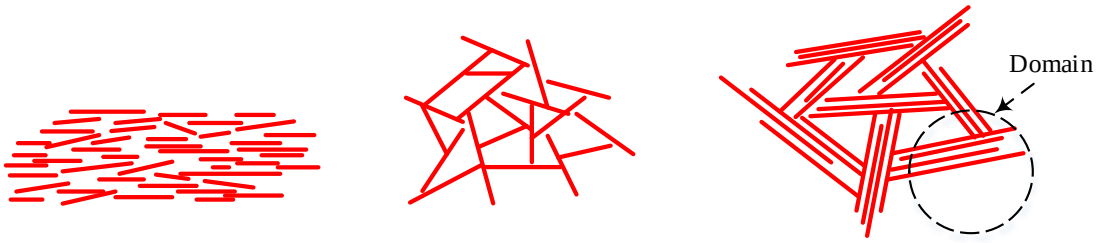


Figure 2.1 Fabric of clays

2.3 Unsaturated Soils

In a general theoretical framework, an unsaturated soil is considered to be a four phase material consisting of solid phase (soil grains), gaseous phase (generically referred to as air), liquid phase (generically referred to as water), and an independent phase called air-water interface or contractile skin (Fredlund and Rahardjo, 1993). The gaseous phase is in fact presented as a mixture of air and liquid vapour. In some special cases, three fluid media can be present in unsaturated soils. This is for example the case in hydrocarbon-bearing soils where oil, water and gas occur as pore fluids. Determination of the hydro-mechanical behaviour of unsaturated soils depends on the mutual interaction between these phases. Figure 2.2 presents an idealised structure of an unsaturated soil. According to Wheeler et al. (2003c), the bulk water exists within the water-filled voids and the meniscus water is developed at the inter-particle contacts around the air-filled voids.

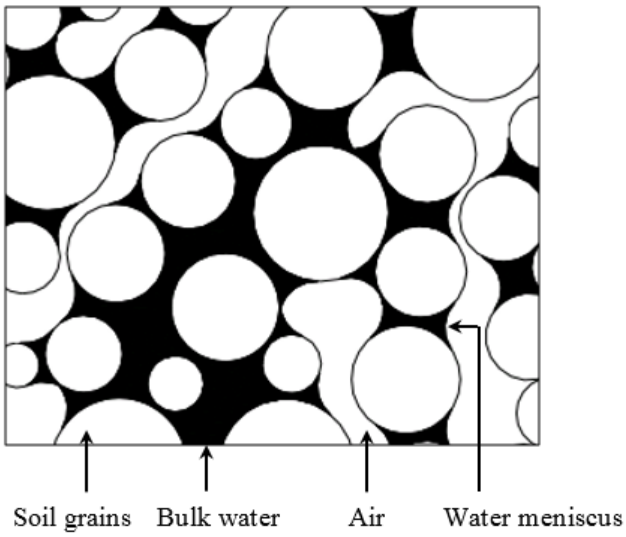


Figure 2.2 Idealised structure of unsaturated soils (after Raveendiraraj 2009)

In this section, typical concepts of unsaturated soil mechanics including definition of suction, role of water menisci in control of volume change, and water retention behaviour are discussed with reference to the literature.

2.3.1 Soil Suction

In general, scientific phenomena such as hydrostatic pressure, change in water level, absorption pressure, and osmotic pressure are the sources of pore-water pressure development (Mitchell, 1993). This fluid pressure, if relative to atmospheric pressure (101.6 kPa absolute pressure at sea-level), is so called gauge pressure, and is negative if it is lower than atmospheric pressure. Conventionally, negative water pressures imply tension and positive water pressures imply compression if referring to pressure in absolute terms. Environmental variations such as surface evaporation and lowering of the groundwater table cause development of negative pore-water pressure in unsaturated soils of the vadose zone. This is described as suction in unsaturated soil mechanics. Suction is considered to have major impacts on the hydro-mechanical behaviour of unsaturated soils. It can be defined generically as the free energy state of soil-water or, the potential of soil for water attraction (Murray and Sivakumar, 2010). Typically, two components are considered for the soil total suction (ψ); matric suction ($s = u_a - u_w$), and osmotic suction (π). Matric suction is defined as the difference between pore-air pressure (u_a) and pore-water pressure (u_w) within an element of soil, and occurs as a result of capillary mechanism and surface adsorption effects, whereas

osmotic suction is described as the ability of water attraction in a soil's inter-particle spaces, and arises from non-homogeneity of ion concentration in bulk water. In other words, the presence of dissolved salts in pore-water can result in a reduction of relative humidity (RH) in a pore, which is called osmotic suction. Total suction is calculated as;

$$\psi = (u_a - u_w) + \pi \qquad 2.1$$

Experimental results have proven the contribution of suction to hydro-mechanical responses of unsaturated soils. Change in matric suction during cycles of wetting and drying can result in irreversible volumetric deformations (Alonso et al., 1995). Decrease in matric suction during wetting of a partially saturated soil may cause expansion or even collapse depending on the confining stress state (Wheeler et al., 2003c). Increase in matric suction leads to an increase in yield stress during isotropic loading, a phenomenon known as suction hardening (Wheeler and Sivakumar, 1995).

The mechanical response of non-expansive soils is much more influenced by the variation of matric suction than osmotic suction (Alonso et al., 1987). Despite the importance of osmotic suction and total suction, it is the matric suction that is directly related to the negative pore-water pressure in unsaturated soils (Fredlund, 2006). Osmotic suction plays a key role in highly plastic clays (Blatz et al., 2008) and where highly active clay minerals and active dissolved salts are present (Alsharrad, 2013). The material used for this research is a non-expansive stiff clay, namely London Clay. The unsaturated tests (see Chapters 4, 5, and 6) were mainly performed on reconstituted specimens, where in the absence of active dissolved salts, matric suction will have much more influence on the mechanical behaviour than osmotic suction. Therefore, the term "suction" used throughout this manuscript generally refers to matric suction.

2.3.2 Capillarity

The fact that soils contain pore-water at negative pressure above the water table is known as capillary rise. The capillary phenomenon plays a major role in the hydraulic response of unsaturated geo-materials. Capillarity action is the upward movement of water in a capillary system, and is associated with the surface tension of water. In bulk liquid the resultant forces acting on a molecule are null whereas the molecules on the air-water interface (contractile skin) experience attractive forces with a downward resultant force from their neighbours in the liquid phase [Figure 2.3(a)]. As an attempt

to reach equilibrium, they must gain excess energy over those in the bulk liquid, resulting in a surface tension distributed over the interface length. The surface tension is defined as the force per unit length acting in the plane of the surface of a liquid and is developed as a result of intermolecular attraction imbalance at the air-water interface, and causes the surface to act like a membrane in tension (Laloui, 2010). The interface will curve if in contact with a solid surface as a result of a balance between the cohesive forces in the liquid and the adhesive forces between solid and liquid (Marinho et al., 2008), generating a meniscus with contact angle (defined in next section) of less or higher than 90° based on the properties of the liquid. In unsaturated soils, as the water pressure at the back of meniscus is less than the air pressure, the water meniscus, with contact angle of less than 90º, will rise in the capillary tubes of small diameter pores until the hydrostatic conditions are established [Figures 2.3(b) and (c)].

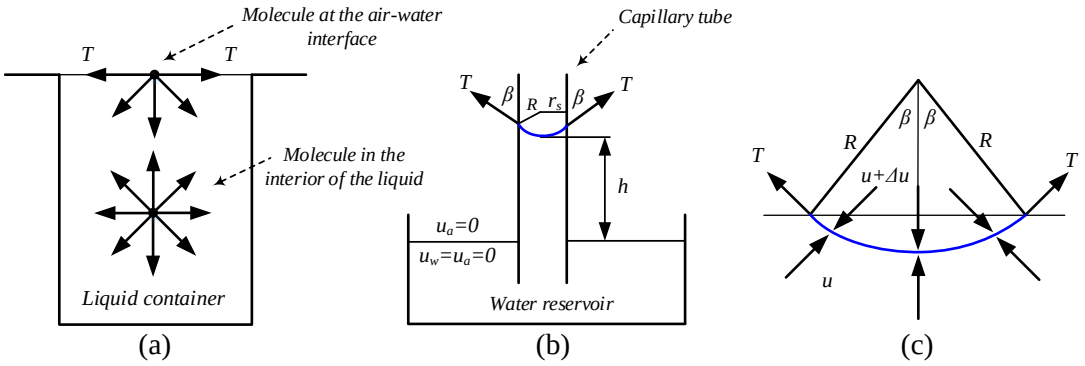


Figure 2.3 Concept of capillary rise: (a) intermolecular forces in a liquid-gas system; (b) capillary mechanism; (c) pressures and surface tension acting on a two-dimensional surface (after Fredlund and Rahardjo, 1993).

The water pressure at the back of the meniscus (u_{wm}) can be calculated by the Young-Laplace equation (Equation 2.2) which is based on the vertical force equilibrium over the contractile skin;

$$u_{wm} = u_a - \frac{4T\cos\theta}{d} = -\frac{2T}{R} \qquad 2.2$$

where T refers to the air-water surface tension, θ is the contact angle, d is the diameter of the capillary tube, and R is the radius of curvature of the interface. Since $cos\theta > 0$ for wetting fluids, the water pressure at the back of the meniscus is less than the air pressure. This also suggests that soils with lower contact angles (higher affinity with water), i.e. hydrophilic clayey or silty soils, will have higher matric suctions for same

water contents (Lourenço, 2008). The maximum negative water pressure that can be sustained without drawing air into the soil is known as the air-entry value (AEV) and is controlled by the value of surface tension T for an air-water interface and the size of throats providing the entry routs to voids. The capillarity mechanism in unsaturated soils is much more complex as the soils comprise discrete particles not uniform tubes (Murray and Sivakumar, 2010).

2.3.3 Contact Angle

The contact angle (θ) is defined as the angle between the solid surface and the gas-liquid interface, and is measured through the liquid. Figures 2.4(a) and 2.4(b) present a schematic definition of the contact angle for a wetting and non-wetting solid surface. The developed contact angles on the opposite sides of the drop can be considered to be equal for the case of a smooth, homogenous, and non-deformable solid surface (Marinho et al., 2008). However, if the drop is placed on a tilted surface, the advancing (leading) and receding (trailing) contact angles, denoted respectively by θ_a and θ_r, will be different as shown in Figure 2.4(c). Note that the θ_a angle is the maximum angle above which the drop will roll off the surface. Further discussions on the concept of contact angle can be found in Marinho et al., (2008).

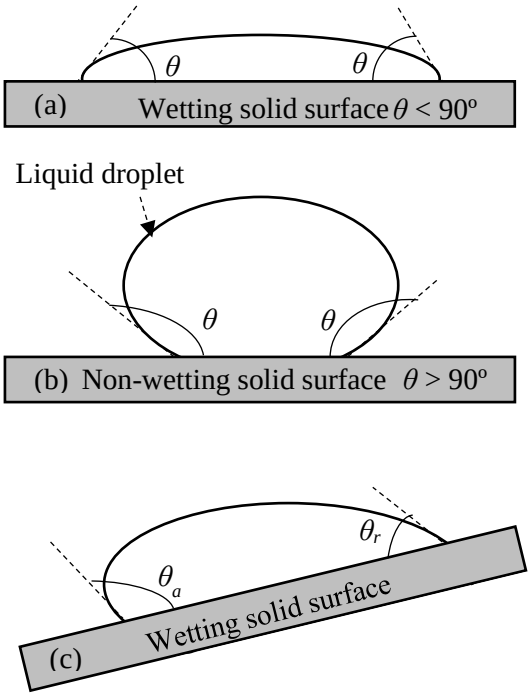


Figure 2.4 Concept of contact angle: (a) wetting surface; (b) non-wetting surface; (c) tilted wetting surface

2.3.4 Adsorption

The other phenomenon that influences the matric suction is the surface adsorption effect, which is particularly associated with the clay minerals in soil matrix. Studies of the mineralogy of clay particles have evidenced distribution of a highly negatively charged electrical layer along the particle surface. Exposure of clay particles to water results in attraction and adsorption of water molecules to the clay surface. Electro-chemical interactions between the water molecules and the clay minerals result in formation of a continuous thin film of water which covers the whole surface area of the particles and so is called "adsorbed water". The greatest amount of adsorbed water is retained around high-activity clay minerals and it effectively reduces the inter-particle pore spaces (Murray and Sivakumar, 2010). The positively charged ions (cations) and free water molecules in the solution are also attracted to the clay surface via electrical forces to form the second cover layer. These parallel layers of charges surrounding the clay mineral comprise the so called "diffuse double layer" (DDL). The term "diffuse" refers to the second layer made of free ions which are not firmly anchored to the soil particles and are free to move in fluid under the influence of electrical attraction or thermal motion. Thermal alterations have inverse impacts on the cation layer thickness, resulting in, for instance, a decrease in layer thickness as a consequence of temperature increase (Craig, 2004). The exerted attractive forces from the clay mineral are reduced with increase in the thickness of the double layer. Where a soil is free to expand or shrink without cracking the thickness of the double layer is proportional to the void ratio. The thickness of the double layer is directly proportional to the void ratio, hence an increase in the thickness of DDL results in an increase in void ratio (Mitchell, 1993). Figure 2.5 presents a schematic view of the adsorbed and diffuse double layers in clays.

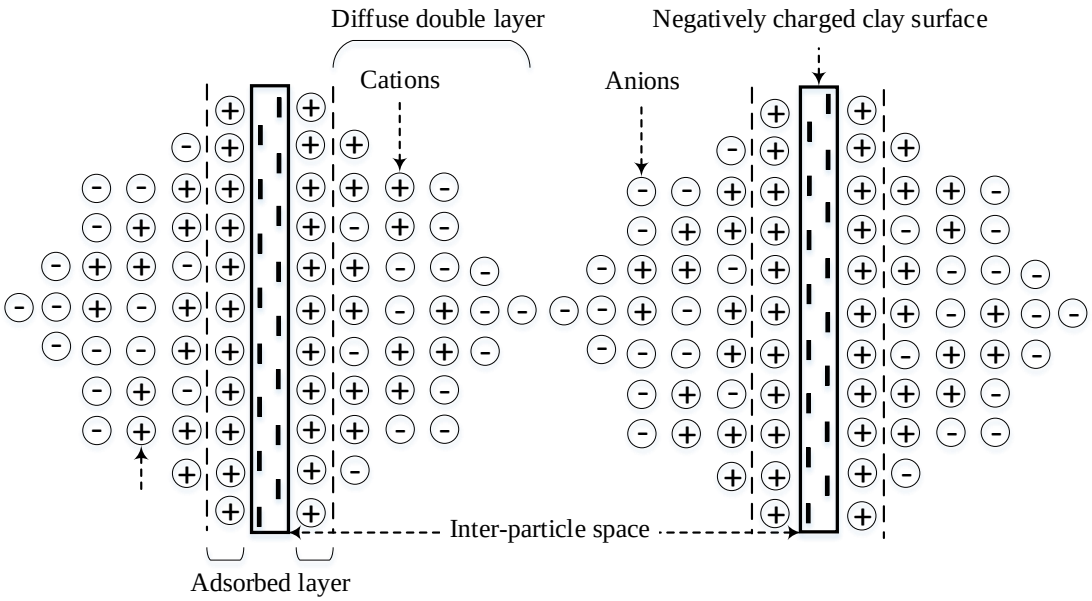


Figure 2.5 Schematic representation of the adsorbed and diffuse double layers in clays.

2.3.5 Water Menisci and Contractile Skin

The intergranular bonding forces in an unsaturated soil matrix are partly exerted by capillary forces acting at the inter-particle contacts. The magnitude of these capillary forces depends on a number of factors such as surface tension, the radius of curvature of the menisci, and the contact angle of the contractile skin (Lourenço et al., 2012). The role of water menisci and the contractile skin in control of strength and deformation of unsaturated soils is clearly confirmed. Water menisci provide attractive forces (meniscus force) that hold the soil particles together (Lourenço, 2008). To better understand the role of water menisci in controlling the strength, stiffness, and deformations in unsaturated soils, Lourenço et al. (2012) conducted a series of microstructural analyses on unsaturated sand, clay, and artificially made spherical grains (organosilicates) using an environmental scanning electron microscope (ESEM). They reported that menisci appear in the soil matrix either as predominantly convex or predominantly concave shapes. If the curvature of the meniscus is concave on the side of the air ($\theta < 90^{o}$), the water pressure will be negative with respect to the air pressure and this applies tensile pressure to the soil grains as does the contractile skin [Figures 2.6(a) and (b)]. Conversely, the water pressure is compressive in a convex shaped meniscus ($\theta > 90^{o}$), pushing the soil grains away from each other and acting against the tensile pressure exerted from the air-water interface [Figures 2.6(c) and (d)]. Unlike the development of continuous films of water with a predominantly concave shape around

the clay particles, a mixture of predominantly concave and convex menisci was observed (at the same RH) around sand and organosilica particles. The authors concluded that "the shapes of menisci are controlled primarily by the nature of the materials involved, irrespective of the size and shape of the individual grains".

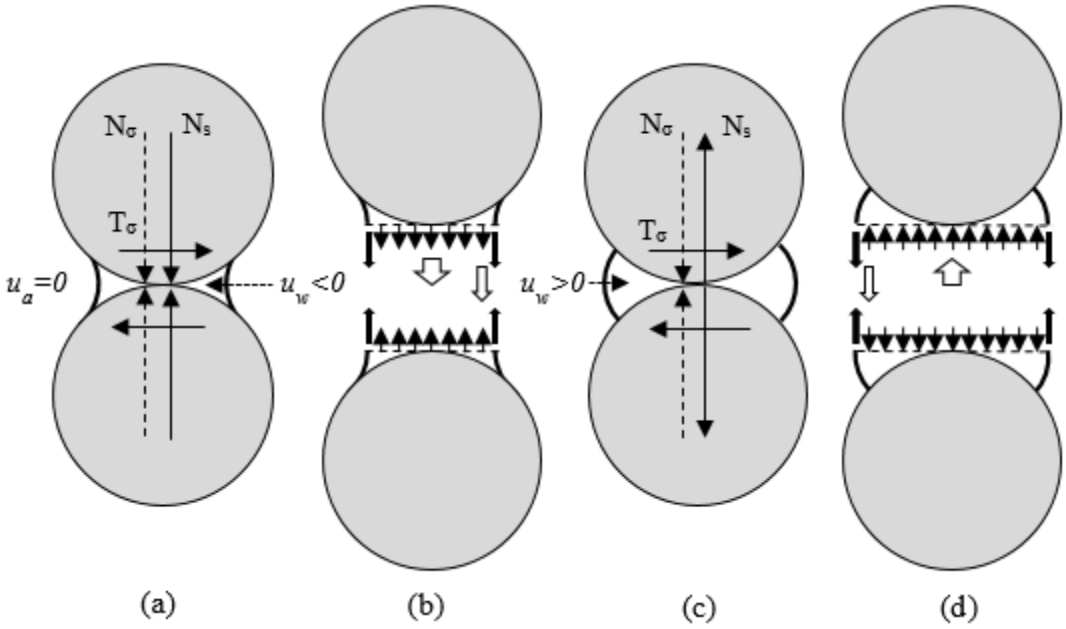


Figure 2.6 Schematic representation of menisci shape at the particle contact of idealised spherical grains: (a) concave menisci; (b) tensile pressure inside the concave meniscus; (c) convex menisci; (d) compressive pressure inside the convex meniscus – T_σ is the tangential component of intergranular force due to the external stress, N_σ is the normal component of the intergranular force due to external stress, and N_s is the intergranular force due to suction

For idealised spherical particles of radius R_i in contact (Figure 2.7), the additional inter-particle force ΔN produced by the meniscus water can be calculated using;

$$\Delta N = \pi T R\left(2 - \frac{r_2}{R_i}\right) \qquad 2.3$$

where, T is the surface tension, and r_2 is the principal radius of curvature of the air-water interface in the water side. The principal radius r_1, shown in Figure 2.7, is defined as the radius of curvature of meniscus water in the air side and can be calculated as;

$$r_1 = \frac{r_2^2}{2(R_i - r_2)} \qquad 2.4$$

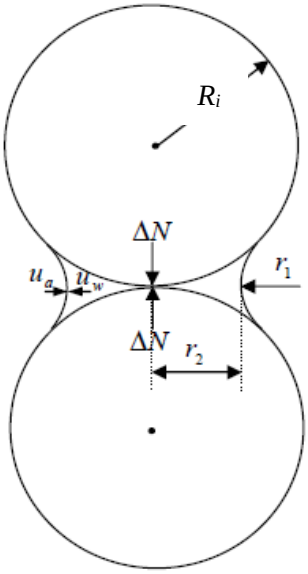


Figure 2.7 The forces diagram of two idealised spherical soil particles in contact (Raveendiraraj, 2009)

The arrangement of water menisci at the contact area with soil particles is affected by the value of the developed contact angle at the particle contacts which, in turn, depends on a number of factors such as the type of the soil and mineral, menisci movement and velocity, super-hydrophobicity related to the surface topography, and the presence of micro-asperities, impurities, solutes, organic matter, microbial cells, and surfactants (Lourenço et al., 2012). The contact angle exhibits hysteresis behaviour in a given system of non-smooth, heterogeneous, and deformable solids (Marinho et al., 2008). Contact angles vary in successive cycles of wetting and drying, based on formation of concave or convex menisci (Lourenço et al., 2012). The importance and influence of the contact angle on the hydro-mechanical behaviour of unsaturated soils is less clearly identified.

The contractile skin acts as a rubber membrane as it induces a normal stress due to the pore-water pressure (Wulfsohn et al., 1996). Although the contractile skin can be considered as part of the water phase in volume-mass alterations of soil properties, there is a strong justification that it is the interaction of the contractile skin, as an independent phase, with the soil structure that causes change in volume and shear strength of an unsaturated soil (Fredlund, 2006). According to Matsumoto and Kataoka (1988) the contractile skin has different properties from that of ordinary water and its water molecular structure is more similar to ice than water. At room temperature, the thickness of the air-water interface region is about 1.5~2 water molecular diameter

(3×10^{-7} mm), and a surface tension of approximately 75 mN/m, subjected to reduction with increase in temperature, is assumed for the contractile skin (Wang and Fredlund, 2003, Fredlund, 2006). Generally, the tensile water pressure acting inside the concave menisci is believed to be the main inter-particle force which provides stability of flocs in an unsaturated soil matrix. However, experimental investigations by Gallipoli et al. (2003b) and Lourenço et al. (2012) indicated the significant role of the tensile forces exerted by the contractile skin, in bonding the soil particles and generating a cohesive component of strength for unsaturated granular materials, especially where positive water pressure inside the convex menisci cause repulsive forces tending to push the particles away from each other.

2.3.6 State Variables

According to Karube and Kato (1994) and Wheeler and Karube (1995), suction (s) can influence the mechanical behaviour of an unsaturated soil in two different ways. First, suction changes the average fluid (air and water) pressure acting in the soil pores which in turn can modify the average skeleton stress. Second, development of suction in a soil element involves formation of water menisci at inter-particle contacts which provides an additional bonding force at particle contacts. These two mechanisms are directly controlled by the state of saturation of the soil. Degree of saturation (S_r) defines the relative area that the fluid pressures act over. Moreover, the number and the intensity of the attractive normal forces exerted by capillary-induced water menisci at inter-particle contacts are a function of the degree of saturation (Gallipoli et al., 2003a). However, due to the hydraulic hysteresis phenomenon (explained later), two samples of the same soil subjected to the same suction can possess significantly different degrees of saturation, and therefore menisci numbers, depending on their position on either the drying or wetting curves of the water retention curve. This statement further stresses the direct influence of S_r on stress–strain behaviour, in addition of the suction impacts (Wheeler et al., 2003c). Therefore, it appears essential to consider the coupled effects of S_r and s in formulating stress state variables for unsaturated soils.

Initial attempts in the early 1960s led to development of various single-valued effective stress variables for unsaturated soils. An example of such equations is the well-known correlation proposed by Bishop (1959);

$$\sigma'_{ij} = \sigma_{ij} - (1-\chi)u_a\delta_{ij} - \chi u_w\delta_{ij} \quad 2.5$$

where σ'_{ij} is the Bishop effective stress, σ_{ij} is the total stress tensor, δ_{ij} is Kronecker's delta, and χ is the effective stress parameter. In fact, the role of χ in Bishop's effective stress equation is to describe the contribution of suction to the macroscopic stress of the soil skeleton. In other words, the effect of matric suction, which acts at a pore-scale level, is scaled up to macroscopic level using the weighting parameter χ. This parameter depends on S_r and soil structure and varies between 0 (dry soil) and 1 (fully saturated soil). Bishop's proposal combines two stress variables namely net normal stress ($\sigma - u_a$) and matric suction ($u_a - u_w$) into a single-valued effective stress equation and forms the basis of the "single effective stress" approach. Other forms of effective stress variables for unsaturated soils were also proposed by Croney et al. (1958), Jennings (1960), Aitchison (1961), and Richards (1966) among others.

Although Bishop's proposal accounts for the first suction mechanism described above, it was soon found to be insufficient for predicting volume change behaviour of unsaturated soils observed in laboratory experiments. In fact, this type of effective stress definition fails to capture the distinctive fundamental features of unsaturated soils such as swelling and collapse in wetting, and increase in apparent preconsolidation pressure (σ'_p) with increasing suction (Wheeler and Karube, 1995). Similar to saturated soils, an unsaturated soil exhibits swelling during wetting due to increase in bulk water pressure. However, during the wetting process, the removal of additional inter-particle bonding forces exerted by water menisci may result in particle slippage and volumetric compression. This volume reduction upon wetting is known as "collapse in compression" (Jennings and Burland, 1962). Some factors such as confining stress, stress history, and the soil's physico-chemical properties can affect the rate and magnitude of such distinctive volume changes in unsaturated soils (Jennings and Burland, 1962, Matyas and Radhakrishna, 1968). The single effective stress approach is unable to predict these two distinct aspects of an unsaturated soil response and will always predict swelling during wetting. Furthermore, this equation combines the externally applied stresses to the soil element boundary with the suction in pore-water in a single effective stress variable. External stresses exert both normal and tangential forces at particle contacts whereas the meniscus lenses of water at negative pressure only produce normal bonding forces at the inter-particle contacts. Later studies by Li

(2003) showed that as the soil fabric is not isotropic so suction will not be either as the menisci will be forced to follow the contacts. Therefore, combining these qualitatively different stresses into a single-valued effective stress equation results in shortcomings in capturing the essential features of unsaturated soils (Ng and Menzies, 2007). From a microscopic point of view, many researchers such as Skempton (1960), Suklje (1969), Nur and Byerlee (1971), Fredlund and Morgenstern (1977), Jardine et al. (2004), and Nuth and Laloui (2008) also argued the validity of combining two stress variables, i.e. net stress and matric suction, into a single equation.

To overcome the abovementioned problems with the use of effective stress as a unique stress state variable, different approaches have been proposed. Biot (1955) performed oedometer and triaxial tests with varied σ_{ij}, u_a and u_w, and proposed the use of net normal stress and matric suction as two independent stress variables with their separate effects on stress–strain behaviour of unsaturated soils. Net normal stress is described at macroscopic scale, whereas matric suction is described at the pore scale. Other researchers such as Skempton (1960) and Fredlund and Morgenstern (1976) also supported this idea and experimentally showed the applicability of two independent stress variables for unsaturated soils. These state variables were extensively introduced and incorporated in formulation of unsaturated elasto-plastic soil models (e.g. Alonso et al. 1990, Gens and Alonso, 1992) to describe the stress states. However, Wheeler et al. (2003c) stated that as there is no unique relationship between S_r and s due to the hydraulic hysteresis, and that expressing the influence of unsaturated conditions solely through the suction could bring errors in predicting the behaviour of unsaturated soils. To account for the hydraulic hysteresis, Wheeler et al. (2003c) introduced two new stress state variables. The first stress variable is called "Bishop's stress" tensor and is defined as;

$$\sigma_{ij}^{*} = \sigma_{ij} - \left[S_r u_w + (1 - S_r) u_a\right]\delta_{ij} = \sigma_{ij} - u_a \delta_{ij} + S_r s \delta_{ij} \qquad 2.6$$

The second stress variable was referred to as "modified suction" and is defined as;

$$s^{*} = ns \qquad 2.7$$

where n is the porosity. This model was a complete mechanical and water retention model, formed on the basis of two stress state variables. Alonso et al. (2010) challenged the "Bishop's stress" tensor in the Wheeler et al. (2003c) model and showed

experimentally that for many clayey soils, the term $S_r s$ becomes unrealistically large at high suctions, as a relatively significant amount of water is retained within the micro-pores of clays even at high suctions. They proposed a microstructurally based effective stress tensor, given by;

$$\sigma_{ij}^{*} = \sigma_{ij} - u_a \delta_{ij} + S_r^e s \delta_{ij} \qquad 2.8$$

In this stress tensor, S_r^e is the effective degree of saturation, and measures the free water in macro-pores. This parameter ranges from zero in the case of dry macro-pores (water is held within micro-pores only), and 1 when macro-pores are fully saturated.

2.3.7 Soil Water Retention Curve

Mechanical behaviour of unsaturated soils is controlled by the pore-water tension (suction) and the ability of the soil for water retention, the latter being characterised by the soil water retention curve (SWRC), which is defined as the relationship between the water content (or degree of saturation) and suction in soils (Fredlund and Rahardjo, 1993). SWRC depicts a continuous and non-linear relationship between water content and suction in soils during wetting or drying. SWRCs have been presented in the literature by different parameters, i.e. gravimetric water content (w), volumetric water content (θ), or degree of saturation (S_r). The corresponding SWRCs are denoted by SWRC-w, SWRC-θ, and SWRC-S_r respectively. Figure 2.8 presents typical graphs of SWRC-S_r and SWRC-w.

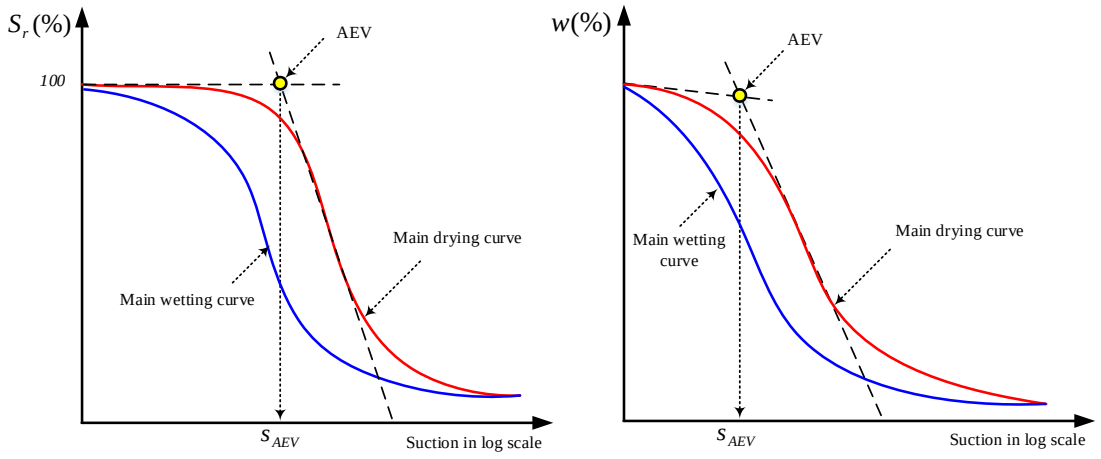
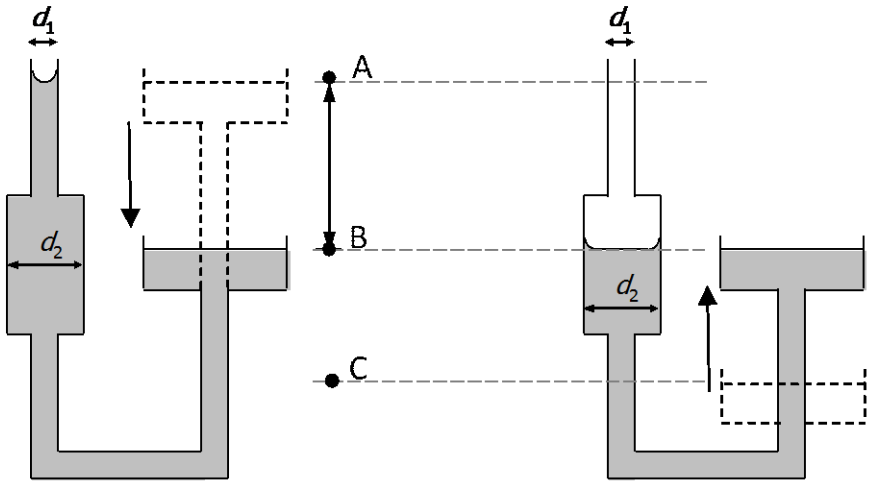


Figure 2.8 Typical water retention curve for non-deformable soils: (a) in S_r – s plane; (b) in w – s plane

Generally, three distinct parts are recognised on a SWRC. Initially, with the soil undergoing drying, the curve remains a relatively flat line until the AEV; during this stage, with increase of suction, the pores remain saturated (S_r = 100%) with pore-water being under tension (saturated state). As suction exceeds the AEV, air breaks into the larger pores and a continuous network of air-filled and water-filled pores is formed. During this stage, the degree of saturation (or water content) is progressively decreased as more water evaporates or leaves the pores (partially saturated state). Finally, with increase in suction, a state is reached where water only remains at the particle contacts and is no longer continuous with the pore space (Laloui, 2010). At this stage, the SWRC almost flattens meaning that much less water will be expelled with increase in suction, and the soil dries without significant volume changes (residual state). In another definition, the first part of the curve until the AEV is named "boundary effect zone", and the portion of the curve between the AEV and the residual state is named "transition effect zone" (Wijaya et al., 2015).

The water retention curve of a soil wetted from the dry state (main wetting curve) follows a different path than the water retention curve obtained by drying from the saturated state (main drying curve). The phenomenon that the water retention curve follows different paths over a drying and wetting cycle is called "hydraulic hysteresis" and can be partially described by the ink-bottle effect. This effect is explained by considering the ink-bottle tube connected to a water reservoir as shown in Figure 2.9. Initially, the capillary tube with diameter d_1 is saturated as it is level with the water in the reservoir (point A). If the water reservoir is lowered to point B, the capillary tube remains saturated because the generated water meniscus at the top of the tube can sustain the exerted suction [Figure 2.9(a)]. Further lowering of the water reservoir to point C, and therefore increasing the applied suction, results in desaturation (depletion) of the capillary tube. At this stage, if the water reservoir is raised back to point B, the capillary tube will not be refilled and will exhibit a different degree of saturation, as this time the capillary rise is controlled by the larger diameter (d_2) tube [Figure 2.9(b)]. Moreover, if from any intermediate state on the drying or wetting curves, the drying or wetting process is reversed, the corresponding $s - S_r$ curve follows a transitional path in the hysteresis domain between the main drying and main wetting curves. These intermediate curves are referred to as scanning curves (Laloui, 2010). Figure 2.10 depicts the different types of scanning curves, known as crossing, converging, and

returning (Tompsett et al., 2005). These curves are further distinguished, according to the direction of the followed paths, as ascending and descending curves.



(a) (b)

Figure 2.9 The ink bottle effect: (a) capillary drainage; (b) capillary rise (after Laloui, 2010).

As discussed in the "Capillarity" section, the size of the pore voids governs the required energy (suction) for flooding or emptying the pores. Therefore, a change in pore size can cause shifting of the main wetting and drying curves (Wheeler et al., 2003c). Because pore size generally reduces with particle size, there is a close relationship between the particle size distribution and the water retention curve of an unsaturated soil. The water retention properties of different soils are varied and strongly depend on the type of soil (Fredlund and Xing, 1994). Other factors such as soil mineralogy (Williams et al., 1983), soil structure (Vanapalli et al., 1999), stress state (Ng and Pang, 2000b), stress history (Vanapalli et al., 1999), initial dry density (Ng and Pang, 2000a), drying-wetting cycles (Sharma and Wheeler, 2000), and temperature (Villar and Gómez-Espina, 2008) can also affect the water retention characteristics of soils. The effect of temperature on water retention has been shown to be small and mainly associated with the thermal expansion of entrapped air, as well as the temperature-dependency of the interfacial tension and wetting coefficient (Grant and Salehzade, 1996, She and Sleep, 1998, Romero et al., 2003).

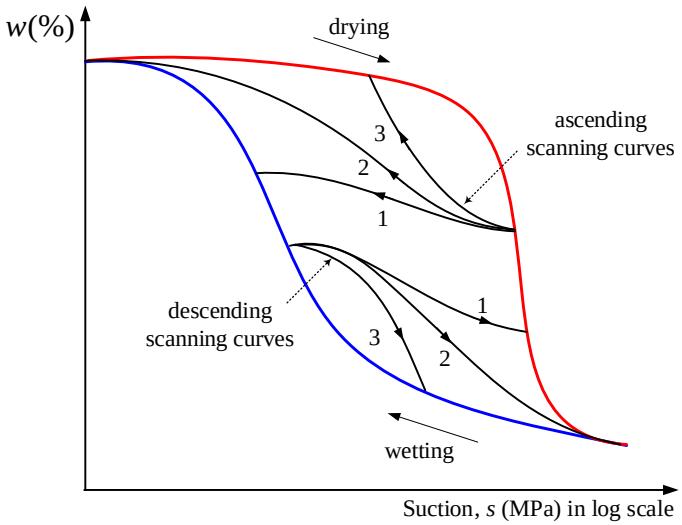


Figure 2.10 Scanning curves from the main drying and wetting curves; 1- crossing, 2- converging, 3- returning (after Tompsett et al., 2005)

The SWRC has proven to be of significant value in engineering practice and has been used for estimation of permeability (Fredlund et al., 1994), hydraulic conductivity (Singh and Kuriyan, 2003), or shear strength (Fredlund et al., 1995, Vanapalli et al., 1996, Lu and Griffiths, 2004) of unsaturated soils. For example, Vanapalli et al. (1996) proposed a semi-empirical non-linear function for prediction of shear strength in terms of matric suction using the SWRC and saturated shear strength parameters. However, it was later shown by Gallipoli et al. (2003b) that although such approaches may result in prediction of some values for the shear strength, the precision and reliability of the obtained results may not be fully guaranteed because of the significant influence of the void ratio on the SWRC which may result in different values of shear strength for different initial void ratios. Nevertheless, the majority of the proposed approaches for interpretation of unsaturated soil parameters from SWRC data are based on simplifying assumptions such as soil non-deformability and stress-history independency of SWRC (Pasha et al., 2016). This can result in misinterpretation and erroneous extraction of soil parameters from the experimental SWRCs, especially in case of fine-grained soils that typically have fabric-related properties and undergo significant volume changes with suction (Fredlund and Houston, 2013).

One of the most important parameters which has been extensively used in deriving unsaturated constitutive models is the AEV (van Genuchten, 1980, Fredlund and Xing, 1994, Ng and Pang, 2000b, Russell and Khalili, 2006, Salimzadeh and Khalili, 2014).

On a SWRC-S_r, the AEV is graphically determined as the intersection point of a horizontal tangent line drawn to the saturated portion, with a tangent line drawn to the transition portion of the curve. Pasha et al. (2016) showed that using the same method to derive AEV from SWRC-w and SWRC-θ curves, can produce highly erroneous results. They proposed a simple method for estimation of AEV from SWRC-w data of deformable soils. This method was based on plotting the SWRC-w data on both semi-log and log–log scales on the same graph. In this way, the saturated part of the curve is identified by a linear or bilinear behaviour in a semi-log plot, and the unsaturated part of the curve is represented by a straight line (linear behaviour) on the log–log plot (Figure 2.11). Therefore, by drawing these two complementary curves on a single graph, the AEV as the boundary between saturated and transition (unsaturated) zones can be readily identified. This graphical technique can be used for evaluation of AEV from SWRC data where the information on the volume change of the sample during testing is not available.

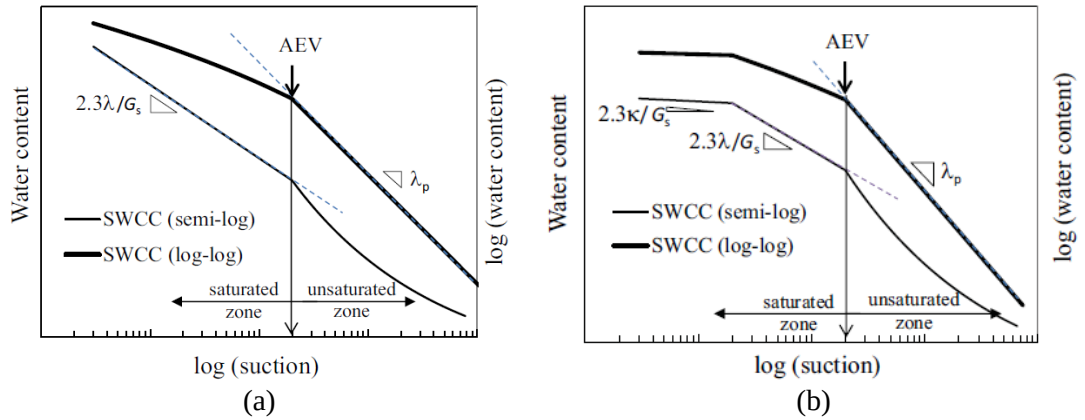


Figure 2.11 Schematic SWRC-w with λ/λ_p different from $G_s w_{AEV}$ along with the proposed graphical method to obtain parameters: (a) NC soils; (b) OC soils with $\sigma'_p < s_{AEV}$ (Pasha et al., 2016).

The experimental methods for development of SWRCs are diverse and in most cases produce discontinuous measurements, bringing difficulties in accurate determination of the AEV. For such measurements, the method proposed by Pasha et al. (2016) appears promising. However, as will be discussed in Chapter 4, direct measurement of soil suction changes using tensiometers can rectify the need for such approximation methods, as an accurate estimation of AEV can be readily obtained from continuous measurements of suction variations with water content.

2.3.8 Suction Measurement and Control Techniques

Various experimental methods are available for measurement of soil suction in the range 0 – 1000 MPa. These methods are typically classified into two groups; methods for suction measurement less than 1.5 MPa, and methods for suction measurement above 1.5 MPa (Fredlund, 2006). At suctions above 1.5 MPa, the matric and total suction can be assumed to be equivalent (Fredlund and Xing, 1994). Lower suction values are usually measured using axis translation, pressure plate, tensiometer, and filter paper methods, whereas high suction values are measured using filter paper, osmotic desiccator, psychrometer, relative humidity, and chilled-mirror hygrometer techniques. Except tensiometers, all other techniques provide indirect measurement of soil suction. Table 2.1 summarises the features of some of these techniques as reported in the literature.

Table 2.1 Methods of suction measurement and/or control

Method	Application		Suction		Range (MPa)	Approximate Equilibrium Time
	Measurement	Control	Total	Matric		
Thermal conductivity sensor [a]	*			*	0-1.5	hours to days
Electrical conductivity sensor [a]	*			*	0.05-1.5	6-50 hours
Time domain reflectometry[b]	*			*	0-1.5	hours
Osmotic desiccator[c]	*	*		*	1-10	hours to days
Tensiometer[d]	*			*	0-2.0	10 minutes
Axis translation[b]	*	*		*	0-1.5	hours to days
Pressure plate[e]	*			*	0-1.5	hours to days
Filter paper (in-contact) [a]	*			*	0.05-30	5-14 days
Filter paper (non-contact) [a]	*		*		0.05-30	5-14 days
Transistor psychrometer [a]	*		*		0.1-10	1 hour
Thermocouple psychrometer[a]	*		*		0.3-7.0	1 hour
Chilled-mirror hygrometer[a]	*		*		0.5-30	10 minutes
Relative humidity[b]	*	*	*		0.1-1000	hours to days

[a]: Bulut and Leong (2008) [b]: Pan et al. (2010) [c]: Delage and Cui (2008) [d]: Marinho et al. (2008)
[e]: Fredlund (2000)

As will be discussed in Chapter 4, for the experimental program of this study tensiometers were used for monitoring suction evolution in soil specimens. Therefore, in this section, the basic principles of axis-translation and thermal conductivity sensors (TCS), which have similar accuracy and *in-situ* application to tensiometers, are briefly explained. A detailed discussion of the tensiometer technique is provided in Chapter 4 where, after a synthesis of recent research on tensiometers, the design and application of a new tensiometer is presented.

2.3.8.1 Axis-Translation

The axis-translation technique is based on the principle of capillary rise. When a capillary pore is subjected to atmospheric air pressure ($u_{a0} = 0$) the water at the back of air-water interface has a pressure less than atmospheric pressure ($u_{w0} < 0$). In this situation, if the capillary tube is close-ended and air pressure is elevated artificially ($u_{a1} > 0$), the curvature of the air-water interface is not significantly changed and therefore the matric suction ($u_a - u_w$) remains almost constant. This results in a rise of water pressure within the capillary tube from negative to positive gauge pressures ($u_{w1} > 0$) if u_{a1} is large enough. This upward translation of the water pressure from the negative meta-stable states to easily measureable positive pressures is referred to as the "axis-translation" technique (Figure 2.12).

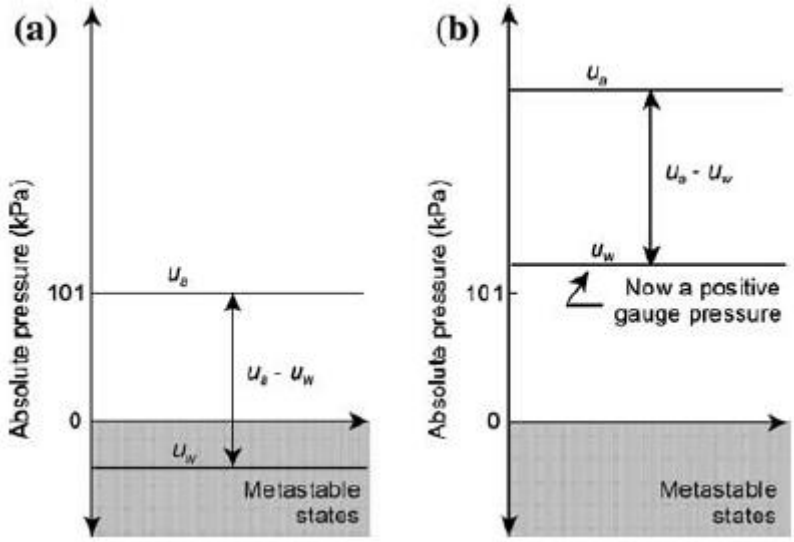


Figure 2.12 Axis-translation technique: (a) atmospheric conditions; (b) axis-translation (Marinho et al., 2008)

The axis-translation technique can be used to control suction in soils. To this end, it is required to control the pore-water pressure by allowing drainage of water through a saturated porous filter (commonly a ceramic disk) placed at the bottom of the soil sample until reaching the equilibrium state. In this case, adequate saturation of the porous ceramic disk is the most important factor determining the success or failure in application of the axis-translation technique. The range of suctions that can be applied by the axis-translation technique is a function of the AEV of the ceramic filter as well as the maximum capacity of the air supply system. Moreover, lack of good contact

between the pore-water and the water in the ceramic disk results in discontinuity of water flow through the porous filter and may dramatically increase the equilibrium time or even prohibit the drainage of water (Marinho et al., 2008).

The axis-translation technique has been widely used in various laboratory apparatuses such as oedometer (Alonso et al., 1995), shear box (Tse and Ng, 2008), and triaxial cell (Wheeler and Sivakumar, 1995, Ng et al., 2009). However, this technique has been shown to involve some limitations. For instance, in suction-controlled triaxial tests using the axis-translation technique, simultaneous application of high suction and high net stress is rather difficult when testing clays and silty clays (Tarantino and Mongiovi, 2003). Furthermore, when using the axis-translation technique, control of soil-moisture evaporation can be difficult (Tarantino and Mongiovi, 2003). Boso et al. (2004) measured the SWRC of a reconstituted silty clay using both axis-translation and high-capacity tensiometer (HCT) techniques, and observed lower water content at suctions above 100 kPa in the axis-translation method in comparison with the HCT method. This small difference was explained to be associated with water evaporation from the top of the sample when using the axis-translation method to control/measure suction.

2.3.8.2 Thermal Conductivity Sensors

A thermal conductivity sensor (TCS) is a device for laboratory and *in-situ* measurement of high negative water pressures. A TCS consists of a small heater embedded in a durable porous ceramic block. When the sensor with initially wet or dry ceramic block is placed in contact with an unsaturated soil, a water flux will occur until an equilibrium in matric suction between the soil and the ceramic block is reached. Change in the moisture content of the block results in change in its thermal conductivity which is quantified by heating the block using the embedded heater and measuring the temperature rise during heating. The measured temperature gradients which are associated with the thermal conductivity of the ceramic and the moisture content are then calibrated against known values of matric suction (Fredlund, 2000). Thermal conductivity sensors have received significant interest in laboratory and *in-situ* suction measurements thanks to their ability for continuous and remote measurement of suctions as high as 1.0 MPa over a long period of time. However, thermal conductivity sensors have been shown to exhibit hysteresis behaviour on drying and wetting cycles (Fredlund, 2000). Some factors such as the temperature gradient and the hydraulic

conductivity of the ceramic block and that of the surrounding soil can also affect their equilibrium time (Hu et al., 2010). Figure 2.13 presents a schematic view of a TCS.

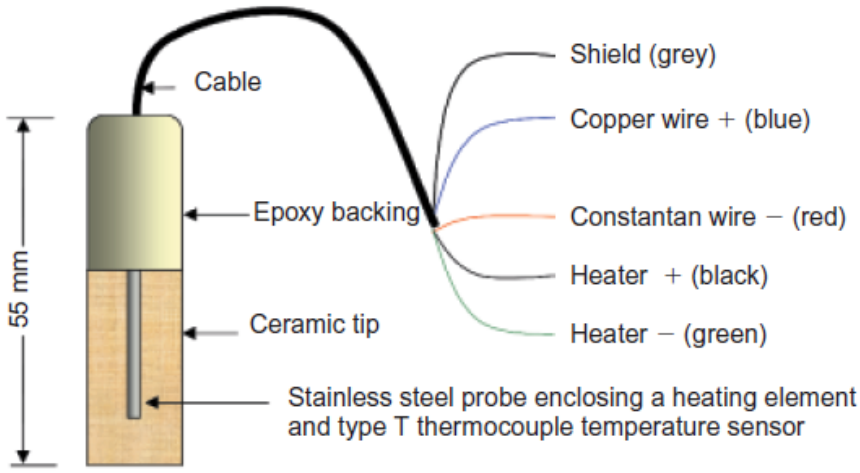


Figure 2.13 Schematic diagram of a thermal conductivity sensor (Leong et al., 2012)

2.4 Primary and Secondary Consolidation in Saturated vs. Unsaturated Clays

In conventional soil mechanics, the mechanism of soil settlement is divided into stress-dependent and time-dependent settlements with the former being a consequence of change in a soil's effective stresses as a result of excess pore-water pressure (u_{exc}) dissipation under applied stress and drained conditions, and the latter being as a result of particle rearrangements under constant applied loads and effective stress with the presence or absence of water having only minor impact (Mitchell, 1993). In other words, the compression and settlement of a soil layer subjected to applied stress is characterised by two successive phases, namely a primary consolidation phase and a secondary consolidation phase. The deformations during the primary consolidation phase involve both stress-dependent and time-dependent (creep) deformations, whereas the secondary consolidation phase is characterised by only creep deformations. In this section, the concepts of primary and secondary consolidation (creep) in clays, both in saturated and unsaturated conditions, are discussed comparatively.

2.4.1 Primary Consolidation in Saturated Clays

The consolidation behaviour of clays is conventionally studied through comparison of compression curves obtained from incremental loading (IL) oedometer tests on

undisturbed and corresponding reconstituted specimens. In contrast to the reconstituted clays which exhibit constant compressibility in the virgin compression range, the compressibility of natural structured clays has been shown to be strain-dependent (Graham et al., 1983). This specific compression characteristic stems from the gradual degradation of inter-particle bonds during plastic straining, a phenomenon known as "destructuration" (Leroueil and Vaughan, 1990). Intact specimens exhibit compression curves which typically lie above the intrinsic compression lines (ICL) induced from testing reconstituted or remoulded specimens. Figure 2.14 schematically illustrates typical compressive behaviour of natural and reconstituted soft clays in an $e - log\ \sigma'_v$ plot. Compression of a natural soft clay involves an elastic response up until the preconsolidation pressure (σ'_p) and follows the reloading compression path with gradient C_r known as the reloading index. At stresses exceeding σ'_p, inter-particle bonds are progressively lost and the soil structure starts to collapse resulting in significant plastic straining and a steep slope (C_c) of the normal compression line (NCL). The slope of the NCL eventually converges with the ICL at high stress levels. The compression characteristic of the natural clay in this region is similar to that of reconstituted clay. Unloading the specimen at this state results in swelling and recovery of some strains. The swelling line exhibits a gradient (C_s) typically of equal value to the reloading index. However, highly structured clays may exhibit steeper slopes in unloading than reloading mainly due to the destructuration of the inter-particle bonds (Mataic, 2016).

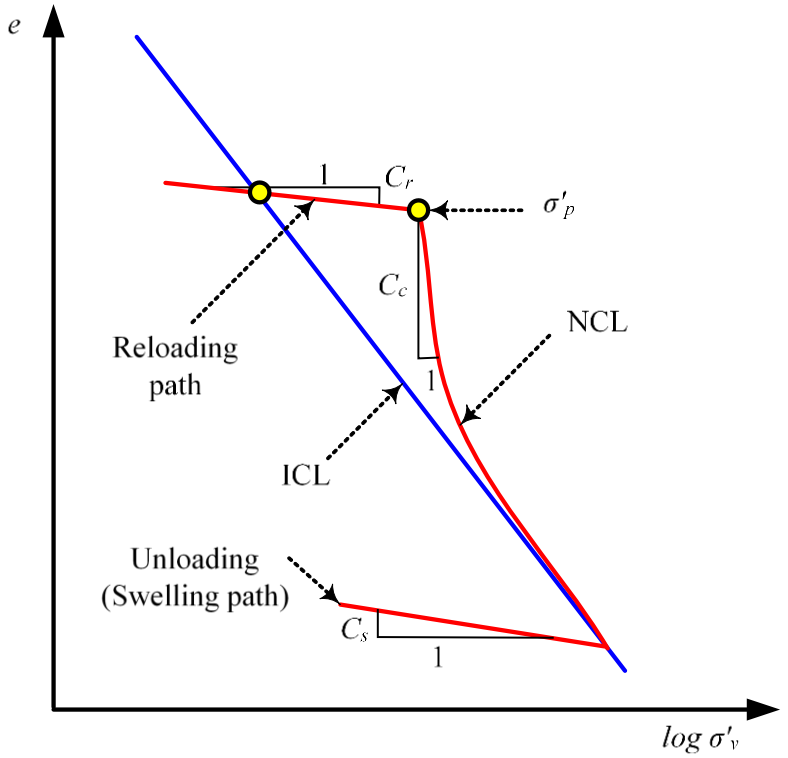


Figure 2.14 Schematic compression curve for natural soft clays (after Mataic, 2016)

Inter-particle bonding (structuration) is not only a feature of undisturbed natural clays. Reconstituted clays may also exhibit some level of structuration if subjected to long-term consolidation. Leroueil et al. (1996) studied the effect of structuration on the oedometric compression of artificially sedimented clay samples and observed a significant increase in σ'_p (from 10 kPa to 18.5 kPa) after 120 days consolidation of samples under 10 kPa applied vertical effective stress. The authors attributed this observation to the development of inter-particle bonds (structuration) during sedimentation.

In a recent investigation of compression characteristics of undisturbed and corresponding reconstituted clays, Sun et al. (2014) explicitly showed the effect of soil structure on the compression behaviour of seven marine clays from the Yangtze River Delta, China (Figure 2.15). The results show that at a consolidation pressure higher than the structural yield stress, most bonding structures will be destroyed, and that fabric anisotropy is solely responsible for the differences observed in compression characteristics of undisturbed and reconstituted clay samples. As shown in Figure 2.15(a), for pressures higher than σ'_p, the compression behaviours of the reconstituted samples are identical and can be expressed as a unique ICL in I_v – log σ'_v plane, where

I_v is an index proposed by Burland (1990) for normalisation of the compression curves for reconstituted clays, and it can be determined as;

$$I_V = \frac{e - e^*_{100}}{e^*_{100} - e^*_{1000}} = \frac{e - e^*_{100}}{C^*_c} \qquad 2.9$$

where e^*_{100} and e^*_{1000} are the void ratios corresponding to σ'_v = 100 kPa and σ'_v = 1000 kPa respectively.

Different compression responses of the undisturbed samples due to their distinct microstructures are shown in Figure 2.15(b). The authors, according to Burland et al. (1996), ascribed the consolidation behaviour of samples with yielding lying between the ICL and the sedimentary compression line (SCL), to the natural micro-fabric and inter-particle bonding phenomena, and those which lay above the SCL to the brittle bonded microstructure.

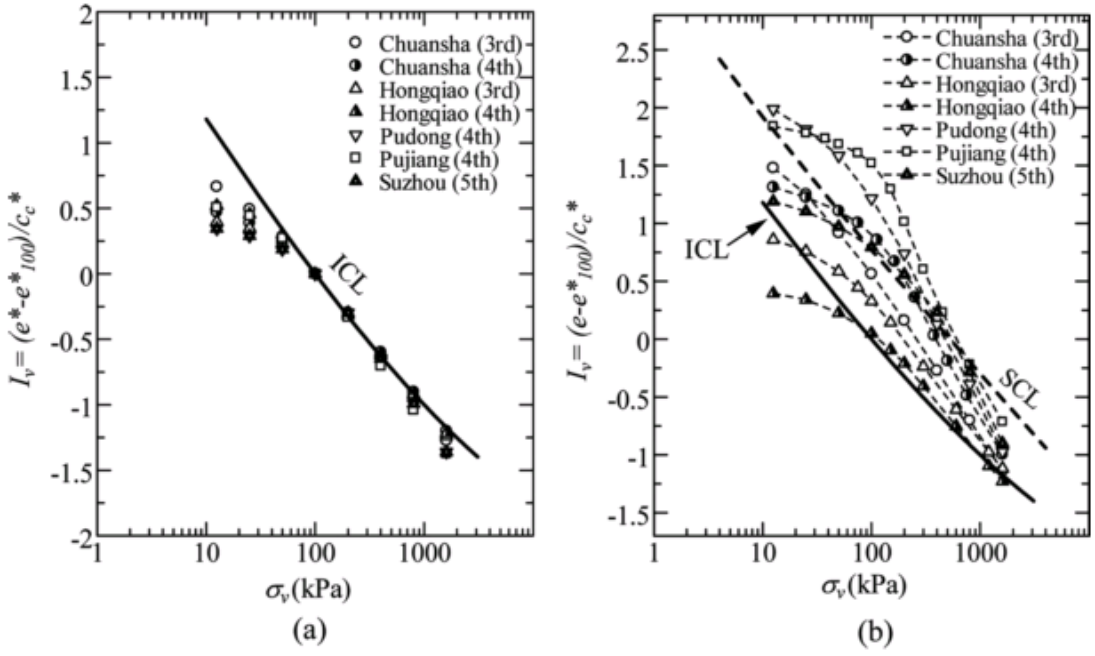


Figure 2.15 Normalised compression curves for Yangtze River Delta clays: (a) reconstituted samples; (b) undisturbed samples (Sun et al., 2014)

The micro-fabric also plays a significant role in compression behaviour of natural clays. From the same preconsolidation pressure, a mass of clay with a flocculated particle arrangement undergoes more relative particle movements than the same clay mass with a dispersed particle arrangement if subjected to the same stress increment (Le et al.,

2012). This is mainly due to the greater orientation of the parallel arranged particles in the dispersed state than the randomly arranged particles in the flocculated state and also the tendency of the randomly arranged clay particles for rearrangement to a parallel state. Pillai et al. (2012) showed that the time required for consolidation of dispersed kaolinite specimens was higher than that of flocculated samples. Moreover, the flocculated specimen exhibited higher creep deformations than the dispersed specimen, further highlighting the effect of micro-fabric in control of volume change in clays (see Figure 2.16).

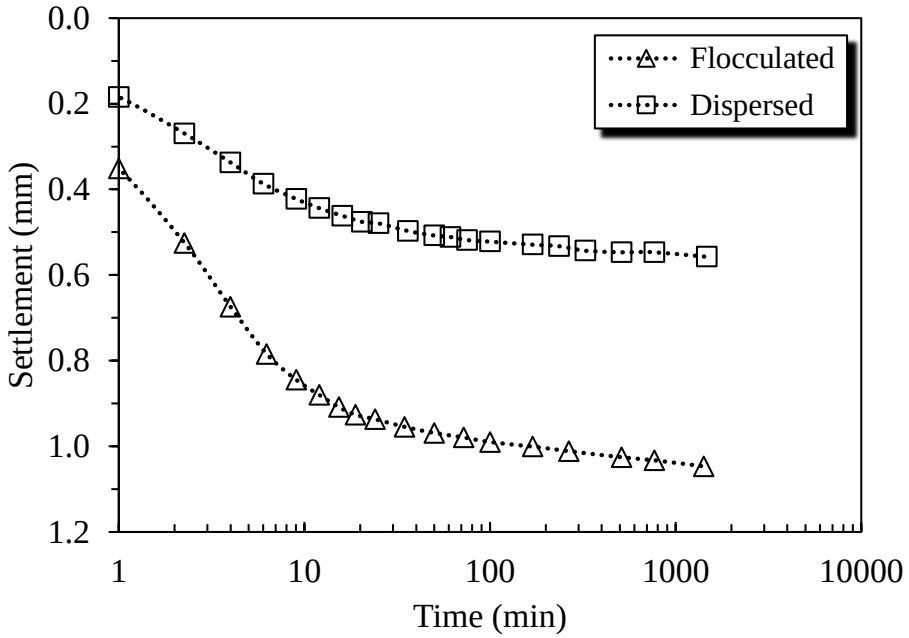


Figure 2.16 Time-settlement graphs for flocculated and dispersed kaolinite samples subjected to 1D consolidation tests under a pressure range of 10–20 kPa (re-drawn from Pillai et al., 2012)

A schematic diagram of the 1D compression and swelling curves of overconsolidated stiff clays, such as London Clay, in their natural and corresponding reconstituted states, is shown in Figure 2.17 (Stallebrass et al., 2007). In contrast to soft clays, as discussed above, overconsolidated stiff clays, do not exhibit a steep slope (λ) of the NCL following a peak preconsolidation pressure. Instead, the transition from reloading state to virgin compression state is smooth and unbroken.

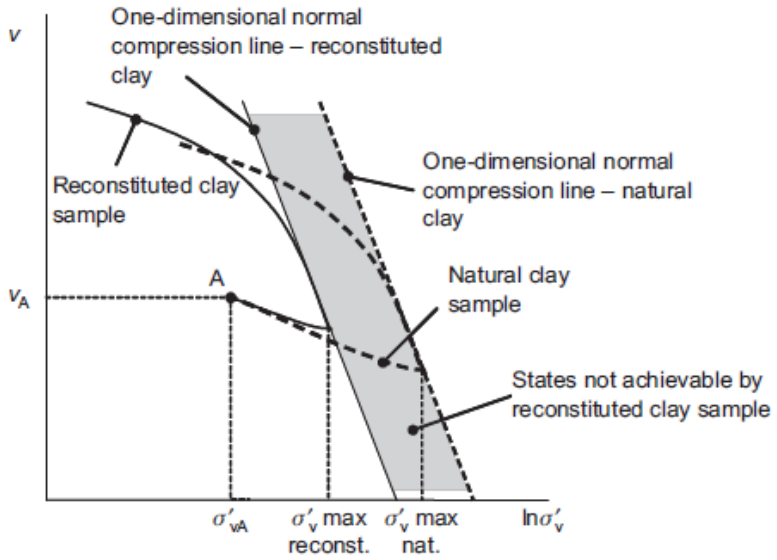
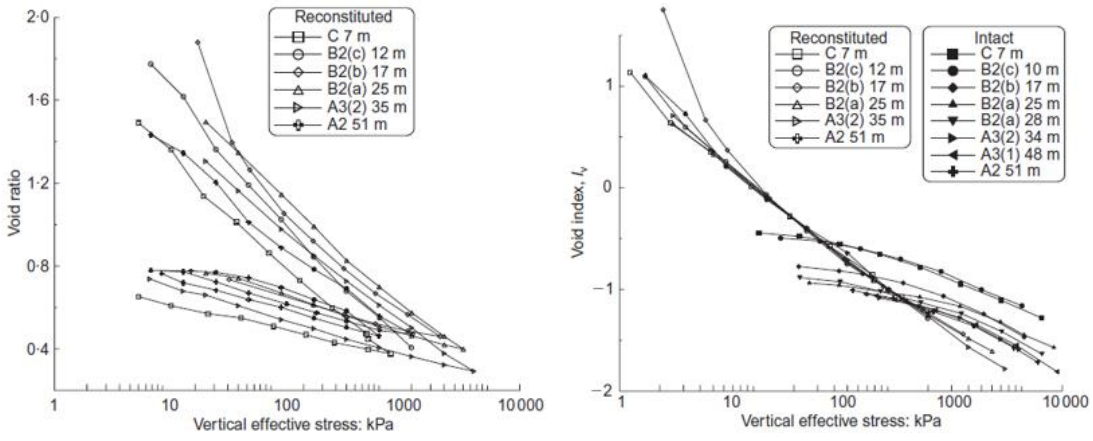


Figure 2.17 Schematic compression curves for natural and reconstituted overconsolidated stiff clays (Stallebrass et al., 2007)

Figure 2.18 presents the results of a series of oedometer tests, carried out by Gasparre et al. (2007), on intact and reconstituted London Clay samples from different lithological units at the Heathrow Terminal 5 site (T5). The authors reported that the intrinsic compression and swelling lines (ICL and ISL) for higher plasticity samples (Unit B2) lie above those of lower plasticity samples (Units A3 and A2).



(a) (b)

Figure 2.18 Oedometer test results on intact and reconstituted London Clay from T5: (a) in terms of void ratio; (b) in terms of void index [Gasparre et al. (2007) in Hight et al., (2007)]

The expansibility of London Clay at T5 was studied by Hight et al. (2003) from oedometer swelling tests on rotary core samples [Figure 2.19(a)]. As it can be seen, the swelling of London Clay at T5 increases significantly at effective stresses below 50-100 kPa. Based on the obtained water content profile [Figure 2.19(b)], the significant

swelling (increase in water content) is restricted to the upper 3.5 m of the clay layer where the vertical effective stresses are less than 50 kPa.

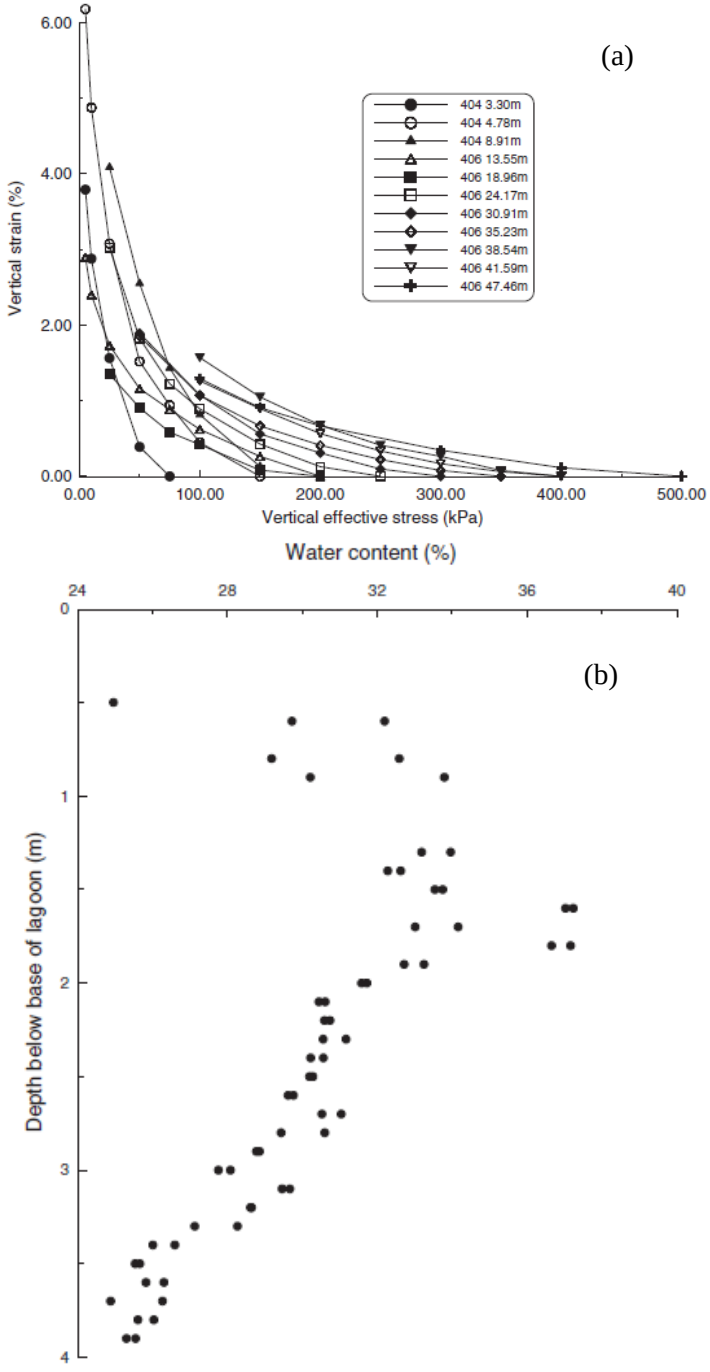


Figure 2.19 (a) Expansibility of London Clay at T5 from oedometer swelling tests; (b) water content profile (Hight et al., 2003)

Table 2.2 presents the relevant correlations used for determination of the compression indices from e – log σ'_v and e – ln p' plots.

Table 2.2 Correlations for determination of compression indices

Plot → / Index ↓	$e - \log \sigma'_v$	$e - \ln p'$
Compression index	$C_c = \frac{\Delta e}{\Delta \log(\sigma'_v)}$	$\lambda = \frac{C_c}{\ln 10} = \frac{\Delta e}{\Delta \ln \sigma'_v}$
Reloading index	$C_r = \frac{\Delta e}{\Delta \log(\sigma'_v)}$	$\kappa_0 = \frac{C_r}{\ln 10} = \frac{\Delta e}{\Delta \ln \sigma'_v}$
Unloading (swelling) index	$C_s = \frac{\Delta e}{\Delta \log(\sigma'_v)}$	$\kappa = \frac{C_s}{\ln 10} = \frac{\Delta e}{\Delta \ln \sigma'_v}$
Intrinsic compression index		$\lambda_i = \frac{\Delta e}{\Delta \ln \sigma'_v}$

2.4.2 Primary Consolidation in Unsaturated Clays

Primary consolidation in unsaturated clays is relatively more complex than in saturated clays. Increase in suction results in an increase in σ'_p, a phenomenon known as suction hardening (Wheeler and Sivakumar, 1995). Suction also influences the slope of the constant suction NCL in the e – log σ'_v plane. A group of researchers e.g. Alonso et al. (1990), Li et al. (2006), and Li et al. (2009), have experimentally shown, for a wide range of geo-materials, that the slope of the constant suction NCL decreases with increase in suction. This is while another group of researchers e.g. Toll (1990), Sivakumar (1993), Wheeler and Sivakumar (1995), Sivakumar and Wheeler (2000), Toll and Ong (2003), and Estabragh and Javadi (2008), showed that the slope of the constant suction NCL increases with increase in suction to reach a peak value then decreases. This second group justify the increase in compressibility with increase in suction by development of highly compressible macro-pores in the soil during drying. Subjecting specimens to mechanical unloading results in an elastic swelling, with the gradient of swelling lines being almost independent of suction level (Sivakumar, 1993). Suction also influences the location and shape of the NCL (Monroy et al., 2008). Figure 2.20(a) presents the results of compression tests carried out on compacted London Clay in an osmotic oedometer equipped with a HCT to monitor change in suction throughout the tests (Monroy et al., 2008). The specimens were prepared by static compaction to an initial suction of 1000 kPa, then hydrated to different equilibrium suctions (zero, 120, and 405 kPa) in free-swell tests under a constant nominal load, followed by a loading–unloading cycle at constant suction. The C_c and C_s indices were found to increase and decrease respectively with increase in suction [Figure 2.20(b)].

Benatti et al. (2010) studied the effect of suction on 1D compressibility of a collapsible silty clay from Brazil. The results obtained are shown in Figure 2.21. An increase in σ'_p with increase in suction was observed. However, for this type of soil, the values of C_c and C_s indices remained unchanged with change in suction level. The shape of the compression curve was also not affected by the change in suction. This unique response might be ascribed to the structural properties of the tested soil having high porosity of 68% and a very low AEV of only 1 kPa.

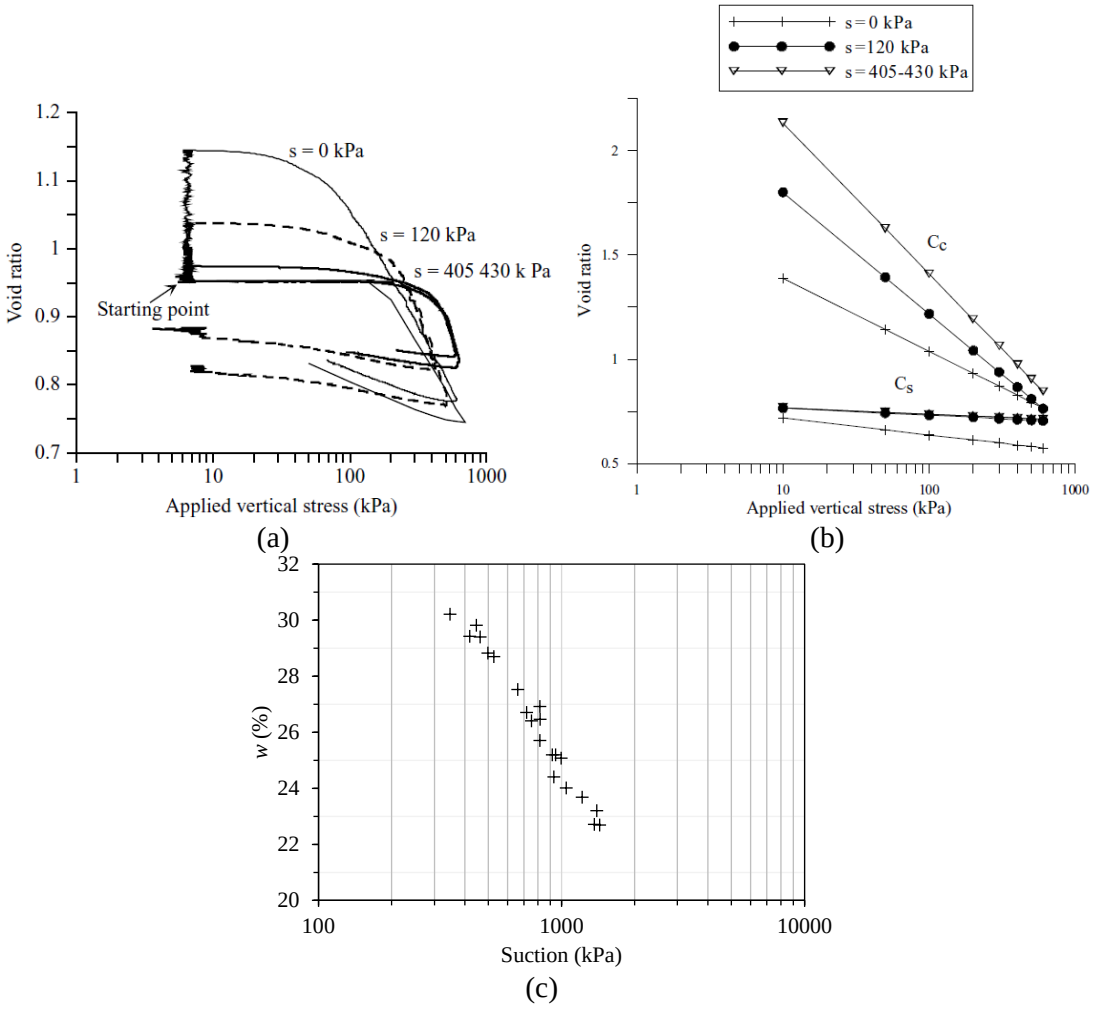


Figure 2.20 Oedometer tests on unsaturated compacted London Clay: (a) compression curves at different suctions (Monroy et al., 2008); (b) normal compression and swelling indices (Monroy et al., 2008); (c) soil water retention curve (re-drawn after Monroy, 2005)

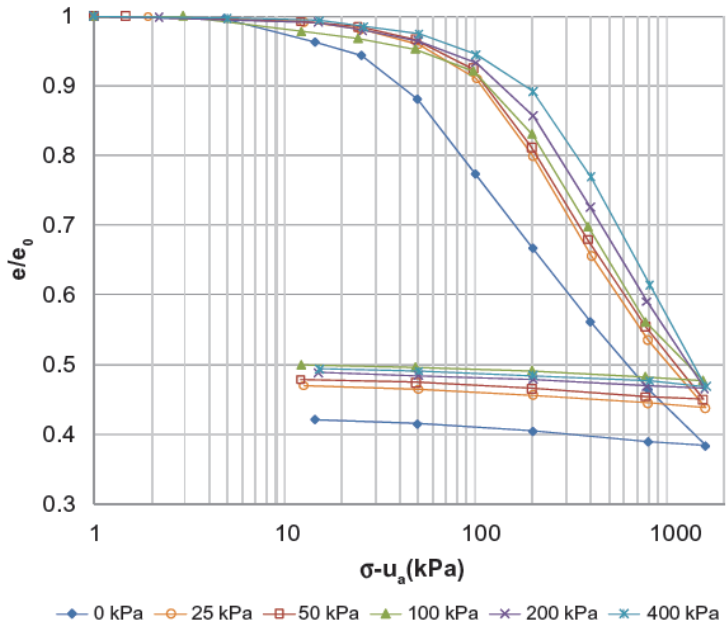


Figure 2.21 Compression curves from oedometer tests with controlled suction on a high porosity silty clay (Benatti et al., 2010)

Haghighi (2011) performed suction-controlled oedometer tests on kaolin clay at two different temperatures (Figure 2.22). An increase in σ'_p was reported with increase in suction. The C_c index appeared to be unaffected by change of suction form 100 kPa to 300 kPa, however, with increase of suction to 500 kPa, the slope of virgin compression line is slightly decreased.

From these and other sets of information on the compression characteristics of the stiff London Clay, a high porosity silty clay, and kaolin clay, one may conclude that the response of unsaturated clays during primary consolidation is not solely governed by the state of the suction, and that, it is in fact the combination of multiple factors such as soil fabric, inter-particle bonding, pore-size distribution, and suction that determines the response of an unsaturated clayey soil.

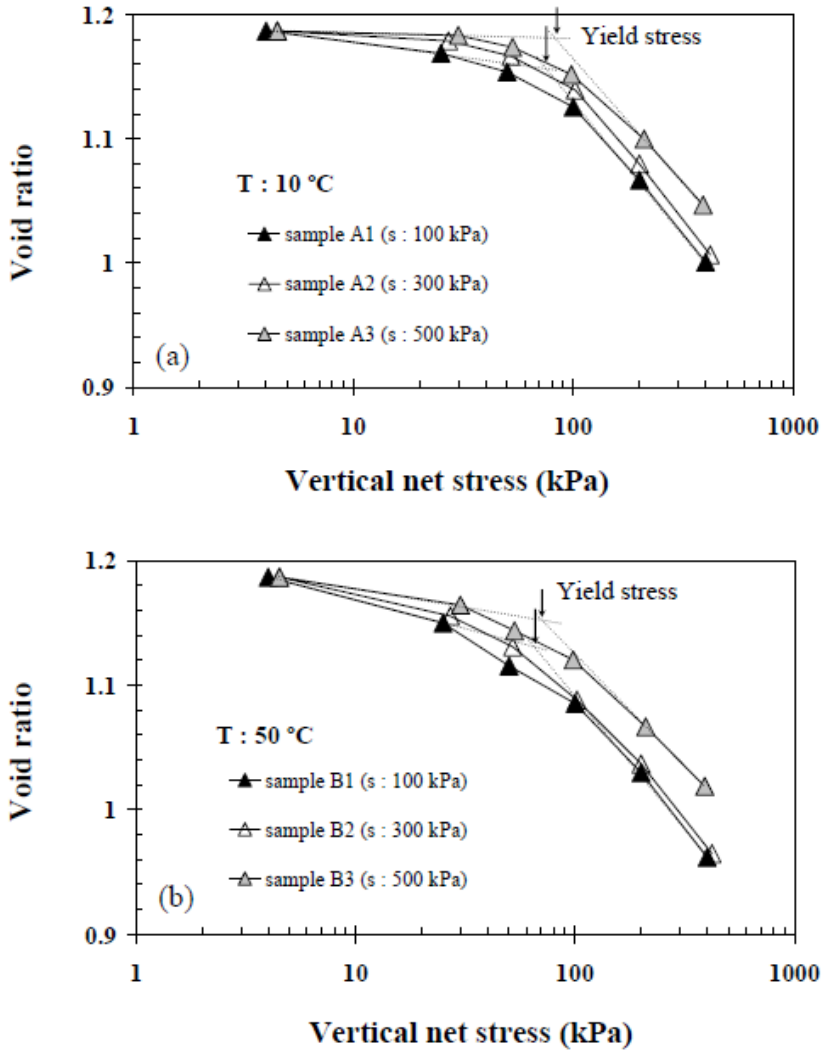


Figure 2.22 Compression curves from oedometer tests on kaolin clay with controlled suction and temperature (Haghighi, 2011)

2.4.3 Secondary Consolidation in Saturated Soft Soils

Craig (2004) defined the secondary compression of clayey soils as the gradual readjustment of the clay particles into a more stable configuration under an approximately constant effective stress state. This time-dependent process is thought to be independent of the pore-water influences. However, looking into the mechanism of creep in micro scale, one can find that it is the flow of the very thin layer of adsorbed water over the clay particles that causes movement of solid particles and their rearrangement into a more packed state. The decreasing rate of secondary compression with time, observed in laboratory experiments (e.g. Leroueil et al., 1985, Yin, 1999), is attributed to the increase in viscosity of the adsorbed water during progressive particles packing and reduction in void ratio (Craig, 2004). Increases in plasticity, water content,

and stress level, are generally known to decrease the viscous resistance of the soil structure (Sorensen, 2006).

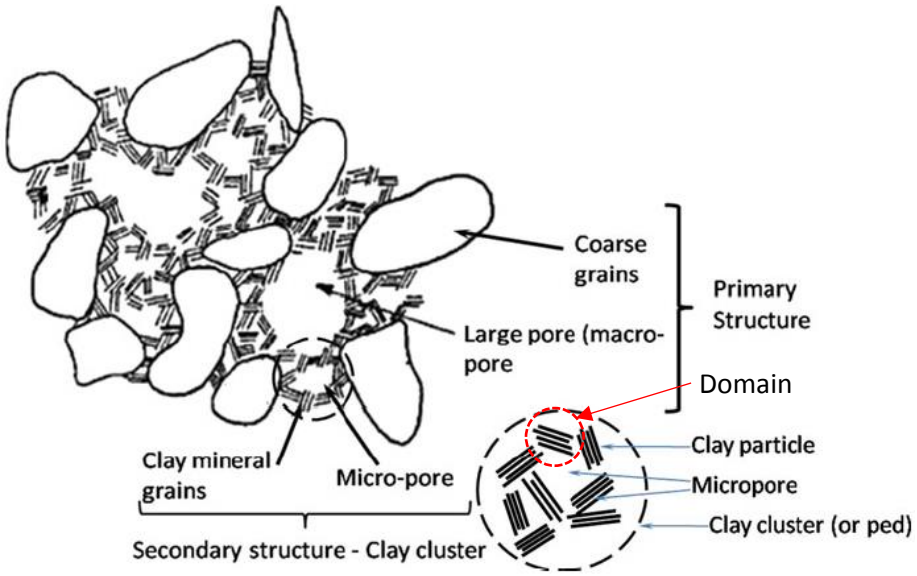


Figure 2.23 Schematic view of the structure of a clayey soil (after Le et al., 2012)

The mechanism of creep in clays can be better explained by considering interactions at micro scale. Figure 2.23 illustrates the schematic structure of a clayey soil. Microscopic observations of clay micro-fabric reveal the presence of clusters or aggregates of low internal porosity, with intra-aggregate (intra-cluster) pore sizes smaller than 10–100 nm (Navarro and Alonso, 2001). Here, in order to distinguish between coarse-grained aggregates and clay clusters, the term "aggregate", used by Navarro and Alonso (2001), is replaced with "floc" (a clumped mass of fine particles). Water is present in the intra-floc pores in the forms of free or adsorbed water, with reduced mobility due to the size of the pores and the electro-physio-chemical interactions with negatively charged clay particles. Navarro and Alonso (2001) used the term "microstructural water" for the combination of free and adsorbed water in intra-floc pores. They presented a microstructural-based model, in which, the secondary deformations were associated with the flow of microstructural water to the bulk (or macrostructural) water occupying the larger inter-floc pores, as a result of micro and macro water potential unbalance. The model also assumed equal densities for micro and macro water. Unlike microstructure water, the macrostructure water is able to move under external gradients, and hence, is responsible for the primary deformations. Flow of microstructure water, assumed to be attached to the clay particles, results in change in micro-porosity and rearrangement of the clay particles. Particle rearrangement, in turn, affects the

tortuosity and porosity which can potentially change the permeability of the floc (Mitchell, 1993). Tortuosity (τ) is defined as the effective hydraulic flow path (L_e) over a unit length (L) of a medium ($\tau = L_e/L$). Different particle arrangement and tortuosity can also result in different permeability values at the same void ratio (Yu and Li, 2004). Figure 2.24 shows the flow path through intra-particle pores for different particle arrangements. Orientation of particles perpendicular to the direction of the applied load restrains the fluid flow and therefore lowers the permeability. Moreover, it is known that the adsorbed water is structurally different from the free water and has different thermodynamic properties (Hueckel, 1992). Therefore, reduction in micro void ratio, can lead to an increase in the viscosity of the micro water, which can further decrease the floc's permeability and restrict the flow of microstructural water towards the bulk water.

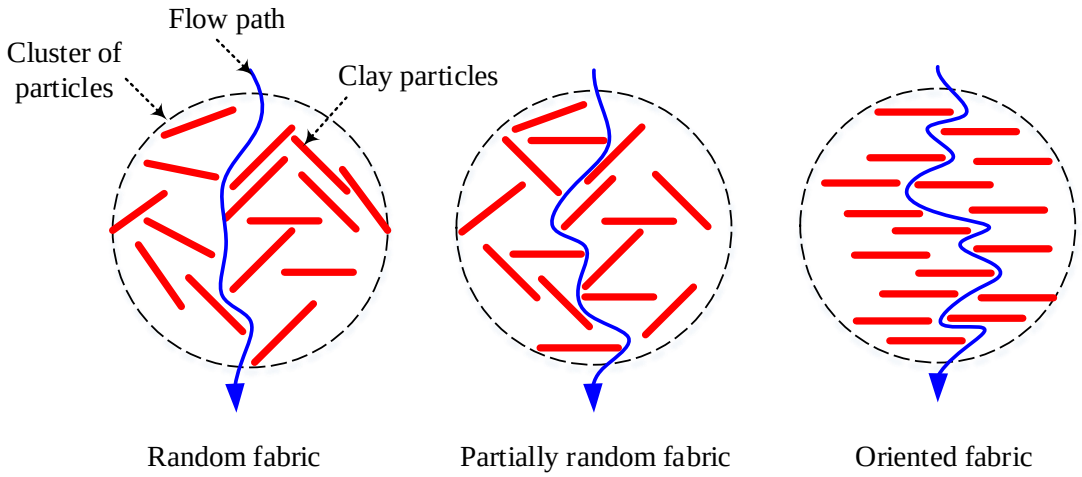


Figure 2.24 Flow path through intra-particle pores for different particle arrangements (after Bayesteh and Mirghasemi, 2015)

The interaction of micro water and clay particles also plays a crucial role in controlling the delayed deformations. The micro water contributes positively in bringing the particles into a more packed state, by decreasing the frictional forces at particle contacts. In contrast, when the negatively-charged plate-shaped clay particles approach each other very closely, the overlap of the electron clouds around particles results in development of strong repulsive forces which can influence the orientation of the particles. Interaction of the clay particles with pore-fluid and development of local electrical fields, can also exert attractive van der Waals forces (Bayesteh and

Mirghasemi, 2015). A comprehensive review of creep mechanisms was performed by Le et al. (2012), and the results are shown in Table 2.3.

Table 2.3 Mechanisms of creep (Le et al., 2012)

Author	Mechanism	Main Factors
Taylor & Merchant (1940), Terzaghi (1941), Gibson & Lo (1961), Mesri (1973, 2001), Mesri & Godlewski (1977), Crooks et al. (1984).	Breakdown of inter-particle bonds	Relative movement of particles, soil structure rearrangement.
Murayama & Shibata (1961), Christensen & Wu (1964), Mitchell (1964), Kwok & Bolton (2010).	Breaking of molecule bonds	Activate energy, temperature and deviatoric stress.
Grim (1962), Gupta (1964), Kuhn & Mitchell (1993).	Sliding particles	Activate energy, contact forces.
De Jong & Verruijt (1965), Berry & Poskitt (1972), Zeevaart (1986), Navarro & Alonso (2001), Mitchell & Soga (2005), Wang & Xu (2006).	Water flows with two drainage structure (Macro– micro structures)	Two levels of soil structures, water flows in two pore structures and deformation of pores.
Terzaghi (1941), Barden (1969), Bjerrum (1967), Garlanger (1972), Christie & Tonks (1985), Graham & Yin (2001).	Structural viscosity	Different viscosity of absorbed water system, clay mineral–water interaction.

Experimental characterisation of creep in clays is a relatively complex procedure that requires a thorough understanding of the influencing factors. Characterisation of creep in the laboratory requires performance of long-term compression tests at constant effective stress. However, keeping the effective stress throughout the course of a test is not an easy task. For example, in undrained triaxial creep tests, possible development of pore-water pressure with time can change the effective stress conditions. Furthermore, in drained triaxial creep tests, correcting the applied load for changes in cross-sectional area can alter the state of effective stress in the specimen.

Creep tests can be performed in both compression and swelling stages (Kamao, 2016). Creep strains after a significant unloading stage are negative and cause additional swelling. This process is known as “creep recovery” (Li et al., 2003). After a period of time, the negative creep strains may shift to positive strains (den Hann and van den Berg, 2001). It must be noted that the creep behaviour described here is the characteristic of creep tests under an oedometric state, isotropic stress, or anisotropic

stress state far from failure. Creep rupture is beyond the scope of this work and therefore will not be covered here.

2.4.3.1 Creep Hypotheses

In geotechnical practice, the time-dependent consolidation of soft soils is normally studied based on the results of standard oedometer and triaxial tests in the laboratory. The results obtained are then extrapolated to emulate the field conditions. This approach has been criticised as posing shortcomings in the aspects of:

- The use of thin soil samples in the laboratory to analyse the time-dependent settlement of thick soil layers in the field.
- The shorter time scale for completion of primary consolidation in thin laboratory soil samples in comparison with the thick soil layers in the field (Degago et al., 2011).

Assessment of creep settlements observed in fast laboratory tests on thin samples, and their extrapolation to the slow settlement rates in thick soil layers in the field, has been a topic of active debate among researchers (Yin, 1999, Leroueil, 2006, Degago et al., 2011). Ladd et al. (1977) were the first who challenged the classical theory of consolidation by introducing two hypotheses, namely hypotheses A and B, for assessment of consolidation behaviour. These hypotheses are differentiated based on the assumption of occurance of creep strains after completion of primary consolidation (hypothesis A) or during dissipation of u_{exc} (hypothesis B). According to hypothesis A, for a given vertical effective stress (σ'_v) increment, the vertical strain (ε_v) at the end of primary (EOP) consolidation is independent of the duration of the primary consolidation. This implies that the thickness of the consolidating soil layer (H) does not affect the ε_v at EOP, and hence the corresponding value of the preconsolidation pressure, meaning that for both laboratory and field conditions, there is a unique relationship between the EOP void ratio (strain) and the effective stress (σ'_v) (Mesri and Choi, 1985). In contrast, according to hypothesis B, ε_v at EOP is not unique and is influenced by H and the duration of primary consolidation. This implies a higher *in-situ* EOP strain than the corresponding EOP strain obtained from fast laboratory tests on thin soil samples. Accordingly, a lower *in-situ* EOP preconsolidation pressure than its corresponding laboratory value is expected.

Later research by Feng (1991), Mesri (2001), Mesri and Vardhanabhuti (2006), and Mesri (2009) supported hypothesis A while accepting the existance of creep strains during dissipation of u_{exc}. In fact, this group of hypothesis A advocates, believed that the total strain during primary consolidation is caused by (1) change in effective stress (stress-induced compression), and (2) change in time (time-induced compression). The proportional effectiveness of these two components varies in thin laboratory samples and thick *in-situ* soil layers possessing different durations of primary consolidation and effective stress rate. It can, therefore, be assumed that these interrelated components counteract each other to yield an EOP void ratio (strain) that is independent of the consolidation duration (Degago et al., 2011). This statement disagrees with the Isotach concept (Suklje, 1957) which considers a unique relationship between effective stress, strain, and strain-rate during primary and secondary consolidation (explained further later). Figure 2.25 schematically presents the differences of creep hypotheses in a ε_v – log t plane.

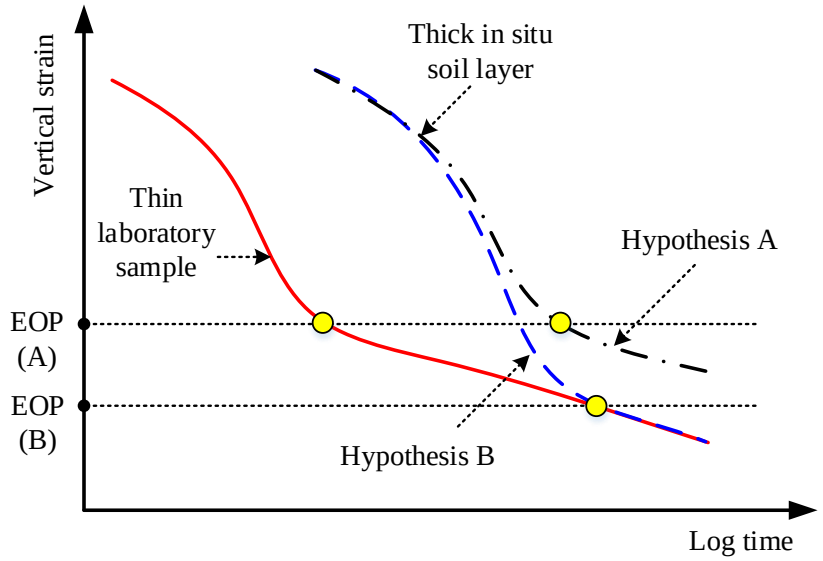
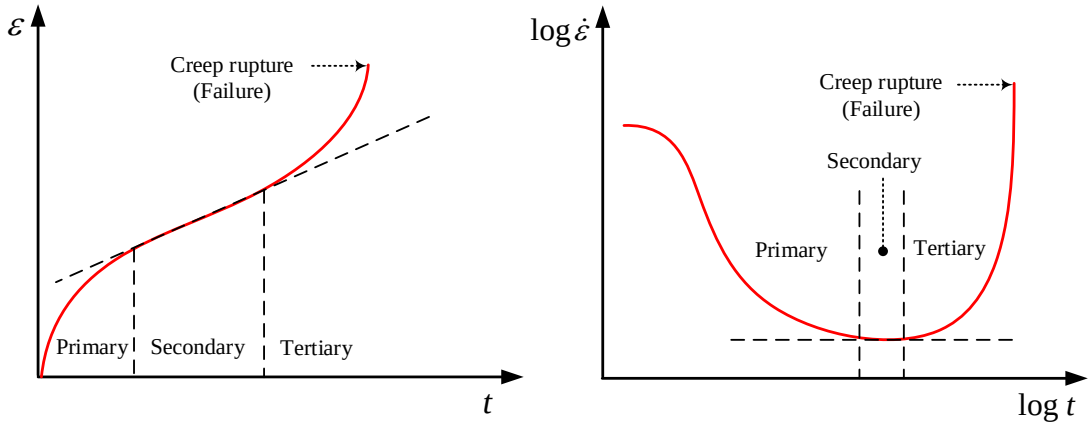


Figure 2.25 Creep hypotheses A and B (after Ladd et al., 1977)

2.4.3.2 Creep Phases

Creep deformation, in triaxial conditions, can be divided into primary creep (transient creep), secondary creep (stationary creep) and tertiary creep (acceleration creep) phases based on the strain-rate evolution during secondary compression (Augustesen et al., 2004). As shown in Figure 2.26, these phases can be defined as the creep deformations at decreasing, constant, and increasing strain-rates respectively. Hicher (1985) stated that during deviatoric creep tests, secondary creep is rarely detected, whereas the

primary creep and tertiary creep are normally observed, with the latter being related only to the stress states near the failure states. Tertiary creep will not be observed in one-dimensional or isotropic compression tests.



(a) (b)

Figure 2.26 Definition of creep stages in triaxial creep tests: (a) ε – t plane; (b) log $\dot{\varepsilon}$ – log t plane (after Augustesen et al., 2004).

Table 2.4 gives the volumetric strain-rate values during creep phases of conventional oedometer tests as reported in the literature.

Table 2.4 Volumetric creep strain-rate values observed in conventional oedometer tests

Authors	Soil	Strain rate range (s^{-1})
Leroueil et al. (1983a)	Canadian soft clays	4×10^{-8} – 4×10^{-5}
Leroueil et al. (1985)		10^{-9} and 10^{-6}
Leroueil (1988)	Canadian soft clays	10^{-7}
Leroueil (1996)		5×10^{-8} and 5×10^{-6}
Leroueil (2006)		10^{-8} and 3×10^{-7}
Sorensen (2006)	Reconstituted Kaolin Clay	10^{-8}

2.4.3.3 Creep Index

In conventional long-term oedometer tests a straight line is usually fitted to the data points after EOP consolidation in the e – log t or ε_v – log t graphs (Figure 2.26). The slope of this straight line is considered as the conventional secondary compression coefficient, or creep index, and is calculated using;

$$C_{\alpha e} = \frac{\Delta e}{\Delta \log t} \qquad 2.10$$

$$C_{\alpha \varepsilon} = \frac{\Delta \varepsilon}{\Delta \log t} = \frac{\Delta e}{(1+e_i)\times \Delta \log t} = \frac{\varepsilon_v}{\Delta \log t} = \frac{C_{\alpha e}}{1+e_i} \qquad 2.11$$

where $C_{\alpha e}$ and $C_{\alpha \varepsilon}$ are the coefficients of the secondary compression with respect to e and ε respectively, Δe and $\Delta \varepsilon$ are the changes in void ratio and vertical strain respectively under a constant effective stress within the time t_0 to t, and e_i is the initial void ratio. Alternatively, the coefficients α and $\alpha\varepsilon$ have been used in many of the elasto-visco-plastic constitutive models for expressing the creep or time-dependency. These parameters are related to the conventional $C_{\alpha e}$ and $C_{\alpha \varepsilon}$ coefficients using the following correlations:

$$\alpha = \frac{C_{\alpha e}}{\ln 10} \qquad 2.12$$

$$\alpha\varepsilon = \frac{C_{\alpha \varepsilon}}{\ln 10} \qquad 2.13$$

This approach, as discussed in Liingaard et al. (2004), is known as the semi-logarithmic law of creep. Assuming a constant value for C_α with time, the vertical creep strain is calculated as;

$$\varepsilon_v^c = C_{\alpha\varepsilon} \log\left(1 + \frac{t}{t_i}\right) \text{ for } t \geq 0 \qquad 2.14$$

where t_i is the reference time corresponding to the EOP, and t is the time lapsed post EOP. In this model, as the creep rate is continuously decreased, only the primary creep phase can be captured as shown in Figure 2.27. The assumption of constant C_α with time is, however, in many cases, non-realistic and several authors have shown the dependency of C_α on a number of factors such as soil structure, consolidation pressure, and temperature (see Mesri, 1973, Karstunen and Yin, 2010, and Mataic et al., 2015).

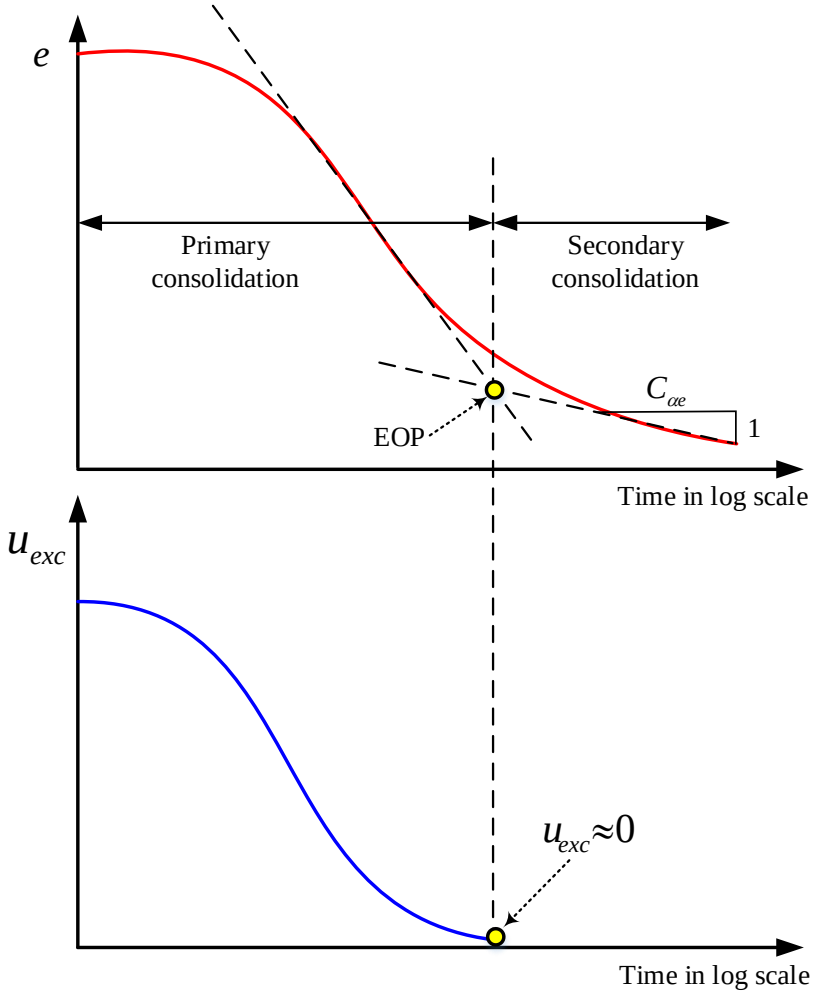


Figure 2.27 Estimation of creep index from conventional consolidation tests

2.4.3.4 Factors Affecting Creep Index

Effect of Soil Structure

The influence of soil structure and particle arrangement on the secondary compression of clayey soils was studied by Mitchell (1956). The experimental results on 14 undisturbed and remoulded clays demonstrated higher secondary compression ratio for undisturbed samples in comparison with remoulded samples. These observations were attributed to the presence of more random particle arrangements in undisturbed samples than the remoulded samples which tend to re-orient to parallel arrangements under compressive overburden pressures.

Effect of Consolidation Pressure

It was found by Mesri and Godlewski (1977) that C_α is dependent on the applied vertical effective stress. As shown in Figure 2.28(a), the values of C_α increase slowly with

vertical stress up to σ'_p, after which they exhibit a sudden increase to a peak value followed by a gradual smooth reduction. It was also reported that remoulded specimens of natural clays do not exhibit pressure-dependency mainly due to their destroyed naturally-developed structure. Similar results were reported by Fodil et al. (1997) for soft clay samples of the Le Flumet dam foundation in France, Bilotta et al. (2008) for ashy soils (silty sand) of the Campania region in Italy, Yin et al. (2011) for Vanttila Clay [Figure 2.28(b)], and Mataic et al. (2015) for Perniö Clay in Finland.

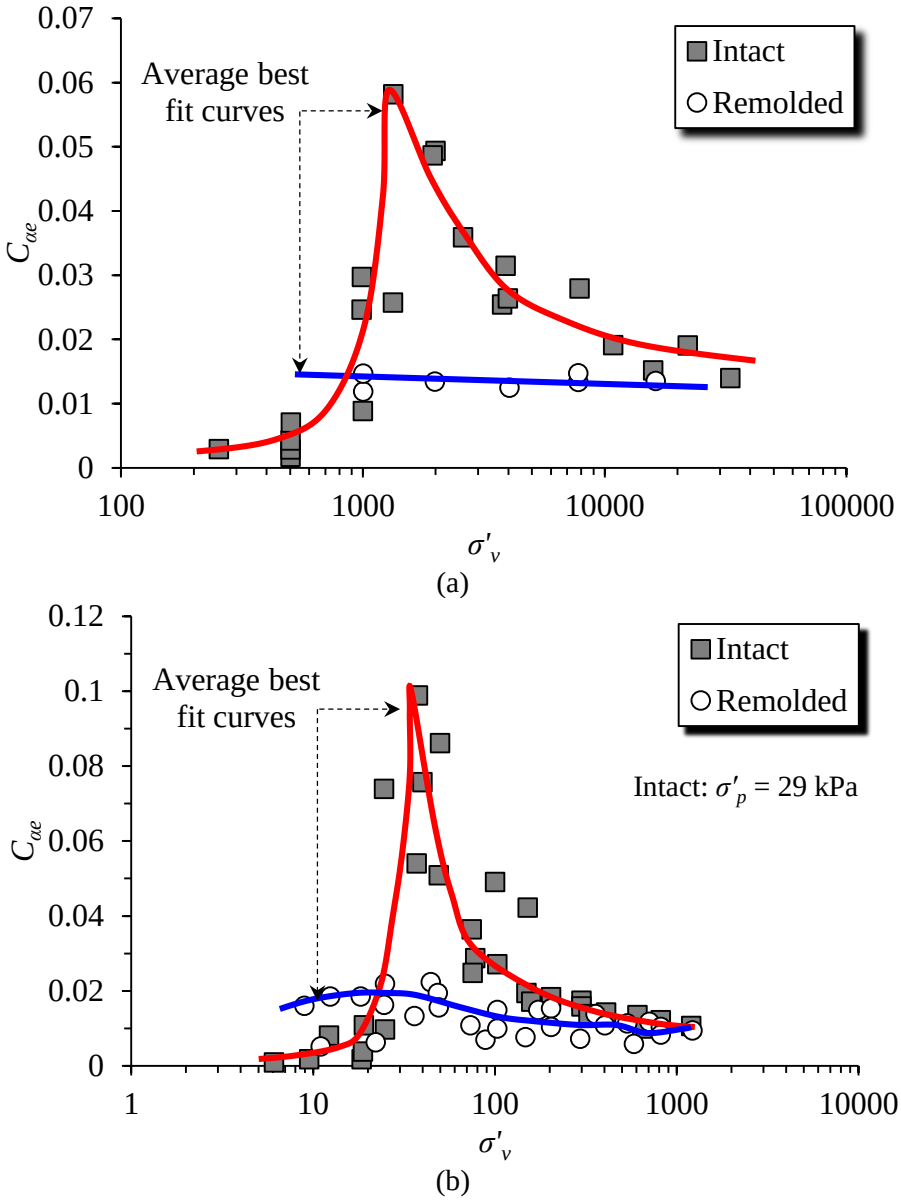


Figure 2.28 Variation of $C_{\alpha e}$ with consolidation pressure for undisturbed and remoulded specimens: (a) Leda clay (re-drawn after Mesri and Godlewski, 1977); (b) Vanttila Clay (re-drawn after Yin et al., 2011).

Mesri and Godlewski (1977) and Mesri and Castro (1987) also showed that the ratio C_α/C_c remains approximately constant with change in effective stress. Mesri et al. (1994) defined four groups of soils based on the C_α/C_c ratio (Table 2.5). This ratio (α) was defined as the slope of the curve in the log $\dot{\varepsilon}$ – log σ'_p plane;

$$\alpha = \frac{C_{\alpha\varepsilon}}{C_c} = \frac{\Delta \log \dot{\varepsilon}}{\Delta \log \sigma'_p} \qquad 2.15$$

A value of α = 0.05 was also reported by Graham et al. (1983) for Belfast Clay loaded at $\sigma'_v = 2\,\sigma'_p$. However, it was observed that α was significantly higher at stresses close to σ'_p if the ratio was evaluated for each stress increment. A C_α/C_c range of 0.02 – 0.04 was reported by Deng et al. (2012) for stiff Boom Clay. Leroueil et al. (1985), Yin et al. (2011), and Mataic et al. (2015) could not, however, find a constant α for the Batiscan Clay, Vanttila Clay, and Perniö Clay respectively.

Table 2.5 Soil categories based on the values of C_α/C_c (Mesri et al., 1994)

Material	C_α/C_c
Granular soils including rockfill	0.02 ± 0.01
Shale and mudstone	0.03 ± 0.01
Inorganic clays and silts	0.04 ± 0.01
Organic clays and silts	0.05 ± 0.01
Peat and muskeg	0.06 ± 0.01

Effect of Temperature

According to Mitchell (1993), variations of temperature can significantly influence the volume change behaviour and shear strength of the soils. This can be attributed on the one hand to the higher volumetric expansion of the pore-water in comparison with the soil grains, and on the other hand, to the decrease in shearing strength of the inter-particle contacts by increase in temperature. Effect of temperature on creep deformations has not received significant attention in previous studies. Mesri (1973) conducted a series of temperature controlled 1D consolidation tests on both organic and inorganic Paulding Clay and reported that temperature does not significantly influence the relationship between C_α and the consolidation pressure. Similar results were reported by Leroueil and Marques (1996). Moreover, Tsuchida et al. (1991) and Towhata et al. (1993) showed that under long-term consolidation, a structural resistance against deformation is developed inside the soil specimen which is accelerated under

high temperatures. Burghignoli et al. (2000) observed an increase in the rate of thermal secondary consolidation with increase in temperature from drained triaxial creep tests on reconstituted Todi Clay performed in the range 25 to 80°C. Similar results were reported by Jarad (2016) from temperature controlled CRS tests on a lightly overconsolidated illitic clay in a temperature range of 20 to 70°C. In general, increase in temperature can result in decrease in viscosity of water in soil pores, and this consequently increases the hydraulic conductivity of the soil medium (Delage et al., 2009). With increase of fluid permeability in intra-floc and inter-floc pores, an increase in creep deformations is expectable.

The assumption of a linear relationship between the creep strain and the logarithm of time is not valid for most cases. Figure 2.29 presents the results of triaxial creep tests on various clays (Mitchell et al., 1997). It can be seen that the creep strains exhibit non-linear variations with logarithm of time.

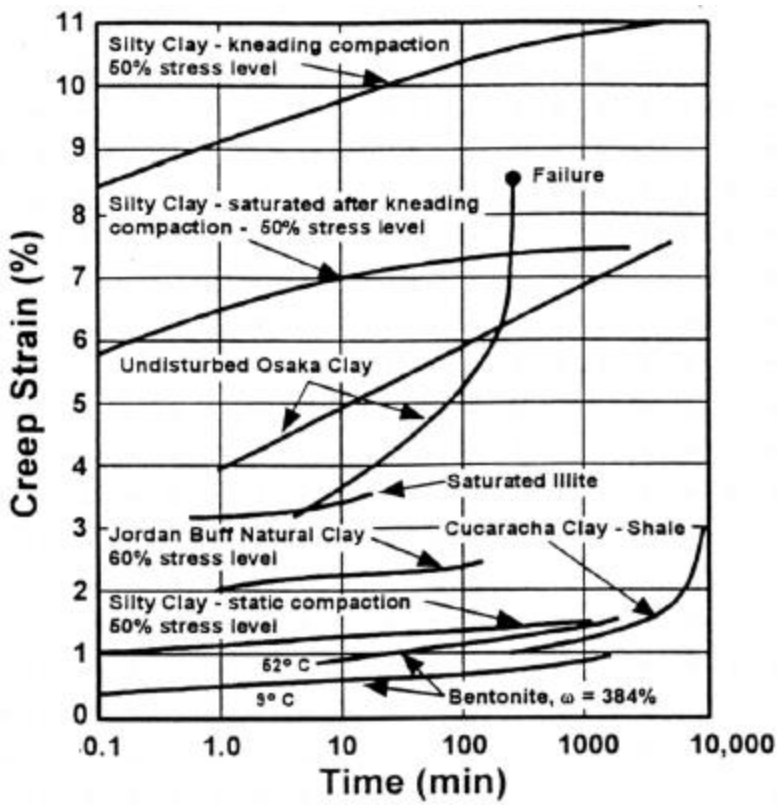


Figure 2.29 Variation of creep strain with logarithm of time for various clays and under various stress states (Mitchell et al., 1997)

Nevertheless, it has been shown by various researchers (e.g. Singh and Mitchell, 1969, Vaid and Campanella, 1977, Tavenas et al., 1978, Fodil et al., 1997) that there is a linear

relationship between the logarithm of creep rate and logarithm of time. The slope of the line in the log $\dot{\varepsilon}$ – log t plane is given by;

$$m = -\frac{\Delta \log \dot{\varepsilon}}{\Delta \log t} \qquad 2.16$$

Figure 2.30 presents the results of drained triaxial creep tests on London Clay as reported by Mitchell et al. (1997), where the linear $\dot{\varepsilon}$ – t relationship in a log-log scale is clearly observed.

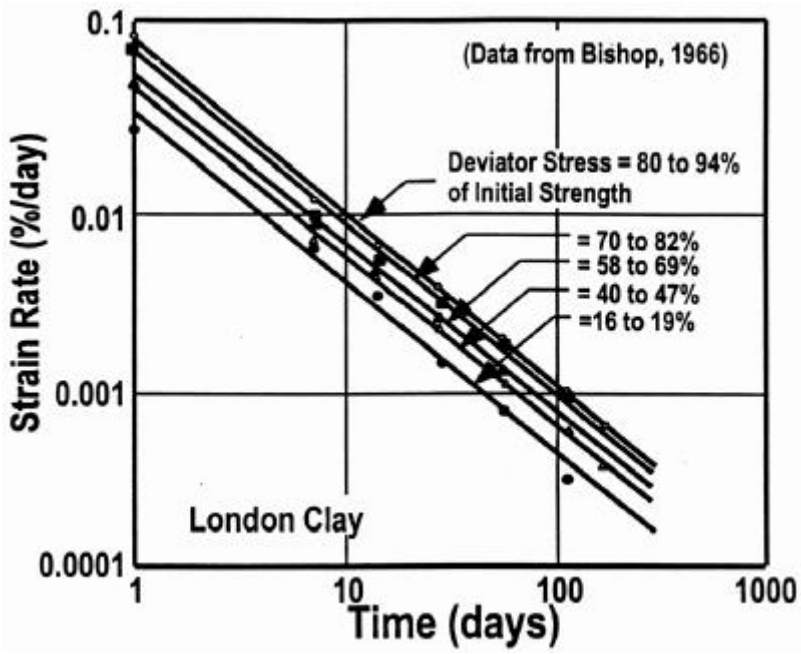


Figure 2.30 Variation of logarithm of creep strain rate with logarithm of time for London Clay under various deviator states levels in drained triaxial creep tests (Mitchell et al., 1997)

Sorensen (2006) performed a 1D long-term creep test on reconstituted London Clay under a constant vertical effective stress of 785 kPa, and reported a near-linear variation of void ratio with logarithm of time with $C_{\alpha e}$ = 0.016 and $m \approx 1$ in log $\dot{\varepsilon}$ – log t plot.

2.4.3.5 The Concept of Isochrones or Time Lines

Bjerrum (1967) proposed the concept of isochrones or time lines based on the results of 1D creep tests on soft clays. Based on this model, the soil response in compression and swelling is defined as a function of effective stress and time. The time lines are parallel curves in e – log t space. Each line represents the equilibrium void ratio for the duration of sustained loading (creep). Reduction in void ratio as a result of prolonged

sustained loading (delayed compression) leads to an increase in σ'_p. Loading a sample, initially having a state on a time line corresponding to a higher sustained loading period (e.g. 3000 years time line in Figure 2.31), will result in an increase in σ'_p without significant volume change, after which the state path re-joins the original NCL.

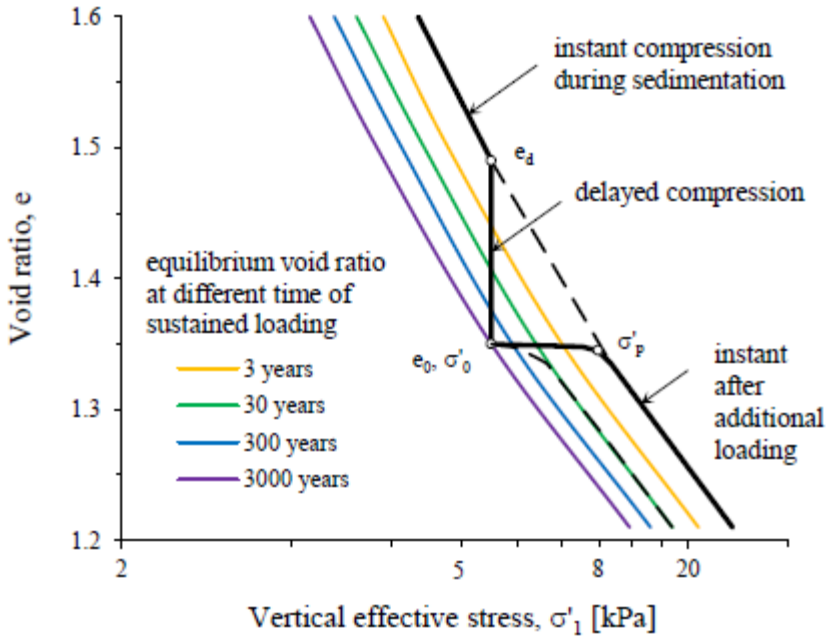


Figure 2.31 Illustration of the time lines concept (Mataic, 2016)

2.4.4 Secondary Consolidation in Unsaturated Clays

As discussed in Section 2.4.3., the concept of creep in saturated soft soils is a complex process that is influenced by various factors. In a very general definition, creep in saturated soils, subjected to a prolonged constant load increment, can be defined as rearrangement of the particles into a more packed state under constant effective stress. This definition, however, cannot be truly applied to unsaturated soils as either an external or internal stress will be changing. For example, as compression takes place, with reduction in void ratio, the degree of saturation increases and suction reduces changing the effective stress. This process becomes even more complex with presence of localised and non-uniformly distributed unsaturated pockets in a soil mass. Hence, unlike saturated soils, the phenomenon of particles rearrangement under prolonged sustained loading may not be regarded as true creep. Nevertheless, as the observed time-dependent deformations of unsaturated soils subjected to sustained loading have been referred to as "creep" in the literature, for sake of consistency and to provide a comparison platform, the same terminology is used in this manuscript.

Very few studies have been reported in the literature concerning creep deformations in unsaturated clays. Therefore, complementary information with regard to the creep response of unsaturated chalks and rockfills will be reviewed in this section with the aim of providing an insight into the viscous response in unsaturated conditions. Usually, models of such behaviour are based on extending the existing creep models developed for saturated soils, thereby often involving unrealistic assumptions and simplifications.

2.4.4.1 Creep in Oedometric Conditions

As discussed in section 2.3.6, if the suction variation of a soil, following the main drying or main wetting curves in $S_r - s$ or $w - s$ planes, is reversed, the soil scans a curve from main drying to main wetting curves or vice versa. These scanning curves are associated with the hydraulic hysteresis forces arising from the bulk and the meniscus water. These hysteresis forces can also result in plastic deformations during repeated wetting and drying cycles (Wheeler et al., 2003c). Alonso et al. (1995) proved the plastic deformations during cyclic wetting and drying of Boom Clay in suction-controlled oedometer tests (Figure 2.32). The observed deformation might be attributed to rearrangement of particles, however, it cannot be regarded as true creep, as the state of pore-water pressure (suction) and hence, effective stress, is changed during the course of wetting and drying.

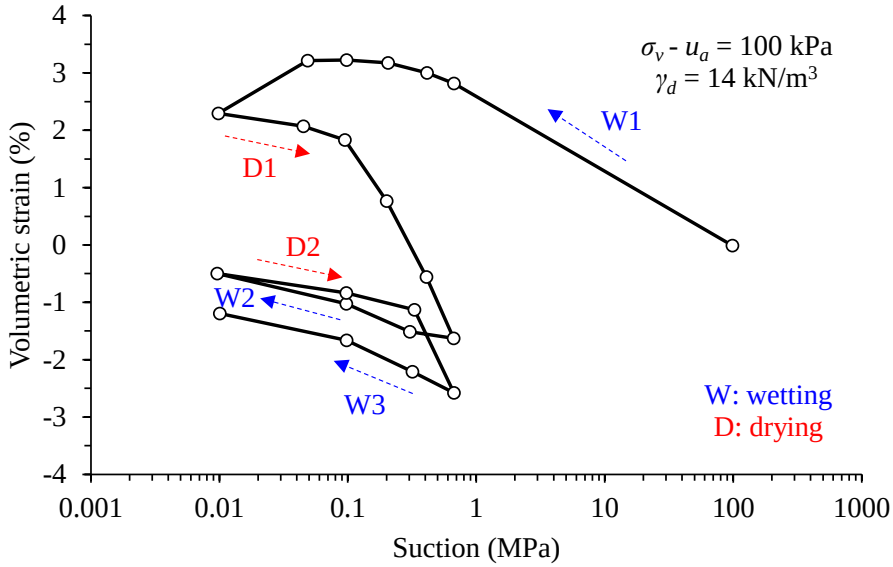


Figure 2.32 Plastic deformations during cyclic wetting and drying tests on Boom Clay in oedometric conditions (re-drawn after Alonso et al., 1995)

Long-term (10 days) oedometer creep tests on unsaturated volcanic ashy soils (silty sand) of the Campania region in Italy, was reported by Bilotta et al. (2008). Undisturbed and remoulded (from slurry) samples were tested in a suction-controlled oedometer cell where different suctions in the range 0–200 kPa were applied using the axis-translation technique. Specimens were loaded incrementally to a maximum vertical stress of 2400 kPa. Each load increment was sustained for a period of 10 days (Figure 2.33). With increase in suction, C_α values for undisturbed specimens were decreased for vertical stress levels lower than 600 kPa. Such trend was disappeared for higher stress levels. For remoulded specimens, regardless of the stress level, the C_α values did not show any specific trend with increase in suction. Moreover, at the same stress level, greater C_α values were observed for undisturbed specimens than for remoulded ones.

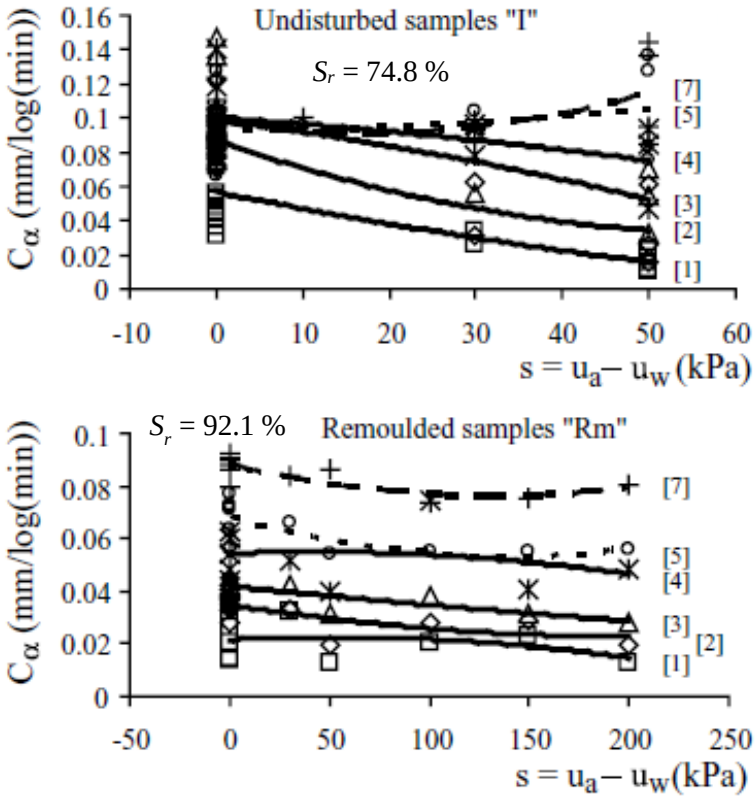


Figure 2.33 Variation of C_α with suction and applied vertical stress for undisturbed (top) and remoulded (bottom) volcanic ashy soils (Bilotta et al., 2008) – numbers in brackets indicate applied vertical stresses in kPa. Symbols are also given in parentheses: [1]=36.9 (□), [2]=87.9 (◊), [3]=160.4 (Δ), [4]=298.1 (<*>), [5]=599.9 (○), [6]=1193.1 (-), [7]=2379.6 (+).

Oil reservoir chalks have been the subject of numerous experimental and theoretical studies in recent years, as it was believed that some concepts of unsaturated soil

mechanics are also applicable to multiphase chalk behaviour (Delage et al., 1996). Priol (2005) and Priol et al. (2007), performed a set of multiple step loading creep oedometer tests on oil-saturated, water-saturated, partially-saturated, and dry Lixhe chalk (an outcrop chalk from Belgium) and reported that at high pressures the creep coefficient values increased with increase in vertical stress and decreased with increase in suction (Figure 2.34). Similar results were reported by De Gennaro et al. (2005) who evaluated the suction- and stress-dependency of the creep coefficient in MSL compression tests on Estreux chalk under dry, water-saturated, and unsaturated (s = 1.5 MPa) conditions using a suction-controlled osmotic oedometer cell (Figure 2.35).

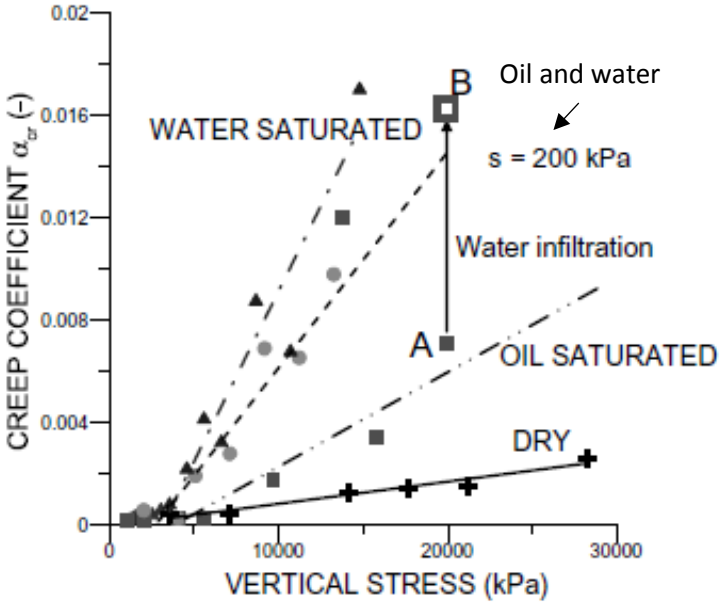


Figure 2.34 Oedometer creep tests on Lixhe chalk; effect of stress level and suction on the creep coefficient (Priol et al., 2007)

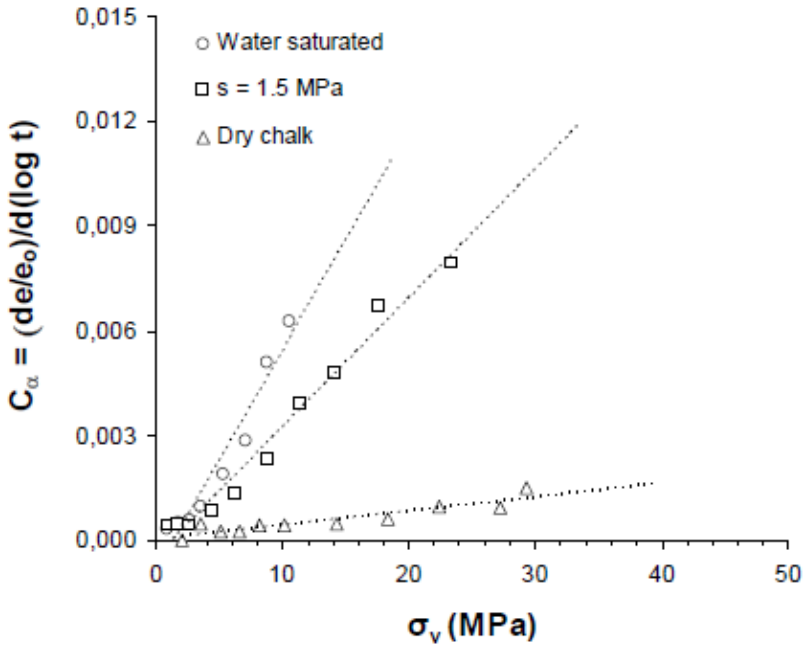


Figure 2.35 Oedometer creep tests on Estreux chalk; effect of stress level and suction on the creep coefficient (De Gennaro et al., 2005)

2.4.4.2 Creep in Triaxial Conditions

A number of drained and undrained saturated triaxial creep tests have been reported in the literature, however the accuracy of the undrained creep tests has been questioned mainly due to the change in effective stress as a consequence of u_w development during undrained creep tests (Augustesen et al., 2004). Lai et al. (2010) performed two sets of unsaturated drained triaxial creep tests on remoulded samples taken from sliding zone soils (a clayey soil) of the Qianjiangping landslide in China and showed that increase in matric suction results in decrease in creep strain-rate and amount under constant net confining pressure and deviatoric stress. The results also showed improvement of the shear strength during multi-stage loading. Similar observations were reported by Zou et al. (2013) from the results of unsaturated drained triaxial creep tests on the same soil samples (Figure 2.36). The creep tests were performed over a one week time period. It was found that increase in matric suction results in a decrease in elasto-plastic and maximum value of the visco-plastic deformations. Zhu and Yu (2014) also conducted unsaturated triaxial creep tests on weak intercalation soils in soft rocks of the Badong formation in China, under different deviatoric stress levels and matric suctions, and reported a non-linear increase of volumetric creep strains with an increase in deviatoric stress in constant suction tests, and an increase in creep strains with a decrease in suction in constant deviator stress tests.

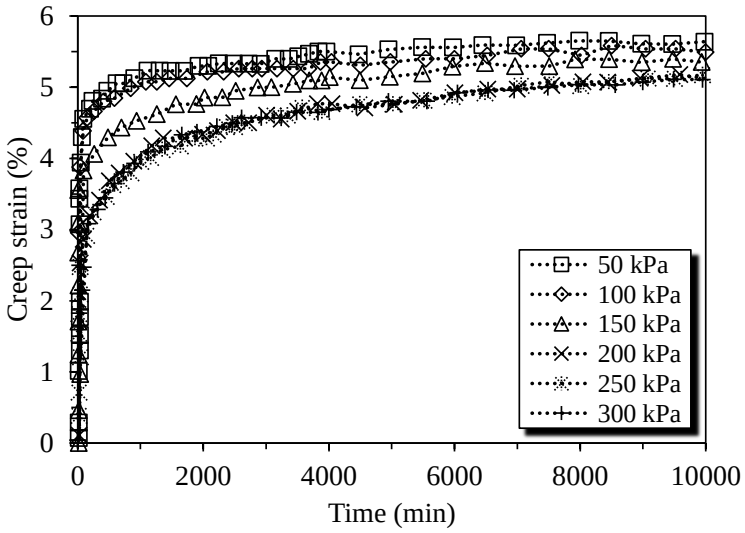


Figure 2.36 Triaxial creep tests under different matric suctions (re-drawn after Zou et al., 2013)

2.4.4.3 Unsaturated Creep Models

Since the 1950s a number of empirical and constitutive correlations have been proposed for prediction of creep behaviour of soils (e.g. Suklje, 1957, Bjerrum, 1967, Singh and Mitchell, 1969, Mesri and Castro, 1987, Zhu et al., 1999, Karim, 2010). Nevertheless, despite these attempts, the limitations of the proposed creep functions such as their applicability for certain test conditions, complexity, and dependency on other soil parameters have resulted in the lack of a unified and widely accepted creep correlation for prediction of creep strains for a variety of soil types and stress states. Some of these models have recently been used as the base models for developing time-dependent empirical and constitutive models for unsaturated geo-materials.

Oldecop and Alonso (2002) performed suction-controlled oedometer tests on rockfill material and proposed a phenomenological relationship to define the long-term volumetric creep strain-rate;

$$\dot{\varepsilon}_v^c = \frac{\mu p}{t}\left(1-\beta^c \ln\left(\frac{s+p_a}{p_a}\right)\right) \qquad 2.17$$

where p is the confining stress, μ is a kind of creep index, β^c is a model parameter, p_a is atmospheric pressure, and s is suction. This model was later modified by Alonso et al. (2005) to obtain an equation for deviatoric creep strain-rate in triaxial conditions. In the proposed equation, p was substituted by q, and μ was replaced by $\eta = 0.3\,\mu$. Note

that, the intrinsic creep deformation in rockfill material was attributed to the particle breakage in these studies.

The Barcelona Basic Model (BBM), proposed by Alonso et al. (1990), forms the base of unsaturated creep models for reservoir chalks (e.g. Collin et al., 2008; Pereira and De Gennaro, 2010). In BBM, two independent stress variables namely, net stress ($\sigma_v - u_a$) and suction ($u_a - u_w$), are used as effective stress fields. This model is an elasto-plastic hardening model that allows for reproduction of the irreversible response of the soil against suction and stress reversals. This model also accounts for collapsibility of the soil due to suction changes. Two yield curves namely, loading-collapse (LC) and suction-increase (SI), are used for characterisation of the isotropic stress states. In modelling triaxial stress states, these two curves become yield surfaces (Alonso et al., 1990). Viscous behaviour of reservoir chalks was first studied by De Gennaro et al. (2003) who extended the Pasachalk elasto-plastic model (Collin et al., 2002) to account for viscoplastic responses. A modified version of the viscoplastic Pasachalk model was later proposed by Collin et al. (2008) which takes into account the creep behaviour as a function of suction. In this model, Perzyna's over-stress theory (Perzyna, 1964) was adopted to account for the time-dependent response of chalk, whereas the suction effects were incorporated in the model based on the formulation of the loading-collapse (LC) curve in the BBM. This model was validated based on the experimental data on creep response of Lixhe chalk presented by Priol (2005), as shown in Figure 2.37.

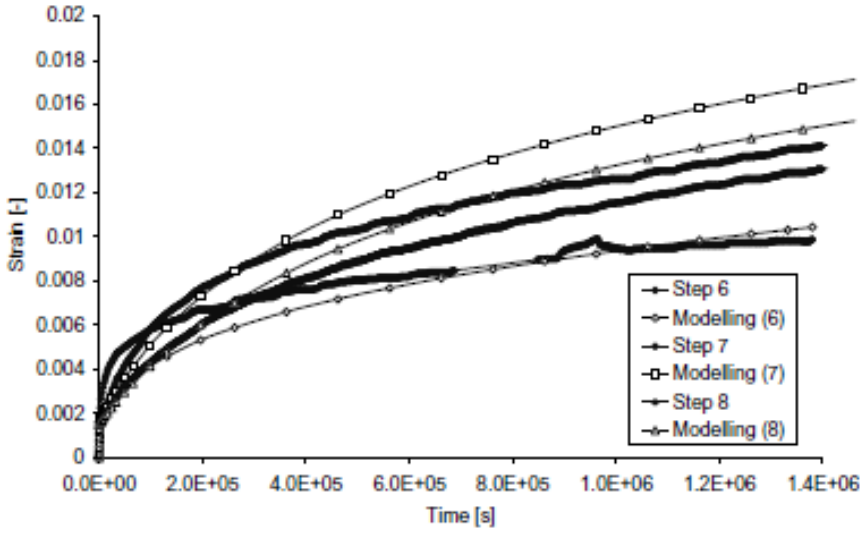


Figure 2.37 Numerical modelling of creep phase for unsaturated chalk samples at s = 200 kPa (Collin et al., 2008)

Pereira and De Gennaro (2010) proposed a rate-dependent elasto-visco-plastic constitutive model, called RASTRA, for modelling coupled effects of time and partial saturation. The model is an extension of the BBM for partially-saturated geo-materials and developed based on the Isotach approach (Suklje, 1957, Bjerrum, 1967). As in BBM, the model assumes inviscid mechanical behaviour in the elastic regime and a non-associated plastic flow rule. The RASTRA model extends the BBM by including the rate effects and assuming the BBM suction-dependent preconsolidation stress also to be dependent on the volumetric strain-rate. The model was further validated based on CRS compression tests on Lixhe reservoir chalk under constant oil-water suction of 0.2 MPa, and a standard MSL oedometer test on dry Estreux chalk having an initial suction of about 30 MPa.

An empirical correlation for quantitative determination of matric suction effects on creep behaviour of soils was also suggested by Lai et al. (2010). The model was developed by incorporating matric suction in the stress intensity function of the well-known Singh-Mitchell creep model (Singh and Mitchell, 1969). Similar to the Singh-Mitchell creep model, the unsaturated version of this model also considers the unrealistic assumptions of time- and stress-independency of the parameters. The Singh-Mitchell creep strains can be computed using

$$\varepsilon_v^c = A\left(\frac{t_1}{1-m}\right)\exp(\delta D_r)\times\left(\frac{t}{t_1}\right)^{1-m} \qquad 2.18$$

where D_r is the stress intensity defined as the proportion of the deviator stress (q) to the drained shear strength (q_f), t is the test time, t_1 is the reference time representing the time at the beginning of the creep stage, m is the slope of the plot of $ln\ \dot{\varepsilon} - ln\ t$ ($m \neq 1$), δ is the slope of the graph of $ln\ \dot{\varepsilon} - D_r$, and A is the strain-rate at $D_r = 0$ and $t = t_1$. In the unsaturated version of the Singh-Mitchell model, a new stress intensity function was proposed incorporating the effect of matric suction;

$$D_R = D_r \times \frac{\sigma_3'}{u_a} \qquad 2.19$$

In Equation 2.19, $\sigma'_3 = \sigma_3 - u_a$ is the net confining pressure. Note that unsaturated drained shear strength values are to be used in calculation of the D_r values. The unsaturated creep strain is essentially expressed as;

$$\varepsilon_v^c = B\exp(\beta_{D_R} D_R) \times \left(\frac{t}{t_1}\right)^{\lambda'} \qquad 2.20$$

where $B = At_1 / \lambda'$, $\lambda' = 1 - m$, and β_{DR} is the corresponding value of δ under the new stress intensity. The model was further validated against the experimental data obtained from two drained triaxial creep tests performed on the sliding zone soils (a clayey soil) of Qianjiangping landslide in China.

In an another attempt to develop a rheological model for unsaturated soils, Zou et al. (2013) proposed a creep model for sliding zone soils of Qianjiangping landslide. This model is based on the extended Burgers creep model which is typically used to simulate viscous processes in geo-materials (Sun, 1999). The extended Burgers model is capable of capturing the primary and secondary creep phases, however, it does not account for tertiary (acceleration) creep. The extended Burgers model was adopted to incorporate the effect of matric suction on creep deformations. Moreover, taking into account the suction-dependency of the extended Burgers creep model parameters, the developed unsaturated Burgers model was further modified and validated against the experimental results of drained triaxial creep tests on remoulded specimens under constant net confining pressure (100 kPa) and deviator stress level (q/q_f).

An empirical model accounting for creep of unsaturated soils was developed by Zhu and Yu (2014) from the results of unsaturated triaxial creep tests on weak intercalation soils in soft rocks of the Badong formation in China. This model was constructed by incorporating matric suction in the Mesri creep model (Mesri et al., 1981). The volumetric creep strains are calculated using;

$$\varepsilon_v^c = \left[\frac{q_f}{Ap_a(s/p_a)^y}\right] \frac{D_r}{1-(R_f)_r D_r} \left(\frac{t}{t_1}\right)^{aD_r^b} \qquad 2.21$$

where p_a is the atmospheric pressure (101 kPa), A, y, a, and b are material constants, and R_f is the average slope of $\varepsilon/D_r - \varepsilon$ curves at different times.

As can be seen, a range of different models have so far been proposed to take into account the effect of partial saturation on the 1D or 3D creep strains. Furthermore, the proposed models have been developed and validated based on limited experimental data, restricting their application to specific stress states and material types.

2.5 Rate-dependency in Saturated vs. Unsaturated Clays

It is well known that the mechanical behaviour of soils, in particular natural clays, is highly influenced by time and rate effects (Fodil et al., 1997, Tanaka, 2005, Degago et al., 2013, Bagheri et al., 2015). In this section, effects of strain-rate on 1D behaviour of clays in saturated and unsaturated conditions is discussed comparatively.

2.5.1 Strain-Rate Effects on Oedometric Behaviour of Saturated Clays

Conventional IL oedometer tests are widely used for determination of 1D compression and consolidation characteristics of soils mainly due to their simplicity, cost efficiency, and ease of data interpretation. However, these types of test are typically associated with a number of disadvantages and drawbacks which can be outlined as; (1) due to the widely spaced results, it is difficult to draw the e – log σ'_v curve and estimate the σ'_p, (2) the process of step loading is highly time-consuming, and (3) sudden loading can cause sample disturbance (Leroueil et al., 1983a). Implementation of continuous loading (CL) tests using, for instance, the hydraulic loading Rowe cell (Rowe and Barden, 1966), appears to be an effective solution for significantly shortening the testing time and more accurate characterisation of the 1D consolidation process. CL tests including constant-rate-of-strain (CRS), constant-rate-of-loading (CRL), and constant gradient of pore-water pressure (CG) tests have rapidly become popular as more advantages of these tests such as improved estimation of σ'_p, permeability coefficient (k_v), and consolidation coefficient (c_v) were discovered (Premchitt et al., 1996).

2.5.1.1 CRS Oedometer Test

The CRS test was first introduced by Hamilton and Crawford (1959) as a mean for rapid determination of σ'_p. Accurate determination of this parameter is of high importance for design engineers, as beyond this point, significant deformations can take place. CRS testing is a standardised method (ASTM-D4186-06, 2006) for consolidation testing and has been widely described in the literature (e.g. Hamilton and Crawford, 1959,

Crawford, 1964, Gorman et al., 1978, Leroueil et al., 1983b). Basically, the soil specimen is set up in the cell which is then mounted and fastened on a displacement-controlled loading frame. A continuous load is then applied as a result of axial movement of the piston with constant rate of displacement. The stress–strain relationship is then obtained from the measurement of stresses. The variation of u_w is also measured at the base of the specimen. The results of a series of CRS tests by Gorman et al. (1978) on samples from three sites in Kentucky, USA, demonstrated the ease of σ'_p determination from CRS tests in comparison with the IL and CG tests. It was observed that at effective stresses just exceeding σ'_p, a significant and sudden increase in u_w occurs. Leroueil et al. (1983a) and Leroueil et al. (1983b) performed a series of different laboratory experiments (IL, CRS, and CG) on Champlain clays and found a better match between the σ'_p values obtained from CRS tests and those obtained from field measurements. Comparison of CRS test results with other conventional tests can be also found in Leroueil et al. (1985), Leroueil (1988), Hanzawa (1989), and Leroueil et al. (1996).

The CRS test offers, in general, several advantages including; (1) sample disturbance is reduced by smooth loading procedure, (2) a continuous record of stresses and strains can be obtained and plotted from the test results, (3) by choosing appropriate strain-rates, the secondary compression is minimised, allowing the test to be completed in a considerably lower time than conventional oedometer tests (Premchitt et al., 1996), and (4) horizontal and vertical coefficients of permeability can be obtained from horizontal and vertical CRS tests (Näätänen et al., 1998). The main disadvantage of the CRS test is its inapplicability for measurement of the rate of secondary compression. However, as will be discussed in the following sections, this problem can be overcome by performing stress-relaxation stages at certain strain levels and correlating the obtained relaxation coefficient to the compression and creep indices.

2.5.1.2 Determination of Appropriate Strain-Rate for CRS Tests

The dependency of the e – log p curve and u_{exc} on the imposed strain-rate highlights the importance of selection of appropriate $\dot{\varepsilon}_v$ for CRS tests. Imposing high rates of strain may result in generation and non-uniform distribution of u_{exc} throughout the specimen, with the maximum value of u_{exc} occurring at the base of the specimen and zero or very small u_{exc} developing at the top of the specimen. This phenomenon can result in

variation of effective stress state and void ratio across the specimen's height, leading to a variable rate of deformations during the test. On the other hand, very low strain-rates, in addition to significantly increasing the test time, may prevent generation of the minimum u_{exc} required for determination of the consolidation parameters such as k_v and c_v. Moreover, typical strain-rates in the range 10^{-8} to 10^{-4} s^{-1} are of practical interest in engineering practice (Pereira and De Gennaro, 2010). Therefore, caution must be applied in selection of the $\dot{\varepsilon}_v$ so that (1) generation of u_{exc} is controlled during the test, and (2) the selected $\dot{\varepsilon}_v$ falls within the practical range. In this regard, several criteria have been proposed in the literature. For instance, Gorman et al. (1978) suggested a range of 8.33×10^{-7} s^{-1} (i.e., 0.005 $\%min^{-1}$) to 1.67×10^{-6} s^{-1} (i.e., 0.01$\%min^{-1}$) as a guideline for selection of $\dot{\varepsilon}_v$. The upper limit was proposed to suit soils with a liquid limit w_L > 60%. A typical range from 1.67×10^{-8} s^{-1} (i.e., 0.0001$\%min^{-1}$) to 6.67×10^{-6} s^{-1} (i.e., 0.04% min^{-1}) was also proposed by Head (1992). Another approach by Lee et al. (1993), based on a series of CRS tests on undisturbed and reconstituted samples of soft marine clays from Singapore, offers an upper bound β with a magnitude of 0.1, where $\beta = \dot{\varepsilon}_v H_0^2/c_v$, in which, H_0 is the initial height of the test sample. In this approach, the maximum value of $\dot{\varepsilon}_v$ is obtained by $\dot{\varepsilon}_v = 0.1c_v/H_0^2$. Using this approach, Almeida et al. (1995) performed a set of IL and CRS tests on Rio de Janeiro estuary clays and observed a good consistency of c_v values obtained from IL and CRS tests for $0.15 \leq \beta \leq 0.28$ and a pore-water pressure ratio (PPR) range of $0.18 \leq PPR \leq 0.31$. PPR is defined as the ratio of the u_{exc} to the applied vertical total stress (σ_v) and is determined based on the c_v value of the test soil. ASTM-D4186-06 (2006) suggests that the maximum value for $\dot{\varepsilon}_v$ to be used in CRS testing must be limited to a value such that the maximum pore-water pressure ratio (PPR_{max}) is less than 3 – 15%. Other values of PPR_{max} recommended in the literature are 50 – 70% (Smith and Wahls, 1969), 5% (Wissa et al., 1971), 10 – 15% (Sällfors, 1975), 30 – 50% (Gorman et al., 1978), 15% (Larsson and Sällfors, 1986), and 3 – 20% (Head, 1992). Indeed, the dependency of this approach on the reliability of measured c_v values is considered as a major drawback as discused in Dobak (2003). Table 2.6 presents the strain-rate values used by various researchers for CRS testing on clays.

The strain-rate values chosen for CRS tests are generally higher than the observed strain-rates during creep phases of conventional oedometer tests as reported in Table 2.4. This, as will be explained in the next section, results in CRS compression curves

lying above the compression curves obtained from IL oedometer tests. Selection of very slow strain-rates, in addition to significantly increasing testing time, can give rise to aging effects and gradual development of inter-particle bonding, which leads to an increase in σ'_p and shift of the CRS compression curve to the right (Leroueil et al., 1996). This is also the case when a specimen subjected to prolonged creep at very low strain-rates is loaded (Sorensen et al., 2010). A CRS compression curve with very slow strain-rate may also lie above a CRS compression curve with much faster strain-rate, due to the aging effects (Figure 2.38). The aging effect is, however, outside the scope of this work.

As it can be seen, an overwhelming amount of information and guidelines can be found in the literature for determination of an appropriate strain rate for CRS tests on saturated soils. However, as of today, there is no available guideline for determination of a suitable strain rate for CRS tests on unsaturated soils (Wijaya et al., 2014). As suggested by Wijaya et al. (2014), a strain rate that provides a good match between the compression curves from conventional oedometer test and CRS test, can be considered as an appropriate strain rate. Indeed, this method is not a practical method as it may involve several trial and error tests to obtain a good match with the oedometer test results.

Table 2.6 Strain-rate values used for CRS testing on clays

Authors	Soil	Strain-rate range (s^{-1})
Hamilton and Crawford (1959)	Undisturbed Leda Clay	8.3×10^{-7}, 2.5×10^{-5}, 1.3×10^{-5}
Sällfors (1975)	Swedish high plastic Bäckebol clay	$5\times10^{-7} – 2\times10^{-5}$
Leroueil et al. (1983a)	Canadian soft clays	$4\times10^{-8} – 4\times10^{-5}$
Leroueil et al. (1985)	Canadian soft clays	$1.7\times10^{-8} – 4\times10^{-5}$
Mesri and Feng (1986)	Berthierville Clay	8×10^{-7}
Yin and Graham (1989)	Reconstituted illite	3.7×10^{-6}
Kim and Leroueil (2001)	Berthierville Clay	6.35×10^{-6}
Seah and Juirnarongrit (2003)	Bangkok Clay	$0.3\times10^{-6} – 5\times10^{-6}$
Cheng and Yin (2005)	Hong Kong Marine Clay	1.7×10^{-5} and 1.7×10^{-4}
Leroueil (2006)	Canadian soft clays	10^{-6} and 4×10^{-6}
Sorensen (2006)	Reconstituted London Clay	2.3×10^{-7}
Sorensen (2006)	Reconstituted Kaolin Clay	$2.3\times10^{-7} – 3\times10^{-5}$
Tsutsumi and Tanaka (2012)	Reconstituted Osaka and Kasaoka Clays	3×10^{-8} and 3×10^{-6}
Tong and Yin (2013)	Hong Kong Marine Clay	1×10^{-5}
Jarad (2016)	Arginotech Clay	3.3×10^{-5}, 3.3×10^{-4}, 1.7×10^{-4}

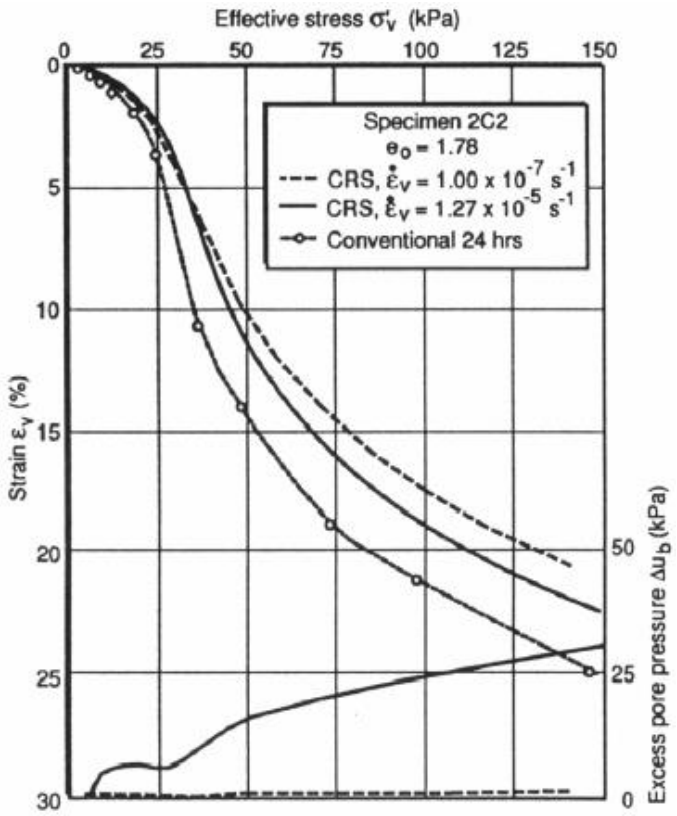


Figure 2.38 Aging effects on 1D stress–strain behaviour (Leroueil et al., 1996)

2.5.1.3 Strain-Rate Effects on Compression Behaviour

Leroueil et al. (1985) conducted a series of CRS tests on a variety of Chaplain Sea Clays and showed that the σ'_p tends to increase with increase in $\dot{\varepsilon}_v$ (Figure 2.39). The authors also observed higher pore pressure increase at higher strain-rates from the CRS tests conducted on Batiscan Clay. The u_{exc} values were very small and negligible at strain-rates lower than 5×10^{-7} s^{-1}. Similar results, i.e. the higher the strain-rate, the higher the effective stress at a given strain, were reported by Cheng and Yin (2005) from a series of CRS tests on Hong Kong marine clays. The authors also obtained higher σ'_p values from CRS tests than the conventional MSL oedometer tests (Figure 2.40). Increase in σ'_p with increase in $\dot{\varepsilon}_v$ was also reported by Seah and Juirnarongrit (2003) from a series of CRS consolidation tests with permitted radial flow on soft Bangkok Clay. The authors also pointed out the independency of the horizontal coefficients of permeability and consolidation to the strain-rate.

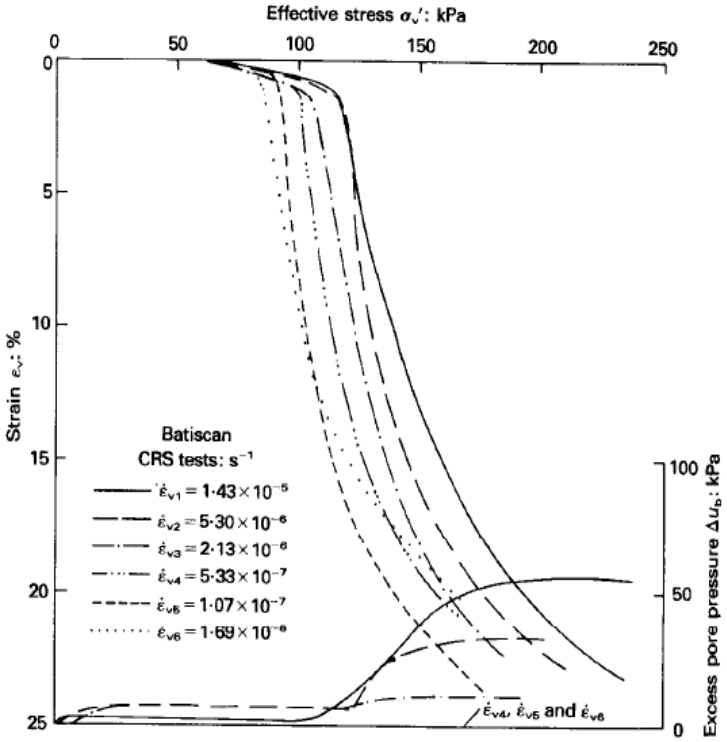


Figure 2.39 Effect of strain-rate on preconsolidation pressure from CRS oedometer test results on Batiscan Clay (Leroueil et al., 1985).

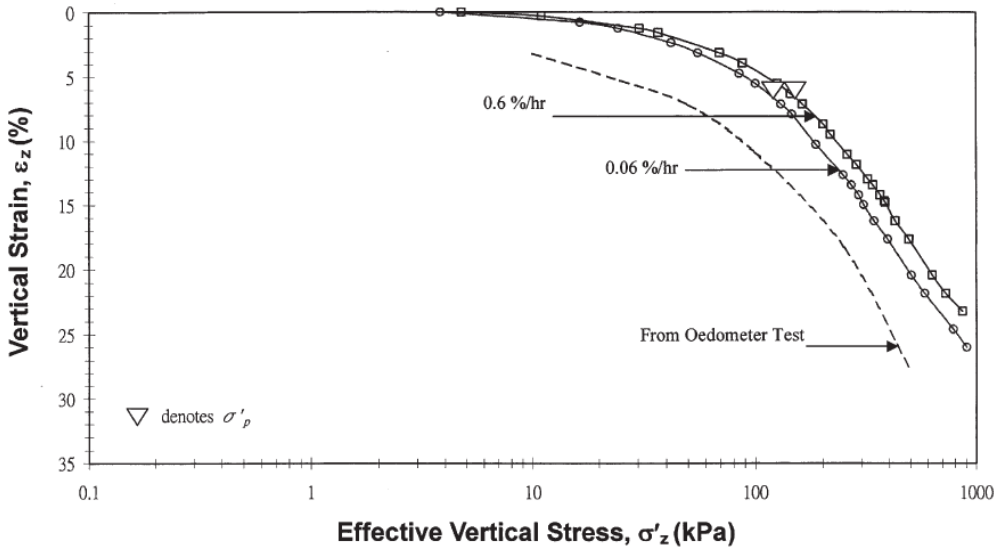


Figure 2.40 CRS oedometer test results on Hong Kong marine clay (Cheng and Yin, 2005).

In one of the most recent studies, Jarad (2016) studied the effect of strain-rate on compression behaviour of two lightly overconsolidated (OC) clays in a series of CRS tests, and reported an increase in σ'_p with increase in strain-rate (Figure 2.41). A slight increase of m_v and c_v coefficients with increase in strain-rate was also observed.

However, the C_c and C_s indices were found to be independent of the strain-rate change. It was also shown that the permeability and hydraulic conductivity of the specimens increased with increase in strain-rate.

Soga and Mitchell (1996) reviewed the published results of 1D compression tests on a variety of clays and reported that the apparent σ'_p increases linearly with $\dot{\varepsilon}_v$, if plotted on a log-log scale, for about 10–20% per log cycle increase in $\dot{\varepsilon}_v$ (Figure 2.42).

The following relationship for coupling apparent σ'_p (yield limit) with $\dot{\varepsilon}_v$ was proposed by Leroueil et al. (1985);

$$\log_{10}(\sigma'_p) = A + \frac{1}{m'}\log_{10}(\dot{\varepsilon}_v) \qquad 2.22$$

where, A and m' are material parameters. Equation 2.22 reveals a linear relationship between σ'_p and $\dot{\varepsilon}_v$ on a log σ'_p – log $\dot{\varepsilon}_v$ plot.

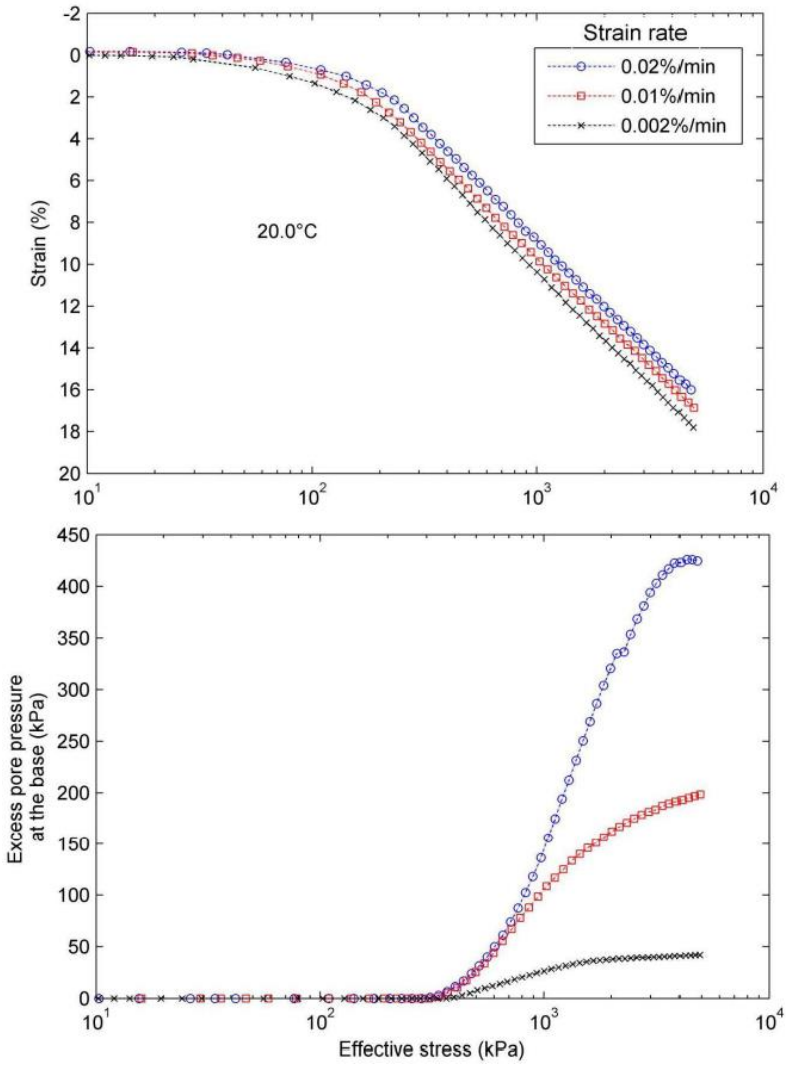


Figure 2.41 Effect of strain-rate on the effective stress–strain curve and u_{exc} (Jarad, 2016)

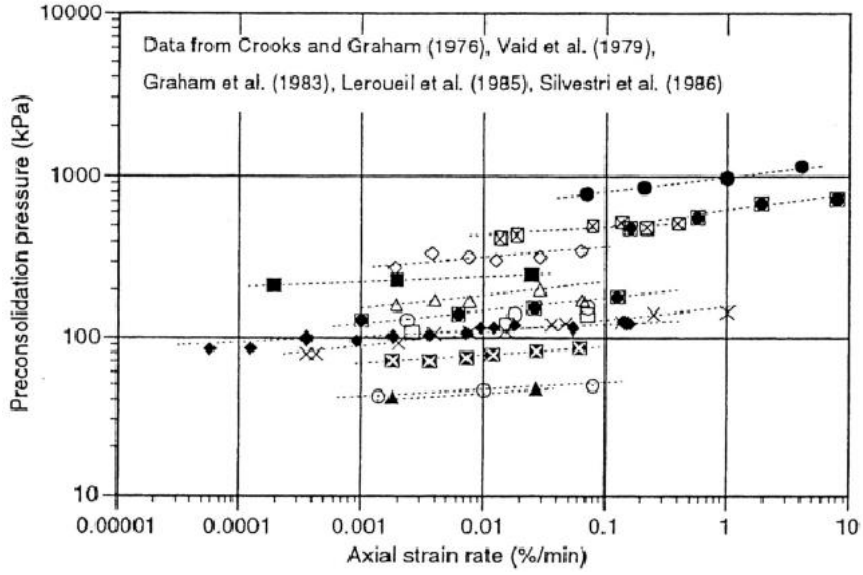


Figure 2.42 Effect of strain-rate on σ'_p from 1D compression tests on NC and slightly OC soft clays (Soga and Mitchell, 1996)

Richardson and Whitman (1963) suggested step-wise change in strain-rate (SRS) tests to be performed for investigation of the effect of change in strain-rate on the stress–strain behaviour. During a SRS test, the portions of the stress–strain curves corresponding to different strain-rates are obtained. These portions are then extrapolated to obtain the complete stress–strain curves. Several researchers including Leroueil et al. (1985), Cheng and Yin (2005), and Sorensen (2006) have performed SRS tests. It was, however, found that the SRS curves did not completely match with the continuous CRS curves.

2.5.1.4 The Concept of Isotach or Strain-Rate Lines

Leroueil et al. (1985) showed that there is a unique relationship between the vertical effective stress (σ'_v), strain (ε_v), and strain-rate ($\dot{\varepsilon}_v$). This relationship is known as Isotach behaviour and was first introduced by Suklje (1957). In other words, the Isotach concept states that the current stress is a unique function of strain and its rate. The Isotach concept also indicates that in the case of change in $\dot{\varepsilon}_v$, the stress–strain curve will be immediately shifted to that corresponding to the new $\dot{\varepsilon}_v$ and it stays on the same stress–strain curve until the $\dot{\varepsilon}_v$ is changed again (Figure 2.43). Vaid and Campanella (1977) stated that the unique $\sigma'_v - \varepsilon_v - \dot{\varepsilon}_v$ relationship is independent of the test type. The Isotach behaviour is also independent of the strain history, and has been reported as the characteristic of the majority of soft clays, stiff clays, and soft rocks, in both reconstituted and intact states, under drained and undrained conditions, and in oedometric and triaxial stress spaces (Sorensen, 2006). For instance, the Isotach behaviour was captured in CRS oedometer tests reported on Hong Kong marine clays (Cheng and Yin, 2005), stiff plastic Kitan and Oimachi clays (Komoto et al., 2003), and reconstituted Kaolin Clay and London Clay (Sorensen, 2006). However, it has also been shown in the literature that development of structural resistance during compression at very small strain-rates or non-isothermal conditions, can result in non-Isotach stress–strain behaviour (Tatsuoka et al., 2008, Tsutsumi and Tanaka, 2011, Tsutsumi and Tanaka, 2012).

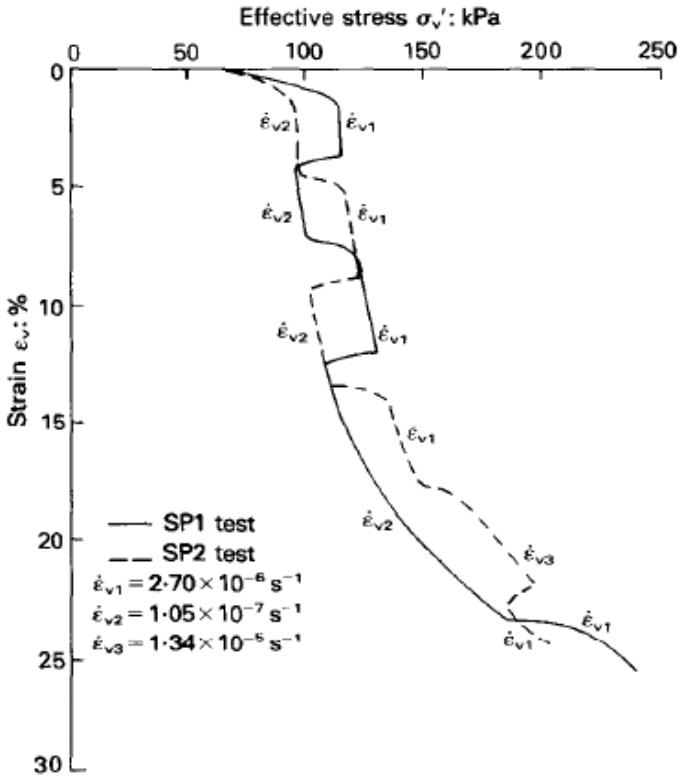


Figure 2.43 The Isotach concept from SRS oedometer test results on Batiscan Clay (Leroueil et al., 1985).

2.5.2 Strain-Rate Effects on Oedometric Behaviour of Unsaturated Clays

From the literature review, it is found that the different aspects of rate-dependent behaviour for a variety of saturated geo-materials, especially soft clays, and under diverse testing conditions have been relatively extensively studied. Yet, very few studies have been reported on the rate-dependent behaviour of clays, in particular stiff clays, under unsaturated conditions. Similar to the saturated clays, CRS tests can be used to investigate the compression behaviour of unsaturated clays. However, as there is no available guideline for appropriate strain-rate selection, the unsaturated CRS test procedure may become more complicated. For unsaturated soils, the CRS test can be conducted in two ways; (1) constant matric suction (CS-CRS) tests, and (2) constant water content (CW-CRS) tests (Wijaya et al., 2014).

Muñoz-castelblanco et al. (2011) investigated the behaviour of a natural aeolian loess by conducting a series of CW-CRS oedometer tests at three different strain-rates of 0.003, 0.010, and 0.059 %/min (Figure 2.44). The fast test was found to match better with the results of the incremental loading (IL) oedometer test. Increase in strain-rate

also appeared to increase the slope of NCL in the post-yield regime. The ordering of σ'_p with strain-rate was, however, not clear. Instantaneous and fast loading associated respectively with IL and fast CW-CRS tests, could have caused destruction of the specimens' structure and hence, development of lower σ'_p values.

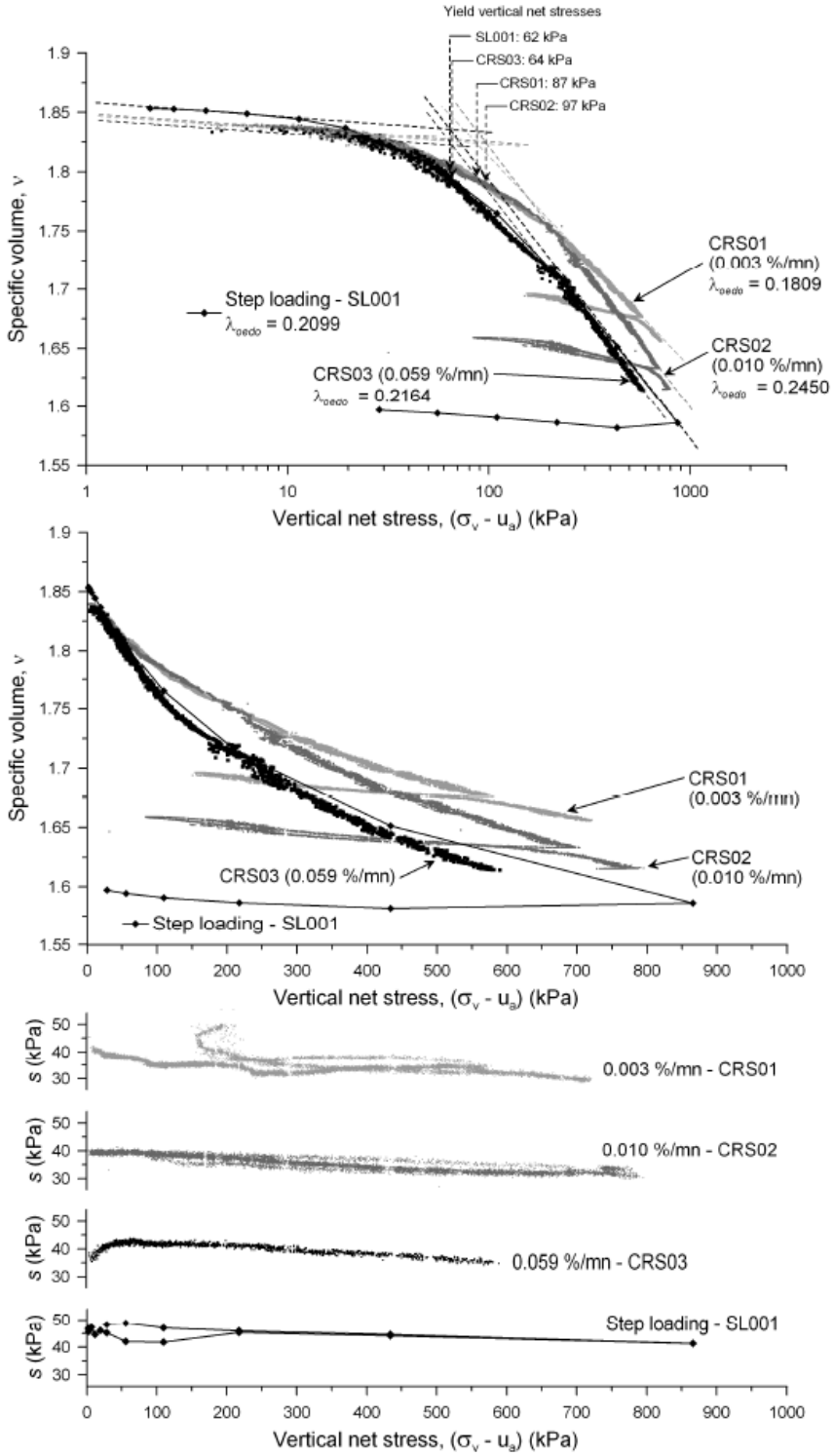


Figure 2.44 Effect of strain-rate in CW-CRS tests on aeolian loess (Muñoz-castelblanco et al., 2011)

Results of CW-CRS tests performed on unsaturated reconstituted kaolin clay at different strain-rates were reported by Wijaya et al. (2014). Change in u_w was measured throughout the tests using a HCT accommodated at the base of the specimen. The authors stated that increase in strain-rate resulted in a decrease in compressibility of the specimens before reaching the saturated compression curve (apparent unsaturated σ'_p), from which the unsaturated compression curves were merged with the saturated compression curve (Figure 2.45). For the fast compression test, having a strain-rate of 0.1 mm/min (corresponding to 8.3×10^{-5} s^{-1}), development of a higher u_{exc} was observed. Moreover, the deviation of the pore-water pressure curve of the fast test from those of the medium and slow rate tests was attributed to non-uniform change of u_w in the specimen due to the fast loading rate, which resulted in development of a time-lag in measurement of u_w by the tensiometer.

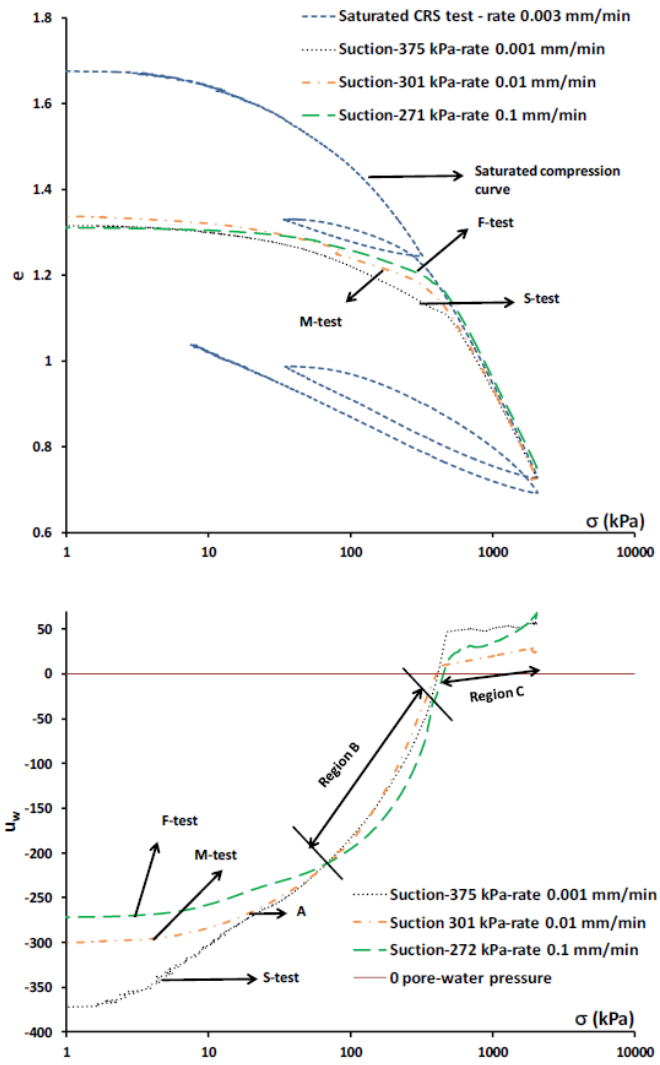


Figure 2.45 Results of unsaturated CRS tests on reconstituted kaolin clay at different strain-rates (Wijaya et al., 2014)

From these two sets of information, a firm conclusion as to whether the increase in strain-rate results in decrease or increase of σ'_p, or the slope of NCL in unsaturated clays, may not be drawn. Further investigations on various soil types are needed to confirm the existence of such trends, as reported for saturated clays (section 2.5.1.3).

2.6 Stress-Relaxation in Saturated vs. Unsaturated Clays

In this section, the concept of stress-relaxation, an important time- and rate-dependent phenomenon in clays, and the correlations between time- and rate-dependent soil parameters are discussed. Stress-relaxation in unsaturated states has not received much attention in the literature. The only reported work by Wang et al. (2017), is, however, discussed.

2.6.1 Stress-Relaxation in Saturated Clays

In practice, construction often involves stages of constant total strain in a soil body during which the deviatoric stress decreases continuously with time at a very slow rate. This phenomenon is known as "stress-relaxation" and is defined as the change in effective stress with time at zero rate of strain. According to Lade et al. (2009), the mechanism of relaxation at a micro-level is controlled by the variations in geometrical configuration of the soil particles with time. Stress-relaxation has been observed in problems associated with excavations where a short-term change in lateral earth pressure is observed after installation of retaining and support systems. In the literature relatively few studies can be found that investigate the stress-relaxation behaviour under various conditions (Lacerda and Houston, 1973, Yin and Graham, 1989, Sheahan et al., 1994, Ladanyi and Benyamina, 1995, Fodil et al., 1997, Kim and Leroueil, 2001, Yin and Hicher, 2008, Tong and Yin, 2013, Yin et al., 2014). According to Ladanyi and Benyamina (1995), investigation of the stress–strain–time behaviour of soils can be done more conveniently by performing stress-relaxation tests rather than conventional creep tests, especially for monitoring failure states. However, due to the lack of a unified and widely accepted formulation for correlating stress-relaxation and strain-rate-dependency and creep parameters, stress-relaxation tests have not been widely used for determination of the time-dependent response of soft soils (Yin et al., 2014).

The relaxation test is in fact a special CRS test with zero strain-rate. If at stress state A [Figure 2.46(a)] the stress-relaxation process is initiated by keeping the total strain

constant over time [Figure 2.46(b)], the sample undergoes a decrease in stress over time towards point B [Figure 2.46(c) and (d)]. This is called relaxation of stresses. Relaxation tests are carried out to measure change of effective stress with time in 1D or triaxial straining conditions. The 1D relaxation tests on a saturated clayey soil can be performed in both creep and swelling regions. To observe the effect of stress-relaxation in swelling (increase of effective stress with time), the strain-rate is set to zero after unloading the specimen to certain stress states (Tong and Yin, 2013). In saturated stress-relaxation tests in the swelling region, the sample will absorb water during zero straining. During this stage, the pressure required to keep the sample at the required strain level is called the swelling pressure (Yin and Tong, 2011).

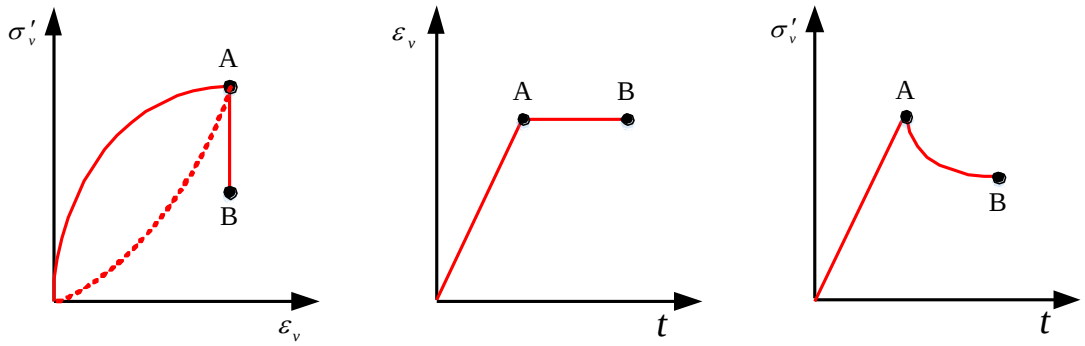


Figure 2.46 Relaxation test (A→B): (a) stress-strain relationship; (b) strain history; (c) stress history

Lacerda and Houston (1973) stated that for states not close to failure, the pattern of stress-relaxation is very similar to deformations observed during creep. Stress-relaxation in clays have been extensively studied in the past few decades from drained and undrained triaxial tests on various clays (e.g. Arai, 1985, Oda and Mitachi, 1988). The results obtained have indicated linear change in principal stress with logarithm of time. However, no unified conclusion has been made on the effects of stress application mode, imposed strain level, and strain-rate prior to the stress-relaxation stage. Fodil et al. (1997) performed drained triaxial stress-relaxation tests on clay samples, obtained from 9 m depth of the Le Flumet dam foundation in France, at different initial strain-rates (3.33×10^{-8} s^{-1}, 3.33×10^{-7} s^{-1}, and 3.33×10^{-6} s^{-1}) and measured relaxation of stresses at different strain levels (1.0%, 3.5%, and 6.7%). The authors concluded that:

- The subsequent stress–strain behaviour was not affected by the stress-relaxation phases and the same stress–strain trend was followed by the sample as that of obtained from tests without relaxation steps.
- Stress-relaxation is directly proportional to the applied strain-rate before the start of relaxation. In fact, a higher applied strain-rate results in a higher change in effective stress with time during zero straining (see also Tong and Yin, 2013).
- At constant initial strain-rate, change in effective stress level is decreased with increase in strain level.

Leroueil and Marques (1996) proposed a relationship between stress-relaxation and creep at constant stress state. In the elastic region, and in a given direction, the change in the current stress ($\Delta\sigma$) is linked to the change in current elastic strain (ε^e) and is given by;

$$\Delta\sigma = E_{\max}\Delta\varepsilon^e \qquad 2.23$$

where E_{max} is the elastic stiffness modulus. Total strain-rate ($\dot{\varepsilon}^t$) is also calculated as the sum of elastic strain-rate ($\dot{\varepsilon}^e$) and the visco-plastic strain-rate ($\dot{\varepsilon}^p$);

$$\dot{\varepsilon}^t = \dot{\varepsilon}^e + \dot{\varepsilon}^p \qquad 2.24$$

During a creep test, the applied stress is constant, hence $\dot{\varepsilon}^e = 0$ and $\dot{\varepsilon}^t = \dot{\varepsilon}^p$. In a stress-relaxation test the total strain is constant, hence $\dot{\varepsilon}^t = 0$ and $\dot{\varepsilon}^e = -\dot{\varepsilon}^p$. Considering $\dot{\varepsilon}^p$ to be positive during a creep stage after loading, $\dot{\varepsilon}^e$ becomes negative. This implies that during stress-relaxation, both ε^e and σ will reduce. Therefore, it can be concluded that the rate of change in stress and elastic strain during a stress-relaxation stage is directly linked to the rate of change of visco-plastic strains during a creep stage.

2.6.1.1 Stress-Relaxation in Oedometric Conditions

Inspection of the experimental stress-relaxation results indicates a linear relationship between the vertical effective stress and time in ln σ'_v – ln t space during relaxation of the stresses (Yin et al., 2014). Hence, the slope of this line can be considered as the coefficient of stress-relaxation, R_α;

$$R_\alpha = -\frac{\Delta \log(\sigma'_v)}{\Delta \log(t)} \qquad 2.25$$

Yin and Graham (1989) performed a stepped CRS oedometer test on reconstituted illite with a single stage relaxation at the end of stepped loading. The relaxation coefficient was reported as R_α = 0.042. A CRS oedometer test with three relaxation stages at different strain levels was conducted by Kim and Leroueil (2001) on Berthierville Clay. The specimen was loaded at a constant rate of strain of 6.35×10^{-6} s^{-1} and the relaxation stages were set at 0.59, 4.45, and 13.40% strain levels (Figure 2.47). An average R_α = 0.0657 was measured. Stress-relaxation tests on reconstituted London Clay were reported by Sorensen (2006). The specimen was loaded in a CRS cell to 2.0 MPa vertical stress and then stress-relaxation was allowed for 4 days. The time required for dissipation of u_{exc} , developed during the drained loading stage, was more or less equal to the period considered for the stress-relaxation stage (i.e. 4 days), although it was reported that the total vertical stress continued to reduce linearly with logarithm of time after the EOP state was achieved. Dissipation of u_{exc} typically results in change in strain level and hence specimen volume change. In such a case, the reduction in stress may not be fully associated with the stress-relaxation phenomenon.

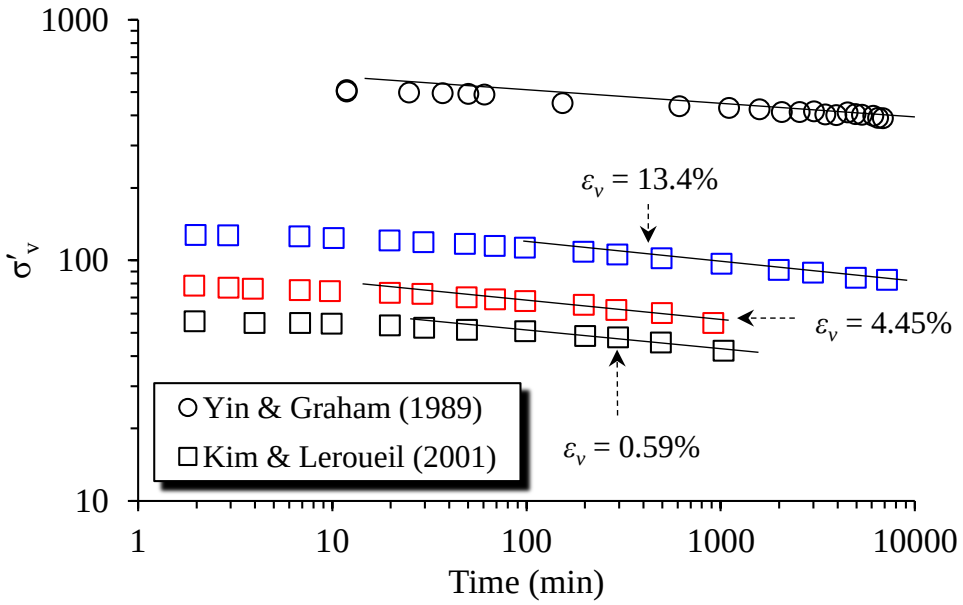


Figure 2.47 Results of stress-relaxation tests on reconstituted illite (re-drawn after Yin and Graham, 1989) and Berthierville Clay (re-drawn after Kim and Leroueil, 2001)

2.6.1.2 Empirical Approaches for Formulation of Stress-Relaxation

Different approaches for formulation of stress-relaxation in oedometric and triaxial stress space are available. As the focus of this thesis is on 1D time- and rate-dependency in clays, the mathematical descriptions of the empirical approaches for characterisation of stress-relaxation in oedometric conditions will be presented here.

In one of the first attempts, the effective vertical stress decay with time observed in 1D stress-relaxation tests was formulated by Yin and Graham (1989) as;

$$\sigma'_v = \sigma'_{vi}\left(\frac{t_{ie}+t_0}{(C_c/C_s)t+t_{ie}+t_0}\right)^{C_{\alpha e}/C_c} \qquad 2.26$$

where σ'_{vi} is the initial effective vertical stress at the start of stress-relaxation, t_0 is the reference time, and t_{ie} is the equivalent time and expressed as;

$$t_{ie} = -t_0 + t_0 \exp\left(\left(\varepsilon_v - \varepsilon_{v0}^{ep}\right)\frac{1+e_0}{C_{\alpha e}}\ln 10\right)\left(\frac{\sigma'_v}{\sigma'_{v0}}\right)^{-C_c/C_{\alpha e}} \qquad 2.27$$

In Equation 2.27, ε_{v0}^{ep} is the elastoplastic strain at $\sigma'_v = \sigma'_{v0}$.

An analytical solution for 1D stress-relaxation was proposed by Yin et al. (2014). This model which was developed based on the rate-dependent elasto-viscoplastic model of Yin et al. (2010), expresses the evolution of vertical stress during relaxation as;

$$\sigma'_v = \left[A(1-m)t + \sigma'^{1-m}_{vi}\right]^{1/(1-m)} \qquad 2.28$$

where A and m are constant values and determined using;

$$A = -\dot{\varepsilon}_v^r \frac{\ln 10(1+e_0)(C_c-C_s)}{C_c C_s}\left(\frac{1}{\sigma'^r_{pi}.\sigma'^{C_s/(C_c-C_s)}_{vi}}\right)^{\beta} \qquad 2.29$$

and

$$m = \frac{C_c\beta}{C_c-C_s}+1 \qquad 2.30$$

In Equation 2.29, $\dot{\varepsilon}_v^r$ is the reference volumetric strain-rate, σ'^r_{pi} is the initial value of the current reference stress corresponding to the start of stress-relaxation, and β is the rate-dependency coefficient representing the slope of the linear relationship log (σ'_p) – log ($d\varepsilon_v/dt$). Leoni et al. (2008) defined the rate-dependency coefficient as;

$$\beta = \frac{C_c - C_s}{C_{\alpha e}} \tag{2.31}$$

Consequently, the relaxation coefficient can be derived using;

$$R_\alpha = \frac{C_c - C_s}{C_c \beta} \tag{2.32}$$

or

$$R_\alpha = \frac{C_{\alpha e}}{C_c} \tag{2.33}$$

The sequence of the above equations indicates a unique relationship between R_α, $C_{\alpha e}$, and β, highlighting the advantages of stress-relaxation tests for deriving time-dependent parameters. As mentioned earlier, the stress-relaxation test is a CRS test with zero strain-rate. Therefore, the time required for determination of time-dependent parameters such as $C_{\alpha e}$, can be significantly reduced by simply measuring the relaxation coefficient from a relatively fast (2-3 days for compression up to ε_v = 20%) CRS compression test followed by a one day stress-relaxation stage.

2.6.2 Stress-Relaxation in Unsaturated Clays

Stress-relaxation in unsaturated conditions has not received much attention in the literature. To the best of the author's knowledge, the only reported work on unsaturated stress-relaxation behaviour is the work of Wang et al. (2017) who performed a set of triaxial stress-relaxation tests on unsaturated lime-treated expansive clays of Hefei Xianqiao Airport site in China, at suctions of 50 and 100 kPa, and studied the effects of pre-relaxation strain level, pre-relaxation strain-rate, and relaxation time. The authors reported that the stress-relaxation stage can be divided into three phases. At the start of the relaxation stage, first a sharp decline in the relaxation curve, resulting from fast dissipation of the accumulated energy in the specimen, is observed (instantaneous

relaxation). The rate of dissipation of energy is then decreased slowly (decelerated relaxation) until it reaches a steady state (nearly non-relaxation). Moreover, for stress levels below peak deviator stress, larger relaxed stresses were observed with increase in pre-relaxation strain. Conversely, for stresses higher than the peak strength, smaller relaxed stresses were observed for higher pre-relaxation strain levels. Unlike the linear relationship suggested for saturated clays in the literature (e.g. Arai, 1985, Oda and Mitachi, 1988), the change in deviatoric stress with logarithm of time during the relaxation stage was found to be nonlinear. Furthermore, similar to the observations reported by Fodil et al. (1997) on saturated clays, a small pre-relaxation strain level was found to increase the magnitude of the instantaneous relaxation, and the duration to reach the non-relaxation state for unsaturated lime-treated clays. Lower stress relaxation rates were also observed for higher pre-relaxation strain-rates. Overall, the pre-relaxation conditions were reported to have negligible effects on the general stress relaxation characteristics, i.e. the consequence of three relaxation phases as explained above. The brittleness of the tested sample was also reported to have a significant influence on the relaxation process. Despite these findings, a clear explanation of the effect of suction on the stress-relaxation response was not provided.

2.7 Concluding Remarks

In this chapter, the time- and rate-dependent behaviour of clays in saturated and unsaturated states was reviewed. The following remarks can be drawn:

- The response of unsaturated clays during primary consolidation is not solely governed by the state of suction, and that, it is, in fact, the combination of multiple factors such as soil fabric, inter-particle bonding, pore-size distribution, and suction that determines the response of an unsaturated clayey soil.
- The mechanism of creep in clays is relatively complex. Several mechanisms for creep have been proposed in the literature highlighting the influence of factors such as viscosity of pore fluid, soil structure and particle arrangement, clay mineral–water interactions, deviatoric stress, and temperature gradients. However, as of today, the mechanism of creep in unsaturated clays, including the role of water menisci and contractile skin, has not been studied.

- The assumption of a linear relationship between the creep strain and the logarithm of time is not valid, as it has been shown that C_α is influenced by several factors such as soil structure, consolidation pressure, and temperature.
- The ratio C_α/C_c, initially believed to be a constant value, was found, from recent experimental investigations on soft clays, to be actually inconstant. However, the C_α/C_c ratio in stiff clays such as London Clay has been rarely investigated. Moreover, there is not currently any reported work evaluating the C_α/C_c ratio for unsaturated clays.
- There is a linear relationship between the logarithm of creep rate and logarithm of time for saturated clays. However, as yet, the influence of change in degree of saturation, and consequently suction state, on this relationship has not been investigated.
- Under unsaturated conditions, increase in suction results in a decrease in 1D creep strain-rate for ashy soils, chalks, and rockfill material. Similar results have also been reported for clayey soils in triaxial stress space. Analogous to saturated soils, creep strains increase with increase in applied vertical stress in unsaturated conditions.
- The rate-dependent behaviour of clays can be conveniently studied from 1D CRS oedometer tests. The CRS test is a standardised test and an overwhelming amount of information on selection of appropriate strain-rate for a saturated CRS test is available. However, there is no available guideline for determination of a suitable strain-rate for unsaturated CRS tests.
- The apparent preconsolidation pressure (σ'_p) increases linearly with strain-rate, if plotted on log-log scales. However, the effect of strain-rate on m_v, c_v, C_c, and C_s is not clear and requires further investigation.
- Most clays, including soft and stiff clays, have been shown to exhibit Isotach behaviour in CRS tests. Whether the Isotach concept will be followed by a clayey soil subjected to suction variations, is a question that has not yet been answered.
- Relatively few works have been reported on the effect of strain-rate on compression behaviour of unsaturated clays. As a result, a firm conclusion as to whether the increase in strain-rate results in decrease or increase of σ'_p, or the slope of NCL in unsaturated clays cannot be drawn. Further investigations on

various soil types are needed to confirm the existence of such trends, as reported for saturated clays.

- The phenomenon of stress-relaxation in saturated clays, both in oedometric and triaxial stress states, has been rather comprehensively studied in the past few decades. However, the reported results exhibit discrepancies, resulting in the lack of a unified statement on the effects of stress application mode, imposed strain level, and strain-rate prior to the stress relaxation stage.
- CRS oedometer tests with stages of stress-relaxation can be effectively used for determination of time-dependent parameters such as $C_{\alpha e}$. A unique relationship between the relaxation coefficient (R_{α}), creep index ($C_{\alpha e}$), and rate-dependency coefficient (β) has been proposed in the literature. However, the applicability of such a relationship for unsaturated clays has not yet been validated based on 1D stress-relaxation tests on unsaturated clays.

As can be seen, the viscous behaviour of unsaturated clays, in particular stiff clays, has not received much attention, leaving a significant gap of knowledge regarding the mechanics of unsaturated clays. In the following chapters, it will be attempted to answer some of the questions raised based on an extensive experimental program conducted on London Clay.

CHAPTER 3: SOIL SAMPLING & BASIC CHARACTERISATION

3.1 Introduction

Characterisation of time- and rate-dependent response of saturated natural soft clays has received a significant attention in the past few decades and a large number of studies can be found in the literature. This is deemed to be mainly due to the significant amount of primary and secondary consolidation (creep) in soft clays that if not controlled may cause significant damages to the geostructures. The concepts of creep and time-dependency in natural stiff clays, however, have not been the subject of numerous studies, perhaps due to the observation of lower time-dependent deformations in stiff clays in comparison with the soft clays. This is while the ratio of the secondary to primary deformations in stiff clays is significant, arising the need for further characterisation of the factors (e.g. stress level, suction, etc.) influencing the consolidation process in stiff clays. A natural stiff clay, namely London Clay, was, therefore, chosen for this study. A large number of studies can be found in the literature on characterisation of the hydro-mechanical properties of this material. This fact, allows for comparison of the new findings with the existing data. Moreover, a number of active engineering sites on deep London Clay deposits were also available, where the available on-site machinery could help in facilitating the soil sampling procedure.

The samples of London Clay used in this study were extracted from a site on the Isle of Sheppey, near Kent, UK. In this chapter, first a description of the undisturbed soil sampling techniques and the quality of obtained samples from each method are discussed. Afterwards, an overview of the geological origin and physical properties of the London Clay formation in general, and the London Clay deposits in the east of England (Sheppey Member) in particular, is presented. Then, the details of the site where the undisturbed soil samples were extracted, along with the procedures followed for sampling, transportation, and storage of the undisturbed block samples, are described. The different types of laboratory specimens and the methods used for preparation of the testing specimens are then discussed. Finally, the measured physical and hydro-mechanical properties of the recovered samples are presented and discussed with reference to the literature.

3.2 Samples Quality and Sampling Techniques

The quality of soil samples is a key factor for adequate determination of the geotechnical properties. For example, Fodil et al. (1997) stated that sample disturbance can have significant impacts on determination of σ'_p. Typical sampling techniques are outlined as; block sampling, rotary core sampling, drive sampling (open drive samplers and piston drive samplers), and augur sampling.

Block sampling is referred to as careful excavation of a soil profile around the sample position, and the hand trimming of a regular-shaped block (Clayton et al., 1982). Block sampling allows for complete stress relief, and hence soil expansion, however, this method is believed to produce the best quality samples of heavily overconsolidated soils such as London Clay.

Another method for undisturbed soil sampling is the use of drive samplers. Drive samplers, including thin-walled and thick-walled open-drive samplers, thick-walled open-drive split barrel samplers, the British Standard general purpose U100 sampler, Swedish piston samplers, and Laval samplers are in general screw-threaded tubes with a sharp cutting edge at their end, that are gently pushed into the ground without rotation. The cut soil mass is slid into the tube and collected by separating the soil and tube from the cutting shoe and sampler head after sampling.

Rotary core sampling is another method for undisturbed soil sampling. The rotary core samplers are relatively thicker than drive samplers and possess a less sharp cutting surface (Clayton et al., 1982). The sampler is basically a powered rotary cutting head on the end of a hollow steel shaft which is rotated and driven gently into the soil. This method is typically used for coring samples in weak and weathered rocks, and stiff and hard clays.

Augur sampling is the simplest method of soil sampling and often produces disturbed samples (ASTM-D1452-09, 2009). The augers are drilled into the soil to the certain depths, and when withdrawn to the ground surface, the soil samples are collected. Its application is restricted to the drilling of shallow depth unconsolidated materials (Shuter and Teasdale, 1989).

Normally, the drive, rotary core, and auger sampling methods exert some degree of disturbance to the soil structure. Several criteria have been proposed in the literature for assessment of the quality of undisturbed soil samples. Lacasse et al. (1985) stated that volumetric strain at effective overburden pressure, obtained from compression curves, can be used as an index for measurement of the quality of undisturbed samples. Using this criteria, Sun et al. (2014) studied the quality of undisturbed samples of seven marine clays (from the Yangtze River Delta, China) retrieved using block sampling, thin-wall open-drive sampling, and thick-wall open-drive sampling methods and categorised the quality of the obtained samples as fair, poor, and very poor quality respectively (Figure 3.1). The effect of degree of sample disturbance was also confirmed from the results of compression tests on the undisturbed samples, where the block samples with minimum degree of disturbance presented a clear structural yielding point on the compression curve, whereas the thick-wall samples exhibited a compression characteristic very similar to that of reconstituted samples, mainly due to the significant disturbance of the samples during sampling. Hight et al. (2007) reported that the quality of rotary-cored samples of London Clay from Heathrow Airport Terminal 5 site was in general similar to the quality of block samples, highlighting the influence of structural properties of stiff clays such as London Clay that allows for retrieving high quality samples using the rotary core sampling method.

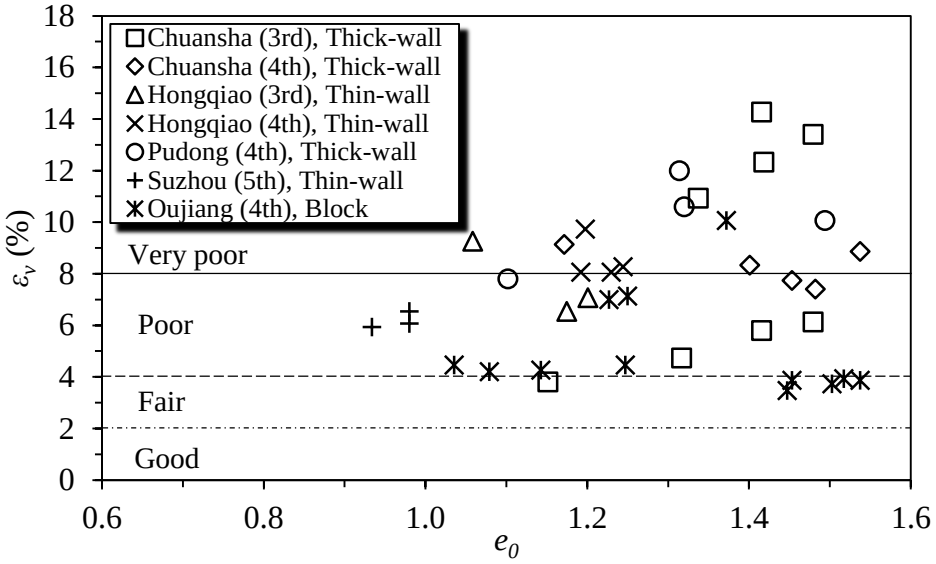


Figure 3.1 Quality analysis of undisturbed samples taken by different sampling methods – The numbers in the brackets correspond to the number of the soil layer (re-drawn from Sun et al., 2014)

EN-ISO-22475:1 (2006) classifies the quality of samples obtained from different sampling methods into three categories;

- Category A: This category contains block, rotary core, and drive sampling methods. Using these methods, samples of quality class 1 to 5 can be obtained.
- Category B: This category contains rotary core, drive, and augur sampling methods. Using these methods, samples of quality class 3 to 5 can be obtained.
- Category C: This category contains augur sampling method. Only samples of quality class 5 can be obtained using this sampling technique.

The five sample quality classes are classified based on the soil properties that remain unchanged during the procedures of sampling, transportation, and storage (BS-EN-1997:2, 2007). Table 3.1 describes the quality classes together with the recommended sampling categories to be used.

Based on the above discussion, block sampling can be considered as a suitable sampling method which if performed adequately can produce class 1 quality samples of natural clays with minimum to negligible level of disturbance to the soil structure. It must be mentioned here that, apart from the possible disturbance to the soil samples during sampling, packing, transport, and storage, other interrelated factors such as stress release, mechanical deformation, change in water content, chemical changes and temperature changes can also cause sample disturbance (Clayton et al., 1982).

Table 3.1 Quality classes of soil samples for laboratory testing (BS-EN-1997:2, 2007)

Soil Properties/Quality Class	1	2	3	4	5
Unchanged Soil Properties:					
Particle size	*	*	*	*	
Water content	*	*	*		
Density, density index, permeability	*	*			
Compressibility, shear strength	*				
Properties that can be determined:					
Sequence of layers	*	*	*	*	*
Boundaries of strata – broad	*	*	*	*	
Boundaries of strata – fine	*	*			
Atterberg limits, particle density, organic content	*	*	*	*	
Water content	*	*	*		
Density, density index, porosity, permeability	*	*			
Compressibility, shear strength	*				
Sampling category according to EN-ISO-22475:1	**A**				
			B		
					C

3.2.1 Effect of Sampling Method on Soil Suction Measurement

Information on the *in-situ* soil suction has various applications in characterisation of soil profiles. For instance, Skempton (1961) suggested an equation to derive the k_0 profile from block samples of London Clay;

$$s_k = \sigma'_v[k_0 - A_s(k_0 - 1)] \tag{3.1}$$

where, s_k is the initial suction corresponding to the triaxial stress state at which the sample neither swells nor consolidates, and A_s is the excess pore-water ratio corresponding to the removal of the deviatoric stress (Bishop et al., 1965). In order to obtain the variations of k_0 with depth, suction measurements are carried out on undisturbed samples retrieved from both shallow and deep depths. Rotary core, thick-wall, and thin-wall sampling methods are typically used for deep sampling. Suction measurements on rotary core and thin-wall samples of London Clay from Heathrow Terminal 5 site were reported by Georgiannou and Hight (1994). The authors used a HCT developed at Imperial College (Ridley and Burland, 1993) to measure suction on extracted samples immediately after sampling. Suction measurements on rotary core samples were assumed to be lower than the true *in-situ* values due to the effect of the fluid in the core barrel which wets the sample and, therefore, lowers the suction. Suction measurements on thin-wall samples were assumed to be more representative of the actual *in-situ* suction. The local consolidation of the samples due to the edge effects associated with thin-walled samplers can increase the suction. However, it was believed that the centreline effect counterbalanced the edge effect by slightly reducing the suction, hence, enhancing the reliability of the measurements. Although the use of thin-walled samplers can to some extent minimise the soil disturbance, however, this method is not recommended for sampling stiff and very stiff clays, hard soils, soils containing gravel or larger size soil particles, cemented soils, or unsaturated soils (ASTM-D1587-00, 2000). Most recently, Tarantino et al. (2016) proposed an effective method for deep suction measurements which eliminates the need for deep sampling and its associated errors. The authors installed a HCT on a penetrometer shaft having the same size as a CPT shaft, and pushed into the ground using the common method of CPT shaft penetration.

There is a relation between the suction of a sample and the state of the stress corresponding to the depth at which the sample has been extracted (Skempton and Sowa, 1963, Bishop et al., 1975, Doran et al., 2000). Bishop et al. (1975) reported that in the case of isotropic elastic samples extracted from the field, employing a "perfect sampling" procedure, the soil suction is equal to the mean effective stress supported by the sample prior to extraction. However, it was found by Doran et al. (2000) that this hypothesis cannot be true in the case of anisotropic elastic soils mainly due to the coupling of the volumetric strain with deviatoric stress during unloading. Bishop et al. (1975) proposed a range of $s_0/\sigma'_v = 0.35 – 0.75$ during unloading of natural clays. Here, s_0 is the initial soil suction and σ'_v is the *in-situ* vertical effective stress. Delage et al. (2007) obtained a range of $s_0/\sigma'_v = 0.94 – 1.42$ from the oedometer tests on block samples of Boom Clay extracted from a deep excavation (223 m) in Mol, Belgium. The authors attributed this higher obtained range to the effects of drying that occurred in the period between sampling and performing the tests (3 years). It can be concluded, from the above discussion, that careful precautions must be taken when measuring suction on undisturbed soil samples, as the disturbance caused during sampling can result in misleading measurements.

3.3 Sampling Programme

3.3.1 The London Clay Formation

According to Aldiss (2014), "The London Clay mainly comprises bioturbated or poorly laminated, blue-grey or grey-brown, slightly calcareous, silty to very silty clay, clayey silt and sometimes silt, with some layers of sandy clay". London Clay is normally classified as an overconsolidated fissured stiff clay of high plasticity (Nishimura, 2005). A sketch map of the London Clay formation outcrop (Bouch, 2006) is shown in Figure 3.2.

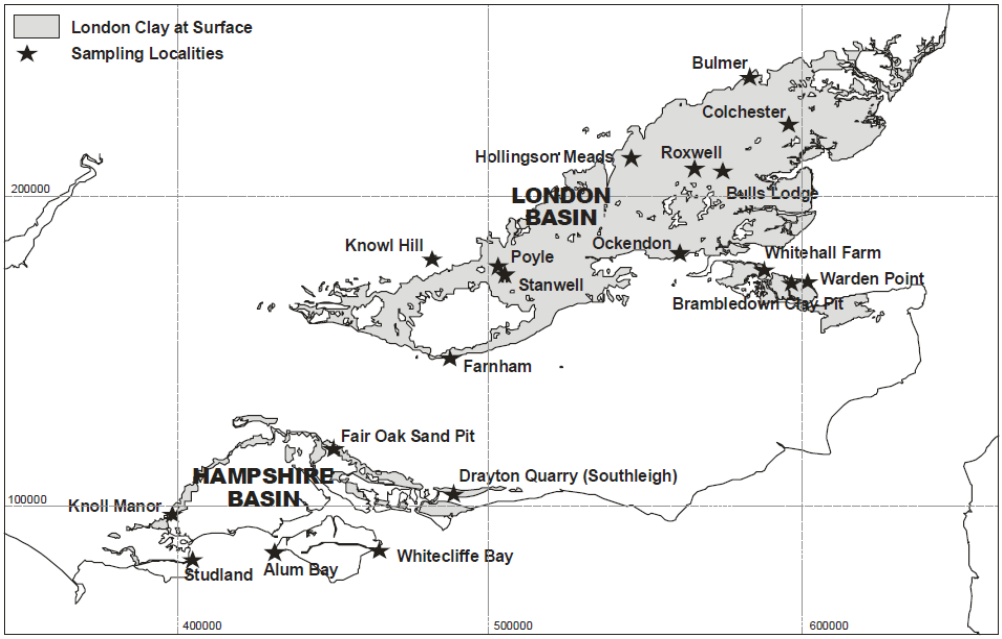


Figure 3.2 Sketch map of the London Clay formation outcrop (Bouch, 2006)

As shown in the figure, London Clay deposits are mainly present in the south-east of England (London basin) as well as the south coast and Isle of Wight (Hampshire Basin). The thickness of the London Clay deposits is estimated to be between 50 m and 150 m in the London basin and 50 m to 130 m in the Hampshire basin (Gasparre, 2005). Its clay fraction varies between 40~60%. The dominant clay minerals are montmorillonite and illite (Gilkers, 1968). Other minerals are mainly kaolinite and chlorite. The plasticity index (I_p) across the London Basin has been estimated to be in range of 40~50 in the west and around 70 in the east (Nishimura, 2005). The brown, brownish grey, or mottled brown and grey coloured London Clay, typically found in the top 5 to 10 m depths, has been recognised as weathered London Clay and contains selenite crystals (a form of gypsum – hydrated calcium sulphate) (Hight et al., 1993, Aldiss, 2014). Figure 3.3 shows the presence of selenite crystals in London Clay samples.

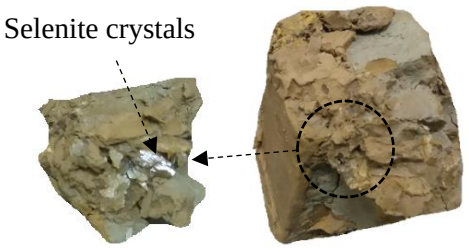


Figure 3.3 Selenite crystals in London Clay sample from Isle of Sheppey

King (1981) studied the biostratigraphy and lithological variations of London Clay formation and based on the identification of marine flooding events, cycles of sea rise and fall, presence or absence of laminations, and variations in silt and sand content, suggested a division of the formation into five principal units, named Divisions A to E (see Figures 3.4 and 3.5). This division has been found to be laterally and vertically consistent with the observations of stratigraphic boreholes drilled throughout the London Basin (Royse et al., 2012). Another series of divisions was also suggested by Ellison et al. (2004). The divisions of King (1981) are subdivided into several members within the London Clay Formation, named as; Walton, Claygate, Ockendon, Aveley, Sheppey, and Bracknell Members. Further information about the stratigraphy of London Clay and associate deposits can be found in King (1981) and Freeborough et al. (2006).

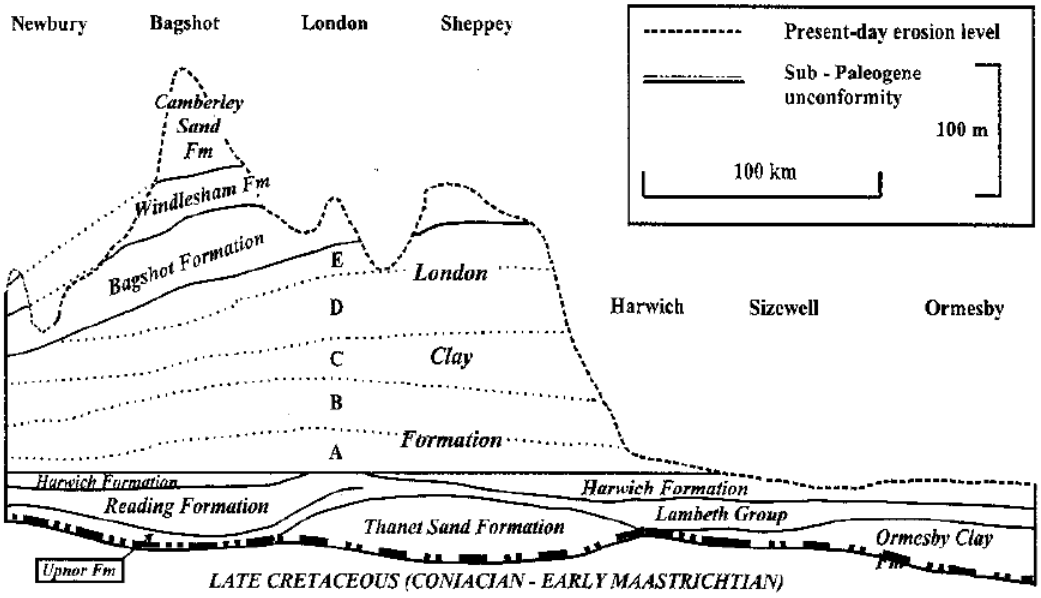


Figure 3.4 Divisions of London Clay formation (King, 1981)

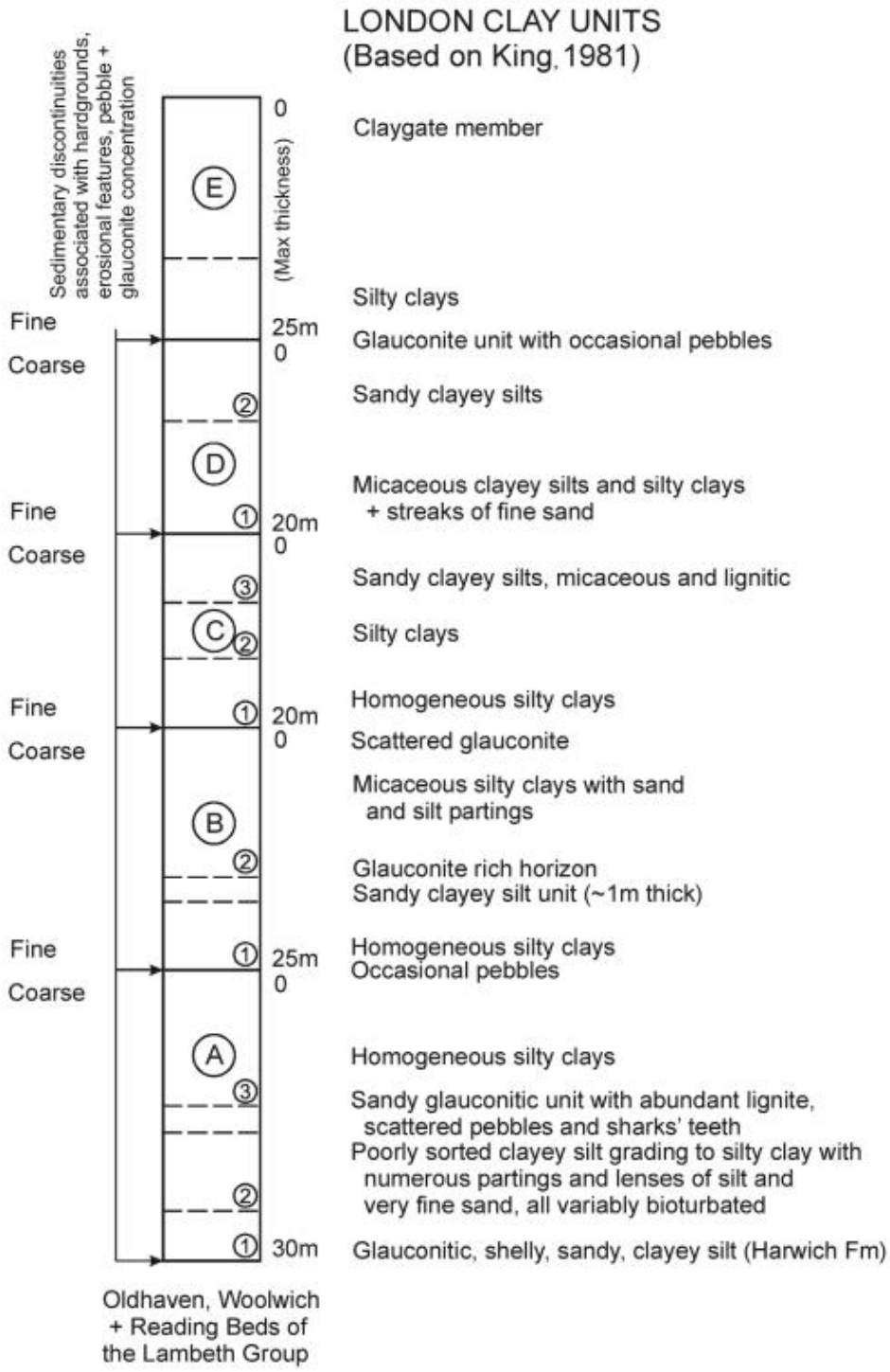


Figure 3.5 Lithological units in London Clay (from Hight et al., 2003)

3.3.2 Geological History and Physical Properties of the Sheppey Member

The London Clay formation in Sheppey Cliffs, Isle of Sheppey, Kent, which exposes the upper part of the London Clay formation is named Sheppey Member and corresponds approximately to the upper part of Division C, Division D and most of Division E (King, 1981). The thickness of the Sheppey Member is approximately 55 m

and is classified as Thames Group. According to Aldiss (2014) "The Sheppey Member comprises silty clay diffusely interbedded with sandy clayey silt; it is commonly glauconitic. There are several layers of calcareous concretions. The top of the Sheppey Member is marked by a change upwards from silty clay with common sandy clayey silt interbeds to silty clay with sandy laminae, of the Claygate Member. The base of the Sheppey Member is marked by a change upwards from mainly homogeneous silty clay of the Aveley Member to silty clay with common sandy clayey silt interbeds". Figure 3.6 presents the geological formations in Isle of Sheppey. Burnett and Fookes (1974) reported that the Sheppey London Clay comprises of 58% of particles less than 2 µm size and 42% particles greater than 2 µm size. The particles < 2 µm size were approximately 90% clay minerals which were found to comprise 57% montmorillonite, 24% illite, 12% kaolinite, and 7% chlorite. The particles > 2 µm size were mainly silt which was found to comprise 70% quartz carbonates, 15% pyrite, and 15% clay minerals.

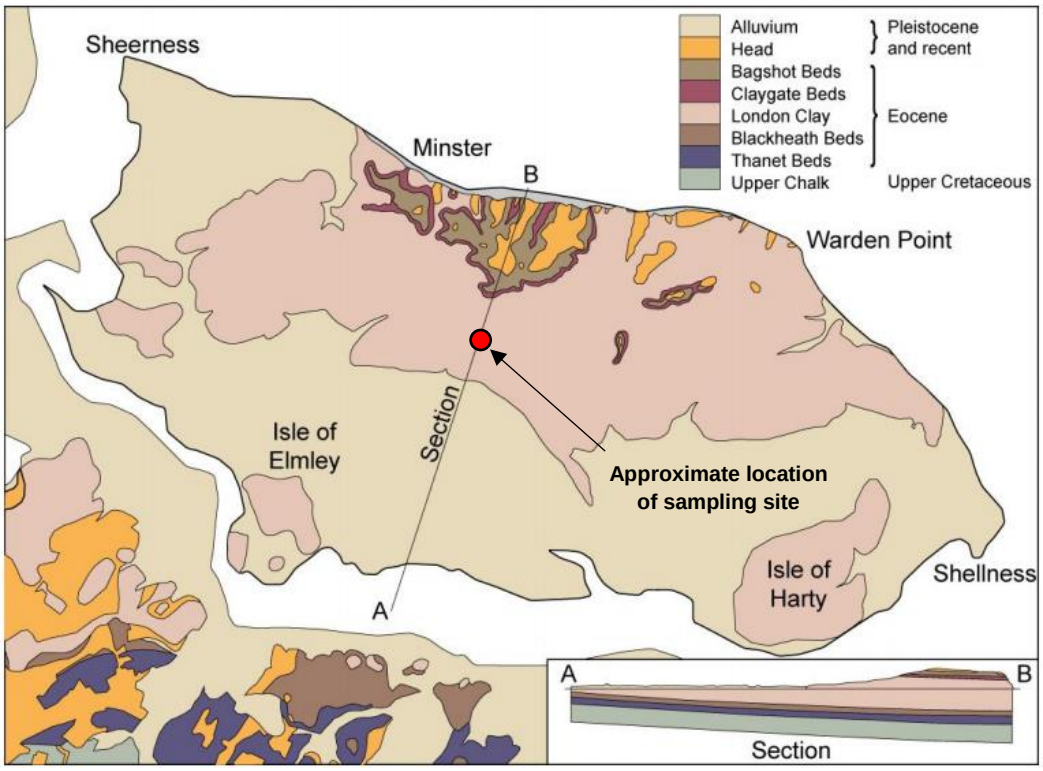


Figure 3.6 Geological formations in Isle of Sheppey (Young, 2014)

3.3.3 Sampling Site

The required information about the location of the London Clay formations was obtained from the Geology of Britain Viewer Web App provided by The British

Geological Survey (BGS). Active sites with London Clay deposits were identified through communication with corresponding companies and organisations. New Hook Farm located on the Isle of Sheppey was selected as a suitable site for soil sampling. New Hook Farm reservoir site is located on the outskirts of Sheerness town on the Isle of Sheppey, and is owned by SW Attwood & Partners Ltd. The principal operation of the site is a fishing pond and water reservoir and at the time of sampling it was in its initial stages of excavation. Figure 3.7 presents the site map of the sampling site.

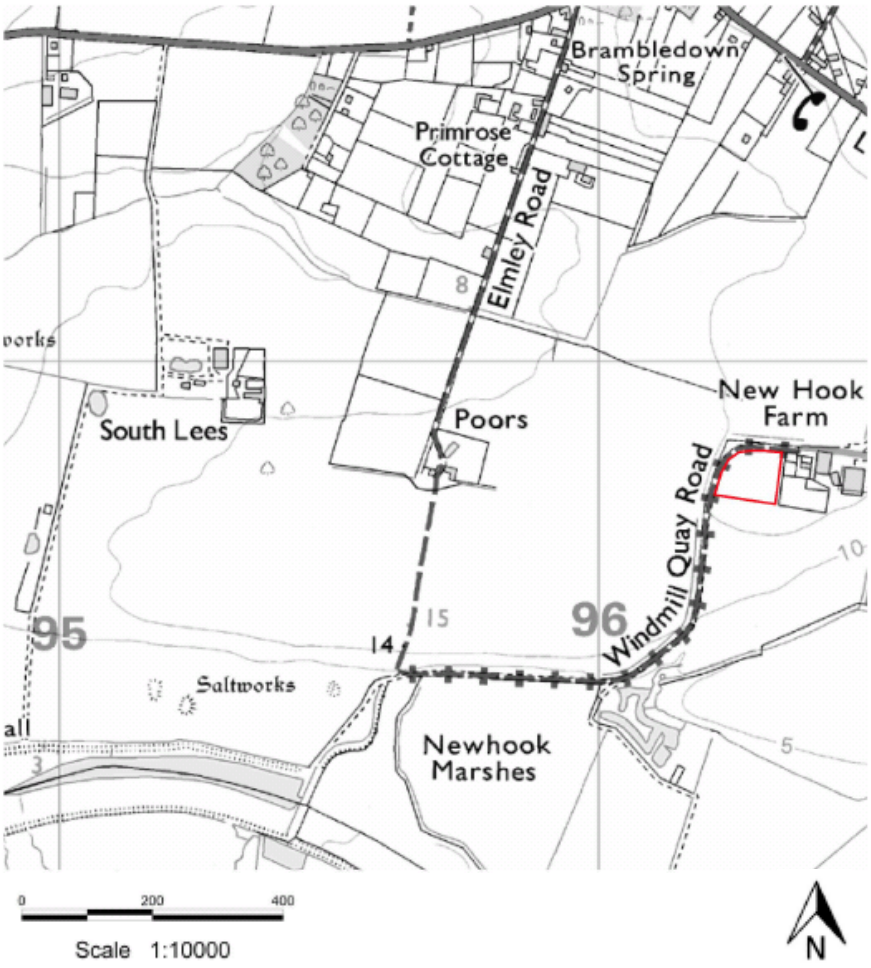


Figure 3.7 Site map provided by SW Attwood from Ordnance Survey National Geographic Database, 2014

3.3.4 Sampling Procedure

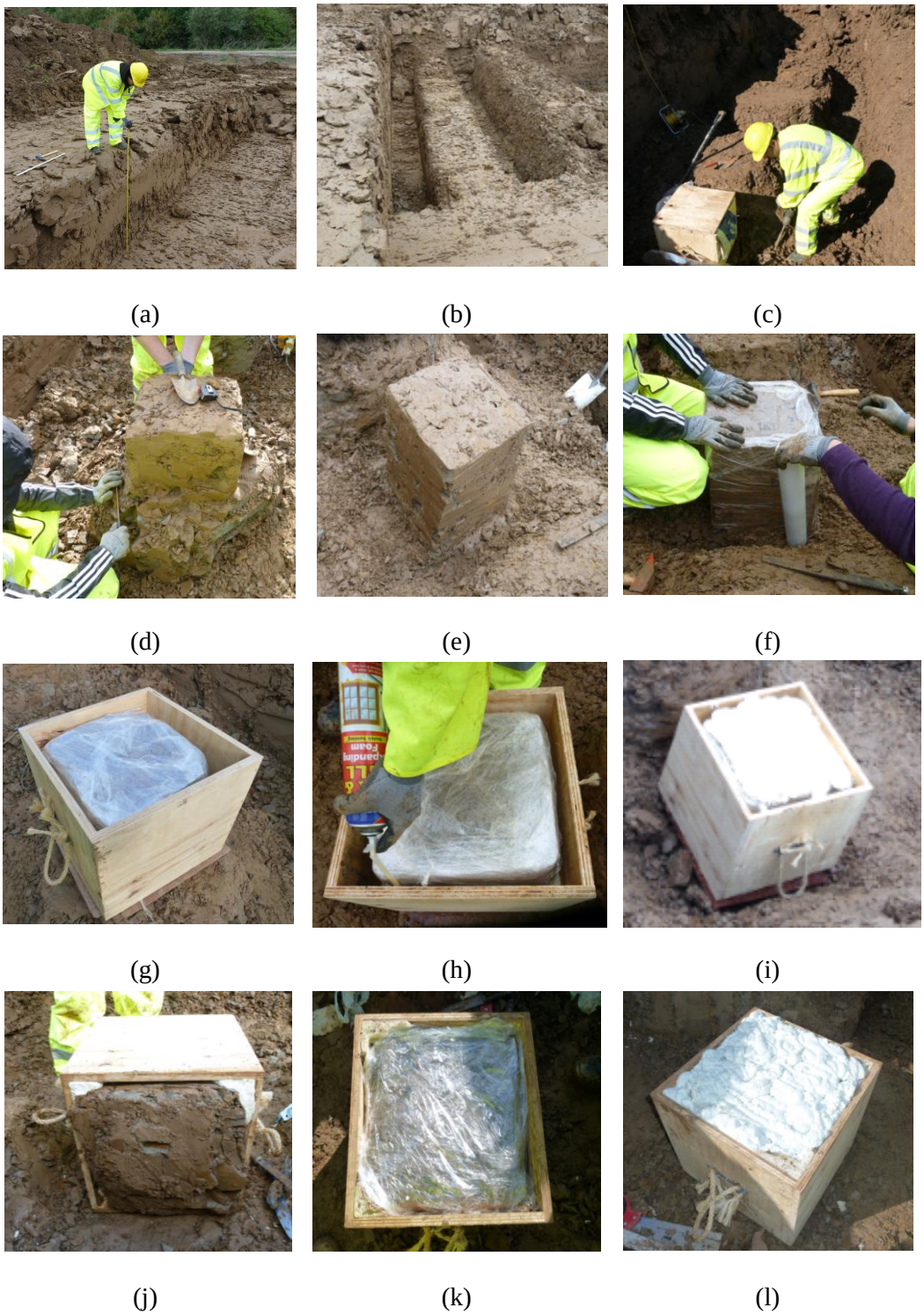
A comprehensive plan for sampling from New Hook Farm was developed including health and safety training, risk assessment, equipment preparation, excavation plan, travel and accommodation arrangements, sampling procedure, and transportation and storage of the recovered samples. Organisation and arrangements of the required

machinery for excavation was made by the site management (Attwood & Partners Ltd). The sampling procedure is described in the following steps;

a) Initially, an intact part of the ground was excavated to a depth of 4 m below the ground level. In order to avoid any disturbance to the samples, the material around the temporary profile was removed carefully so that a trench of approximately 0.8 m height, 1.5 m width, and 10 m length was made [Figures 3.8(a) and (b)].
b) From the trench, large cubical block samples of approximately 60 cm dimension were then prepared using a pneumatic clay spade [Figure 3.8(c)]. Careful operation of the clay spade at this stage was essential as the induced vibration during shaping of the block samples could cause major disturbance to the core block sample.
c) Final preparation and shaping of the block samples to the intended dimensions of 35×35×35 cm was then carried out manually using a soil saw and trimming knife. Due to the fissured nature of the soil (see also Gasparre, 2005), special attention was required during hand trimming the sample to its targeted dimensions [Figures 3.8(d) and (e)].
d) The prepared block samples were then thoroughly wrapped with several layers of Clingfilm to avoid moisture loss. It was also attempted to remove any air trapped between the sample and Clingfilm layers so that a perfect sealing was assured [Figure 3.8(f)].
e) Prefabricated loose lid and base plywood boxes with internal dimensions of 40 cm were then placed over the wrapped block samples [Figure 3.8(g)]. Polyurethane expanding foam was then injected in the gap between the sample and the internal walls of the wooden boxes in order to create a protective semi-elastic coating around the sample to prevent any possible sample disturbance during transportation [Figure 3.8(h)]. Although the required time for complete curing of the foam was 6 hours, it reached a workable condition about an hour after being exposed to the atmosphere. Nevertheless, the samples were left on the site for 12 hours in order to assure full curing of the foam [Figure 3.8(i)].
f) Samples were then cut and detached from the ground very carefully using soil saw [Figure 3.8(j)]. The cut bottom ends were shaped to a flat surface, covered with Clingfilm, and coated with polyurethane expanding foam [Figures 3.8(k)

and (l)]. Attention was given to establishing continuity between the cured foam on the sides of the sample and the applied fresh foam on the sample's base. Accurate sample depths and *in-situ* orientation were also noted.

g) Finally, the box lid was placed and screwed to the box body.



(a) (b) (c)

(d) (e) (f)

(g) (h) (i)

(j) (k) (l)

Figure 3.8 Block sampling procedure

3.3.5 Transportation and Storage

A plan was considered for safely transferring the prepared block samples to the ground surface and then transportation to the university and storage in the lab with minimum disturbance. Samples were brought up to the ground surface with the aid of an excavator. Samples were first placed very carefully in the excavator's bucket, lifted to ground level and then secured on wooden pallets. A lift truck was then used for lifting and accommodating the samples in the transit van. Samples were afterwards tightly fastened in the van using safety rope to minimise their displacement during the journey. Finally, the samples were stored in a temperature and humidity controlled room and the wooden boxes were wrapped again with Clingfilm and adhesive tape in order to avoid any unexpected moisture loss from the soil samples. Figure 3.9 illustrates the transportation and storage stages.



(a) (b)

(c) (d)

Figure 3.9 Transportation and storage of block samples: (a) loading samples to the excavator's bucket; (b) securing samples on the pallets at ground level; (c) accommodating samples in the transit van; (d) storage in a temperature- and humidity-controlled room.

3.4 Types of Specimens for Laboratory Testing

An important factor for selection of suitable types of samples for any experimental research in soil mechanics is the ability to reproduce samples with repeatable initial conditions such as structure, initial water content, and initial stress levels that best reflect the *in-situ* conditions (Saihi et al., 2002, Yin and Miao, 2013). In general, test specimens for laboratory experimental programs can be classified into three distinct categories; (1) undisturbed natural samples, (2) reconstituted samples, and (3) compacted samples. Natural clay samples are known with their structural features; fabric anisotropy and inter-particle bonding. Burland (1990) used the term "intrinsic properties" for the properties of reconstituted samples and stated that these properties are inherent to the soil and independent of natural states. Compacted samples are the artificially prepared samples where the totally remoulded soil materials are typically mixed with water at low water contents and compacted in a Proctor mould.

3.4.1 Undisturbed Specimens

Generally, the *in-situ* settlement rates of full-scale structures are much greater than those obtained from conventional oedometer tests on small size specimens (e.g. 75 mm diameter × 30 mm thickness). This can be attributed to the effect of the clay macro-fabric on drainage behaviour (Rowe and Barden, 1966). In fact, the macrostructural properties of clay layers such as the presence of thin layers of silt and sand, organic inclusions, and silt-filled fissures can increase the overall permeability of the clay deposit and hence increase settlement rates (Craig, 2004). Therefore, in order to obtain more realistic predictions of soil settlements in the laboratory, it is necessary to perform consolidation tests on specimens large enough to represent structural (macro-fabric) features of natural clays. It must be also noted that preparation of two identical natural samples is rarely the case (Hight et al., 2003).

Undisturbed soil specimens of natural clays are typically extracted and trimmed from block samples, U100 tubes, and thin-wall samplers. U100 samples can be directly (without trimming) used to prepare large diameter oedometer specimens and 100 mm diameter triaxial specimens. However, smaller size specimens should be trimmed from block samples or cylindrical U100 samples.

3.4.2 Reconstituted Specimens

There are normally two methods for preparation of reconstituted samples in the laboratory; column sedimentation, and conventional consolidation from slurry. In the column sedimentation method, a dilute soil slurry with a water content of up to 1200% is added to a column of saline water usually in several steps (Stallebrass et al., 2007). At each stage, the slurry is allowed to sediment under gravity forces until an equilibrium state is achieved. Finally, the sedimented sample is consolidated inside the column by applying incremental dead-weight loads to a submersible piston. At the end of the consolidation, subsamples of smaller sizes are cored or trimmed from the obtained soil cake. It must be mentioned here that the presence of salt in the water is basically to reproduce the condition that is more likely to occur during sedimentation of natural clays. Furthermore, water salinity can positively contribute in acceleration of the sedimentation process (Stallebrass et al., 2007). In general, with exception of sensitive clays, the pore-water chemistry has shown little impact on the mechanical response of reconstituted clays (Masin et al., 2003, Stallebrass et al., 2007).

The conventional method for preparation of reconstituted clays involves remoulding, de-airing, reconstitution of natural clay into a slurry with a water content of 1.5–2 times the liquid limit, and consolidation in floating ring consolidation tubes or large diameter moulds to the desired vertical effective stress levels (Saihi et al., 2002, Cunningham et al., 2003). Upon unloading, a small suction is generated in the sample. Therefore, a drained unloading stage might be reqired to release the initial developed suction (Cunningham et al., 2003).

Stallebrass et al. (2007) observed a layered soil fabric for London Clay samples prepared by the sedimentation method, whereas a random fabric was noted for samples prepared using the conventional consolidation method. A distinct difference in 1D compression behaviour of the reconstituted and sedimented specimens was reported by Masin et al. (2003) and Stallebrass et al. (2007). As mentioned in Chapter 2, the samples with flocculated (random) fabric exhibit more relative particle movements than the samples with dispersed fabric under the same stress increment. In the absence of inter-partcle bonds associated with the undisturbed clay samples, the reconstituted samples prepared from conventional 1D consolidation, can better serve for studying creep behaviour of saturated and unsaturated stiff clays where less creep deformation is

typically observed in comparison to soft clays. The main advantage of reconstituted samples is the ease of preparing identical samples. This is an important factor for studying the pre-failure deformation of stiff sedimentary clays, such as London Clay, that can be influenced by a number of factors (Hight et al., 2003).

3.4.3 Compacted Specimens

Raveendiraraj (2009) stated that pore-size distribution of reconstituted clay samples prepared from slurry is uni-modal and pore sizes are predominantly associated with micro-pores between particles rather than macro-pores. Such samples therefore possess high AEV of hundreds of kilopascals. This brings difficulties in investigation of properties of unsaturated soils in the laboratory where application or direct measurement of high soil suctions (i.e. using axis-translation or HCT) are limited. In such cases, compacted specimens can be considered as an alternative. Compacted samples are artificially prepared samples where the totally remoulded soil materials are typically mixed with water at low water contents and compacted in a Proctor mould. The pore-size distribution of samples compacted dry of optimum is essentially bi-modal (Raveendiraraj, 2009). These samples possess relative portions of micro-pores and macro-pores, and therefore, exhibit a lower AEV, which makes them more suitable for laboratory investigations where application or direct measurement of high suctions is restricted. Moreover, compacted soils are more suitable for investigation of collapse compression in wetting, than reconstituted (from slurry) samples as the absence of macro-pores in the latter may prevent observation of this phenomenon (Raveendiraraj, 2009). Compacted samples seem therefore to be a better choice for laboratory testing under unsaturated conditions. However, this method is also associated with some drawbacks. Compacting samples on the dry side of optimum results in aggregation of clay particles and hence development of a double-structure flocculated fabric, whereas, compacting samples on the wet side of optimum leads to development of a dispersed fabric (Alonso and Pinyol, 2008, Pillai et al., 2012). The initial conditions (e.g. dry density γ_d) of the compacted samples are highly dependent on the compaction method (dynamic or static), compaction energy, and initial water content. The density changes of the compacted soils are associated with the volume of macro-pores. At high suction values (low water contents), the macro-pores are relatively empty and therefore the effect of density on suction is negligible (Romero et al., 1999), whereas, at low suction

values (high water contents), this effect is more pronounced. Different microstructure and pore-size distribution are expected for soil samples compacted dry or wet of optimum to the same target density (Alonso and Pinyol, 2008). This can result in non-unique water retention behaviour even for a given density. Cycles of wetting and drying can also significantly modify the fabric of the compacted clayey soils (Cuisinier and Laloui, 2004). During drying, samples compacted dry of optimum exhibit higher stiffness than samples compacted wet of optimum (Sivakumar and Wheeler, 2000). Much attention is therefore to be given when preparing identical compacted samples for laboratory testing.

3.5 Preparation of Testing Specimens

To avoid complications associated with the micro-fabric of undisturbed and compacted samples, reconstituted samples were prepared to study the 1D stress–strain–time and stress–strain–strain-rate behaviours under unsaturated conditions. The intact soil samples were only used to study the 1D stress–strain–time behaviour under saturated conditions. To characterise the intrinsic response of the saturated London Clay samples, a series of 1D consolidation tests was also performed on corresponding reconstituted specimens (see Chapter 5).

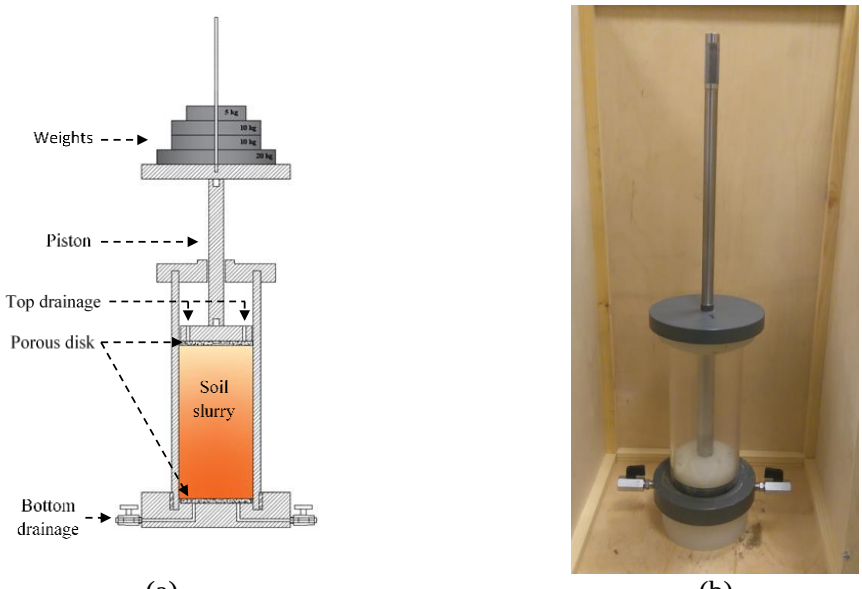
3.5.1 Undisturbed Specimens

To prepare undisturbed oedometer specimens from the block samples, the following procedure was followed. Initially, the block sample was trimmed into four pieces using an electric saw. Due to the fissured nature of the London Clay, during this step the soil sample was laterally supported by the plywood box. One of the quarter samples was used and the other three were immediately sealed with wax and Clingfilm and stored in air-tight containers to be used in the future. After carefully removing the plywood supports, foam layer, and Clingfilm, a cylindrical sample of approximately 100 mm diameter and 200 mm height was trimmed from the quarter sample using a wire saw. As suggested by Gasparre (2005), during hand trimming, about 5 measurements of water content of the sample were taken from the top and the sides of the sample to obtain the average water content of the prepared soil sample. The soil cylinder was then carefully cut into three equal pieces and oedometer specimens were cored from the subsamples using a 75 mm diameter and 20 mm high oedometer ring. It must be mentioned here that the fissured nature of the samples brought difficulties during the

hand trimming stage as the fissured samples tended to crumble. The same problem was also reported by Nishimura (2005) and Gasparre (2005) who performed a series of conventional and advanced laboratory experiments on undisturbed specimens of London Clay extracted from the Heathrow Airport Terminal 5 site.

3.5.2 Reconstituted Specimens

For preparation of reconstituted samples, initially the disturbed clay samples were oven dried at 105° C for a duration of 72 hours, then crushed into powder. Reconstituted soil samples were prepared by mixing the soil powder with distilled water at $1.5w_L$ until a homogenous paste was obtained. The paste was then consolidated in 100 mm and 120 mm diameter Perspex consolidometers (Figure 3.10) under a vertical stress of 80 kPa for durations of 5 and 6 days respectively. The samples were then quickly unloaded to minimise swelling and water absorption. Cylindrical samples were then cut into three equal pieces and allowed to dry at room temperature to pre-specified water contents (Figure 3.11). The unsaturated samples were then stored in air-tight containers for a duration of one week to attain moisture equilibrium. Finally, oedometer specimens were cored from the subsamples using a 75 mm diameter and 20 mm high oedometer ring. CRS oedometer specimens were cored from the 120 mm diameter subsamples using a 95 mm diameter and 35 mm high cutting ring. Preparation of the specimens is very important as the success of this research depends on the reproducibility of the initial state of the specimens.



(a) (b)

Figure 3.10 Perspex consolidometers: (a) schematic diagram; (b) photo



(a) (b)

Figure 3.11 Preparation of reconstituted samples: (a) cylindrical soil cake removed from the consolidometer; (b) approximately equal size cut pieces for oedometer and CRS specimens

Tarantino et al. (2011) described the path followed by a reconstituted sample during the course of 1D consolidation in a consolidometer and subsequent unloading and drying (Figure 3.12). The loading path starts from an initial state with void ratio being equal to water ratio e_w defined as the volume of water per volume of solids. With increasing vertical stress, the sample follows the normal consolidation line towards point A corresponding to the maximum value of the vertical stress σ'_{vc}. At this state the mean effective stress p'_c is given by;

$$p'_c = \frac{1+2k_0}{3}\sigma'_{vc} \tag{3.2}$$

Upon unloading the sample, and reducing the total vertical stress to zero, some water enters the pores, even if the unloading is done very quickly. The mean effective stress is therefore reduced to p'_0 (Point B). By removing the sample from the consolidometer, a suction equal to p'_0 is generated in the saturated sample. Since the AEV of the sample is higher than p'_c, drying the sample from this point follows the path B–A–C, with point C corresponding to s_{AEV} where the sample starts to desaturate. Note that for the suction range where the specimens remain saturated, the saturated mean effective stress equation $p' = p + s$, in which p is the mean total stress, can be used. In the normally-consolidated state, the coefficient of earth pressure at rest k_0 can be calculated as $k_0 = 1 - \sin\phi'$, with ϕ' being the effective angle of friction. This is, however, an assumption and may not be generalised.

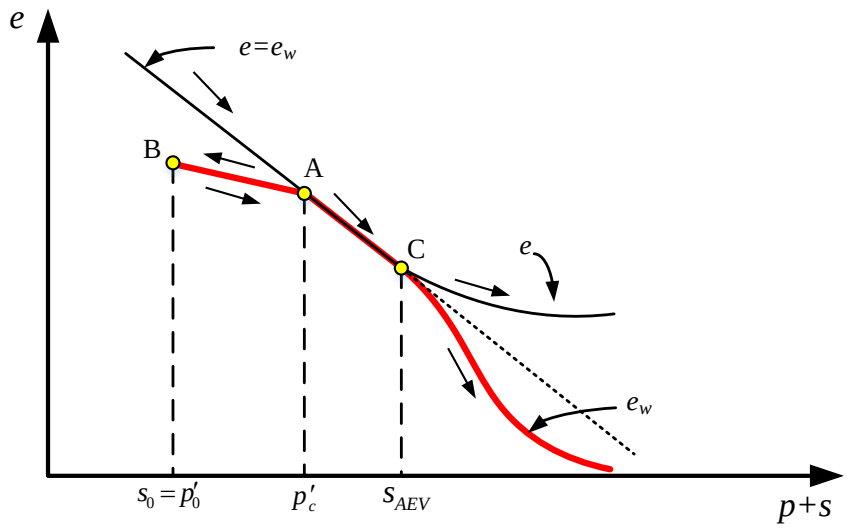


Figure 3.12 Hydraulic and mechanical paths associated with consolidation and drying (re-drawn from Tarantino et al., 2011)

3.6 Properties of the Sheppey London Clay

3.6.1 Index properties

The grading curve obtained from dry sieving and sedimentation tests (BS1377, 1990) is shown in Figure 3.13. The particle size distribution (PSD) curve of natural London Clay presents 98% particles passing through the 0.063 mm sieve. The clay, silt, and sand contents were obtained as 64%, 34% and 2% respectively. The sand and clay contents are important factors in governing the shrinkage and swelling of the samples. A lower clay content in the representative volume of the sediment, will induce less impact on the shrinking and swelling capacity of the sediment.

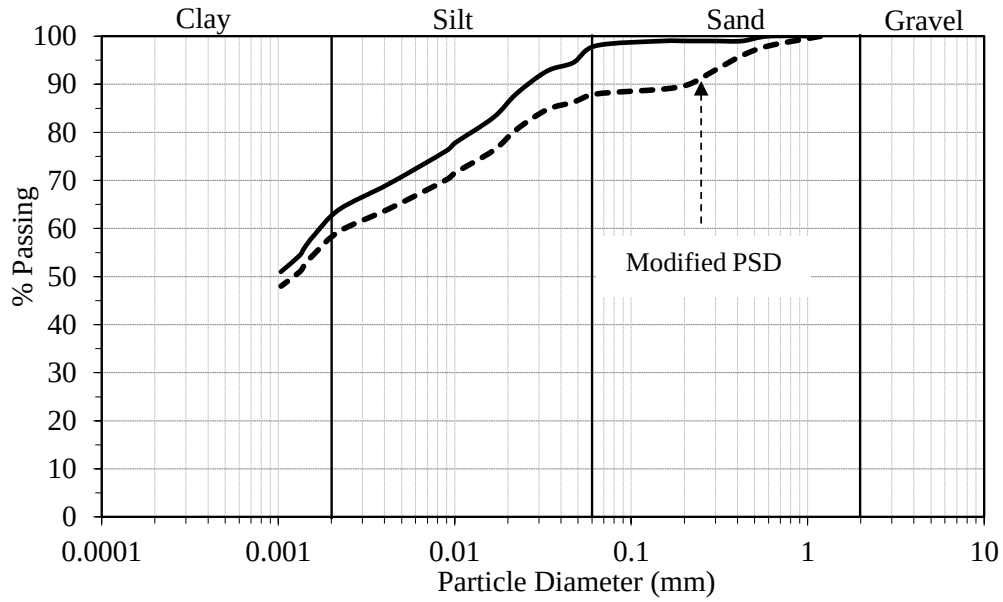


Figure 3.13 Particle size distribution (PSD) curve for Sheppey London Clay

The high content of fine grain inclusions results in an AEV of several megapascals as will be discussed later. In order to decrease the AEV, it was decided to slightly modify the PSD by adding some coarse-grained particles. The PSD was therefore modified by including larger sized peds, resulting from crushing the oven-dried samples, and passing through 1.18 mm sieve. The modified PSD exhibited an AEV of around 250 kPa which allows for testing specimens over a wider range of suctions lying on the transition (de-saturation) phase of the SWRC. It must be mentioned here that this material is not a dry version of the original material (Sheppey London Clay) but an artificially constructed material. The fabric, and probably chemical make-up, of the reconstituted samples are slightly different from the dried natural material and this, therefore, introduces some artificially and atypical fabric into the composite soil.

The index parameters and physical properties of the natural samples were measured and reported by CET Structures Ltd and are summarised in Table 3.2. Laboratory determination of index parameters confirmed the upper bound values of 24% and 78% for respectively plastic limit (w_p) and liquid limit (w_L) indices. These values are closely matched with w_p = 28% and w_L = 77% reported in literature for Sheppey London Clay (Jardine et al., 2003). Based on the USCS classification, the samples are classified as clay of high plasticity (CH).

Table 3.2 Physical properties of Sheppey London Clay samples as reported by CET Structures Ltd

Clay [%]	Silt [%]	Sand [%]	*in-situ* w [%]	w_P [%]	w_L [%]	G_s	k_v [m/s] at 20° C
64	34	2	29 – 35	19 – 24	70 – 78	2.67	2.5×10^{-10}

3.6.2 Macro-fabric

The macro-fabric of London Clay is characterised by the presence of discontinuities which play a significant role in its mechanical behaviour. These discontinuities are in the form of fissures, joints (or backs), bedding surfaces (or laminations), tectonic shear surfaces, recently formed shear surfaces, and minor faults (Skempton, 1964, Hight et al., 2003). For example, Skempton (1964) showed that the joints (large fractures) and fissures (small fractures) reduce the mass strength and allow the clay to soften. He also reported observation of local concentrations of shear stress, caused by joints and fissures, which if they exceed the peak strength can lead to progressive failure. Further information on the effects of laminations and fissures on standard tests can be found in Ward et al. (1965), Bishop et al. (1965), and Skempton et al. (1969).

Figure 3.14 depicts the heavily fissured and jointed pattern of the London Clay at shallow depth at New Hook Farm. Undisturbed block samples of London Clay were taken at 4 m depth below non-quarried ground level, where a slightly less fissured pattern was present.



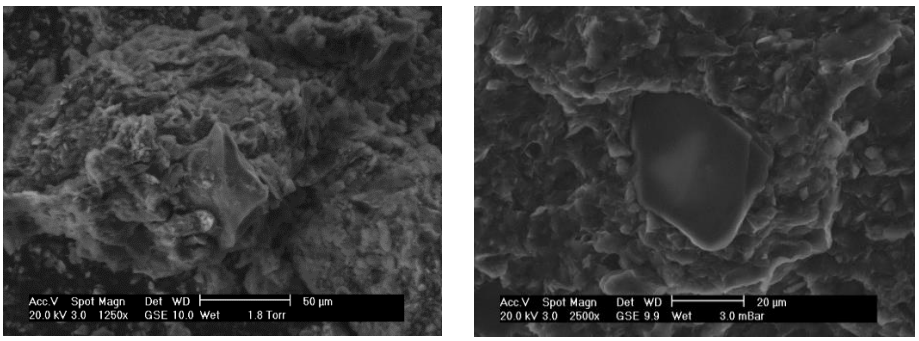
Figure 3.14 Fissured pattern at shallow depth at New Hook Farm reservoir site

3.6.3 Microstructure

To identify the basic structural properties (soil fabric) and chemical compositions of the retrieved London Clay samples, a microstructure and mineralogy analysis was carried out using an Environmental Scanning Electron Microscope (ESEM) and X-ray diffraction (XRD).

For ESEM analysis, cubic subsamples of approximately 1 cm^3 size were excavated from the central portions of the intact samples, and were air-dried. Fresh fracture surfaces were prepared for each stub by cutting with a scalpel. Special attention was given to minimise the specimen disturbance. As noted by Bouch (2006), the preparation of the surfaces using scalpel disturbs the soil structure to some extent. However, the relatively flat surfaces obtained allow for proper identification of the compositional variations. The air-dried ESEM specimens were then carbon-coated prior to testing. Note that in soft clays, as water evaporates from the pores, the soil fabric is modified. Therefore it is necessary to employ the freeze-drying technique to minimise disturbance to the soil fabric (Monroy et al., 2010). However, in stiff clays, the sample shrinkage during air drying does not significantly influence the soil structure (see Figure 3.18), thus the alternative method of air drying can be adopted (Gasparre, 2005). The stubs were analysed using a Philips XL30 FEG ESEM. The microscope has an Oxford Instruments INCA microanalysis system fitted with a Silicon Lithium detector and ultra-thin window for light element detection together with programs for digital X-ray mapping and line scanning for quantitative mineral identification and elemental analysis.

A general view of the specimen showing its relatively silty nature is presented in Figure 3.15. The sample contains irregular silt and sand-sized grains imbedded in the clay matrix.



(a) (b)

Figure 3.15 ESEM micrographs showing the coarser-grained particles imbedded in the clay matrix at magnification of: (a) 1250x; (b) 2500x

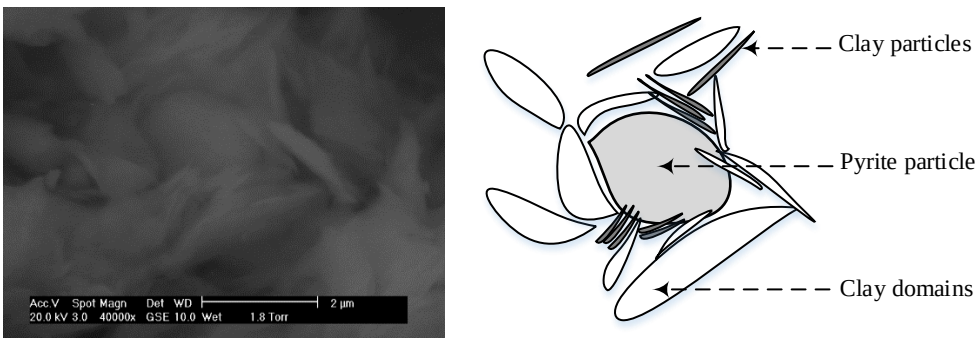
The soil fabric is shown in Figure 3.16. The fabric appears to be composed of proportionally equal large flocs and single plate-shaped particles with edge-to-edge, edge-to-face and face-to-face contacts. As can be seen, the edge-to-edge contacts of the clay domains have resulted in development of large pores in the clay cluster.

The micrograph of Figure 3.17 depicts a pyrite particle surrounded by clay domains and single particles.



(a) (b)

Figure 3.16 ESEM micrograph: (a) soil fabric; (b) schematic diagram of particles and domains arrangements and presence of large pores in flocculated soil fabric



(a) (b)

Figure 3.17 Clay particles and domains around a pyrite particle: (a) ESEM micrograph; (b) schematic diagram

Figure 3.18 shows the steps of drying a flooded specimen in the ESEM. As can be seen, the drying process does not noticeably affect the macrostructure and arrangement of the clay flocs. Also shown in the figure, is the removal of the water menisci developed at inter-floc pores (throats) during sequential drying of the specimen.

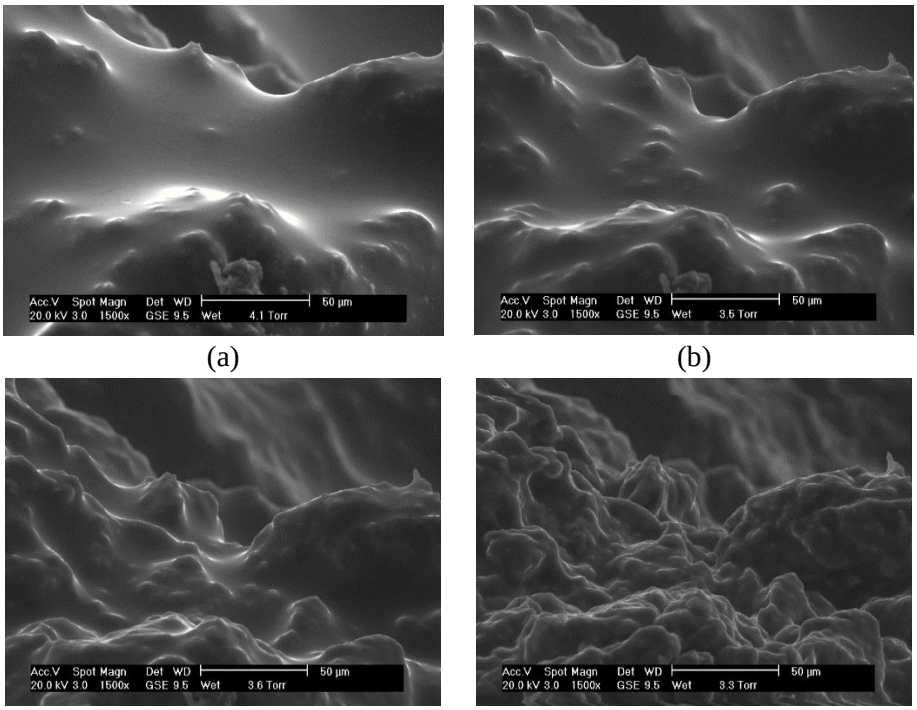


Figure 3.18 ESEM micrographs showing the progressive drying of the clay sample

The diagenesis analysis carried out by Huggett (1994) on London Clay samples recovered from Warden Point on the Isle of Sheppey, revealed the similarity in compositions of Sheppey London Clay with Ockenden London Clay, with differences being only in the relative proportions of some diagenetic minerals. The principal authigenic minerals in Sheppey London Clay are carbonates, apatite and pyrite. The Fibrous calcite, present in Sheppey concretions, comprises a maximum of 5% total Mg, Mn, and Fe. About 50% of the concretions comprise predominantly detrital clay minerals of illite and smectite, with the presence of a slight amount of coarsely crystalline authigenic kaolinite. Silt grains are predominantly quartz and K-feldspar. A clay/quartz ratio of 3.2:1 was also reported. Similar results were obtained from the X-ray analysis carried out in this research, as shown in Figure 3.19. The key petrographical characteristics of the sample are summarised in Table 3.3. It is observed that Silicon dioxide (SiO_2), Aluminium oxide (Al_2O_3), Calcium carbonate ($CaCO_3$), and Iron

disulphide (FeS_2) are predominant constituents of the samples. Calcium (Ca) and Iron (Fe) are the products of weathering of silicate minerals. Calcium carbonate precipitates are formed from the chemical interaction of Ca and CO_2 molecules dissolved in sea water. Similarly, Fe reacts with Sulphur (S), resulting from rotting organic matter, and forms pyrite (FeS_2) (Gasparre, 2005).

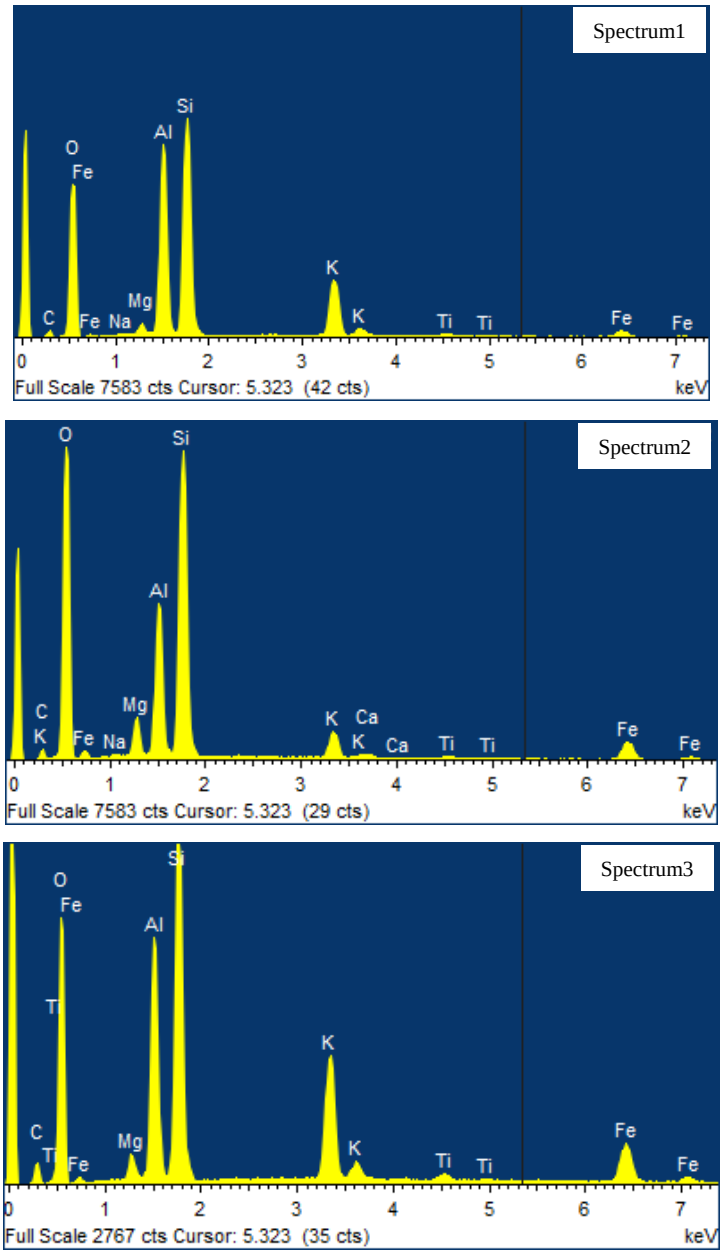


Figure 3.19 The X-Ray spectra acquired from different points on the same sample

Table 3.3 Average chemical composition (% by weight) of Sheppey London Clay

Spectrum	C ($CaCO_3$)	O (SiO_2)	Na (Albite)	Mg (MgO)	Al (Al_2O_3)	Si (SiO_2)	K (Feldespar)	Ca (Wollastonite)	Ti	Fe (Metal)	Total
Spectrum 1	5.16	50.13	0.21	0.77	14.03	19.39	7.37	0.22	0.49	2.23	100.00
Spectrum 2	5.64	56.31	0.24	2.41	8.51	19.21	2.33	0.37	0.40	4.59	100.00
Spectrum 3	6.75	53.67	0.12	1.55	8.65	20.76	3.62	0.17	0.33	4.38	100.00
Mean	5.85	53.37	0.19	1.57	10.40	19.79	4.44	0.25	0.41	3.73	100.00
Std. deviation	0.81	3.10	0.06	0.82	3.15	0.85	2.62	0.10	0.08	1.31	
Max.	6.75	56.31	0.24	2.41	14.03	20.76	7.37	0.37	0.49	4.59	
Min.	5.16	50.13	0.12	0.77	8.51	19.21	2.33	0.17	0.33	2.23	

3.6.4 Mechanical Properties

As mentioned earlier, London Clay is characterised as a fissured stiff clay. The presence of fissures influences the shear strength as reported by Burland (1990), Hight and Jardine (1993), and Hight et al. (2003). Burland (1990) reported the strength sensitivity (S_t) of London Clay to be higher than two. Very few works have been reported in literature on characterisation of the Sheppey London Clay. Jardine et al. (2003) reported some geotechnical parameters for reconstituted Sheppey London Clay as summarised in Table 3.4.

Table 3.4 Geotechnical parameters of reconstituted Sheppey London Clay

Parameters	Dried and reconstituted London Clay at OCR ≈ 1.5
Peak c_u/σ'_v in compression	0.233
Peak c_u/σ'_v in extension	0.210
E_u/p'_0 at 0.01% in compression	844
E_u/p'_0 at 0.01% in extension	484
φ' peak in compression	21°
φ' peak in extension	25°
φ' residual at 100 kPa	10°
Max C_c when normally consolidated	0.45
Max C_α for σ'_v < 100 kPa	0.006

An undrained shear strength (c_u) of 105 kPa under a shearing rate of 1.5 %/min and isotropic pressure of 200 kPa was measured and reported by CET Structures Ltd for the disturbed samples recovered from New Hook Farm.

As the plasticity of the London Clay deposits increases from west to east of the London basin (Hight et al., 2007), a compression curve lying below the curves presented in

Figure 2.17, Chapter 2, is expected for the Sheppey London Clay samples. The oedometric behaviour of intact and corresponding reconstituted Sheppey London Clay samples will be discussed in detail in Chapter 5. The information in Table 3.4 and Figure 2.17 will serve as a platform to compare and validate the results obtained from 1D characterisation of the Sheppey London Clay samples.

3.6.5 SWRC

To the best knowledge of the author, the unsaturated properties of Sheppey London Clay have not been investigated so far. Therefore, in this section, only the general water retention characteristics of London Clay are presented.

Dineen (1997) presented the variation of suction with degree of saturation for reconstituted London Clay over a cycle of drying and wetting (Figure 3.20). According to Fredlund and Houston (2013), the water content corresponding to AEV is generally close to the plastic limit of the soil. For the London Clay, with 19% < w_p < 28%, air-entry values in a range of 1 to 3 MPa have been reported in the literature (e.g. Dineen, 1997).

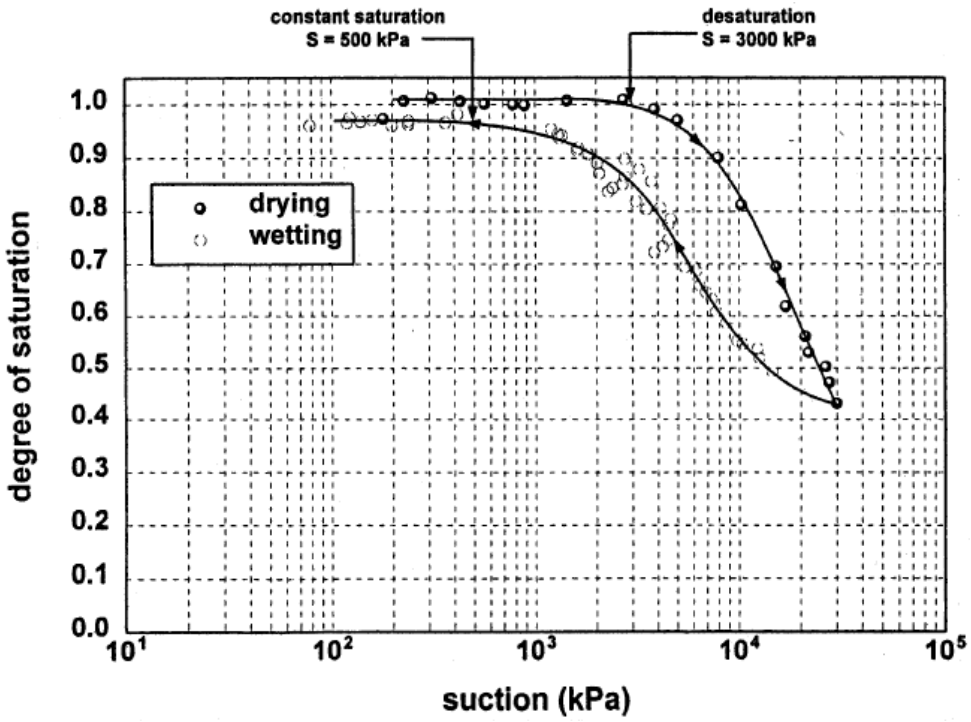


Figure 3.20 SWRC-S_r for London Clay (Dineen, 1997)

The SWRCs for compacted London Clay samples extracted from Harlesden in north London (Monroy, 2005), and from an excavation at Westminster Bridge in the city of London (Mavroulidou et al., 2013) are presented in Figure 3.21. Monroy (2005) used the Imperial College HCT for suction measurements, whereas Mavroulidou et al. (2013) employed the filter paper technique for measurement of SWRC-*w* of specimens compacted dry of optimum then saturated, and presented the results based on the average of the total and matric suction values at corresponding water contents. The compacted samples exhibit significantly lower air-entry values, falling approximately in a range of 0.5 to 1.0 MPa.

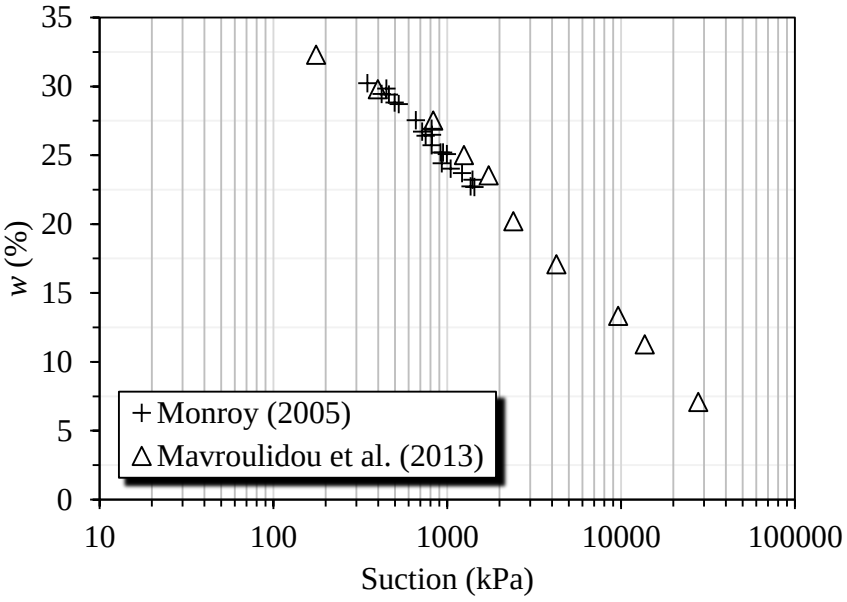


Figure 3.21 SWRC-*w* for compacted London Clay over drying path (data points from Monroy, 2005 and Mavroulidou et al., 2013)

Measurement of SWRC for reconstituted samples of Sheppey London Clay will be discussed in detail in Chapter 4.

3.7 Concluding Remarks

In this chapter, the basic geological properties of London Clay with emphasis on the formation in the Isle of Sheppey were briefly discussed. The procedure followed for preparing undisturbed block samples of Sheppey London Clay was presented. It was shown, with reference to the literature, that block samples provide the best possible quality of undisturbed soil samples in comparison to other undisturbed soil sampling techniques.

The measured physical and geotechnical properties of the Sheppey London Clay, relevant to this research, were reported. The ESEM analysis on representative structured samples indicated the fabric and structure of the intact samples. It was also shown, with reference to literature, that the reconstituted samples prepared based on conventional consolidation from slurry exhibit a uni-modal PSD and layered structure similar to that of sedimentary clays, hence, approving their suitability for the specific experimental program of this research (i.e. creep tests). The microstructural and mineralogy analysis carried out helps in better understanding of the mechanism of creep deformations in London Clay possessing active minerals.

Compacted samples possess relatively low AEV and are also suitable for investigation of unsaturated behaviour such as collapse in compression. However, the dependency of their initial condition on a number of factors such as compaction method, compaction energy, and initial water content, is the major drawback of this type of soil sample, requiring significant attention in preparation of identical compacted samples for laboratory testing.

Few studies can be found in the literature on characterisation of the hydro-mechanical properties of Sheppey London Clay. Therefore, the mechanical and hydraulic properties of London Clay from different sites were presented, with the focus on undrained shear strength, compression characteristics, and water retention properties. This information will serve as a platform to validate the results obtained on 1D characteristics of the Sheppey London Clay samples in subsequent chapters.

CHAPTER 4: A NEW HIGH-CAPACITY TENSIOMETER

4.1 Introduction

Experimental investigation of unsaturated soils' properties requires continuous monitoring of suction evolutions throughout the experiments. High-capacity tensiometers (HCTs) have recently received significant interest in laboratory measurements of soil suction mainly due to their fast response time, accurate measurements, and ease of transport and installation in geotechnical apparatuses. The main drawback of these transducers is cavitation at suctions lower than the bubbling pressure of their ceramic filter. Moreover, these sensors have typically shown poor performance in long-term measurement of high suctions (> 1MPa).

In this chapter, first a synthesis of recent research on HCTs with emphasise on the phenomenon and importance of cavitation, design characteristics of HCTs, and their calibration, saturation, preconditioning procedures, measurement reliability, and applications will be presented. Afterwards, the design characteristics and fabrication process of a new HCT developed at the University of Warwick will be presented. A novel technique for improving the cavitation resistance of the HCTs, based on minimising the surface roughness of the diaphragm on the water reservoir side, will be discussed. After that, the experimental program for calibration, saturation, and evaluation of the performance of the new HCT in the aspects of maximum sustainable suction, sudden pressure change, and long-term stability of measurements will be discussed in details. Finally, application of the developed HCTs for measurement of SWRC of reconstituted London Clay specimens, along with the mathematical curve fitting approach used to attain the entire retention curve over a wide range of suctions, will be discussed.

4.2 Background of HCTs

As mentioned in Chapter 2, the difficulties in the measurement and control of suction in laboratory- and field-based experiments has led to development of a number of techniques such as filter paper, psychrometer, thermal conductivity sensors, axis-translation, pressure plate, and tensiometers. Among these techniques, only tensiometer is capable of directly measuring soil suction under normal atmospheric conditions. The

mechanism of suction measurement in tensiometers is based on the theory of water tensile strength. Standard tensiometers typically constitute of a porous ceramic filter attached to a water-filled tube connected to a pressure measurement system. The working mechanism of the tensiometer is to allow water in the reservoir to flow from the instrument at atmospheric pressure into the soil with negative pore-water pressure (u_w). When pressure equilibrium is attained the water flow will stop. The water-saturated ceramic filter transmits the tensile stress from the soil pore-water to the water reservoir. The exerted tensile stress to the water is then simply measured by the connected pressure measuring system (e.g. manometer, vacuum gauge or electric pressure transducer) (Ridley and Burland, 1996). Figure 4.1 schematically shows the working mechanism of a tensiometer. The maximum sustainable suction (s_{max}) is a function of the AEV, an inherent property of the porous ceramics, which is defined as the maximum pressure difference across the two surfaces of the water-saturated ceramic, above which, air can overcome the surface tension of the water menisci developed in the surface pores and find a passage through the ceramic filter to the water reservoir. Formation of gas bubbles in the water reservoir is called "cavitation" and is the only constraint in measurement of high negative water pressures. Up until early 1990s, ceramic filters of -1 bar AEV were used for fabrication of the tensiometers, hence limiting their suction measurements to values up to 100 kPa (Stannard, 1992). To further enhance the range of suction measurements, considerable efforts were made by Ridley and Burland (1993) at Imperial College (IC) for development of the HCT. The developed HCT at Imperial College has shown the capability of measuring suctions up to 2 MPa. The HCT shares a similar structure with the standard tensiometer and comprises of a pressure measurement device, a water reservoir and a high AEV porous disk as the interface between the soil and the pressure measurement device. Following the success of the Imperial College tensiometer in measurement of high suctions, the device received significant interest in geotechnical community and many similar HCTs have been so far developed with specific technological improvements (Delage et al., 2008). Table 4.1 presents the reported properties of the so far developed HCTs.

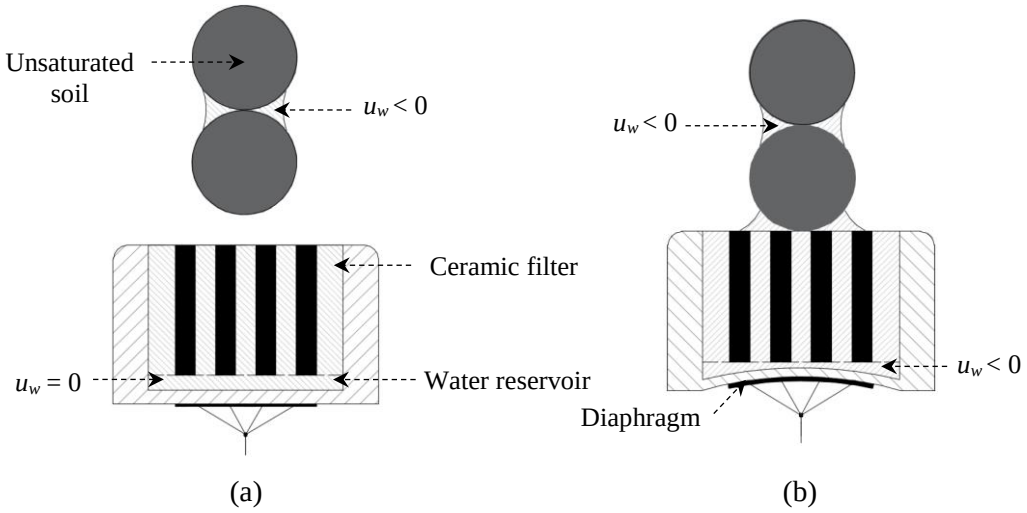


Figure 4.1 Schematic diagram of the working mechanism of a tensiometer: (a) before contact with unsaturated soil; (b) after contact with unsaturated soil

HCTs have recently received significant interest in laboratory measurements of soil suction mainly due to their fast response time, accurate measurements, and ease of transport and installation in geotechnical apparatuses (Lourenço et al., 2011). The response time of the tensiometers is typically within a few minutes in comparison to several hours to several weeks for axis-translation and pressure plate methods (Rahardjo and Leong, 2006). Their miniature size enables them to be relatively easily incorporated in various laboratory testing equipment including triaxial cell (Jotisankasa et al., 2007a), oedometer (Dineen and Burland, 1995, Delage et al., 2007, Cui et al., 2010), shear box (Tarantino and Tombolato, 2005), unconfined compression apparatus (Li and Zhang, 2014), and centrifuge model box (Take and Bolton, 2003, Zhou et al., 2006). Furthermore, the modified version of HCTs have been successfully utilised in field measurements of low suctions (Ridley et al., 2003, Mendes et al., 2008, Toll et al., 2011, Tarantino et al., 2016). However, despite these advantages, HCTs have shown poor performance in long-term measurement of high suctions which hinders their extensive application for field measurements where continuous monitoring of u_w variations is crucial for stability and serviceability analysis of constructions, for example, in arid areas where the negative u_w in shallow depth foundations remains below -1 MPa. Moreover, implementing HCTs in mechanical testing, also requires ensuring continuous measurements over the time period the tests are carried out. This fact is more highlighted when long-term consolidation tests are to be performed on clay specimens with high initial suctions. The long-term performance of HCTs have been examined in some studies. Cunningham et al. (2003) reported measurement of 850 kPa

suction for 8 days without cavitation occurring in the HCTs. Measurement of 320 kPa suction was also reported by Mancuso and Papa (2014) for a time period of about 10 days. All these studies indicate the limitations associated with the use of HCTs. In general, the performance of HCTs can be evaluated from (1) the maximum attainable suction, and (2) the stability and duration of measurements under high suctions. These factors are governed by design characteristics of the HCTs, the AEV of their ceramic filter, and the degree of saturation of the porous ceramic prior to the testing (Mancuso and Papa, 2014). In the next section, the phenomenon of cavitation in HCTs is discussed in details.

4.3 Water in Tension and Cavitation

It has long been recognised that a mass of water is in a metastable state when it is under tension. This means that reduction of pressure beyond a certain threshold will cause rupture and formation of vapour cavities. The tensile pressure at the onset of cavitation is called "tensile strength". For years, the physicists have tried to measure the tensile strength of liquids in general and water in particular in the laboratory experiments. Hydrostatic liquid tension was first measured in Berthelot tubes (Berthelot, 1850). The Berthelot-type systems were then extensively used in the experimental works of Vincent and Simmonds (1943), Lewis (1961), Rees and Trevena (1964), and Chapman et al. (1975) for measurement of water tensile strength. The reported experimental values are widely scattered and fall within a range of 0.9 to 7.7 MPa (Temperly, 1946, Rees and Trevena, 1966). This range exhibits discrepancy with the estimated theoretical tensile strength of water reported in the order of 100 MPa (Vincent, 1941, Temperly, 1946, Temperly, 1947, Harvey et al., 1947, Fisher, 1948), and 405 MPa (Tabor, 1969). The closest measured value to the maximum tension that water can sustain was in the range of 140 MPa (Zheng et al., 1991).

Table 4.1 Properties of the developed HCTs

Authors	AEV (MPa)	Pressure measurement system	Size of water reservoir (mm^3)	Max measured suction (kPa)	Max measurement duration (min)
Ridley and Burland (1993)	1.5	Entran EPX (3.5 MPa)		1370	1440 at 700 kPa
Ridley and Burland (1995)	1.5	Strain-gauged diaphragm (4MPa)	4	1800**	
Guan and Fredlund (1997)	1.5	Brand not given (1.5 MPa)	Min=3.85 Max=19.24	1200-1250	4320 at 700 kPa
Ridley and Burland (1999)	0.1	Strain-gauged diaphragm		164	
	0.5			740	
	1.5			1800	
Sjoblom (2000)	1.5	Strain-gauged diaphragm		2200	
Meilani et al. (2002)	0.5	Druck PDCR 81 (1.5 MPa)		495	
Mahler et al. (2002)	0.5	Ashcroft K8		350	
Tarantino and Mongiovi (2002)	1.5	Strain-gauged diaphragm (4MPa)	<4.5	2063	22540 at 1000 kPa
Take and Bolton (2003)	0.1	Druck PDCR 81 (1.5 MPa) and Entran EPB (0.7 MPa)	~3	~130	
	0.3			530	
Ridley et al. (2003)	1.5	Strain-gauged diaphragm (8MPa)	3		
Toker et al. (2004)	1.5	Data Inst. Inc. AB-HP 200		1300	
Chiu et al. (2005)	0.5	Druck PDCR 81 (0.7 MPa)		472	~18000 at 110 kPa
Mantho (2005)	1.5	Strain-gauged diaphragm		1573	
Lourenço et al. (2006)	1.5	Ceramic transducer by Wykeham Farrance (1.0 MPa)	5	1231	
He et al. (2006)	0.5	Entran EPX-10I-250A (3.5 MPa)	2	550	
Mahler and Diene (2007)	0.5	Entran EPXO (0.5 MPa)	5-112	800	
	1.5	Entran EPX (1.5 MPa) Ashcroft (0.5-1.5 MPa)		1465	
Jotisankasa et al. (2007b)	0.5	Brand not given	60	350	
Lourenço et al. (2008)	1.5	Ceramic transducer by Wykeham Farrance (1.0 MPa)	5	2087	
Cui et al. (2008)	1.5	Strain-gauged diaphragm			~30000 at 20-160 kPa
Rojas et al. (2008)	0.5	Strain-gauged diaphragm	3	450	~8400 at 350 kPa
Mendes and Buzzi (2013)	0.5	147F Precision Measurement Company (3.5 MPa) and	1100	920	
	1.5	Entran EPX (3.5 MPa)		1520	
Mancuso and Papa (2014)	0.5	Strain-gauged diaphragm	3		~14400 at 320 kPa
Li and Zhang (2014)	1.5	EPXO pressure transducer		1100	
Mendes et al. (2016)	0.7	Ceramic flush diaphragm transducer (2.0 MPa)	40 and 430	~700	
	1.5	Ceramic cavity diaphragm transducer (2.0 MPa) Stainless steel flush diaphragm transducer (2.0 MPa)		~2100	
Wijaya and Leong (2016)	0.5	Entran EPX-10I-250A (3.5 MPa)	<19	1300	
Tarantino et al. (2016)	0.8	Strain-gauged diaphragm		800	~18720 at 800 kPa

** A maximum value of 2900 kPa was measured by Tarantino and Mongiovi (2002) using this HCT

In tensiometers, and in a very general definition, the fact that undissolved gas nuclei often appear in the corners of the water reservoir is called "cavitation". Marinho et al. (2008) described the two types of cavitation that may occur in a closed system of water under tension; homogeneous cavitation and heterogeneous cavitation. By definition, homogenous cavitation is referred to as nucleation of the ephemeral microscopic voids developed as a result of thermal motions within the liquid. The tension necessary to cause homogeneous cavitation has been reported to have a magnitude of 823 MPa, a value that has never been measured in laboratory experiments (Marinho et al., 2008). Heterogeneous cavitation is referred to as expansion and transformation of the entrapped air and water vapour in the crevices at the boundary between the liquid and the solid wall of the water reservoir or between the liquid and small particles suspended in the liquid (Harvey et al., 1944). This type of nucleation can happen if the water pressure inside the reservoir is dropped progressively resulting in the gas cavity to be pulled out from the crevice and form a free cavity. Air diffusion into the cavity will also cause volume expansion of the trapped gas and can result in formation of free cavities. The gas pressure inside these unstable cavities is initially close to the water vapour pressure (2.3 kPa at 20°C). Expansion of these free cavities can result in measurement of a gauge pressure (absolute pressure minus atmospheric pressure) of approximately -100 kPa by the tensiometer (Marinho et al., 2008).

Apart from the gas bubbles trapped in the crevices of the water reservoir walls, other sources of potential cavitation nuclei are (1) gas micro-bubbles trapped in crevices of the solid particles suspended in the water (Ishida et al., 2000, Bremond et al., 2005), (2) bubbles covered by surface active substances, and (3) air bubbles stabilised by ionic phenomena (Marinho and Chandler, 1995). Another mechanism for cavitation can be the air diffusion from the air-saturated water in the soil to the de-aired water in the porous stone and the water reservoir of the tensiometer (Ridley et al., 2003). Therefore, it is reasonable to conclude that, in HCTs, cavitation can occur both in the water reservoir and the porous ceramic.

Cavitation can therefore be considered as a major drawback of the tensiometers which may occur before pressure equalisation. Various studies have been conducted on identifying the factors that may affect the cavitation pressure and time of cavitation occurrence. In fact, in order to minimise the likelihood of cavitation occurrence and to

prolong the suction measurements by tensiometers, it is necessary to remove the air from the water reservoir and the porous ceramic filter. However, as removing all entrapped air is almost impossible, one option is to adopt design and experimental procedures to minimise the presence of air bubbles in the system. As it will be discussed in the sequel, adequate saturation of the porous ceramic can significantly improve the magnitude and duration of the tension measurements. Such improvement can be also attained through adaptation of suitable design and fabrication procedures which, in turn, influences the robustness, sensitivity, response time, ease of saturation, and resistance against cavitation of the HCTs (Take and Bolton, 2003).

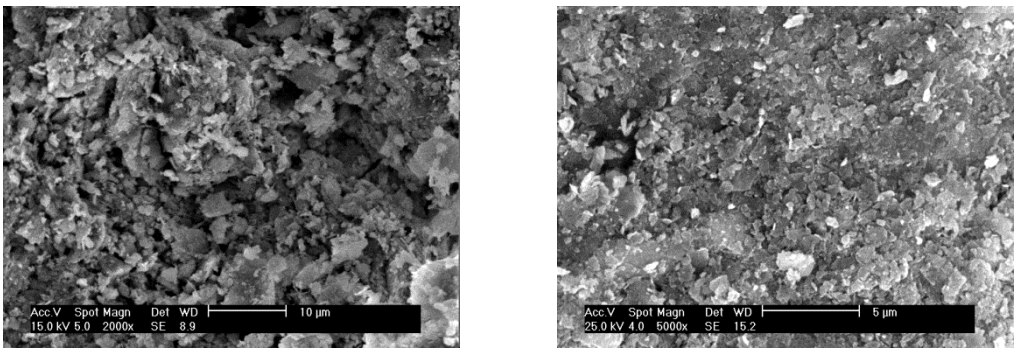
4.3.1 Effect of the Size and Properties of the Water Reservoir

Ridley et al. (2003) stated that if a tensiometer cavitates at a suction close to the AEV of its ceramic filter, the cavitation mechanism can be explained by air breaking into the ceramic filter from the atmosphere. On the other hand, cavitation occurrence at suctions below the AEV of the porous ceramic can be attributed to the release of trapped gas bubbles from the small crevices on the walls of the water reservoir (Ridley, 1993, Ridley et al., 2003, Take, 2003). To reduce the number of crevices and hence, possible nucleation sites, it is necessary for the surfaces in contact with water to be as smooth as possible (Marinho and Chandler, 1994). Mahler and Diene (2007) reported the smoothness of the acrylic material used for fabrication of their tensiometer housing as an important factor in achieving high suctions (800 kPa with a 5 bar ceramic filter). Ensuring clean surfaces within the measurement system as well as using clean and pure water (Henderson and Speedy, 1980) are the other important factors in minimising cavitation occurrence during suction measurements. Reduction in the number of potential cavitation nuclei can be also achieved by reducing the amount of free water in the water reservoir of the instrument (Ridley and Burland, 1993, Marinho and Pinto, 1997, Tarantino and Mongiovi, 2002). The large size of the water reservoir also increases the saturation time as well as the pressure equilibrium time during suction measurements (Mendes and Buzzi, 2014). From the high-speed photography analysis carried out to capture the cavitation mechanism in HCTs, Mendes and Buzzi (2013) observed simultaneous growth of air bubbles from the water reservoir wall on the pressure sensor side and the ceramic wall during cavitation, suggesting the initiation of cavitation in both reservoir and ceramic filter. According to Mendes and Buzzi (2013), cavitation occurs when the air bubbles (developed either in the ceramic or on the

reservoir wall) reach the water reservoir. This means that maximum suction can still be sustained even if some air cavities are formed within the porous ceramic. In other words, the small air bubbles developed either in the ceramic filter or reservoir, can only collate to create an air cavity inside the water reservoir having a larger volume than the ceramic filter (Lourenço, 2008). Therefore, considering a small-sized reservoir with minimised numbers of crevices on its walls can significantly contribute in elevating the cavitation threshold.

4.3.2 Effect of the Size and Properties of the Ceramic Filter

The high AEV porous disk also plays a significant role in suction measurements. The AEV and the hydraulic conductivity of the porous ceramic are directly influenced by the size of the pores. Furthermore, the porosity of the ceramic filter varies according to the size and distribution of the pores. Microscopic analyses have shown that the size and distribution pattern of the pores of ceramics are not uniform and pores exhibit irregular formation patterns (Figure 4.2). Similar observations were also reported by Lourenço et al. (2011). Therefore, the air entry process is not instantaneous and is a function of pore-size distribution (PSD). The PSD and pore connectivity are the important factors governing the bubbling or cavitation. Other factors such as advancing and receding contact angles of the air-water interfaces, and air and liquid pressures can also influence the air entry process (Lourenço, 2008). It must be noted here that there exists small differences between the measured bubbling pressure and the AEV of the ceramic discs (Tarantino, 2004).



(a) (b)

Figure 4.2 SEM micrographs of a Soil Moisture Corp. ceramic disc at magnifications of: (a) 2000x; (b) 5000x

The shape and thickness of the ceramic filter is another crucial factor in design of HCTs. At tension pressures just passing the AEV, the water menisci at the exposed surface start receding into the ceramic until nucleation takes place. It is obvious that the thicker the ceramic filter the longer will be this process and the larger will be the measured tension in the water reservoir (Take and Bolton, 2004). Measurement of water tensions higher than the AEV of the porous ceramic have been reported by a number of researchers (e.g. Sjoblom, 2000, Tarantino and Mongiovi, 2002, Lourenço et al., 2008, Pedrotti et al., 2014). However, these water tensions are not indefinitely sustainable and occurrence of cavitation after a period of time is inevitable mainly due to the air diffusion process (Tarantino, 2004). Sjoblom (2000) reported an increase in s_{max} value from 1500 to 2000 kPa by replacing the ceramic filter initially provided from Soil Moisture Corp., by a uniformly graded porous disk fabricated in Japan.

4.3.3 Effect of Saturation and Pre-conditioning Procedures

Adequate saturation of the ceramic filter directly influences the maximum sustainable suction as well as the measurement duration. Saturation and preconditioning of the water in the tensiometer reservoir and ceramic filter is the most important factor in successful performance of the instrument (Marinho et al., 2008). Different experimental procedures can be found in the literature for saturation of the tensiometer. Indeed, the most agreed method is the one proposed by Ridley and Burland (1993) which involves three stages; (1) evacuation of the dry ceramic filter, (2) flooding the filter with de-aired and demineralised water under maintained vacuum, and (3) pressurisation to high positive pressures for at least 24 hours.

Using water infiltration under vacuum for initial saturation of the ceramic filter has been recognised to be an efficient method for ensuring proper saturation of the filter (Ridley and Burland, 1999, Tarantino and Mongiovi, 2002, Take and Bolton, 2003, Lourenço et al., 2006). Regarding pressurisation stage, it was shown by Guan and Fredlund (1997) that proper saturation and maximum sustainable tension in suction probe can be achieved by applying cycles of cavitation and subsequent pressurisation rather than a single application of high positive pressures. Later studies by Tarantino and Mongiovi (2001) and Tarantino (2004) showed that cycles of cavitation and pressurisation in addition to increase of the maximum sustainable tension, can also improve the stability of measurements during time specially in HCTs with high AEV

porous ceramics (e.g. 1.5 MPa). Rojas et al. (2008) also experimentally approved that s_{max} depends on the past history of the HCT, i.e. the applied cycles of cavitation and pressurisation. Chiu et al. (2005) and Lourenço et al. (2006), however, could not find clear evidences of performance improvement in the HCTs subjected to cycles of cavitation followed by pressurisation. This might be attributed to the relatively low pre-pressurisation pressures applied by them following the cavitation phase.

To better understand the importance of pre-pressurisation on cavitation mechanism, let us discuss the cavitation model presented by Take (2003), as shown in Figure 4.3. As it can be seen in Figure 4.3(a), the initially trapped air bubble inside a crevice on the water reservoir wall, grows as the water tension magnitude is increased. Having received enough tension pressure, the bubble is released from the crevice, causing cavitation in the water reservoir. However, as shown in Figure 4.3(b), pre-pressurising water results in recession of the air-water interface and development of a resistance against applied tensile stress. Hence, under the increasing tension pressure, the cavitation would not occur as the air bubble remains entrapped in the crevice. Now, by subjecting the water to a higher tension pressure, the air bubble expanded in the crevice will be eventually released to form a small free air cavity. Re-pressurisation of the water will dissolve the free cavity into the water and hence increase the degree of saturation of the system [Figure 4.3(c)]. Repeating the cycle of cavitation and pressurisation for a few more times, can significantly reduce the amount of entrapped air in the crevices of the water reservoir, resulting in elevation of cavitation threshold and measurements duration.

In another attempt to improve the saturation of HCTs, Acikel and Mancuso (2010) proposed a new method of saturation based on substituting the present air in the porous ceramic and the water reservoir of the tensiometer with CO_2. It was believed that the higher hydrophilicity of the CO_2 in comparison with air can improve the instrument's resistance against cavitation. The proposed saturation procedure involves several stages; (1) exposing the dry porous ceramic to a low pressure (below 1 bar) circulation of CO_2 in the saturation chamber, (2) pressurising the CO_2 to 2 bar for one hour, (3) drying the porous stone by applying vacuum and heating the ceramic up to 70 °C for 16 hours, (4) flooding the porous ceramic with de-aired water and maintaining the vacuum for around 20 hours, and (5) pre-pressurising the chamber by applying cycles of pressurisation to 800 kPa at regular time intervals up to 72 hours. The authors

observed an improvement by around 50% in measured s_{max} by the probes saturated with this method in comparison to those saturated based on the procedure described by Rojas et al. (2008). Although the efficiency of this method has been experimentally approved, the highly time-consuming nature of this method as well as the need for relatively complex experimental setup, hinder its application for routine saturation of HCTs in laboratory.

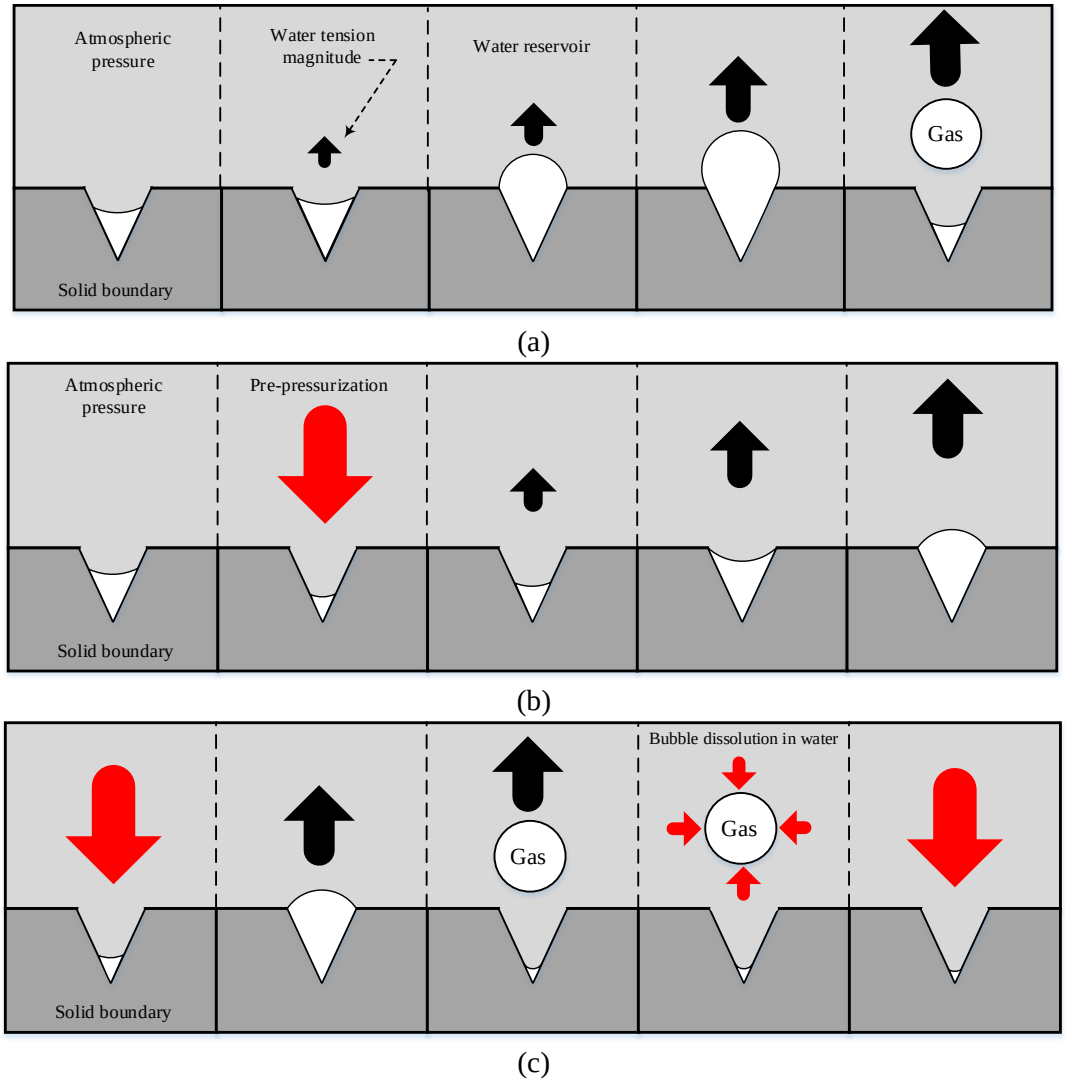


Figure 4.3 Effect of pre-pressurisation and cycles of cavitation and pressurisation on cavitation in tensiometers: (a) no pressurisation of water (cavitation occurs); (b) pressurisation of water (cavitation does not occur); (c) a cycle of cavitation and pressurisation (after Take 2003).

Marinho et al. (2008) theoretically explained the significance of pre-pressurising the HCTs under large positive pressures prior to use for measurement by giving an example of an air bubble trapped in an ideal conical crevice. The application of a high positive

pressure can retract the developed air-water interface into the crevice and as a result dissolve more air into the water. The amount of gas within the total system can be therefore reduced if most of the dissolved air does not return into the crevice when positive pressure is reduced to atmospheric pressure. However, although it is desirable that the recently dissolved air is exsolved from the system, there is no guarantee for this to happen and there exists the possibility that a considerable amount of dissolved air on the reservoir walls form stable nucleation sites. Minimising the size and number of the crevices on the diaphragm's inner surface appears to be a more practical solution to restrict formation of stable nucleation sites on the reservoir walls.

4.3.3.1 Pressurisation Magnitude

The magnitude of the positive water pressure during pre-pressurisation stage has been also the subject of recent studies. Although some researchers such as Ridley and Burland (1993), Guan (1996), and Tarantino and Mongiovi (2002) preferred pre-pressurisation to high positive pressures of 4 to 12 MPa, others such as Chiu et al. (2005), Lourenço et al. (2006), Rojas et al. (2008), Lourenço et al. (2011a) and Li and Zhang (2014) have shown that pre-pressurisation under such high positive pressures is not necessary and lower pressures in range of 0.6 to 1.5 MPa are enough for proper saturation of the HCTs and that the higher positive pressures can only speed up the saturation time. However, pressurisation at high positive pressures is necessary for saturation of HCTs that have been used for a long time or have been in prolonged contact with fine-grained soils, as pore clogging of the porous ceramic could have occurred as a result of physical deposition or precipitation of the finer materials inside the ceramic filter, leading to decrease of the porosity of the ceramic filter (Lourenço et al., 2011). Delage et al. (2008) reviewed the pre-pressurisation pressures adopted by different authors and reported that HCTs subjected to pre-pressurisation pressures greater than 2.7 times their ceramic's nominal AEV could measure suctions above their nominal capacity.

4.3.3.2 Pressurisation Duration

Arguments about the effect of pre-pressurisation duration are still ongoing. The results of a single experiment by Tarantino and Mongiovi (2001) on an IC tensiometer saturated for 1 year under 4 MPa showed a poor performance of the instrument and

occurrence of cavitation at only 650 kPa after just a few seconds. Air diffusion and expansion of air cavities in the porous ceramic under positive pressures were reported to be the reasons behind such poor performance. Nevertheless, it was shown that after re-saturation and pressurisation under 4 MPa the instrument's capability for suction sustainability increased by 4 times. However, a solid conclusion could not be made based on a single experiment to support the significance of pressurisation duration, although the improvement of the instrument's performance after a cycle of cavitation and pressurisation was apparent. In one of the most recent studies, Pedrotti et al. (2014) proposed a one-shot pressurisation method for initial saturation of an HCT used for field measurements. In this method, the dry ceramic filter was subjected to an immediate 4 MPa positive water pressure and the response of the sensor was recorded. It was found that a residual pressure of about 600 kPa was remained in the sensor after releasing the pressure, a phenomenon that was reported to be associated with development of water menisci in the unsaturated ceramic and was considered as an indication of poor saturation. The authors further stated that a period of minimum 4 days was required for adequate saturation of the ceramic using "one-shot" method. The applicability of this method was confirmed from the observation of s_{max} = 2008 kPa, a value much higher than the nominal AEV of the ceramic (1.5 MPa), after a course of 8 days saturation. Pedrotti et al. (2014) also examined 7 different pre-pressurisation patterns for saturation of two HCTs and reported measurement of suctions up to 3 MPa and concluded that air breakthrough at the ceramic outer surface is predominant over that caused by air cavity expansion in the tensiometer crevices.

4.3.3.3 Saturation Check

Instantaneous response of the HCT to change in pressure during pre-pressurisation can be considered as an index for adequate saturation (Lourenço et al., 2006). A delay in response time indicates deficiency in saturation of the ceramic filter. Furthermore, as stated by Tarantino (2004), an adequately saturated tensiometer should reach pressure equilibrium within 1-2 hours if immediately placed in free water by the end of saturation course. It was also evidently shown by Tarantino and Mongiovi (2001) and Tarantino (2004) that an inadequately saturated tensiometer may give apparently reliable and stable readings, yet these measurements are in fact incorrect. It was explained that if the initial degree of saturation of the filter is low, although expansion of air cavities (cavitation) may happen at high tension pressures, but the present air cavities can

enlarge under low tension pressures resulting in erroneous response of the instrument. Moreover, the water pressure in the water reservoir may differ from the actual water pressure at the soil-filter interface, if the ceramic filter is not adequately saturated.

4.4 Suction Measurements

An overwhelming number of studies can be found in the literature with regards the methodologies for performance improvement of the HCTs. However, despite these technological improvements, the HCTs measurement reliability, continuity, and repeatability is still an area of concern, and brings hesitation in wide use of this instrument (Pedrotti et al., 2014). The HCT's measurement precision can be influenced by various factors such as initial saturation, calibration, design components, contact between the soil and the ceramic filter, osmotic efficiency of the ceramic filter, temperature, and equipment setup for suction measurements (Lourenço, 2008).

To improve the contact between the soil and the tensiometer, a common method is to apply clay paste to the porous stone of the tensiometer. As suggested by Oliveira and Marinho (2008) the paste should be prepared at a water content between liquid and plastic limit of the testing soil sample. High water content of the paste can prolong the moisture equilibrium time. Conversely, low paste water content can prevent establishment of an ultimate contact. Applying clay paste also prevents the drying of the filter during installation on the specimen.

Guan (1996) and Tarantino (2004) examined the osmotic efficiency of the tensiometers using sucrose and salt solution respectively and reported null reading suggesting that the high AEV ceramic disk does not have an osmotic effect as it was claimed by Marinho and Chandler (1994).

Richards and Trevena (1976) stated that at low temperatures, i.e. at 4º C, when water is at its maximum density, the water tension at cavitation reaches a peak value in Berthelot tube. Based on this concept, Lourenço et al. (2011) investigated the effect of temperature on s_{max} and reported that decreasing temperature results in an improvement in cavitation threshold.

Equipment setup also plays an important role in accurate measurement of soil moisture suction at constant water contents. Existence of open spaces inside the cell in which

measurements are carried out, can result in water evaporation from the specimen and, therefore, an increase in measured suction values.

As discussed earlier, the results published in the literature (e.g. Tarantino and Mongiovi, 2001, Lourenço et al., 2008, Pedrotti et al., 2014), show that the HCTs are often capable of measuring suctions much higher than the AEV of their ceramic filter. Take and Bolton (2004) discussed that precautions should be considered in interpretation of the measured suctions in excess of AEV, as the observed values could be an artefact of the air entry process. Overall, detection of the abovementioned errors may be difficult if suction measurements on a soil sample are recorded by only one sensor. It has therefore been recommended, where possible, to use two or more tensiometers for simultaneous suction measurements on a soil sample (Tarantino, 2004).

4.5 Calibration Methods

In principle, tensiometers should be calibrated in the negative pressure range. However, due to the difficulties in applying high negative pressures in conventional soil mechanics laboratories, calibration of tensiometers is normally carried out in positive range and a linear extrapolation to the calibration equation is developed for the pressures in negative range. According to Guan and Fredlund (1997) the extrapolation method of calibration can introduce a small error in range of 0.5 – 8.5% of the measured suction. An error range of 1.0 – 1.5% was also reported by Tarantino (2004). Although the linear extrapolation method does not seem to be an ideal method, but it has been widely accepted by HCT users. Calibrations in negative range have also been reported in the literature (e.g. Tarantino and Mongiovi, 2003, Lourenço, 2008, Mancuso and Papa, 2014). These methods are outlined as isotropic unloading in a triaxial cell (indirect), axis-translation (indirect), pressurisation from the back of the diaphragm (direct), and vacuum application (direct, pressure range of ≥-100 kPa) (Lourenço, 2008).

For calibration using the axis-translation method, an instrumented soil specimen is initially brought to a known value of suction by artificially increasing the u_a while maintaining the u_w at the base of the specimen at atmospheric value. With the water drainage line closed, the air pressure is then reduced in steps and the response of the tensiometer (voltage output) to the generated suction inside the specimen is recorded

and used to derive the calibration equation. This method is prone to the errors associated with the axis-translation method as described in Chapter 2.

The isotropic unloading in triaxial cell is relatively more complex than the axis-translation-based calibration methods. A soil specimen, initially consolidated with a constant back pressure to a known effective stress value, is unloaded under undrained condition. The change in the mean total stress, results in generation of an equal negative u_w which is measured by the tensiometer attached to the specimen (Ridley and Burland, 1993). This method, was reported by Ridley and Burland (1993) to produce errors associated with the differences between the recorded suction by the tensiometer and the imposed effective stress, mainly due to the specimen swelling resulted from development of air cavities in pore-water during unloading.

The direct calibration in negative range using the back pressurisation method (e.g. Tarantino and Mongiovi, 2003) is in fact the most reliable method since the imposed pressure at the back of the diaphragm (e.g. through the electrical wire) results in deflection of the diaphragm in the same direction as when it is subjected to negative pressure in unsaturated soil pores. However, this method may not be regarded as a practical method, since the specific designs of the majority of the developed HCTs are not adaptable for air pressurisation through their cables. Furthermore, using this method for calibration of HCTs with strain-gauged diaphragms, requires special assembly to protect the highly sensitive strain gauges under the applied high air pressures. Limitations in application of high air pressures (i.e. up to 1.5 MPa) in laboratories can further restrict the calibration range to values well below the nominal capacity of the HCTs.

4.6 Application for SWRC Development

HCTs have received significant attention for laboratory measurement of soil water characteristic curves for various soil types, thanks to their fast response and short equilibrium time (Toker et al., 2004, Liu et al., 2012, Lourenço et al., 2015). According to Fredlund et al. (1997), the SWRCs obtained from HCTs are equal to ones obtained from conventional methods such as pressure plate and filter paper. This statement was also supported by Marinho and Teixeira (2009) who compared the SWRCs obtained from HCTs (500 kPa capacity) with other conventional methods including filter paper,

suction plate, and pressure plate. However, the recent study by Tarantino et al. (2011) showed that the pressure plate overestimates suction values with respect to tensiometer and axis-translation when employed for measurement of SWRC on a sand-silt-clay mixture.

In laboratory determination of SWRC using HCTs, one method is to place the soil specimen on a digital balance and expose it to continuous air drying. Changes of water content is simultaneously monitored by the electronic balance, while the evolution of suction in the continuously drying specimen is recorded by the HCT (dynamic procedure). This method may involve errors associated with non-equilibrium of suction within the sample during the continuous drying (Marinho and Teixeira, 2009). An alternative method is to air-dry the sample to known water content values and allow the sample to reach moisture equilibrium for at least two days prior to taking measurement of suction using a HCT (static procedure). This method does not require a balance for continuous water content measurements but takes much longer time to complete. Boso et al. (2003) stated that the SWRCs obtained from the dynamic and the static procedures only agree under decreasing evaporation-rate. The effect of evaporation-rate on the SWRC measured by continuous drying (dynamic) method was studied by Cunningham (2000) and Boso et al. (2003) on reconstituted silty clay and clayey silt specimens respectively. In the former study, the evaporation-rate was controlled in a controlled-humidity chamber, and in the latter study, the evaporation-rate was slowed down by wrapping the specimen in a geotextile. Both studies revealed no or little differences between the SWRCs obtained during controlled and uncontrolled evaporation tests. Both static and dynamic procedures may involve other errors associated with, for instance, sample temperature (Fredlund et al., 1997), and influence of the tensiometer cable on sample mass measurements (Toker et al., 2004).

4.7 The New HCT

4.7.1 Design

A total of 12 tensiometers were fabricated at The University of Warwick. Figure 4.4 presents the schematic sketch of the Warwick Tensiometer (WT) and its components.

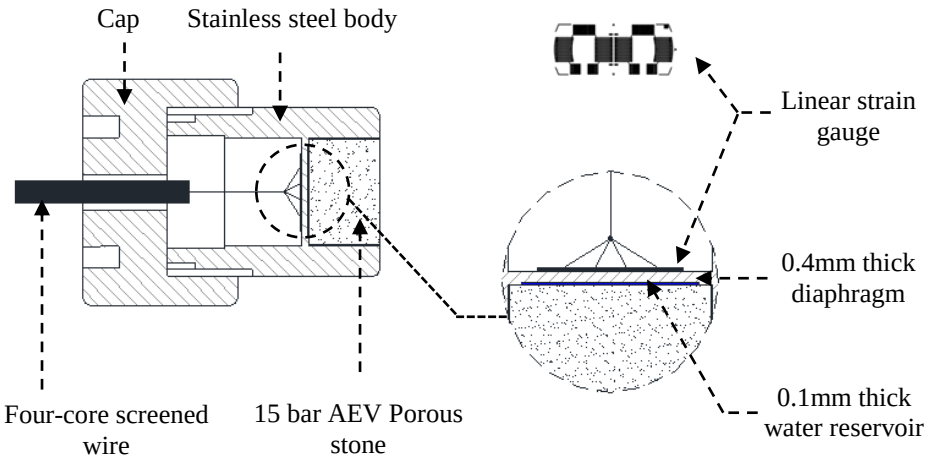


Figure 4.4 Schematic diagram of the tensiometer and its components

The new tensiometer has retained the main features of the tensiometer developed at the University of Trento (Tarantino and Mongiovi, 2002). Modifications were imposed to the size of the water reservoir and the method used for smoothening the diaphragm's surface in contact with water with the aim to minimise the presence of entrapped air bubbles. The diaphragm is positioned at mid-height of the stainless steel body and provides a quasi-symmetric geometry. Design of the diaphragm as an integral part of the body, enables maximum accuracy and minimum hysteresis (Micro-measurements, 2010). The design and manufacturing steps of WTs are discussed in following subsections.

4.7.1.1 Body, Diaphragm, and Water Reservoir

The tensiometer body was machined in the milling machine from one single cylindrical piece of AISI 304 stainless steel. A 3 mm diameter carbide-coated four flute end-mill cutter was used and the material was removed in several milling steps. The WT's diaphragm is 0.4 mm thick and has an internal diameter of 7 mm. The water reservoir has a diameter of 6 mm and a depth of 0.1 mm. In comparison to the Trento tensiometer, the reservoir is smaller in diameter which leads to 17.5% reduction in the volume of the free water in the reservoir. During removing the last 0.1 mm of the diaphragm thickness a refined milling pattern was considered in order to minimise the depth of the developed revolution ridges during machining. A new milling cutter was also used for this stage to eliminate the uneven cutting process associated with eroded cutting edges. The surface roughness of the diaphragm on the water reservoir side was reduced using different metal polishing and surface coating techniques (explained later). The

machined and polished pieces were thermal treated to release the accumulated stresses in the material during metal works.

4.7.1.2 Strain-gauging

In comparison to the Trento tensiometer which incorporates a traditional circular pattern diaphragm gauge, in design of the WTs, a linear-type strain gauge was used which comprised of radial and tangential strain gauges combined in a Wheatstone bridge to generate highest sensitivity. The advantages of using a linear strain gauge are mainly the ease of installation and lower gauge costs. It should be mentioned that both circular and linear configurations function in the same manner although there are minor differences in total gauge output (Micro-measurements, 2010). Figure 4.5 presents a schematic diagram of the linear strain gauge and its internal circuit. The parameters ε_R and ε_T denote radial and tangential strains respectively.

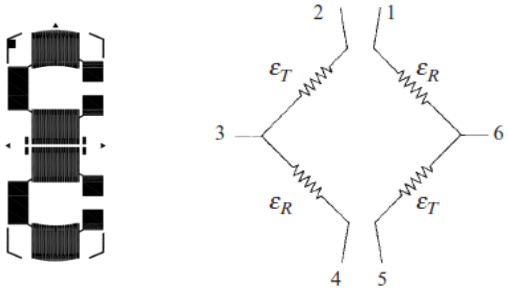


Figure 4.5 (a) Linear strain gauge; (b) Internal circuit diagram (Micro-measurements 2010)

At the centre of the diaphragm, the radial and tangential strains are identical and can be calculated using;

$$\varepsilon_{Rc} = \varepsilon_{Tc} = \frac{3PR_0^2(1-v^2)}{8t_d{}^2E} \tag{4.1}$$

where P is the applied pressure in Pa, R_0 is the diaphragm radius in mm, t_d is the diaphragm thickness in mm, E is the elasticity modulus in Pa, and v is the dimensionless Poisson's ratio.

At the periphery of the diaphragm, the tangential strain ε_{T0} decreases to zero, while the radial strains ε_{R0} become negative with its magnitude being two times the magnitude of the centre strain ε_{Rc}, hence;

$$\varepsilon_{R_0} = \frac{-3PR_0^2(1-v^2)}{4t_d{}^2E} \tag{4.2}$$

The design recommendations by Micro-measurements (2010) indicates that to avoid excessive strain of the diaphragm, the ε_{R0} value should be kept less than 2×10^{-3}. Considering the applied pressure of P = 4 MPa corresponding to the pre-pressurisation pressure suggested by Tarantino and Mongiovi (2002), and the typical stiffness parameters of the AISI 304 stainless steel reported as E=197 GPa and v = 0.275, the ε_{R0} for the WT diaphragm with t_d = 0.4 mm and R_0 = 3.5 mm is computed as 1.08×10^{-3}, a value well below the reference diaphragm strain. This value confirms the safe design of the diaphragm dimensions.

In order to calculate the instrument resolution, the information about the full scale output voltage, the sensitivity, the excitation voltage, and the output signal amplification is necessary. The full scale output voltage is defined as the millivolts the transducer will output when at its maximum range. For the linear strain gauge, the full scale output (V_{out}) in millivolts per volt can be approximately calculated using

$$V_{out} = 0.75\frac{PR_0^2(1-v^2)}{t_d{}^2E}\times10^3 \tag{4.3}$$

For the WT diaphragm, the full scale output is calculated as V_{out} = 1.024 mV/V. Using Equation 4.4, and by considering an excitation voltage of V_{exc} = 5V, the sensitivity parameter (S) is calculated as 1.28 μV/kPa.

$$S = \frac{e_0\times V_{Exc}}{P}\times10^3 \tag{4.4}$$

The obtained sensitivity is compatible with the 24-bit National Instruments NI9237 module used for data acquisition and signal conditioning. Considering an output signal amplification (gain) of 500, the signal resolution is obtained as 0.3 μV. This gives a resolution of 0.23 kPa to the instrument (see Figure 4.6).

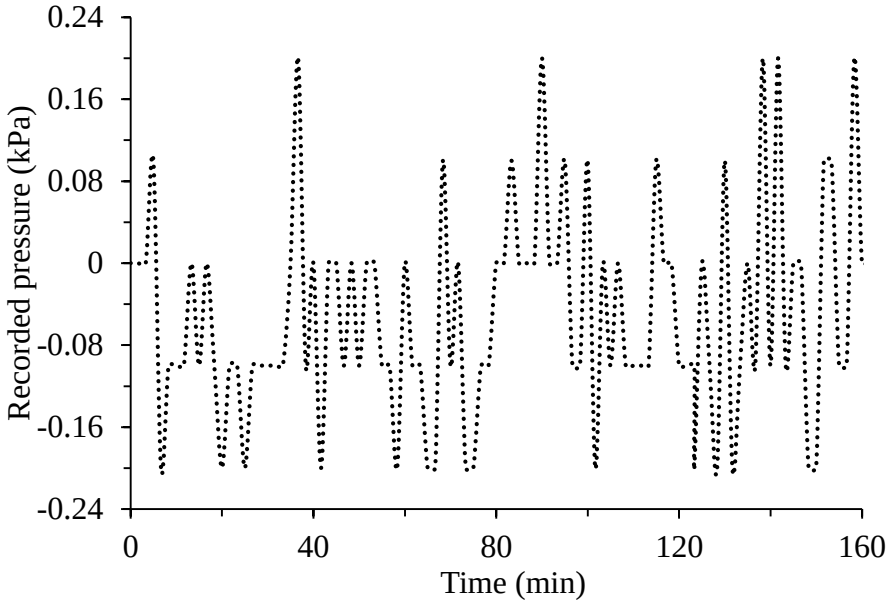
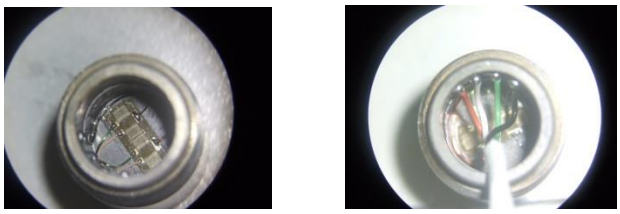


Figure 4.6 Instrument resolution

The strain gauge was initially bonded to the back of the diaphragm using M-Bond-600 adhesive. The installation was protected using M-Coat-C low reinforcement coating. Then, the strain gauge was wired to a terminal using 134-AWN wire. A 2 m miniature screened, twisted pair Teflon jacketed cable was then attached to the terminal. Afterwards, the cap was screwed on the tensiometer's body and sealed using Loctite thread seal. Finally, the cable was anchored to the cap using Raychem S1125 epoxy. Figure 4.7 presents the process of bonding and wiring the strain gauge.



(a) (b)

Figure 4.7 Installation of strain gauge: (a) bonding; (b) wiring

4.7.1.3 Porous Ceramic

In manufacturing WTs, a 1.5 MPa AEV porous ceramic (provided by Soil Moisture Corp.) was machined to the appropriate size and glued within the tensiometers body. A gap of 0.05 mm was considered between the ceramic and the metal and the adhesive was applied uniformly along the sides of the cylindrical ceramic. Once the adhesive

was completely cured and reached its maximum strength, the excess adhesive was machined carefully and levelled with the metallic body.

4.7.2 Minimising Diaphragm's Surface Roughness

In theory, the face milling (called FM hereafter) method, used for machining the diaphragm, should produce very flat surfaces. However, the microscopic inspection of the finished surfaces indicated existence of deep revolution marks [see Figure 4.13(a)] resulted from the motion of the cutter's end face over the material surface. It was therefore essential to reduce the number and the depth of these revolution marks and provide a less rough surface with minimum numbers of potential nucleation sites. To this end, a proper surface polishing technique should be employed.

Typically, conventional polishing tools and techniques such as silicon carbide (SiC) abrasive papers, polishing stones, diamond paste, pneumatic abrading wheels or grinders, and electro discharge machining (EDM) are used for surface finishing (Tsai et al., 2008). These techniques are operationally straightforward and cost-efficient, but typically involve human errors and development of uneven polished surfaces due to the non-uniform force distribution during polishing. In order to improve the surface finish quality, non-conventional polishing techniques such as chemical polishing, electro polishing, abrasive flow polishing, abrasive jet machining, magnetic force polishing, or a combination of mechanical and electro polishing methods have been proposed in the literature (Wang et al., 1998, Yin and Shinmura, 2004, Tsai et al., 2008). These methods, despite producing an improved surface finish, normally involve extended machining costs and time, occasional surface damage, and environmental pollution (Tsai et al., 2008).

The diversity of available polishing methods makes it difficult to select one considering the feasibility and economical aspects of manufacturing HCTs. Therefore, in this work, a comparative study of the efficiency of the most common and cost-efficient metal polishing methods namely EDM, SiC abrasive paper (called SP from now on), and diamond paste abrasive (called DP hereafter) was carried out on dummy cylindrical stainless steel samples. Moreover, a new approach for minimising the diaphragm's surface roughness, namely coating the surface with a thin microscopic layer of a hydrophilic material is presented and discussed in continue.

4.7.2.1 Electro Discharge Machining

The EDM is a thermo-electrical material removal process. A tool electrode shape (also known as work-piece electrode) is introduced to the workpiece and is subjected to an electric voltage. This electrode is separated from the workpiece by a dielectric fluid. The material removal occurs as a consequence of rapidly recurring current discharges between the electrode and the workpiece in the dielectric liquid primarily through conversion of electrical energy into thermal energy. This non-contact material removal procedure is a cost-efficient method and eliminates the common vibration and mechanical stress chatter during machining (Beri et al., 2008). However, the EDM has been reported to leave a large number of craters (large bowl shaped cavities) on the polished surface (Curodeau et al., 2004, Takino et al., 2005). Moreover, the machined surface is found to be prone to thermal damages (Field et al., 1970). This technique was examined by Tarantino and Mongiovi (2002) for polishing the diaphragm surface of the Trento tensiometer and similar results were reported. In this study, the EDM method was examined on two dummy diaphragms and similar observations were obtained. EDM was therefore considered as an inadequate method and was not used for fabrication of the WTs.

4.7.2.2 SiC Abrasive Paper

Another common method for polishing metallic surfaces is the use of abrasive papers. The abrasive papers are fabricated by gluing hard and irregular-shaped particles of abrasive minerals such as sand, corundum, silicon carbide (SiC), etc. on a flexible base such as paper, cloth, or fibre. As the hardness of the abrasive particles is higher than the workpiece, a relatively smooth surface is created through cutting and shearing actions when rubbing the abrasive paper against the workpiece. The rubbing act can be done either by hand or a rotary instrument. Aside from the type of minerals and backings used for fabricating, abrasive papers are typically differentiated by their grit number which depends on the average size and composition of the abrading particles embedded in the paper. Abrasive papers are available in a range of grit sizes typically varying from #100-grit to #2000-grit. A #100-grit abrasive paper contains 100 abrading particles in one square inch. The workpieces are normally polished by abrasive papers with increasing grit starting from a low grit number (coarse abrasives) to a high grit number (fine abrasives). This way, the deep scratch marks developed by using coarse abrasives

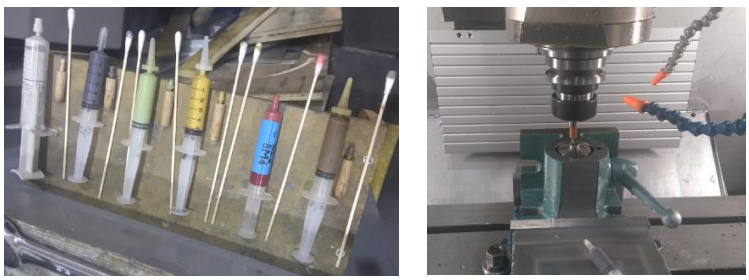
are smoothed and minimised by the finer/softer abrasives which can in turn significantly improve the surface finish quality. The drawback of this method is the dependency on the operator's skills that can affect the reproduction of the polished surfaces with identical roughness properties.

In this study, some dummy samples were polished by SiC abrasive papers with increasing grit from #400- to #1200-grit. Tarantino and Mongiovi (2002) reported that SP with increasing grit can produce smooth diaphragm surfaces. However, the microscopic inspection of the polished samples in this study [see Figure 4.13(b)] demonstrated that a significant amount of scratch marks were developed on the polished surfaces which could potentially lead to development of a considerable number of nucleation sites.

4.7.2.3 Diamond Paste Abrasive

In another attempt to obtain a smooth surface finish, the surfaces of some dummy samples were polished in the milling machine using diamond paste. The paste is made by mixing impurity-free diamond powder with a water soluble oil. The paste provides superior cutting qualities thanks to the high cutting power of the diamond grains. The compound is available in a range of fine to coarse grades.

The samples were polished using diamond paste with decreasing grades i.e., 14 µm, 8 µm, 6 µm, 3 µm, 1 µm, and 0.1 µm grades. An 8-shaped passing pattern was considered for the polishing stage in order to minimise the development of deep revolution marks as a result of diamond grains entrap along typical successive circular passing paths. DP polishing is believed to produce an improved surface finish in comparison to the SP polishing technique [see Figure 4.13(c)]. Figure 4.8 shows the process of polishing the diaphragms using DP polishing method.



(a) (b)

Figure 4.8 Diamond paste polishing method: (a) preparation of the paste with different grades; (b) polishing in milling machine

4.7.2.4 Coating Diaphragms with Hydrophilic Materials

According to Jones et al. (1999), the amount of air trapped in the crevices of the water reservoir depends on the geometry of the crevice as well as the advancing contact angle (θ_a) of the liquid (see Section 2.3.3). The more a surface is hydrophobic (water repelling) the more is the possibility of air being trapped in its crevices due to the development of a higher θ_a at the solid-liquid interface. Conversely, development of a lower θ_a at the solid-liquid interface of a less hydrophobic surface, minimises the possibility of air entrapment in its crevices (Figure 4.9).

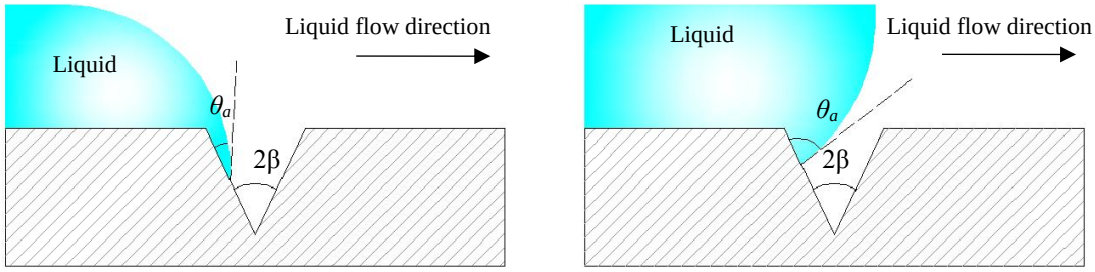


Figure 4.9 Effect of liquid advancing contact angle on air entrapment in a crevice: (a) less hydrophobic surface, low liquid contact angle and less entrapped air; (b) more hydrophobic surface, high liquid contact angle and more entrapped air (after Jones et al. 1999)

A hydrophilic material is a material with strong propensity to attract water and a tendency to be wetted by water. There are two common methods for enhancing hydrophilicity of surfaces; (1) deposition of a microscopic layer of a material more hydrophilic than the substrate, and (2) modifying the chemistry of the substrate using for example plasma or X-ray treatments (Drelich et al., 2011). The latter method is beyond the scope of this study due to its complexity. Hence the former method was applied for producing a smooth and water attracting surface for the diaphragms' inner walls. Deposition of a microscopic layer of a hydrophilic material, in most cases, can significantly reduce the surface roughness by filling the existing crevices on the substrate surface and hence decreasing porosities.

Among many available hydrophilic materials, anti-fog agent, Triton X-100 surfactant, and Titanium Dioxide (TiO_2) materials were chosen for coating the samples. These materials are commercially available at affordable prices. Several techniques including ink-jet printing, spin coating, and sputtering are often used for deposition of films of

Nano-particles on substrates (Drelich et al., 2011). Among these, spin coating technique was found to be a more compatible method for coating the tensiometer diaphragms.

Anti-fog Agent

Anti-fog agents (called AF hereafter) are hydrophilic materials used to prevent fog formation on the surfaces of optical devices such as eyeglasses and goggles. Fog prevention takes place by increasing surface energy hence producing continuous and transparent films of condensed water on the AF treated surfaces. As explained by Chevallier et al. (2011), the main concern in using highly hydrophilic anti-fog coatings are; (1) their solubility in water which can significantly affect their long-term functionality, and (2) their occasional poor adhesion to the substrates which is a function of physical interaction between the two materials. In recently developed AF agents, these problems have been addressed by using crosslinking agents in the composition formulae (for further information see Chevallier et al. 2011).

A microscopic layer of the AF agent (Zero-fog) was uniformly spread over the surface of the DP polished samples using spin coating method. The surface was then left for curing under vacuum at 95°C for a time duration of 6 hours. The coated sample was then aged in deionised water for 24 hours and under constant room temperature, then dried under ambient conditions. The thickness of the film was measured using profilometery (explained later) and found to be in order of 4 µm which was thick enough to fill the valleys of the sample's surface.

Triton X-100 Surfactant

Triton X-100 (or Octylphenol Ethoxylate) is a non-ionic surfactant with excellent wetting characteristics. Surfactants are substances that, except in some limited occasions, reduce the interfacial free energy, and therefore surface tension, between two liquids or between a liquid and a solid (Rosen and Kunjappu, 2012). Their molecular structure contains both hydrophobic and hydrophilic (water attracting) groups. The interaction between the hydrophilic chain and water results in a decrease in surface tension of water. Hence, the coated surface exhibits excellent wetting characteristics. Similar to AF agent, the water-solubility characteristic of Triton is considered as its main drawback for being used in coating the tensiometer's diaphragm. Nonetheless, a microscopic layer of this material was believed to develop relatively

strong bonding with the substrate and hence remain undissolved for a longer period of time. Similar to AF, spin coating method was used for deposition of Triton particles on the samples. The samples were then treated in a vacuum furnace under 240º C for 12 hours to improve the stability of the coating material.

Titanium Dioxide (TiO_2)

TiO_2 nanoparticles have been widely used in epoxy coatings to improve chemical resistance, corrosion resistance, and hydrophilicity of stainless steel substrates, given their high specific area and strong bonding properties to the metallic substrates (Ohkoa et al., 2001, Yu et al., 2003, Conradi and Kocijan, 2016).

Mesoporous TiO_2 material was prepared using the following procedure; initially, 11.27 g ethanol (C_2H_5OH) was poured into a polypropylene bottle. Then 0.32 g of Pluronic F127, 1.02 g distilled water, and 0.14 g of suprapure HNO_3 were added to the bottle. The mixture was stirred at 750 rpm at room temperature using a magnetic stirring plate. Finally, 1.03 g $Ti(OB_4)_4$ was pre-weighed in a separate container and added to the prepared liquor using a pipette. The mixture was then stirred at the same rate for 24 hours in order to age the solution. A thin film of this coating material was deposited on the DP polished stainless steel samples using spin coating method. The samples were then treated in a vacuum furnace under 300º C for 16 hours to improve the stability of the coating material. The microscopic layer of TiO_2 coating was also found to decrease the surface roughness by filling the valleys on the polished surfaces [see Fig. 4.13(f)].

4.8 Surface Roughness Analysis

Analysis of the surface roughness obtained from polishing and coating methods was carried out using three distinctive methods namely surface metrology, microscopic inspection, and contact angle measurement.

4.8.1 Surface Metrology

The random irregularities developed during surface finishing processes including milling, drilling, and mechanical polishing, are known as surface texture or roughness (ISO/DIS4287/1, 1987). Various parameters including roughness or arithmetic average deviation from the mean line (R_a), root mean square value of roughness (R_q), maximum peak of roughness (R_p), maximum valley of roughness (R_v), and maximum peak-to-

valley height (R_t) can be used for characterisation of surface texture (Hasegawa et al., 1976). Figure 4.10 presents a schematic definition of the surface texture parameters. For measurement of these parameters, 3D surface metrology analysis was carried out on the dummy samples using a Bruker contour GT-K profiler (Figure 4.11).

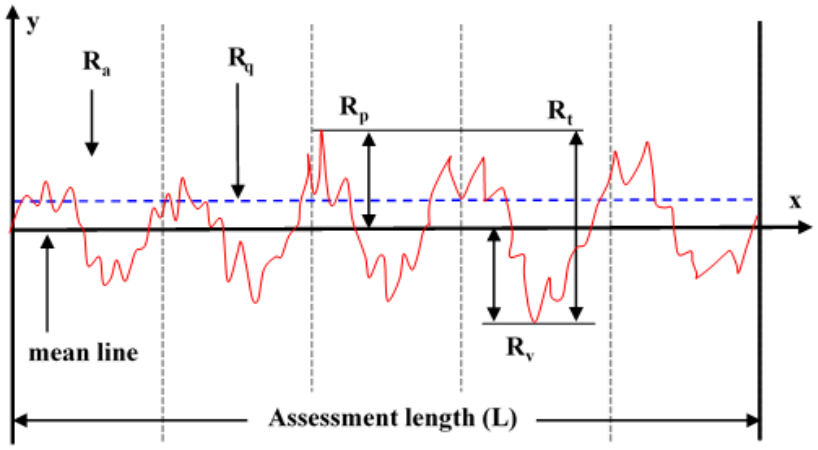


Figure 4.10 Surface texture parameters

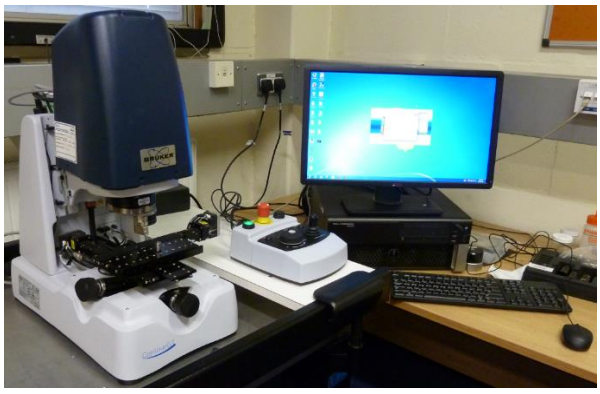


Figure 4.11 The Bruker contour GT-K profiler

Table 4.2 Examples of surface texture parameters obtained from 3D topography analysis on treated AISI 304 stainless steel samples

Sample	Surface texture parameters				Surface treatment method
	R_a	R_p	R_v	R_t	
S1	7.811	18.379	-21.285	39.664	Face-milling
S4	0.433	2.301	-2.657	4.958	SiC abrasive paper polishing
S6	0.308	0.813	-2.031	2.844	Diamond paste polishing
S7	0.212	0.319	-0.731	1.050	Hydrophilic coating (Anti-fog agent)
S10	0.145	0.285	-0.281	0.566	Hydrophilic coating (Triton X-100)
S11	0.163	2.742	-1.938	4.680	Hydrophilic coating (TiO_2)

Figure 4.12 presents the 3D surface topography images. The unevenness of the FM sample and presence of high peaks and deep valleys on the surface are clearly shown

in Figure 4.12(a). These peaks and valleys are reduced on SP and DP polished samples and their values fall within an approximate range of +2.2 μm to -2.2 μm [Figures 4.12(b) and (c)]. The roughness is further decreased on the AF coated, Triton coated, and TiO_2 coated samples [Figures 4.12(d), (e), and (f)], demonstrating the efficiency of hydrophilic coating method in achieving smooth surfaces. The surface texture parameters for some of the tested samples are given in Table 4.2.

4.8.2 Microscopic Inspection

A simple microscopic investigation using an optical microscope was also carried out to evaluate the surface quality obtained from polishing and coating processes. Figure 4.13 presents the microscopic images of the finished surfaces. Also present in Figure 4.13, are the microscopic images obtained from profilometry. It is clear from the images that FM process creates deep revolution marks on the surface which are considered as potential nucleation sites [Figure 4.13(a)]. The SP polishing method significantly improved the surface finish quality, yet development of shallow depth revolution marks appeared to be inevitable [Figure 4.13(b)]. The number of the revolution marks was significantly reduced on the DP polished sample, proving the suitability of this technique for achieving very smooth surfaces [Figure 4.13(c)]. The microscopic images of the AF coated sample [Figure 4.13(d)], Triton coated sample [Figure 4.13(e)], and TiO_2 coated sample [Figure 4.13(f)] were slightly fade due to the viscosity and transparency of the coating materials which cause light reflection. However, the microscopic layers of the hydrophilic coatings provide very smooth surfaces as it can be seen in the profilometry images. Note that the microscopic images of the TiO_2 coated diaphragm present the distribution of the Titanium Nano-particles on the surface. This should not be mistaken as the surface roughness of the sample.

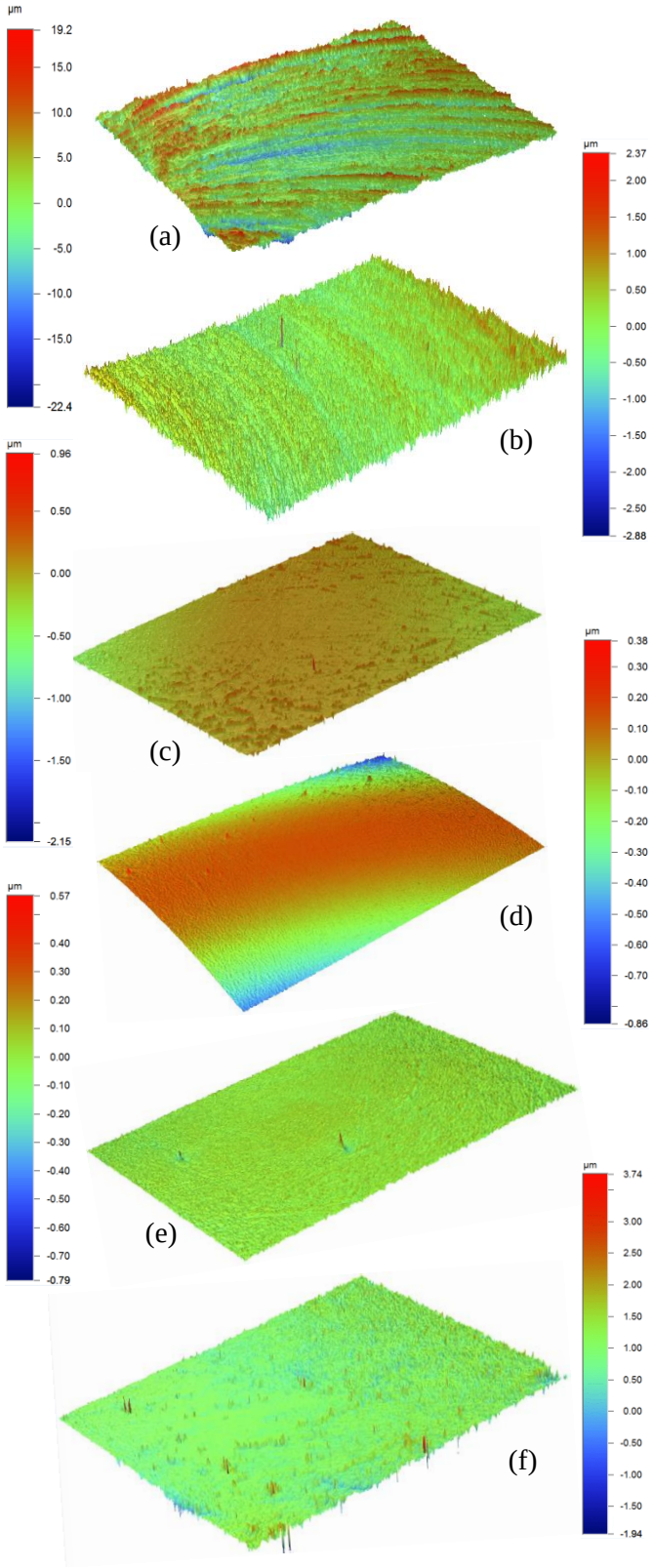


Figure 4.12 3D surface metrology diagrams: (a) FM sample; (b) SP polished sample; (c) DP polished sample; (d) AF coated sample; (e) Triton coated sample; (f) TiO_2 coated sample

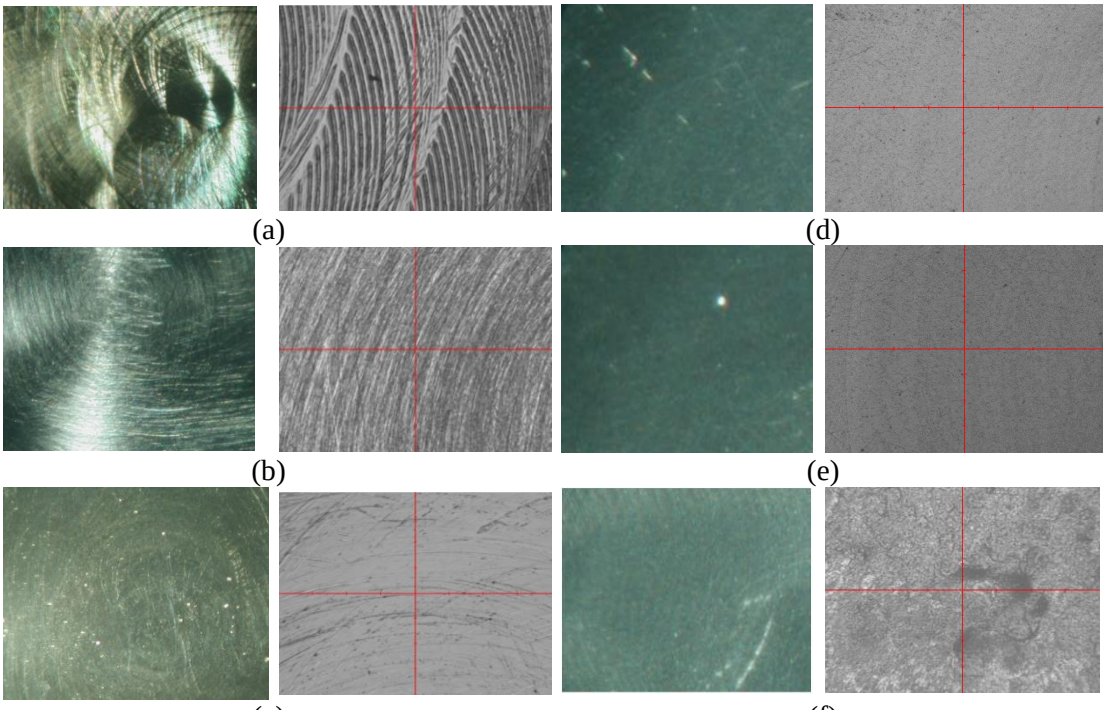
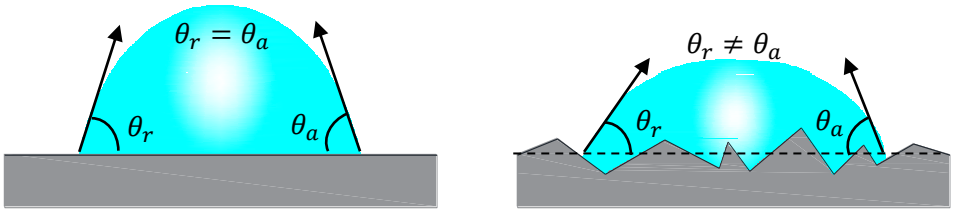


Figure 4.13 Microscopic view of the finished surfaces: (a) FM; (b) SP polished; (c) DP polished; (d) AF coated; (e) Triton coated; (f) TiO_2 coated samples.

4.8.3 Contact Angle

Surface roughness can influence materials' properties such as friction and wettability. By definition, wettability is the natural tendency of a liquid to spread over a solid surface. Under gravity, a liquid droplet, deposited on a solid surface and in equilibrium with its vapour, has a tendency to spread over the solid surface until the cohesive (internal) forces in the liquid, the gravity forces, and the adhesive (capillary) forces between solid and liquid reach an equilibrium state (see Section 2.3.3). At this state, the developed angle between the solid surface and the liquid surface (measured through the liquid) is defined as contact angle and denoted by θ (Figure 4.14).



(a) (b)

Figure 4.14 Definition of contact angles: (a) an ideal surface (higher contact angle); (b) a rough surface (lower contact angle) – θ_a and θ_r are advancing and receding contact angles respectively

The conventional range of contact angle for a well wetting surface is $0^o < \theta < 90^o$. For materials with contact angle range of $90^o < \theta < 180^o$, the penetration (under gravity forces) of liquid into the rough surface asperities is restricted and gas bubbles can be entrapped in the existing crevices. This can result in development of a discontinuous liquid-solid interface and an alternation of gas-liquid and solid-liquid interfaces (She and Sleep, 1998). In the modified classification of hydrophilic and hydrophobic surfaces presented by Drelich et al. (2011), a smooth solid surface is hydrophilic if $\theta \cong 0^o$, weakly hydrophilic if $0 < \theta < (56\text{-}65^o)$, weakly hydrophobic if $(56\text{-}65^o) < \theta < 90^o$, and hydrophobic if $90^o < \theta \leq 120^o$. Figure 4.15 schematically explains the role of hydrophilic coating in enhancing surface wettability and minimising the number of nucleation sites.

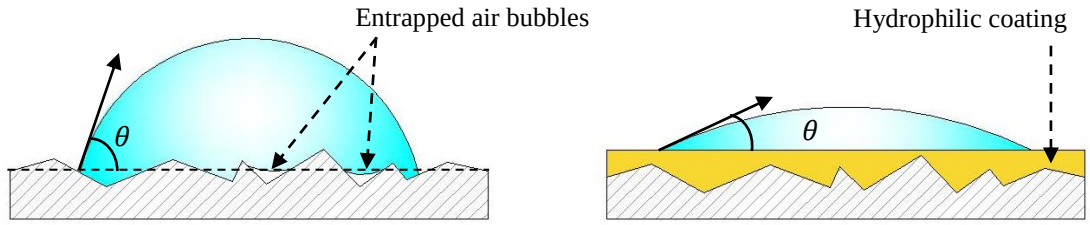


Figure 4.15 (a) Wettability of a rough surface (higher θ); (b) enhanced wettability by coating the rough surface with a hydrophilic material (lower θ)

A difference between advancing and receding contact angles, known as contact angle hysteresis (Chau et al., 2009), indicates surface heterogeneity and non-uniform roughness characteristics (Good, 1992). The contact angle hysteresis value depends on the measurement methods (e.g. sessile-drop or captive-bubble), measurement conditions (static or dynamic), and the volume of the liquid used for measurements (Drelich, 1997, Blake, 2006). Although, contact angle hysteresis is known as a characteristic of a heterogeneous rough surface, it can be also observed on a homogenous smooth surface with hydrophilic properties such as glass and metals. The reason behind this phenomenon is the development of thin water films of different thicknesses on the hydrophilic surfaces subjected to contact angle measurements as a result of adsorption (α-Films) and wetting (β-Films) processes (Starov et al., 2007). These respectively stable and metastable water films remain in equilibrium with the bulk water (droplet) placed on the surface and affect the measured contact angles. In case of metals (other than noble metals) and alloys, contact angle measurements can be

also affected by presence of a thin film of an oxide layer covering the hydrophilic metallic surface. Indeed, the measured contact angle in this case represents the wetting properties of the oxide layer and not the metallic surface (Drelich et al., 2011). Hence, it is necessary to keep the hydrophilic surfaces free of contamination prior to conducting contact angle measurements. Figure 4.16 presents the difference between measured advancing and receding contact angles (see Chapter 2, Section 2.3.3) of a water droplet placed on an AF coated sample.

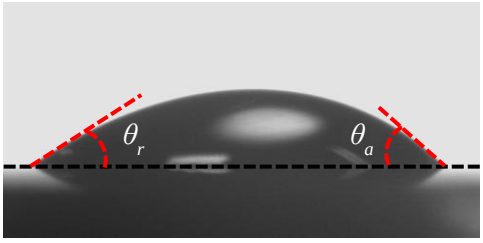


Figure 4.16 Contact angle hysteresis on an AF coated sample θ_a = 45º and θ_r = 35º

Contact angle measurements were carried out using a DataPhysics OCA 20 contact angle measurement apparatus (Figure 4.17). The device is also capable of measuring the hysteresis between the advanced and receded contact angles useful for indication of surface chemical heterogeneity and roughness. The common method of sessile drop was used to study the wettability. The measurements for each sample were repeated 3 times and representative apparent contact angle values were reported based on averaging the obtained values. Prior to measurements, all samples were cleaned with ethanol in an ultrasonic bath and then oven-dried at 80° C. The whole measurement process was carried out under constant room temperature of 21° C and ambient humidity. To further ensure consistency in measurements, the equilibrium contact angles were measured 3 seconds after deposition of the water droplet. For each sample, water droplets of 1 µL volume were placed at three different points over the surface area. This way, the effect of α- and β-films on measurements was minimised and also the non-uniformity of surface roughness, if any, over the surface area could be assessed.

Figure 4.18 presents the results of contact angle measurements on the dummy samples. The measured contact angle on the FM sample (θ = 74º) was lower than that of the SP sample (θ = 81º), yet both were within the θ range associated with weakly hydrophobic materials. Similarly, the DP sample exhibited a larger contact angle (θ = 87º) than the SP sample with a θ value close to the boundary between hydrophobic and weakly

hydrophobic materials. In fact, improvement of surface roughness by polishing the samples using DP and SP methods decreased the hydrophilicity of the treated surfaces. Development of water repelling characteristics in the polished surfaces may, in turn, offset the improvement in cavitation occurrence, achieved by reducing surface roughness. The AF coating significantly improved the surface affinity to water and lowered the equilibrium apparent contact angle to $\theta = 41^{o}$. Further improvement in hydrophilicity was achieved from the Triton-coated sample with an average contact angle of $\theta = 34^{o}$. Similarly, the TiO_2 coated sample showed a contact angle of $\theta = 18^{o}$, representing significantly improved wetting characteristics.



Figure 4.17 The DataPhysics OCA 20 contact angle measurement apparatus

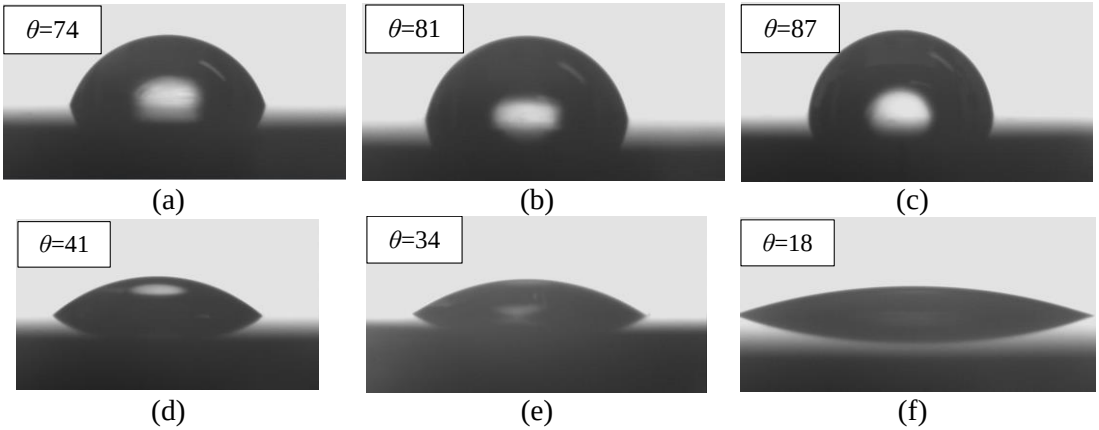


Figure 4.18 Measured contact angles: (a) FM sample; (b) SP polished sample; (c) DP polished sample; (d) AF coated sample; (e) Triton coated sample; (f) TiO_2 coated sample

4.9 Experimental Program for Evaluation of the New HCTs' Performance

In order to examine the effect of diaphragm surface roughness on the performance of the HCTs, several prototypes were manufactured with different surface treatment techniques applied to their diaphragms. Table 4.3 presents the properties of these manufactured HCTs. In the following, the processes of saturation and calibration of the developed HCTs together with the experimental program followed for examination of their performances are discussed in detail.

Table 4.3 Properties of the WTs

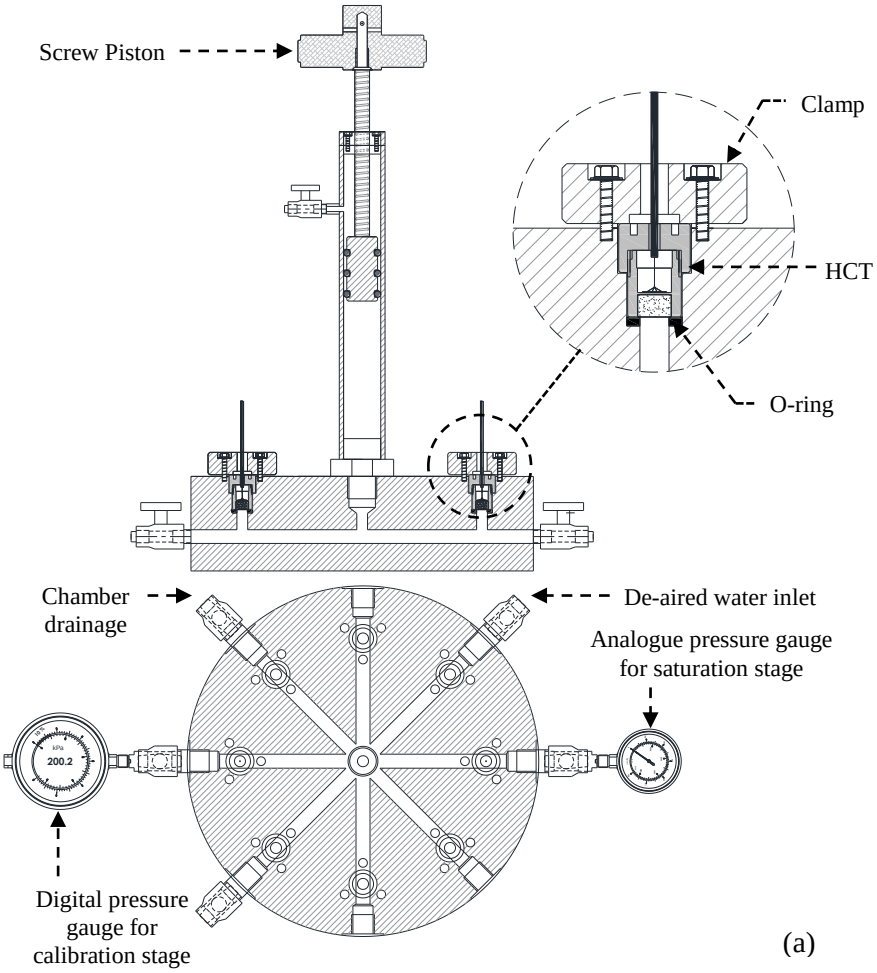
HCT	Diaphragm surface treatment method
WT1, WT2	Face-milling
WT3, WT4	SiC abrasive paper polishing
WT5, WT6	Diamond paste polishing
WT7, WT8	Hydrophilic coating (Anti-fog agent)
WT9, WT10	Hydrophilic coating (Triton X-100)
WT11, WT12	Hydrophilic coating (TiO_2)

4.9.1 Saturation

A purpose built stainless steel chamber (Figure 4.19) was designed and manufactured for saturation and calibration of the tensiometers. The saturation chamber possesses 8 slots to insert and clamp the HCTs in a way that their ceramic filter is faced inward and prone to vacuum, water flooding and pressurisation. A screw piston positioned at the centre of the chamber enables pressurisation of the fluid inside the chamber.

The HCTs were saturated in the saturation chamber following the procedure explained by Tarantino (2004). The tensiometers with their ceramic filter at initially dry state were placed and sealed in the saturation chamber. A vacuum pressure was then applied to the chamber and maintained for one hour to remove as much air as possible from the chamber and the ceramic filters. While maintaining the vacuum pressure, the ceramic filters were flooded with de-aired demineralised water. Subsequently a positive water pressure of 4 MPa was applied to the chamber to force the residual amount of air into solution. A GDS pressure/volume controller was used to increase the water pressure up to 3 MPa. Beyond this value the pressure/volume controller was disconnected and the pressure was increased by means of the screw piston. The pressure drop due to

saturation of the ceramics and dissolution of air bubbles was compensated regularly to maintain a constant pressure during the saturation period.



(a)



(b)

Figure 4.19 Saturation chamber: (a) schematic diagram; (b) photo

At the end of the saturation course, a simple examination was carried out to evaluate the success of the saturation process. First, a loading–unloading cycle was applied to the saturation chamber in steps of 100 kPa and the HCTs responses were monitored. Each loading (unloading) stage was kept for 10 minutes so the sensors reach equilibrium with the applied pressure. According to Lourenço et al. 2006, instantaneous response of the HCT to change in pressure during pre-pressurisation can be considered as an index for adequate saturation. All HCTs were found to respond immediately to the pressure change, and pressure equilibrium stablished in less than 10 minutes for each loading (unloading) stage.

Furthermore, as stated by Tarantino (2004), an adequately saturated tensiometer should reach pressure equilibrium within 1-2 hours if immediately placed in free water by the end of saturation course; therefore, upon removing from the saturation chamber, the tensiometers were placed in free water and the pressure changes were monitored. The residual pressure remaining in the sensors by the end of saturation course was found to vary between 39 to 12 kPa (Figure 4.20). Equilibrium was achieved in 70 to 85 minutes for all tensiometers indicating their adequate saturation.

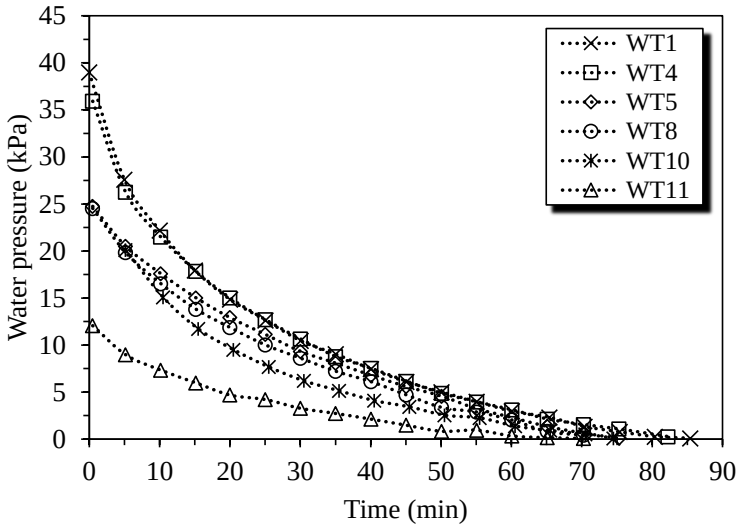


Figure 4.20 Residual pressure equilibrium by the end of saturation course

4.9.2 Calibration

In principle, the HCTs should be calibrated in negative range. However, as explained in Section 4.5, calibration of HCTs in positive range and development of a linear extrapolation to the calibration equation for pressures in negative range can also provide an accurate calibration with a small error in range of 0.5 – 8.5% (Guan and Fredlund,

1997) or 1.0 – 1.5% (Tarantino, 2004) of the measured suction. Calibration in a positive range has been widely accepted by HCT users (see for example Lourenço et al., 2008). In this study, calibration of the tensiometers was performed in positive range. A loading – unloading cycle was applied in steps of 100 kPa and up to 1.5 MPa and the corresponding voltage outputs were recorded. The obtained curves exhibited a linear trend both for loading and unloading cycles. The calibration error, remained at a low range of 0.25 – 0.33%. Figure 4.21 presents an example of the obtained calibration curve.

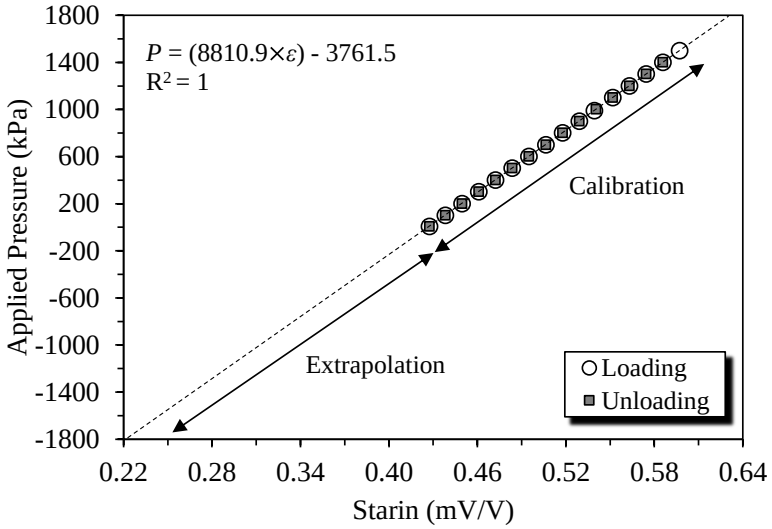


Figure 4.21 Calibration curve for WT4

4.9.3 Determination of Maximum Sustainable Suction s_{max}

A set of experiments was performed to examine the performance of the WTs in terms of s_{max}. For this set of experiments, the ceramic filter was wiped and allowed to dry off at ambient temperature (free evaporation test). Figure 4.22 presents the results of free evaporation (FE) tests carried out on WT1, WT4, WT5, WT8, WT10, and WT11. As it was expected, the tensiometer with FM diaphragm (WT1) cavitated at approximately 65% (-972 kPa) of its nominal capacity. A plausible explanation for cavitation mechanism in this case could be the development of air cavities in the reservoir due to the presence of a large number of gas nuclei entrapped in the crevices of the water reservoir walls. Tensiometers WT4 (SP polished diaphragm) and WT5 (DP polished diaphragm) cavitated respectively at 1809 and 1838 kPa suctions, values up to 122% of the nominal capacity. Comparing these results with the performance of the WT1 (FM diaphragm), validates the significance of having a smooth surface on the interior walls

of the water reservoir to improve cavitation resistance and hence s_{max}. As explained earlier, typically, the air cavities are initially formed in the ceramic disk. However, development of air cavities in the water reservoir, in a faster rate than in the ceramic disk, is also contingent. It is hard, however, to comment on the predominant mechanism of cavitation for WT4 (SP diaphragm) and WT5 (DP diaphragm), as the free air bubbles may have been initially formed in the water reservoir. Finally, the response of the tensiometers with AF, Triton, and TiO_2 coated diaphragms showed greater resistance against cavitation when compared with other prototypes. These HCTs sustained suctions of 1906, 1900 and 2301 kPa, respectively. Identifying the contribution of diaphragms' surface smoothness in increasing the s_{max} might still be premature when comparing the performance of the sensors with AF coated diaphragm, WT8, and Triton coated diaphragm, WT10 (s_{max} values of up to 127% of the nominal capacity), with the performance of the polished diaphragm HCTs. However, the role of the water reservoir surface roughness is more clear when under identical initial conditions (i.e. degree of saturation of the ceramic disks), a s_{max} value of 153% of the nominal capacity was recorded by the HCT with TiO_2 coated diaphragm (WT11).

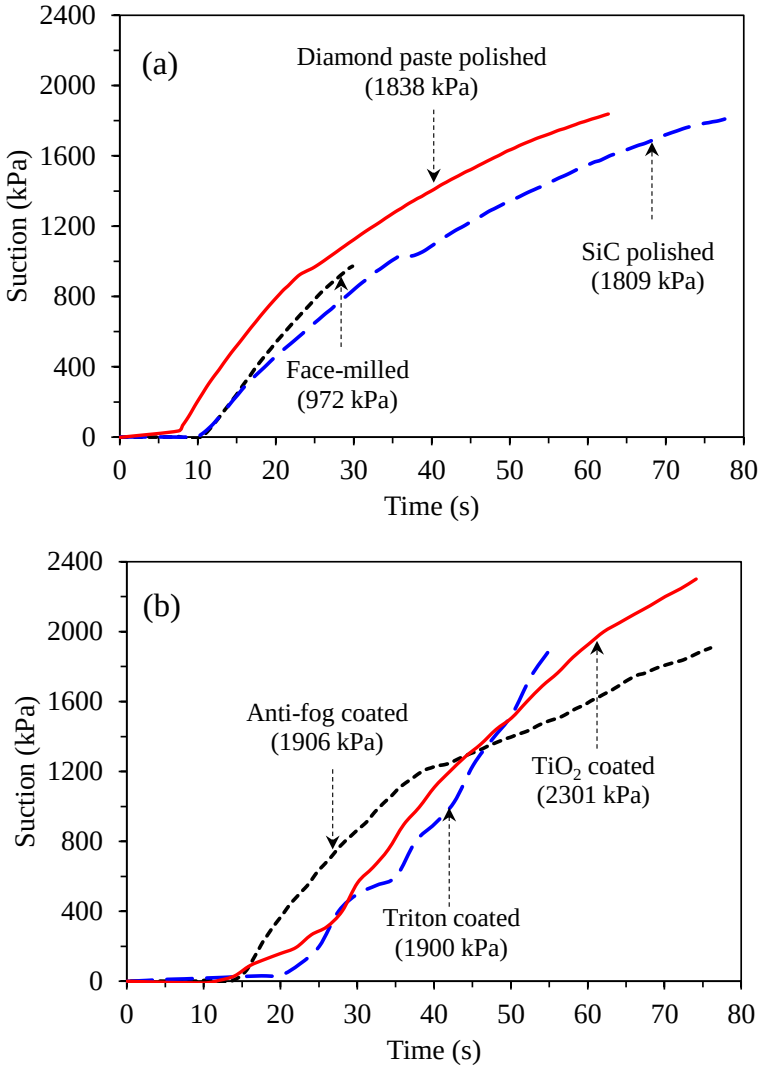


Figure 4.22 Free evaporation tests: (a) HCTs with mechanically polished diaphragms; (b) HCTs with hydrophilic coated diaphragms – values in brackets indicate the s_{max}

4.9.4 Response to Sudden Pressure Changes

Cyclic evaporation (CE) tests were performed on the tensiometers to evaluate the sensors capability in recording sudden changes in suction, as suggested by Guan and Fredlund (1997), He et al. (2006), and Mancuso and Papa (2014). The probes were subjected to cycles of free evaporation up to predetermined suctions and subsequently placed in contact with the free water after each evaporation cycle, and allowed for pressure recovery to atmospheric pressure. Figure 4.23(a) shows the results of CE tests on WT1 (FM diaphragm). The WT1 was cavitated at 976 kPa and after 10 evaporation cycles. It was observed that the HCTs with polished diaphragms exhibited relatively similar performances during CE tests [Figures 4.23(b) and (c)]. However, they recorded significantly lower values (about 300 kPa) of s_{max} during CE tests than the FE tests.

Similar results were obtained from HCTs with AF and TiO_2 coated diaphragms [Figures 4.23(d) and (f)]. The HCT with Triton coated diaphragm (WT10) was, however, able to sustain a suction value very close to its observed s_{max} in the FE test [Figure 4.23(e)]. A possible explanation for the underlying mechanism of cavitation during CE tests is that, by applying cycles of negative pressure, initially microbubbles develop on the reservoir walls, subsequently with increasing the number of cycles, the density of the microbubbles decreases (Bremond et al. 2005) resulting in their detachment from the surface, forming free air cavities, and hence facilitating cavitation at lower suctions than s_{max}. Except WT1 (FM diaphragm), the other HCTs were cavitated at suctions above their nominal capacity. The presence of a fewer number of crevices on the reservoir walls, results in delayed interfusion of detached microbubbles into larger free air bubbles capable of forming discontinuities in the water reservoir. Furthermore, for HCTs with coated diaphragms, an additional tensile force is required to overcome the attractive forces exerted by the hydrophilic surfaces to the water molecules at the air-water interfaces of entrapped microbubbles, resulting in elevation of cavitation threshold.

Another noteworthy observation was that after each cycle of cavitation to pre-specified suctions, and upon placing the tensiometer in free water, the measurements did not return to zero value even if enough time was given for pressure equilibrium. After each cycle of cavitation, the sensors measured a small negative pressure which was increased with increasing the number of cavitation cycles. A possible explanation for this observation can be the development and enlargement of air cavities in the ceramic disk that prevent pressure equalisation between the water in the reservoir, that is under tension, and the free water at atmospheric pressure.

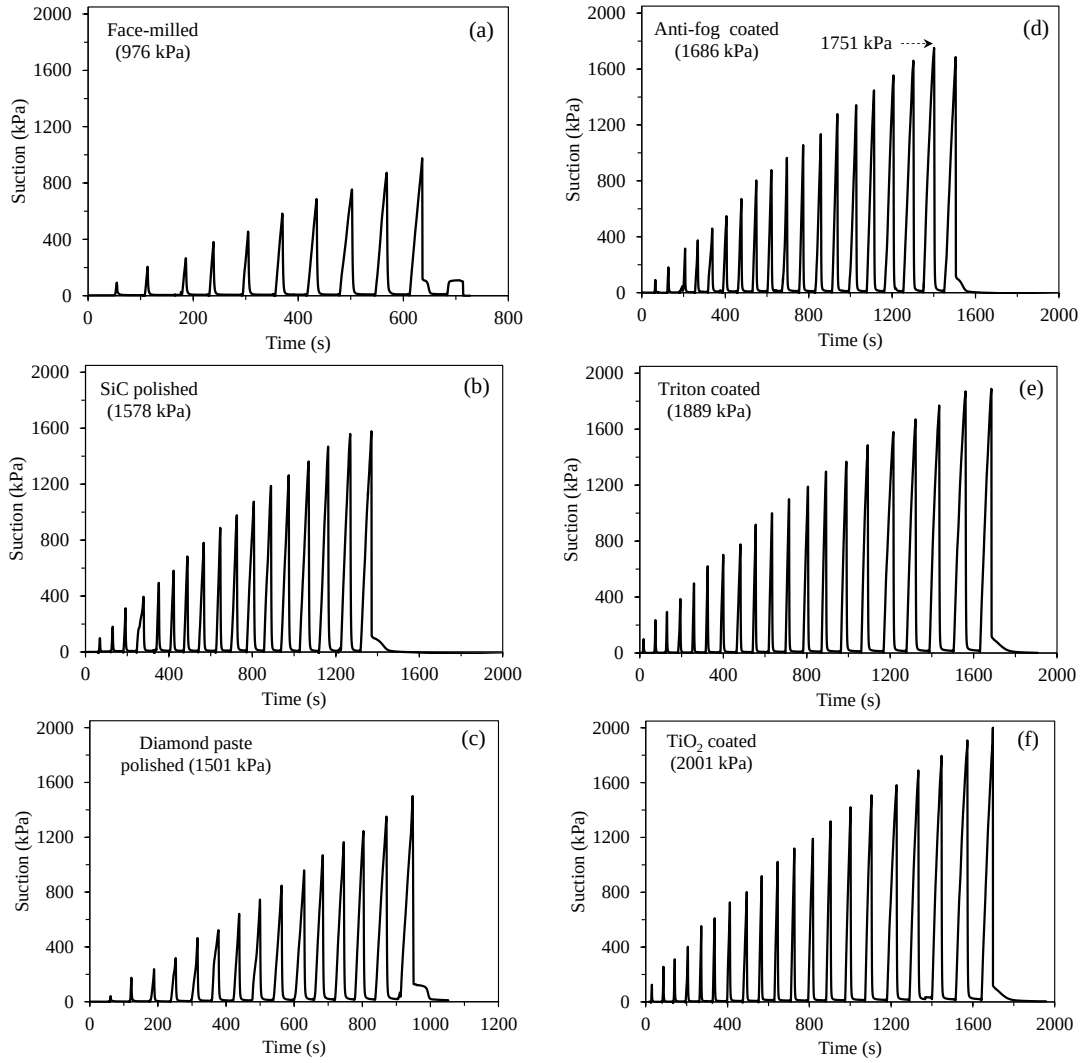


Figure 4.23 Cyclic evaporation tests – values in the brackets indicate s_{max}

4.9.5 Evaluation of Long-term Stability of Measurements and t_{max}

As mentioned earlier, one drawback of the HCTs is their inability for measurement of high suctions (> 1 MPa) for long periods of time. To investigate the effectiveness of the proposed diaphragm treatment methods for improving the long-term performance of the new HCTs, two sets of experiments, namely constant suction tests and increasing suction tests, were carried out on reconstituted London Clay (LC) specimens prepared based on the method explained in Chapter 3. In constant suction tests, HCT measurements were carried out on soil samples air dried to water contents corresponding approximately to suctions of 600 and 1000 kPa, based on the information obtained from the soil water retention curve (see section 4.10). In increasing suction tests, HCT measurements were carried out on initially saturated specimens which were exposed to the atmosphere and allowed to lose moisture at a relatively constant rate.

Both sets of experiments were performed in a new unsaturated oedometer cell (Figure 4.24). The cell accommodates a cylindrical specimen of 75 mm diameter and 20 mm height. The special design of the loading cap allows for installation of two HCTs on the specimen. A transparent nitrile membrane was used to seal the annular gap between the cell body and the loading cap. Prior to the experiments, the ultimate contact between the tensiometer ceramic disk and the specimen was ensured by covering the ceramic disk with some soil paste made by mixing LC powder with demineralised de-aired water at $w \cong 0.50$. The weight of the loading cap also contributes in providing ultimate contact between the HCT and the specimen. All experiments were conducted in a temperature and humidity controlled environment.

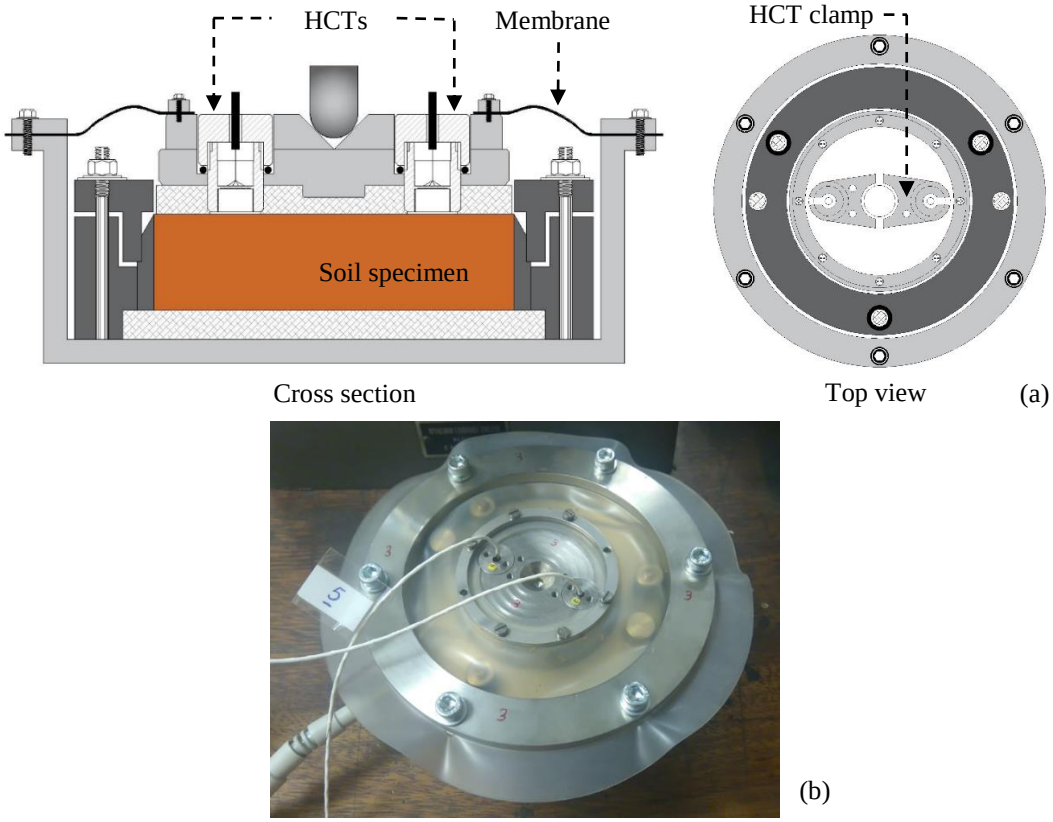


Figure 4.24 New oedometer cell for testing unsaturated soil specimens: (a) schematic diagram; (b) photo

4.9.5.1 Constant Suction Tests

Table 4.4 presents the details of the long-term suction measurements on constant suction specimens. The tests were performed in a temperature- and humidity-controlled environment. The equilibrium suction (s_{eq}) was determined when pressure changes were in the range of ± 0.4 kPa.

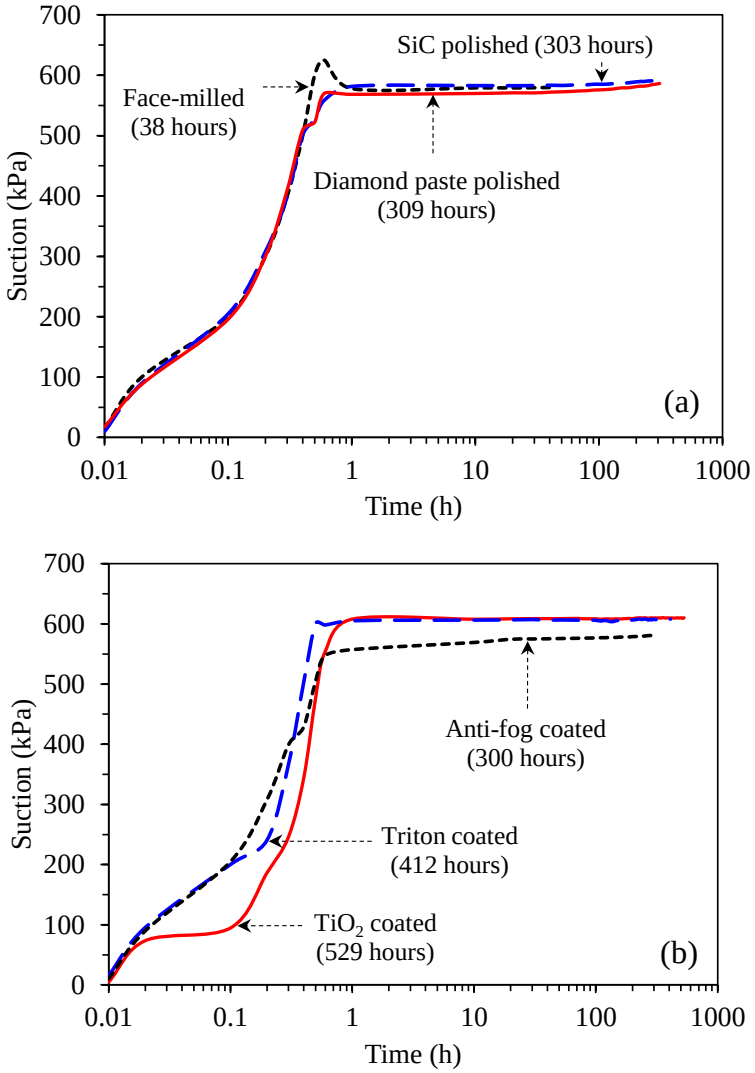
Table 4.4 Long-term suction measurement tests

Test No.	Cell No.	s_{eq} (kPa)	HCT	Duration (hr)*
1	A	579	WT1	38
2	A	582	WT4	303
3	B	570	WT5	309
4	B	575	WT8	300
5	C	606	WT10	412
6	C	608	WT11	529
7	A	973	WT1	1
8	A	977	WT4	268
9	B	971	WT5	262
10	B	968	WT8	267
11	C	991	WT10	360
12	C	996	WT11	475

* includes the pressure equilibrium duration

Figures 4.25(a) and (b) present the results of long-term suction measurements on specimens having approximately 600 kPa suction. The WT1 (FM diaphragm) was able to sustain a suction of 579 kPa for a duration of only 38 hours at which it was cavitated. For this sensor, the possible mechanism of cavitation appears to be controlled by development of air cavities at the diaphragm-water interface. The HCTs with polished diaphragms (WT4 and WT5) exhibited an improved performance and were able to sustain suctions of 582 and 570 kPa for durations of 303 and 309 hours respectively. For these two sensors, the mechanism of cavitation is unknown. However, minimising the presence of air bubbles in the water reservoir almost certainly played a significant role in prolonging the measurement durations, even if cavitation was first initiated in the water reservoir. The performance of the AF coated diaphragm (WT8) was also very similar to the polished diaphragm HCTs, indicating the possibility of dissolution of the AF coating during the continuous use of this sensor and application of cycles of cavitation and pressurisation. This tensiometer measured a suction of 575 kPa for a duration of 300 hours. It must be mentioned here that after about 40 hours of measuring constant suctions, WT4 (SP diaphragm), WT5 (DP diaphragm), and WT8 (AF coated diaphragm) recorded an increasing rate of suction up to their tension breakdown. This could be due to leakage from the sealing membrane of the oedometer cells A and B. The recorded pressure differences were, however, within a range of 10-15 kPa which is small enough not to have any significant impacts on the test results. The WT10 (Triton coated diaphragm) and WT11 (TiO_2 coated diaphragm) tensiometers exhibited significantly improved performances with t_{max} of 412 and 529 hours corresponding to 606 and 608 kPa suctions respectively. This notably improved performance was

believed to be due to; i) minimised number of nucleation sites in the water reservoir, and ii) strong affinity of water molecules to the hydrophilic surfaces of the reservoir walls which requires higher tension and/or sustained tension duration to cause cavitation.



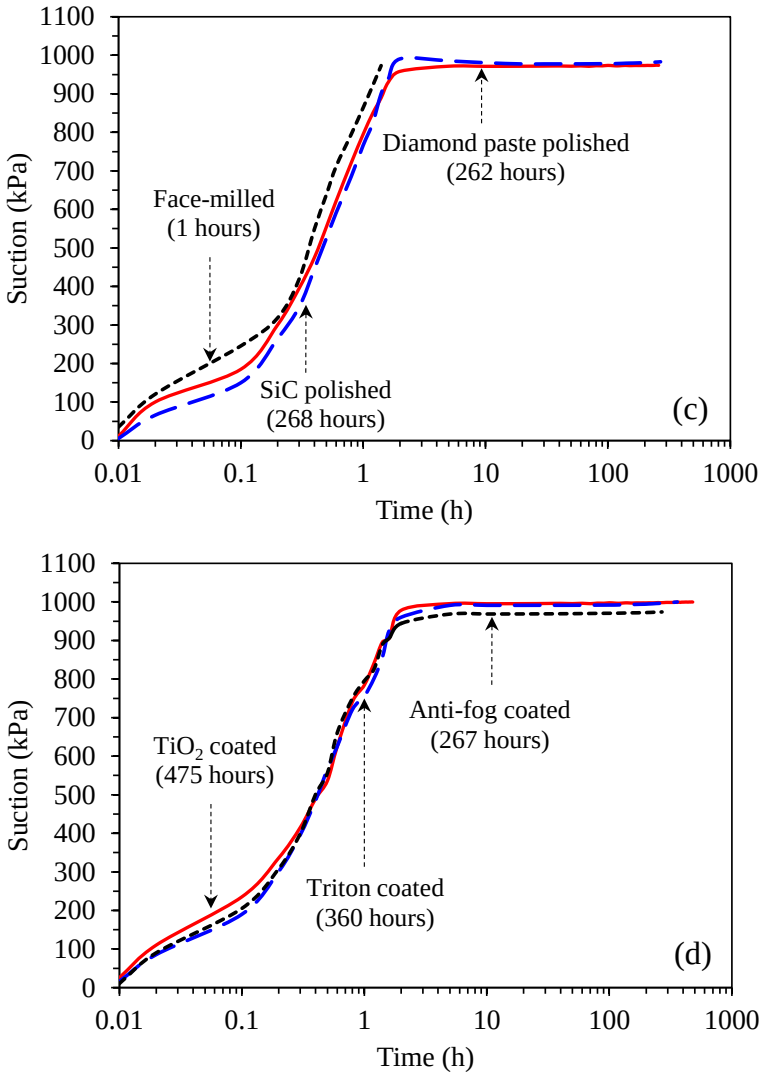


Figure 4.25 Long-term performance of the HCTs during constant suction tests: (a) mechanically polished diaphragms under ~600 kPa suction; (b) hydrophilic coated diaphragms under ~600 kPa suction; (c) mechanically polished diaphragms under ~1000 kPa suction; (d) hydrophilic coated diaphragms under ~1000 kPa suction – Values in brackets indicate the t_{max}

The performances of WTs in contact with specimens having approximately 1000 kPa suction are shown in Figures 4.25(c) and (d). The WT1 (FM diaphragm) cavitated after only one hour and before reaching equilibrium with the specimen's pore-water tension. The pressure equilibrium between the HCT and the specimen is typically achieved in about 10 minutes (Wijaya and Leong 2016), in this case the delayed apparent equilibrium was believed to be due to high water content in the soil paste applied to the ceramic disk of the HCTs. WT4 (SP diaphragm) and WT5 (DP diaphragm) were able to record suctions of 977 and 971 kPa for a time period of 268 and 262 hours

respectively. Once again, the performance of WT8 (AF coated diaphragm) was found to be very similar to the polished diaphragm HCTs. Finally, the WT10 (Triton coated diaphragm) and WT11 (TiO_2 coated diaphragm) showed remarkable records of measuring suctions of 991 and 996 kPa for the durations of 360 and 475 hours, respectively. Under higher suctions, the expansion of air cavities at the diaphragm-water interface and inside the ceramic disk was accelerated, leading to lower t_{max} values. Considering t_{max} values obtained from the WT4 (SP diaphragm) as the reference, the improvements achieved from Triton and TiO_2 coating methods were in the range of 134% – 177% for both sets of experiments carried out.

The HCTs with hydrophilic coated diaphragms were also used in long-term consolidation tests on LC specimens having suctions of around 200 kPa. The HCTs were able to measure the constant suction of 200 kPa for a duration of 37 days without being cavitated. At the end of the tests, free evaporation tests were carried out on the tensiometers (Figure 4.26). As seen in the figure, the HCTs were able to record higher s_{max} values than those obtained prior to the long-term tests (shown in Figure 4.22(b)). This response could be attributed to pore clogging in the ceramic disks due to prolonged contact with a very fine-grained clayey soil that resulted in a decreased porosity of the ceramic disk and consequently increased its AEV. Based on these results, development of gas bubbles in the ceramic filter may be the possible predominant cavitation mechanism in the new HCTs.

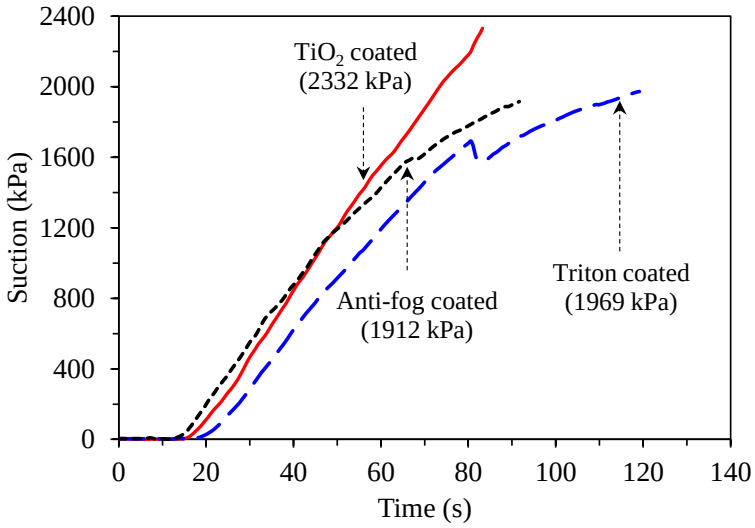


Figure 4.26 Free evaporation tests on HCTs with hydrophilic coated diaphragms after long-term consolidation tests – values in brackets indicate the s_{max}

4.9.5.2 Increasing Suction Tests

Figure 4.27 shows the recorded suction changes with time on continuously drying specimens. As expected, the WT1 (FM diaphragm) was only able to record the evolution of suction for 18 hours and cavitated at 954 kPa. It is more likely that cavitation was first initiated in the water reservoir with the rough surface, rather than in the ceramic disk, although a definite conclusion cannot be drawn. Comparing the performance of this sensor with WT4 and WT5 that had polished diaphragms and cavitated at suctions of 1610 and 1672 kPa, after 24 and 27 hours, respectively, confirms the important role of the diaphragm surface smoothness in improving the cavitation threshold and delaying its occurrence. The WT8 (AF coated diaphragm) showed very similar performance to WT5, with s_{max} = 1693 kPa and t_{max} = 28 hours, further recognising the likelihood of the AF micro-layer dissolution into the water during the long-term use of the HCT. The WT10 (Triton coated diaphragm) cavitated at 1763 kPa and after 32 hours, whereas the WT11 (TiO_2 coated diaphragm) recorded a tension breakdown of 2104 kPa after 28 hours continuous measurement of increasing suction. The significant differences in s_{max} and t_{max} values recorded by WT10 and WT11 placed on the same specimen, may be attributed to the possible differences in evaporation rate at the contact area of the two HCTs and the specimen. A possible reason for the lower s_{max} values observed in this set of experiments, can be due to the effect of air diffusion into the ceramic filter during the course of air drying, facilitating cavitation in HCTs.

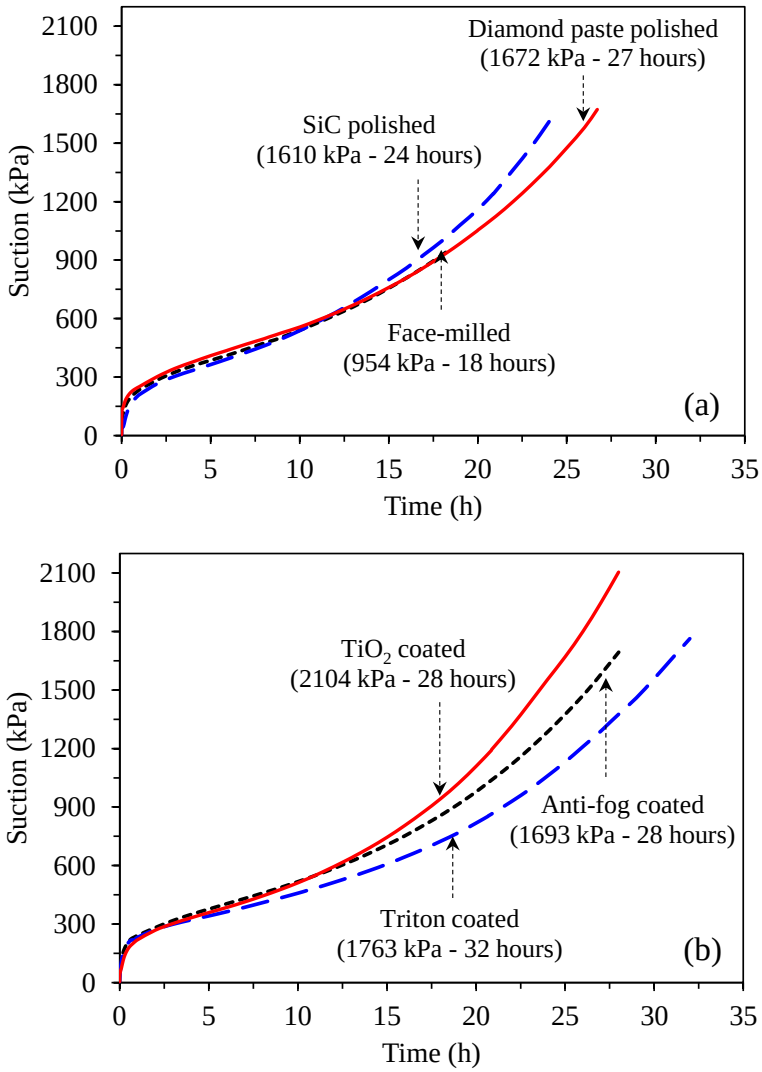


Figure 4.27 Long-term performance of the HCTs during increasing suction tests – Values in brackets indicate s_{max} and t_{max} respectively

4.10 Using the Developed HCTs for SWRC Development

As discussed in section 4.6, the previous studies on the measurement of SWRCs using HCTs have revealed the independency of the SWRC to the specimen moisture evaporation-rate in the dynamic measurement method (Cunningham, 2000, Boso et al., 2003). In this section, the SWRCs of the reconstituted London Clay specimens are determined using the new HCTs. The performance of the HCTs during SWRC measurements are assessed. Moreover, the effect of evaporation-rate on the obtained SWRCs is evaluated.

4.10.1 Experimental Setup and Measurement Procedure

SWRC of London Clay specimens was measured using HCTs and based on the continuous drying method. As shown in Figure 4.28, the soil specimen enclosed in the confining ring (75 mm diameter and 20 mm height) was placed on a porous stone sitting on the digital balance with 0.01 g resolution. The porous stone is used to facilitate the dynamic drying process by exposing the specimen's base to atmosphere, hence minimising the effect of exposed surface area. Two holes of 10 mm diameter and 6 mm depth were created on the sample surface, using a mini augur, to accommodate the HCTs. These holes provide lateral support for the probes' body to keep them in place throughout the measurements (the outer diameter of the tensiometer body is 11 mm). This method is believed to minimise the specimen disturbance at the contact area with the tip of the tensiometer, in comparison with the method followed by Lourenço et al. (2011) to push the probe 3 mm into the specimen which can cause local consolidation and therefore affect the measurements. Moreover, using the suggested method, suction is measured close to the middle height of the specimen where it can be reasonably assumed that evaporation takes place at a constant and uniform rate. This way the effect of non-uniform evaporation at the exposed surfaces is eliminated. In addition, the effect of accelerated drying in localised areas due to the surface cracking during continuous drying, which can result in development of inhomogeneous suction fields across the specimen, is minimised. Two HCTs were gently fitted into the holes on the specimen surface. A thin layer of soil paste (see Section 4.9.5) was also applied to the tip of the sensor to ensure a good contact with the soil. The sensor cable was also supported by a hanger to eliminate the possible mass measurement errors associated with its weight and stiffness. The testing program was carried out under constant temperature and humidity conditions. To minimise the fluctuations of temperature and humidity inside the laboratory due to sequential door openings by the lab users, all the experiments were commenced after the working hours and also during the weekends. Measurements of sample's mass were continuously recorded on the computer using an RS232 interface. The tests were performed on 5 identical specimens cored from a single cylindrical sample (100 mm diameter and 130 mm height) consolidated from slurry in a consolidometer following the procedure described in Chapter 3. In this set of experiments, only the main drying branch (starting from the fully saturated sate) of the SWRC-*w* was produced.

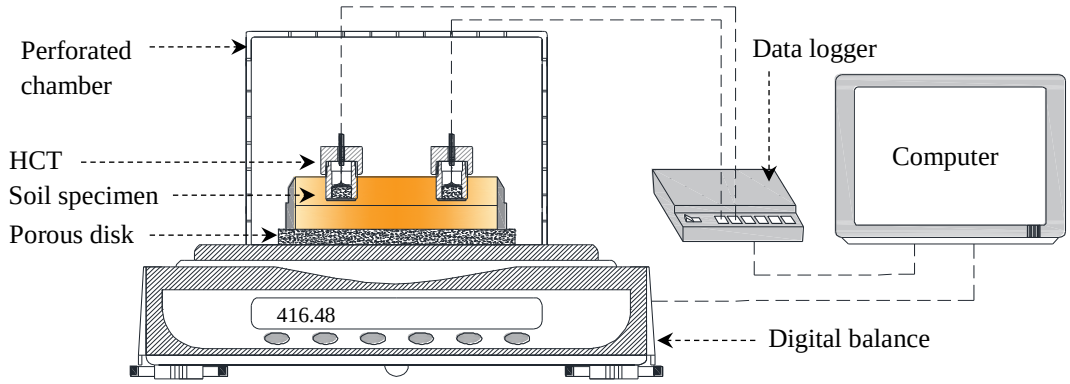


Figure 4.28 Schematic diagram of the experimental setup for SWRC measurement

4.10.2 Continuous Drying Tests

A total of 3 tests were performed on reconstituted London Clay specimens, with two HCTs recording suction evolutions in each specimen. These tests are denoted CD1 to CD3, with CD standing for continuous drying. Figure 4.29 presents a plot of the variation of the mass of water evaporation with time as the specimen is dried out. As it can be seen, the evaporation-rate follows an approximately linear trend for all the three tests. The initial conditions of the specimens as well as the obtained key parameters from CD tests are shown in Table 4.5. Note that e_0 is the initial void ratio, w_{sat} and w_f are the initial (saturated) and final water contents respectively, Δm_w is the evaporated mass of water, Δt is the test duration, and $\Delta m_w/\Delta t$ is the moisture evaporation-rate. Figure 4.30 presents the obtained SWRCs.

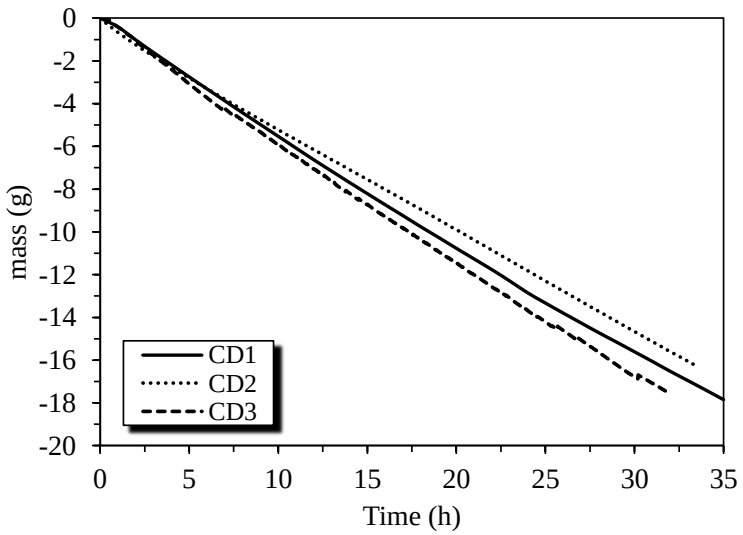
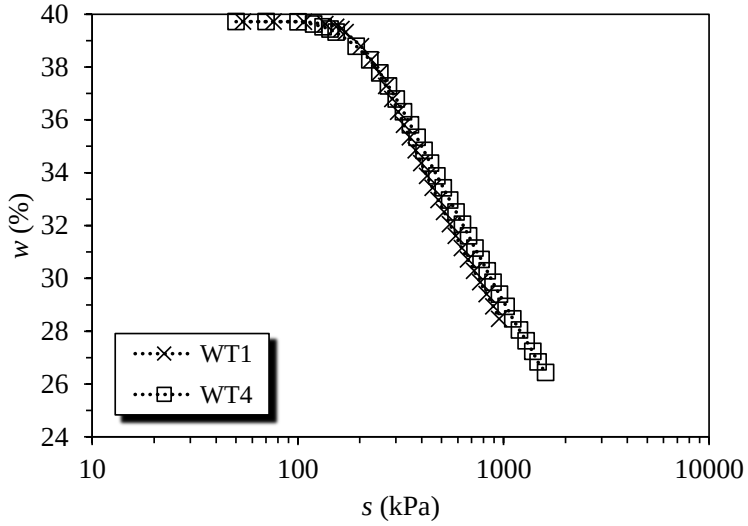
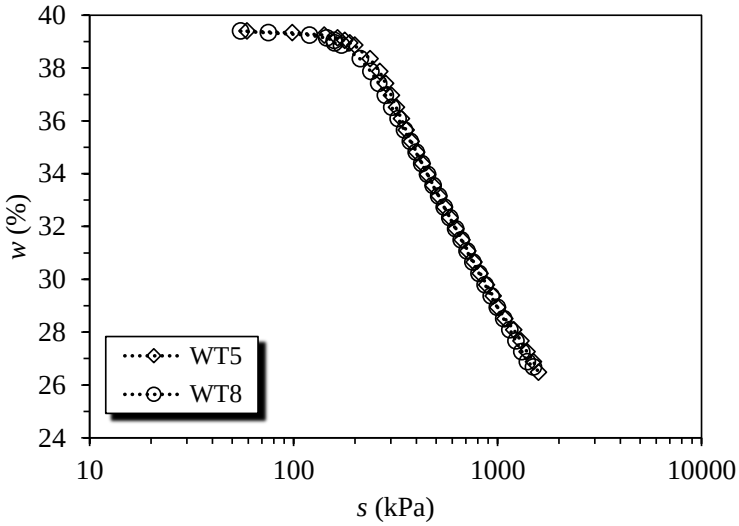


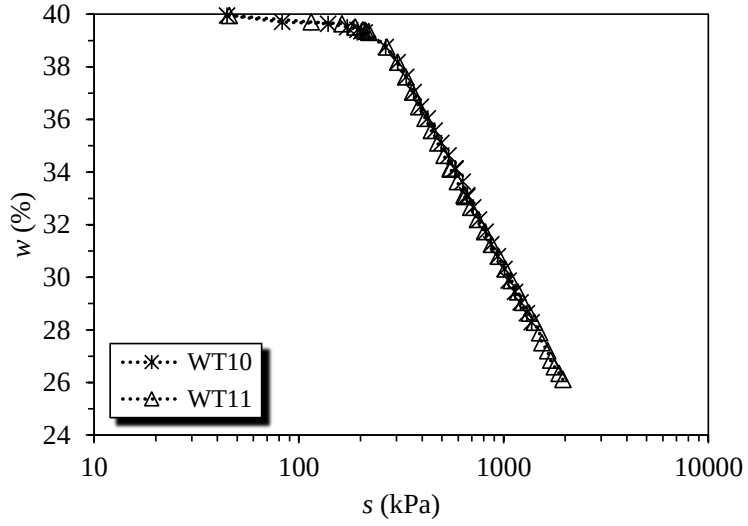
Figure 4.29 Variation of water content with time during CD tests



(a)



(b)



(c)

Figure 4.30 SWRCs from continuous drying tests: (a) CD1; (b) CD2; (c) CD3

Table 4.5 Results of the CD tests

Test No.	HCT	e_0	w_{sat} (%)	w_f (%)	Δm_v (g)	Δt (h)	$\Delta m_v / \Delta t$ (g/h)	s_{AEV} (kPa)	s_{max} (kPa)
CD1	WT1	1.06	39.72	28.47	12.92	25.3	0.51	210	952
	WT4			26.44	15.25	29.9		208	1601
CD2	WT5	1.05	39.14	26.48	14.50	30.2	0.48	227	1584
	WT8			26.68	14.27	29.7		209	1498
CD3	WT10	1.06	39.67	27.51	14.55	26.5	0.55	244	1510
	WT11			26.12	16.17	29.4		248	1946

4.10.3 Continuous Drying Tests with Controlled Evaporation-Rate

In reality, the drying process in the shallow depth soil layers does not normally take place instantly and over a short period of time. The change in humidity and temperature in the field is a time-dependent process which can be extended over the entire dry season. This process is often interrupted with the causal rainfalls and climate variations. This is believed to modify the *in-situ* water retention behaviour of soils compared to that of measured in laboratory using continuous drying procedure. To further study this effect, a series of tests were conducted on the soil specimens subjected to prolonged drying. As shown in Figure 4.28, a perforated plastic chamber was placed over the specimen to reduce the evaporation-rate. The chamber allows for controlled circulation of air around the specimen providing a relatively uniform moisture loss from the top and bottom of the specimen. Two tests were carried out on reconstituted specimens. For each test, four HCTs were used to monitor the evolution of suction as the specimen dried out. These tests are denoted CD1(er) and CD2(er), with "er" standing for evaporation-rate. The initial conditions of the specimens as well as the obtained key parameters are shown in Table 4.6. Figure 4.31 presents the obtained SWRCs.

Table 4.6 Results of the CD(er) tests

Test No.	HCT	e_0	w_s (%)	w_f (%)	Δm_v (g)	Δt (h)	$\Delta m_v / \Delta t$ (g/h)	s_{AEV} (kPa)	s_{max} (kPa)
CD1(er)	WT1	1.05	39.27	30.54	10.14	63.4	0.16	252	908
	WT2			32.83	7.48	46.8		273	725
	WT3			27.57	13.59	84.9		263	1457
	WT4			27.16	14.07	87.9		263	1580
CD2(er)	WT5	1.06	39.75	27.40	12.45	73.2	0.17	251	1603
	WT8			28.51	11.33	66.7		263	1312
	WT10			27.75	12.09	71.1		282	1463
	WT11			26.00	13.86	81.5		268	1900

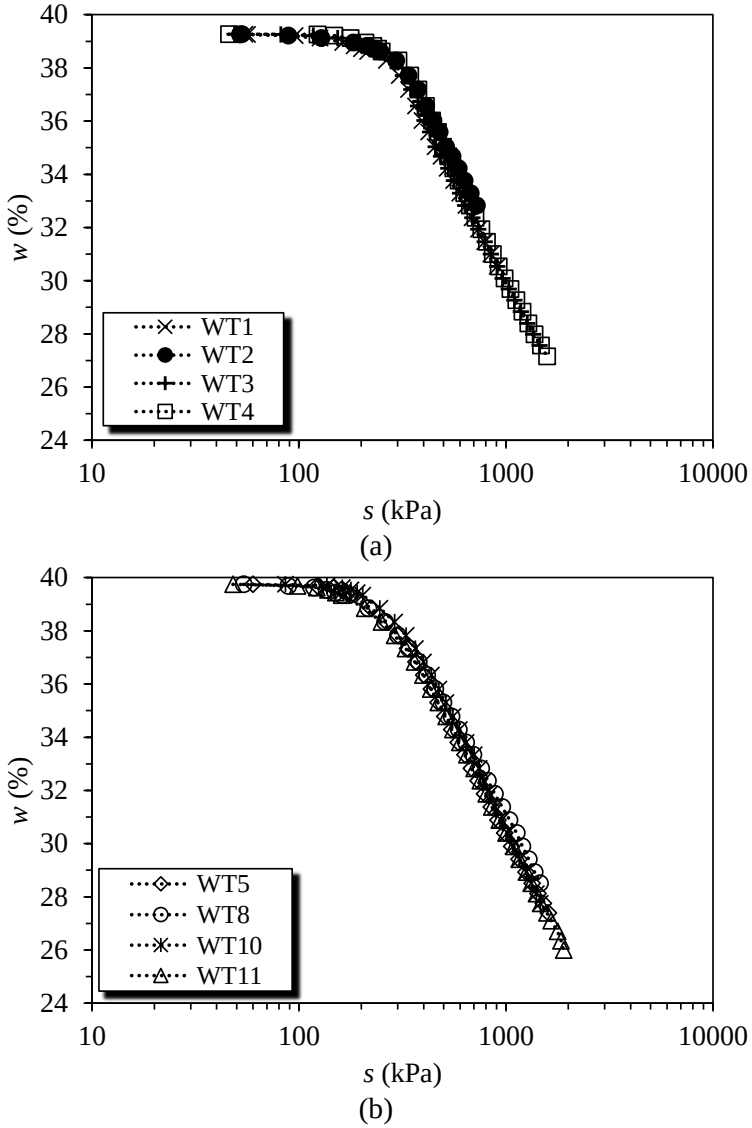


Figure 4.31 SWRC from continuous drying tests with evaporation rate control: (a) CD1(er); (b) CD2(er)

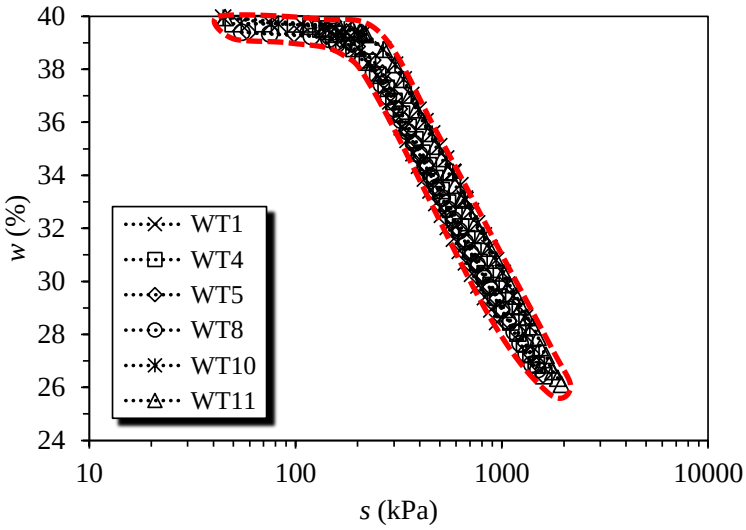
4.10.4 Discussion of the Results

Inspection of the SWRCs obtained from CD and CD(er) tests revealed some interesting findings. Figure 4.32 presents the envelope of the SWRCs obtained from each set of experiments. It is seen that the envelope for the SWRCs from CD(er) tests is slightly narrower than the envelope for the SWRCs from CD tests. Moreover, the CD(er) envelope has been slightly shifted to the right, resulting in an increase of the AEV for an average of about 40 kPa in comparison to the CD tests. This is deemed to be due to the fact that during CD(er) tests the HCTs and the soil specimen had more time to reach equilibrium. Therefore, at a given water content, a higher suction (and a closer value to real suction) is recorded when the evaporation-rate is reduced. The smooth transition

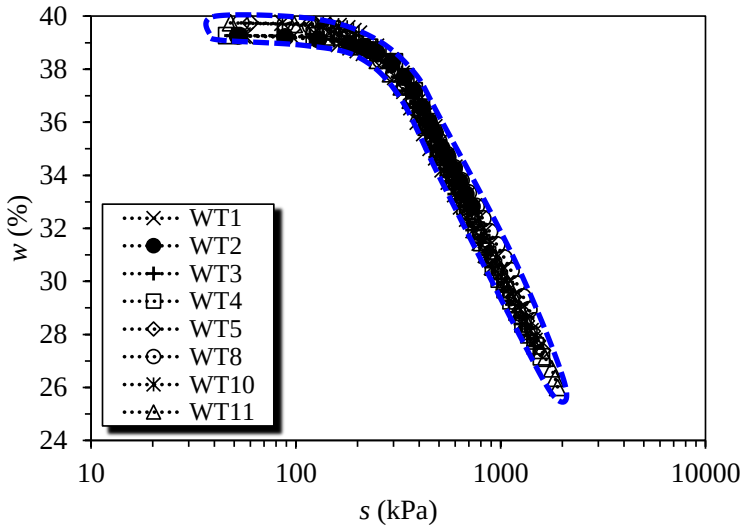
from saturated to unsaturated states observed on SWRCs from CD(er) tests in comparison to the somewhat sharper transition on the SWRCs from CD tests, further justifies the effect of evaporation-rate on the HCTs measurements.

It must be noted here that the presented SWRCs in Figure 4.32 relate local suction to global water content. In fact, suction distribution at the mid-height of the tested specimens might be different, resulting in slightly different SWRCs. Moreover, suction measurements were carried out under non-equilibrium conditions, i.e. where the soil and the HCT were not in ultimate equilibrium. These can help in explaining the differences observed between the CD and CD(er) envelopes.

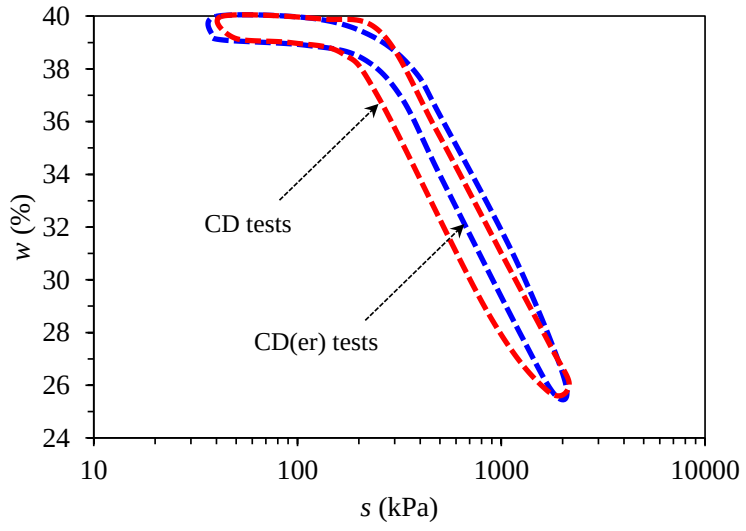
Figure 4.33(a) presents a comparison of the s_{AEV} values measured during CD and CD(er) tests. The s_{AEV} values are higher for the CD(er) tests with the differences varying in range of 20 to 55 kPa. A comparison of the s_{AEV} values recorded during FE, CD, and CD(er) tests is shown in Figure 4.33(b). All HCTs showed significantly lower s_{max} values during CD and CD(er) tests than the FE tests. One possible reason for this observation can be the effect of air diffusion and occurrence of cavitation inside the ceramic filter at suctions below or close to the ceramic's AEV. Moreover, it can be seen that the change in moisture evaporation-rate did only have a minor impact on the recorded s_{max} values from CD and CD(er) tests, where the prolonged contact of the HCTs with the unsaturated specimen during CD(er) tests, resulted in a slight reduction of the recorded s_{max} values, highlighting once again the influence of air diffusion process on the cavitation mechanism in HCTs.



(a)



(b)



(c)

Figure 4.32 SWRC envelopes: (a) CD tests; (b) CD(er) tests; (c) comparison of the envelopes

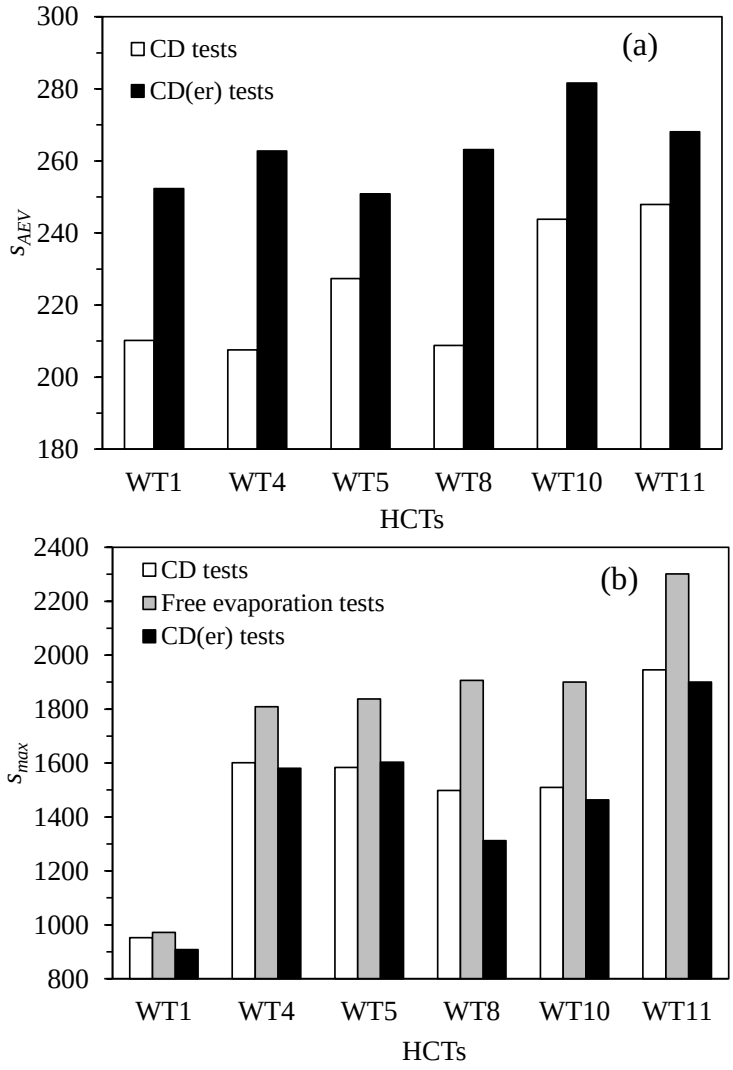


Figure 4.33 Assessment of the HCTs performance during SWRC measurements: (a) s_{AEV} values in CD and CD(er) tests; (b) s_{max} values from FE, CD, and CD(er) tests

4.11 Mathematical Extrapolation of SWRC

Measurement of SWRC using HCTs is limited to the s_{max} value and is typically below 2.0 MPa. The maximum measurable suction from CD and CD(er) tests correspond to a water content of 26%. In order to extend the SWRC to the data points corresponding to the water contents below 26%, one method is to use sigmoidal curve fitting equations to mathematically extrapolate the variation of water content versus soil suction where the data points for high suctions are not available. In this section, the Fredlund and Xing (1994) equation is used in order to extend the SWRC obtained from the CD and CD(er) tests to a wider range of suctions. The extended SWRC will be used in Chapters 5 and 6 for determination of the specimens' suctions having water contents lower than 26%.

4.11.1 The Fredlund and Xing (1994) Equation

In the field, determination of degree of saturation ($S_r = V_w/V_v$) and/or volumetric water content ($\theta = V_w/V_s$) is either not possible or very costly and difficult. Therefore, in geotechnical engineering, SWRCs are usually plotted based on gravimetric water content ($w = m_w/m_s$). The Fredlund and Xing (1994) relationship is, however, capable of best-fitting any of the designations of water content, i.e. gravimetric water content, volumetric water content, or degree of saturation. The proposed equation in terms of gravimetric water content is given by;

$$w(s) = w_{sat}\left[1 - \frac{\ln\left(1+\frac{s}{s_r}\right)}{\ln\left(1+\frac{10^6}{s_r}\right)}\right] \times \left[\frac{1}{\ln\left[\exp(1)+\left(\frac{s}{a}\right)^n\right]}\right]^m \tag{4.5}$$

Where s denotes suction, $w(s)$ is the gravimetric water content at any given suction, w_{sat} is the saturated gravimetric water content, s_r is the residual soil suction, a is equal to s_i being the suction at inflection point as shown in Figure 4.34, and m and n are the fitting parameters given by;

$$m = 3.67\ln\left[\left(\frac{w_{sat}}{w_i}\right) \times \left(1 - \frac{\ln\left(1+\frac{s_i}{s_r}\right)}{\ln\left(1+\frac{10^6}{s_r}\right)}\right)\right] \tag{4.6}$$

where w_i is the water content at the inflection point, and

$$n = 3.72s' \frac{1.31^{m+1}}{m \times \left(1 - \frac{\ln\left(1+\frac{s_i}{s_r}\right)}{\ln\left(1+\frac{10^6}{s_r}\right)}\right)} \tag{4.7}$$

where

$$s' = \frac{s_t}{w_{sat}} - \frac{s_i}{\ln\left(1+\frac{10^6}{s_r}\right)\times\left(s_i+s_r\right)\times 1.31^m} \tag{4.8}$$

And s_t is the slope of the tangent line at inflection point and is given by;

$$s_t = \frac{w_i}{\ln\left(\frac{s_p}{s_i}\right)} \tag{4.9}$$

In Equation 4.9, s_p is the intersection of the tangent line to the inflection point with the horizontal axis as shown in Figure 4.34.

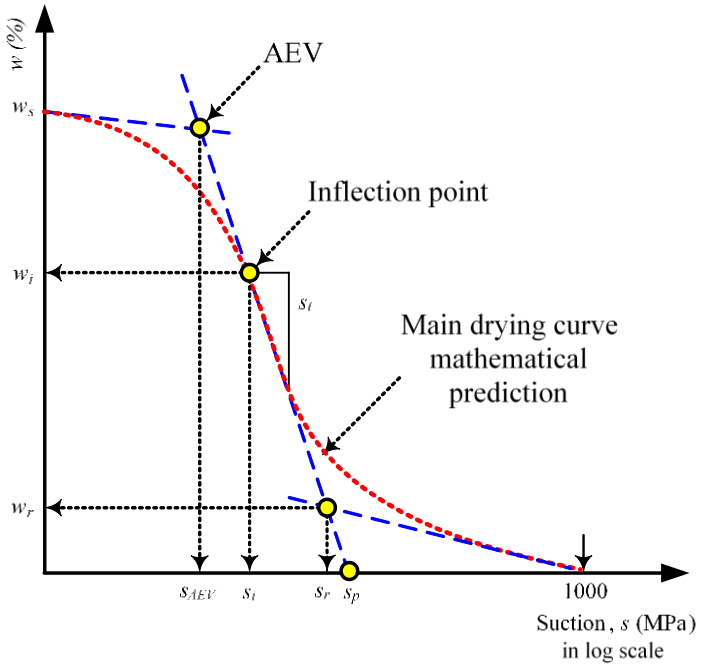


Figure 4.34 Definitions of the parameters of Fredlund and Xing equation in SWRC-*w* space

Fredlund and Houston (2013) proposed an equation for curve fitting the experimental SWRC data of soils that undergo significant volume changes with change in suction, by incorporating the shrinkage curve information into the Fredlund and Xing (1994) equation. The shrinkage curve was suggested to be measured using a digital micrometer for the measurement of the specimen's volume during drying. This method of volume measurement, however, does not seem to be the best possible method, as it is associated with human errors, as well as possible disturbance to the specimen which can cause subsequent errors on dimensions measurements. The London Clay specimens used in

this study were found to have a slight volume variation with increase in suction to the maximum capacity of the HCTs (i.e. 2.0 MPa), as it was also shown in microstructure analysis presented in Chapter 3. Therefore, the equation of Fredlund and Xing (Equation 4.5) was used to best-fit the experimental data and extrapolate the entire SWRC.

4.11.2 Curve-fitting the Experimental Data

The Equation 4.5 requires estimation of four parameters namely, w_{sat}, w_i, s_r and s_i. The estimated values for these parameters obtained from CD and CD(er) tests are given in Table 4.7. Note that accurate estimation of s_r values were not possible due to unavailability of data points for high suctions close to the residual suction, s_r. This is the drawback of the Fredlund and Xing equation for best-fitting the experimental data of tensiometers and prediction of the entire water retention curve. The value of s_r was therefore assumed as 7.0 MPa, a value that provides the best fitting curves to the experimental data in low suction ranges.

Table 4.7 Input parameters for Fredlund and Xing equation

Test No.	HCT	e_0	w_{sat} (%)	w_i (%)	s_i (kPa)	s_{AEV} (kPa)	s_{max} (kPa)
CD1	WT1	1.06	39.72	37.27	258	210	952
	WT4			36.74	316	208	1601
CD2	WT5	1.05	39.14	36.93	290	227	1584
	WT8			36.83	290	209	1498
CD3	WT10	1.06	39.67	37.13	340	244	1510
	WT11			36.72	395	248	1946
CD1(er)	WT1	1.05	39.27	36.61	414	252	908
	WT2			36.13	430	273	725
	WT3			36.56	425	263	1457
	WT4			36.64	402	263	1580
CD2(er)	WT5	1.06	39.75	36.51	399	251	1603
	WT8			36.13	452	263	1312
	WT10			36.41	439	282	1463
	WT11			36.00	444	268	1900

Figure 4.35 presents an example of the best fitting curve obtained from the Fredlund and Xing equation. The best-fit curves for the CD and CD(er) tests are also shown in Figure 4.36. Overall, providing the accurate estimation of the input parameters, the proposed equation was found to be capable of producing best-fit curves that are closely matched to the experimental data.

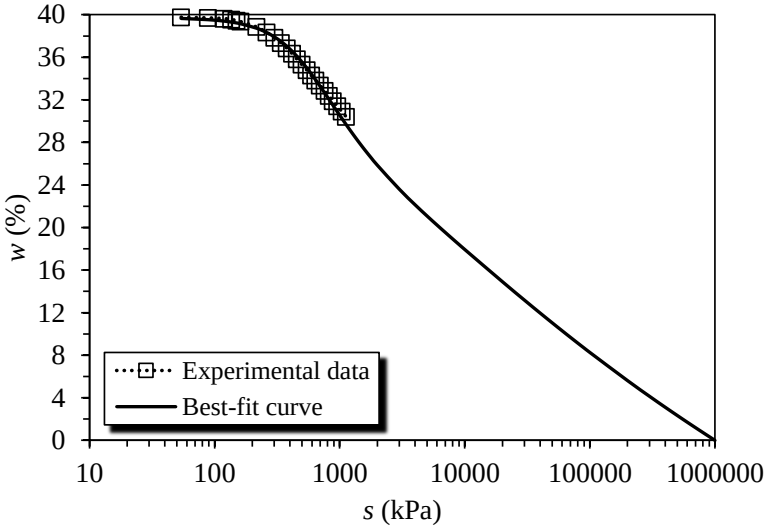
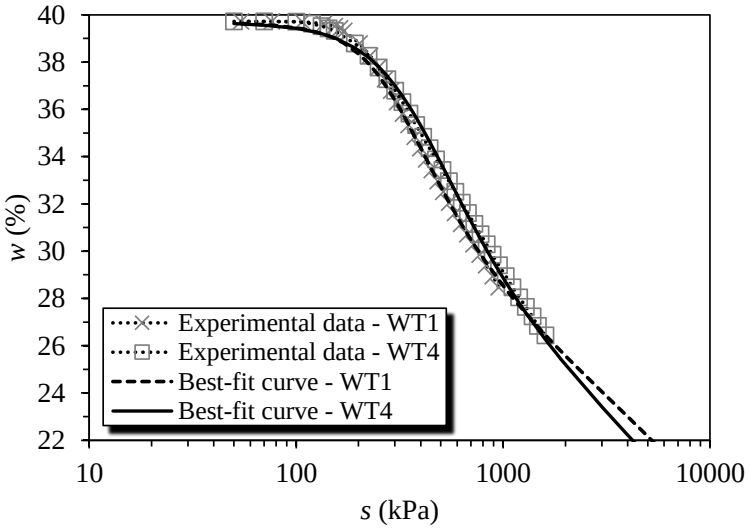
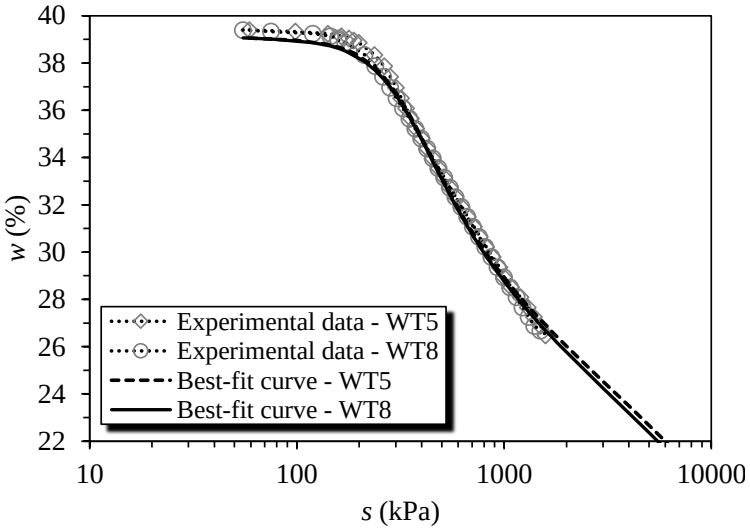


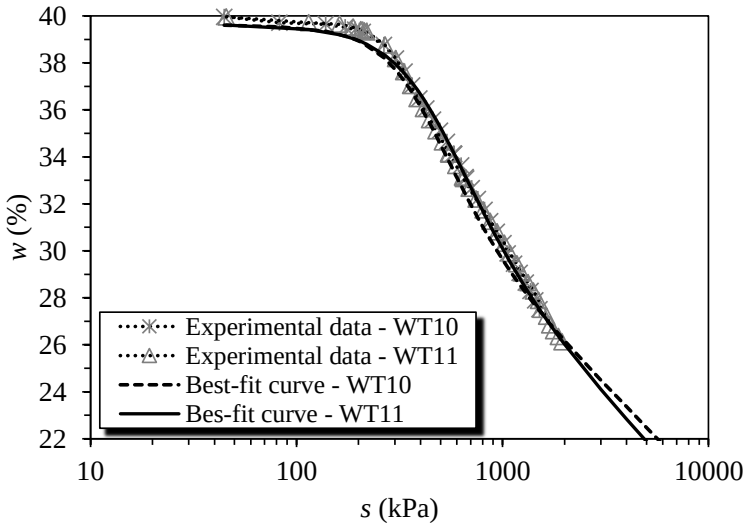
Figure 4.35 A best-fit curve to the experimental data obtained from WT8 in CD2(er) test



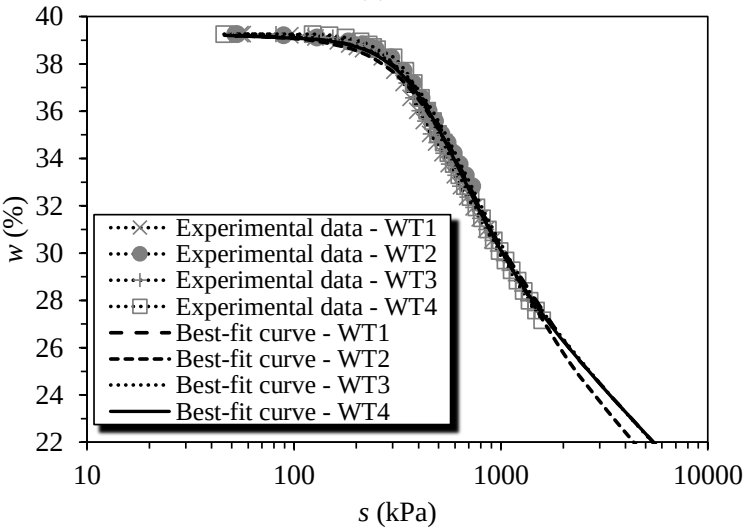
(a)



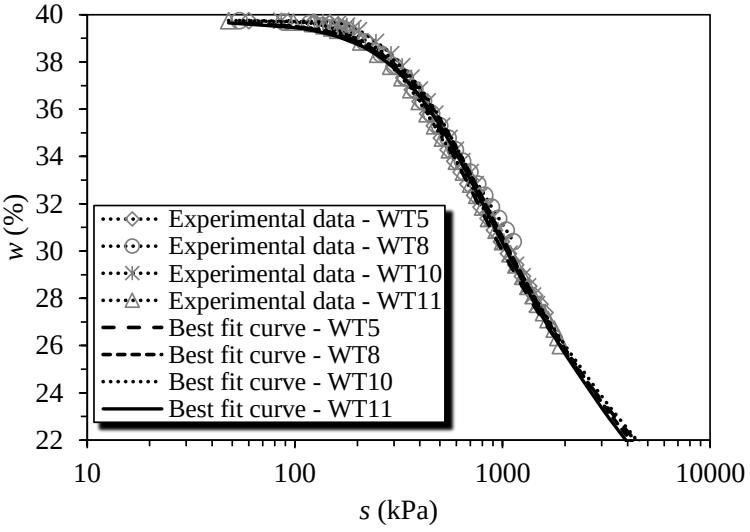
(b)



(c)



(d)



(e)

Figure 4.36 Best-fit curves to the experimental data obtained from: (a) CD1 test; (b) CD2 test; (c) CD3 test; (d) CD1(er) test; (e) CD2(er) test

A comparison of the obtained best-fit curves from CD and CD(er) tests is presented in Figure 4.37. Similar to the experimental results presented in Figure 4.32, the best-fit curves to the CD(er) tests showed a higher AEV than the best-fit curves to the CD tests. The best-fit curves to the CD tests somewhat diverge, whereas almost all of the best-fit curves to the CD(er) test results coincide on the desorption curve at least from the onset of desaturation to the point corresponding approximately to s = 2.0 MPa. From this point, significant differences in the extrapolated suctions corresponding to given water contents along the main drying paths of the extended SWRCs for CD and CD(er) tests were observed. For instance, suctions corresponding to w = 22% vary in a range of 3.9 – 4.5 MPa and 4.8 – 5.8 MPa for the best-fit curves to the CD(er) and CD tests respectively. As the CD(er) test results were previously considered as more reliable representative of the water retention characteristics of the tested specimens, the best-fit curves to the CD(er) tests were also preferred over the best-fit curves to the CD tests, and will be used in the next chapters for estimation of the specimens' suctions having water contents below 26%. It must be mentioned here that this method may not be the most practical approach, and therefore, the use of indirect suction measurement methods, such as filter paper or psychrometer, for measurement of suctions beyond the capacity of the HCTs seems to be inevitable.

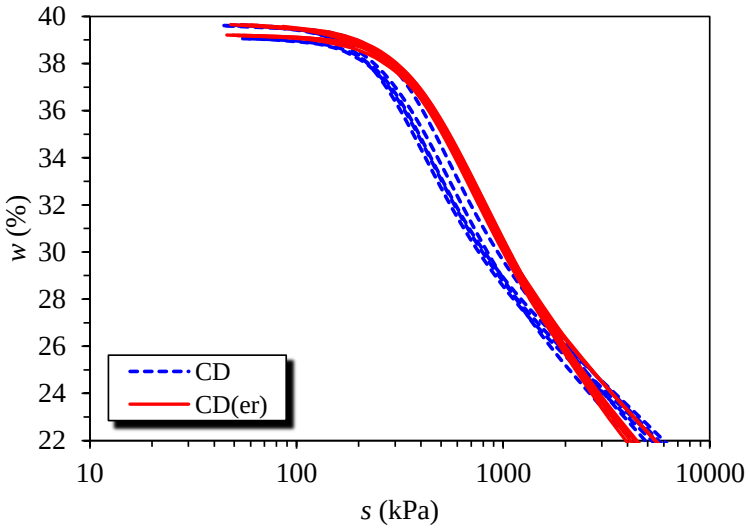


Figure 4.37 Comparison of the best-fit curves from CD and CD(er) tests

4.12 Concluding Remarks

In the first part of this chapter, the effect of water reservoir, with respect to its walls' surface roughness, on the performance of a newly designed HCT was examined. The following conclusions can be drawn from this study;

- The mechanism of cavitation in tensiometers is indeed influenced by the surface roughness of the water reservoir. The smoother and the more water attractive surfaces in water reservoir can significantly reduce the number of entrapped gas bubbles and nucleation sites, hence increasing the cavitation threshold in HCTs.
- While the HCT with FM diaphragm was only capable of measuring suctions up to 65% of its nominal capacity, the surface polishing techniques resulted in an increase of s_{max} values up to 122% of the nominal capacity. Furthermore, AF and Triton coatings and TiO_2 coating increased the s_{max} by 127% and 153% of the nominal capacity, respectively.
- Considering the t_{max} values obtained from the SP polished HCT as an index, the improvements achieved from Triton and TiO_2 coating methods were in the range of 134 – 177%.
- The mechanical surface polishing methods reduce the hydrophilicity of the diaphragms and hence may offset the improvement achieved through reducing surface roughness. This effect is more evident during long-term measurements of constant high suctions.
- The TiO_2 hydrophilic coating appears to be promising in improving the s_{max} and t_{max} values of the HCTs. Its strong bonding properties to the substrate also counterbalances potential issues caused by dissolution or detachment of the coating layer, and hence guarantees the long-term functionality of the HCT.
- The new HCT provides an improved measurement, in terms of the s_{max} and t_{max} values, in comparison to the presented HCTs in the literature, as shown in Table 4.8.
- Further works are to be done for evaluation of the long-term stability and adhesion of hydrophilic coatings to the diaphragms of the HCTs.

Table 4.8 Improvements achieved by the new HCT

Authors	AEV (MPa)	Max measured suction (kPa)	Max measurement duration (min)
Bagheri et al. (2018) – this study		**2301**	**31740** at $s \approx 600$ kPa **28500** at $s \approx 1000$ kPa
Ridley and Burland (1993)	1.5	1370	1440 at 700 kPa
Guan and Fredlund (1997)	1.5	1200-1250	4320 at 700 kPa
Sjoblom (2000)	1.5	2200	
Tarantino and Mongiovi (2002)	1.5	2063	22540 at 1000 kPa
Mantho (2005)	1.5	1573	
Lourenço et al. (2008)	1.5	2087	
Mendes et al. (2016)	1.5	~2100	
Tarantino et al. (2016)	0.8	800	~18720 at 800 kPa

The SWRC-*w* of the reconstituted London Clay specimens over the main drying path were determined using the new HCTs following continuous drying procedures with and without soil moisture evaporation-rate control. In contrast to the works of Cunningham (2000) and Boso et al. (2003) that report the independency of the tensiometric-based SWRCs to the evaporation-rate using the dynamic method, it was found that the evaporation-rate can influence the measured s_{AEV} and, slightly, the shape of the curve in transition between saturated and unsaturated states. Generally, the air-entry values obtained from CD(er) tests were higher than the CD tests for an average of 40 kPa, mainly due to the extended pressure equalisation time during suction measurements in controlled-evaporation tests. Moreover, a smooth transition from the saturated to the unsaturated states was observed in CD(er) tests in comparison to the somewhat sharper transition in CD tests.

The Fredlund and Xing (1994) equation was used for extrapolation of the entire SWRC for the London Clay specimens. Input parameters, i.e. w_{sat}, w_i, s_r and s_i, play a significant role in accurate curve-fitting of the experimental data and extrapolation of the water retention behaviour at high suctions. Hence, their accurate estimation from the experimental data is crucial. However, for HCTs, as the experimental data close to the residual suction in clayey soils is not available, accurate estimation of s_r is not possible. The extended SWRCs obtained for CD(er) tests appear to provide more reliable extrapolation of water retention characteristics corresponding with suctions beyond the capacity of the HCTs. This is not, however, a certain conclusion, and the extrapolated curves need to be checked against the experimental values of soil suction measured using indirect suction measurement methods. Nevertheless, both

experimental results and mathematical extrapolation for CD(er) tests will be used for analysis of the oedometer and CRS tests results in the following chapters.

CHAPTER 5: TIME-DEPENDENCY IN UNSATURATED CONDITIONS

5.1 Introduction

Calculation of soil settlements requires a deep understanding of the compression parameters and the factors which can influence them. The objective of this chapter is to evaluate the 1D time-dependent behaviour of the natural and reconstituted Sheppey London Clay under saturated and unsaturated conditions. To this end, a set of 1D consolidation tests were carried out on dry, saturated, and unsaturated London Clay specimens. These tests included multi-staged loading (MSL) oedometer tests and single-staged loading (SSL) long-term oedometer creep tests. Conventional oedometer cells were used for tests on dry and saturated specimens, whereas the new unsaturated oedometer cells, described in Chapter 4, were used for unsaturated tests with suction measurements. Saturated tests were performed on undisturbed and reconstituted specimens, whereas the unsaturated tests were performed only on reconstituted specimens.

In this chapter, first, the results of MSL tests will be discussed with emphasis on the effects of suction and vertical stress level on the compression response and consolidation indices. The stress- and suction-dependency of $C_{\alpha e}/C_c$ ratio will be also investigated. Afterwards, variation of volumetric creep strains with time, suction, and vertical stress level in oedometeric conditions will be discussed based on the results of SSL oedometer tests. Finally, based on the results of the suction-monitored oedometer creep tests on unsaturated reconstituted specimens, development of a simple creep law accounting for suction effects will be presented and discussed.

5.2 Tests Nomenclature

The nomenclature chosen for MSL oedometer tests is shown in Figure 5.1. The letters “r”, “i”, and “d” represent reconstituted, intact, and dry specimens respectively, letters “s” and “u” indicate the saturated or unsaturated conditions, the number before dash indicates the initial water content, and the number after dash shows the test number for tests with identical initial conditions. For unsaturated tests, the initial suction is also mentioned in brackets after the test number.

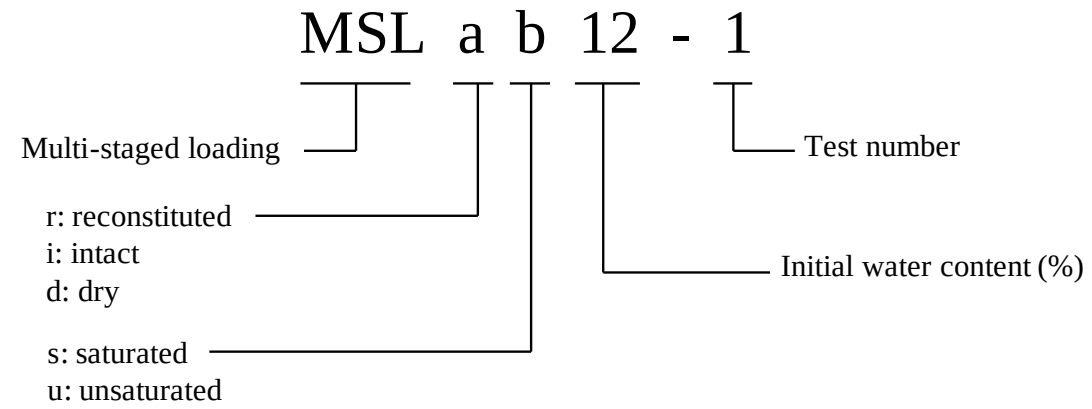


Figure 5.1 Nomenclature of the MSL oedometer tests

The nomenclature chosen for SSL creep oedometer tests is shown in Figure 5.2. The nomenclature is similar to that of MSL tests with the only difference being the number after dash which shows the maximum applied vertical stress in kilopascals. For unsaturated tests, the initial suction is also mentioned in brackets after the test number.

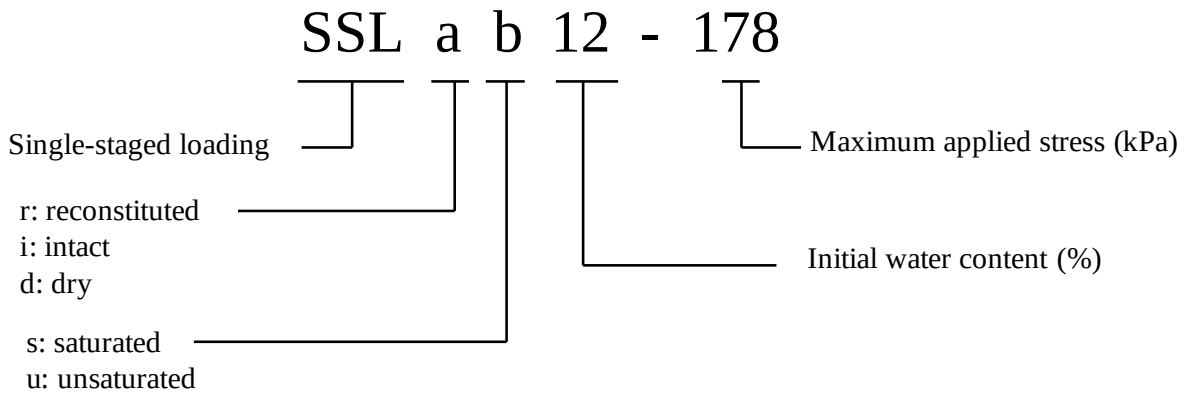


Figure 5.2 Nomenclature of the SSL oedometer creep tests

5.3 Theoretical Framework

5.3.1 Determination of Void ratio

A typical method to obtain the values of the initial void ratio (e_0) at the start of compression is the use of;

$$e_0 = w_0.G_s \qquad 5.1$$

where, w_0 is the initial water content and G_s is the specific gravity of the solids. This method is considered accurate if the initial degree of saturation (S_{r0}) of the specimen is very close to 100%. An alternate method is to calculate e_0 from;

$$e_0 = \frac{V_v}{V_s} = \frac{V_T}{V_s} - 1 = H_0.A_0.\frac{G_s.\rho_w(1+w_0)}{m_0^T} - 1 \qquad 5.2$$

In Equation 5.2, V_v, V_s, and V_T are the initial volume of voids, volume of solids, and total volume respectively. H_0 is the initial height, A_0 is the initial area of the specimen, and m_0^T is the initial total mass of the specimen. This method is more appropriate for reconstituted specimens where accurate measurement of the initial total volume is possible (Sorensen, 2006). However, for undisturbed specimens of fissured London Clay, accurate determination of V_T is rather difficult, and hence, the use of an alternate method for determination of e_0 is recommended.

The information of the final water content (w_f) at the end of the experiment can also be used to obtain the initial and final values of the void ratio;

$$e_f = w_f.G_s = e_0 - (1+e_0).\varepsilon_f^v \qquad 5.3$$

where ε_f^v is the final volumetric strain. The parameters w_f and e_f are highly dependent on the quick removal of the specimen at the end of unloading stage to avoid further ingress of water (Sorensen, 2006).

For reconstituted specimens, e_0 was calculated based on Equation 5.2. The obtained values were also in good consistency with those of obtained from Equation 5.1. For undisturbed specimens, e_0 was calculated based on Equation 5.3. During the tests, the change in void ratio was determined based on the measured change in height of the specimen which corresponds to the volume change where radial straining is prevented.

5.3.2 Determination of Effective Stress

In an oedometer test, the stress–strain conditions are axis-symmetric. In saturated tests, the principle of effective stress is applied. However, as the pore-water pressure (u_w) is not measured, the effective stress is considered to be equal to the applied vertical stress once the excess pore-water pressure (u_{exc}), generated immediately after application of dead weights, is dissipated. The period of 24 hours considered for each loading increment ensures full dissipation of u_{exc}. Moreover, in the conventional oedometric conditions, the radial stress is unknown, hence the information of k_0 and mean effective

stress (p') are not available. Furthermore, since radial straining is prevented, the volumetric strain (ε_v) equals the axial strain (ε_a).

As suggested in the literature (e.g. in Koliji, 2008), the experimental results of unsaturated oedometer tests can be evaluated based on the generalised vertical effective stress;

$$\sigma'_v = \sigma_{vnet} + S_r s \qquad 5.4$$

where S_r is the degree of saturation, s is soil suction, and σ_{vnet} is the net normal vertical stress defined as;

$$\sigma_{vnet} = \sigma_v - u_a \qquad 5.5$$

Estimation of S_r requires the information of the water content of the specimen during the test. However, the suction-monitored oedometer cell, as described in Chapter 4, does not allow for measurement of the specimen water content. Therefore, as suggested by Tarantino (2017), the experimental results of unsaturated oedometer tests were evaluated based on the net normal stress. Since the tests were carried out at the atmospheric air pressure, the net normal stress was equal to the applied vertical total stress.

5.3.3 Determination of Compression and Consolidation Parameters

The compression index (C_c) and swelling index (C_s) were calculated as the slope of respectively the normal compression line (NCL) and the swelling (unloading) line of the compression curve plotted in e – log σ'_v space. As suggested by Mataic et al. (2015), the creep index ($C_{\alpha e}$) was defined as the slope of the plot of e versus log t from the time period of 6–24 hours for each load increment. The decrease in void ratio during this time scale represents the creep phase as the end of primary consolidation (EOP) was found to be within the first 5–6 hours of each loading increment.

5.4 Saturated MSL Oedometer Tests

5.4.1 Test Procedure and Apparatus

In order to evaluate the saturated 1D compressibility characteristics of the Sheppey London Clay, MSL oedometer tests with 24 hours loading periods were performed on

intact, reconstituted, and low-quality undisturbed specimens. Figure 5.3 shows the oedometer test apparatuses used at the University of Nottingham for conducting saturated oedometer tests. As explained in Chapter 3, the oedometer specimens, having dimensions of 75 mm diameter and 20 mm height, were prepared by penetrating the cutting ring into the undisturbed samples or the reconstituted soil cakes. The inner wall of the confining ring was slightly lubricated with grease before preparing the specimen, in order to minimise the side friction effects on the stress–strain response. The specimen top and bottom surfaces were trimmed and flattened in order to minimise the errors associated with the alignment of the loading platen which can result in erroneous displacement measurements. Prior to the start of the tests, the initial water content (w_0) and the specimen dimensions were precisely measured and recorded. The specimen was then set up in the oedometer cell and the loading cap and the hanger were placed. Drainage was allowed through the saturated porous disks placed at the top and bottom of the specimen. The specimen was then allowed to reach equilibrium overnight under an equivalent stress of about 8 kPa due to the weight of the hanger and the loading cap. Any possible swelling was also recorded. Afterwards, vertical load was applied step-wise to the submerged specimens and sustained for 24 hours to ensure full dissipation of u_{exc} during each loading step. Typically, for conventional oedometer tests, vertical load is doubled at each stage of loading. This can, however, cause significant unfavourable disturbance to the structural properties of the testing specimen especially at high stress levels. In order to reduce such effects, in addition to the doubling vertical stress method, other loading patterns, as will be explained later, were also implemented. By the end of loading to the desired stress levels, the specimens were unloaded step-wise in order to evaluate the swelling response. Each unloading stage was kept for 24 hours to ensure complete swelling and that most of the generated suction was released. The compression curves were finally obtained based on the final settlement values recorded by the end of each loading/unloading stage. This method, although involves some minimal errors associated with the occurrence of creep deformations following dissipation of u_{exc} during each loading stage, enables comparison of the obtained compression curves with those reported in the literature for London Clay samples. Vertical deformations during compression and swelling were measured by a linear vertical displacement transducer (LVDT) with travel length of 25 mm and accuracy of 0.001 mm. A LabVIEW code was developed for data acquisition during the long-term tests. The code enables varying the time intervals for data logging, which is useful for

capturing the instantaneous deformations immediately after loading and unloading. Furthermore, this feature helps in reducing the amount of logged data during delayed consolidation phases (i.e. primary and secondary consolidation phases). Moreover, in order to minimise the effect of temperature fluctuations, the experiments were performed in a controlled-temperature room. The main objectives of this set of experiments are (1) to evaluate the effect of soil structure on the consolidation response, and (2) to evaluate the effect of consolidation pressure on C_c, $C_{\alpha e}$, and $C_c/C_{\alpha e}$ ratio.



Figure 5.3 Conventional oedometer apparatuses at the University of Nottingham

The stages of loading and unloading performed on saturated specimens are given in Table 5.1. The "*" sign at the end of some of the test IDs indicates the low-quality intact specimens.

Table 5.1 Loading – unloading pattern for MSL tests on saturated specimens

Test ID	Loading/unloading pressures (kPa)
MSLis32-1	22-44-89-178-355-710-1421-710-355-178-89
MSLis32-2	22-44-89-178-355-710-1421-710-355-178-89
MSLis32-3	22-44-89-178-355-710-1421-710-355-178-89
MSLis32-4	11-22-44-89-178-222-333-444-666-888-1110-1332-1110-888-666-444-333-222-178
MSLis32-5	11-22-44-89-178-222-333-444-666-888-1110-1332-1110-888-666-444-333-222-178
MSLis32-6	11-22-44-89-178-222-333-444-666-888-1110-1332-1110-888-666-444-333-222-178
MSLis32-7*	22-44-89-133-178-222-333-444-666-888-1110-888-666-444-333-222-178-133
MSLis32-8*	22-44-89-133-178-222-333-444-666-888-1110-888-666-444-333-222-178-133
MSLis32-9*	22-44-89-133-178-222-333-444-666-888-1110-888-666-444-333-222-178-133
MSLrs39-1	11-22-44-89-178-355-710-1421-710-355-178-44
MSLrs39-2	11-22-44-89-178-355-710-1421-710-355-178-44
MSLrs39-3	11-22-44-89-178-355-710-1421-710-355-178-44
MSLrs43-1	11-22-44-89-178-355-710-1421-710-355-178-44
MSLrs43-2	11-22-44-89-178-355-710-1421-710-355-178-44
MSLrs43-3	11-22-44-89-178-355-710-1421-710-355-178-44

5.4.2 Test Results

Figure 5.4 presents the normalised compression curves for intact specimens. As can be seen, the change in loading pattern, which was aimed at reducing the effects of sudden loading and subsequent damages to the soil structure, does not have a notable influence on the obtained compression curves. The only exception is the MSLis32-5 curve which is slightly shifted to the right, and exhibits lower compressibility. This different compression behaviour might be due to the factors such as lower degree of saturation (S_r) of the specimen at the start of the test, or errors in measurement of the initial water content. Moreover, the highly structured nature of the specimens resulted in high C_s values. Similar observations were also reported by Gasparre (2005) for London Clay samples retrieved from Heathrow Airport Terminal 5 site. Average C_c and C_s values of respectively 0.218 and 0.096 were obtained from the compression tests on intact specimens having an average initial void ratio of 0.85 and initial water content of 32%.

A comparison of the normalised compression curves for Sheppey London Clay and the natural London Clay from Unit C (block sample retrieved from 5–10 m depth) of the Heathrow Terminal 5 site is shown in Figure 5.5. The curves exhibit very similar characteristics with almost equal compression and swelling indices. The specimen from T5, however, is less compressible than the Sheppey specimen, mainly due to its lower plasticity index (I_p = 37%) and initial water content (w_0 = 24%).

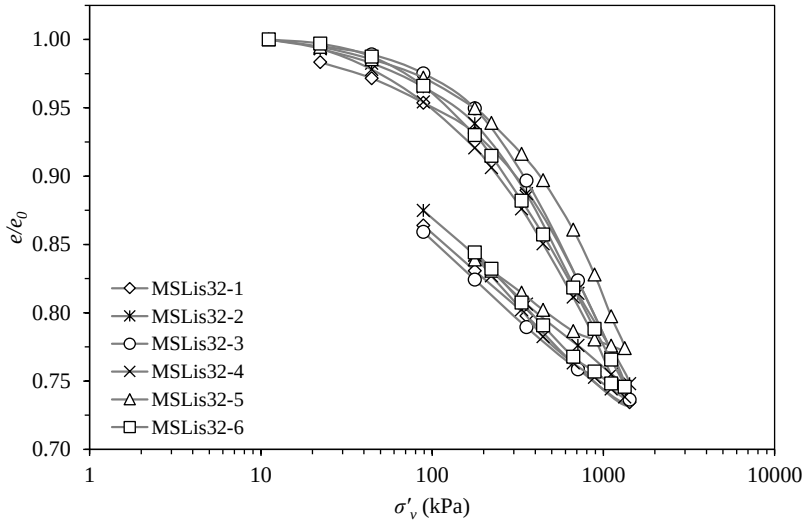


Figure 5.4 Compression curves for intact Sheppey London Clay

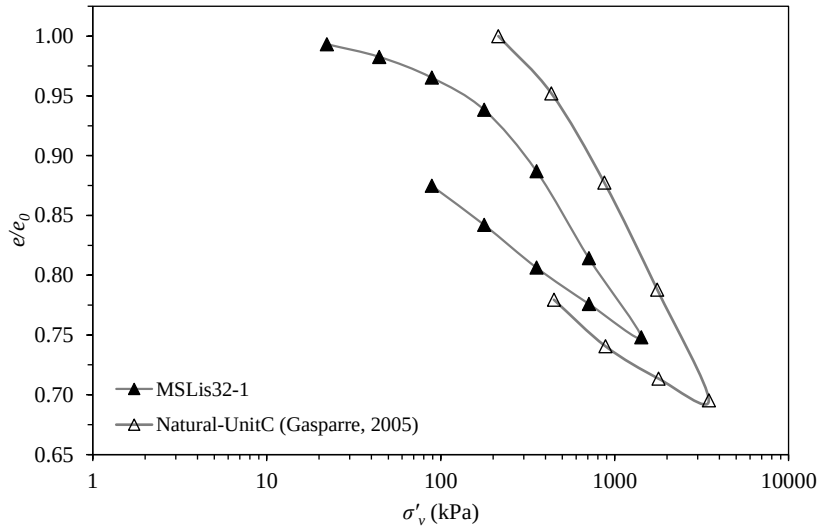


Figure 5.5 Comparison of the compression curves for intact Sheppey London Clay and natural London Clay from Unit C of Heathrow T5 site

Figure 5.6 presents the results of MSL compression tests carried out on reconstituted specimens. It is seen on the graphs that with increase of initial water content, compressibility of the specimens is increased. Average C_c and C_s values of respectively 0.383 and 0.125 were obtained from the compression tests on reconstituted specimens having an average initial void ratio of 0.93 and initial water content of 39%. For specimens with initial water content of 43%, the average C_c and C_s values of respectively 0.408 and 0.133 were obtained. Similar C_c values of 0.41 to 0.51 were reported by Sorensen (2006) from isotropic compression and oedometer tests on reconstituted London Clay from Heathrow Terminal 5 site. Similar to intact specimens, the reconstituted compression curves of Sheppey London Clay and T5 London Clay, as reported by Gasparre (2005), were compared as shown in Figure 5.7. The reconstituted Sheppey specimen exhibits less compressibility in comparison with the reconstituted T5 London Clay specimen. This behaviour might be attributed to the modified particle size distribution (PSD) of the reconstituted Sheppey specimens (as explained in Chapter 3) and presence of sand-sized peds that results in an increased resistance against compression.

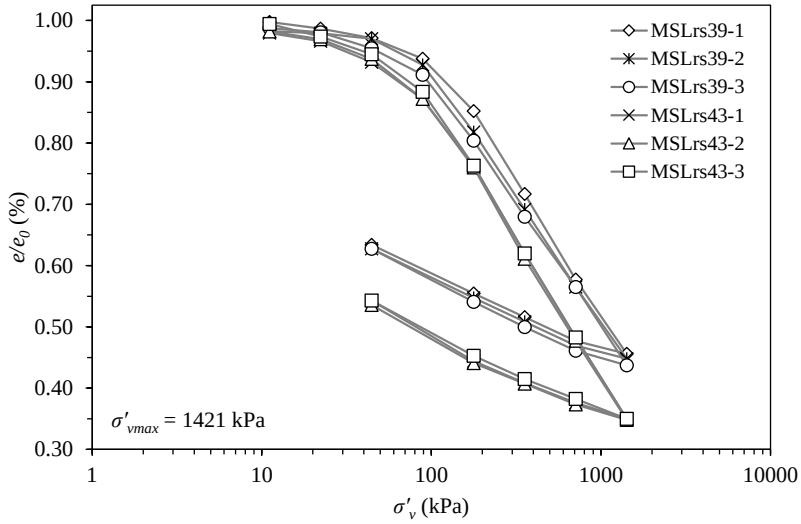


Figure 5.6 Compression curves for reconstituted Sheppey London Clay

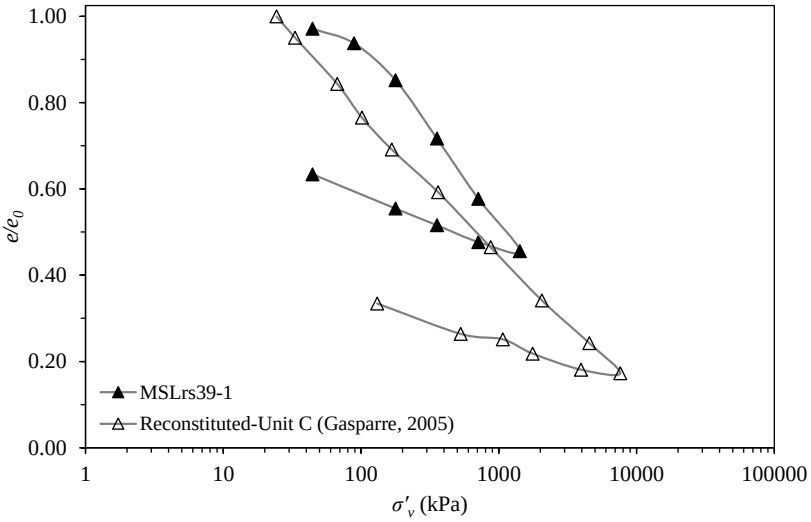


Figure 5.7 Comparison of the compression curves for reconstituted Sheppey London Clay and reconstituted London Clay from Unit C of Heathrow T5 site

To further investigate the effect of soil structure on the compressibility of Sheppey London Clay, a set of three MSL oedometer tests were carried out on low-quality undisturbed specimens having an average initial void ratio of 0.85 (Figure 5.8). A comparison of compression curves for intact, reconstituted, and low-quality undisturbed specimens is shown in Figure 5.9. The compression curve of the low-quality specimen with partly destroyed structure lies in between the compression curves of intact and reconstituted specimens. The curve is more similar to the reconstituted compression curve, highlighting the greater influence of soil structure than the initial water content on the compressibility of stiff London Clay. However, the effect of initial

water content on the compressibility response must not be neglected. Evaluation of this issue, however, is beyond the scopes of this study and will not be addressed here.

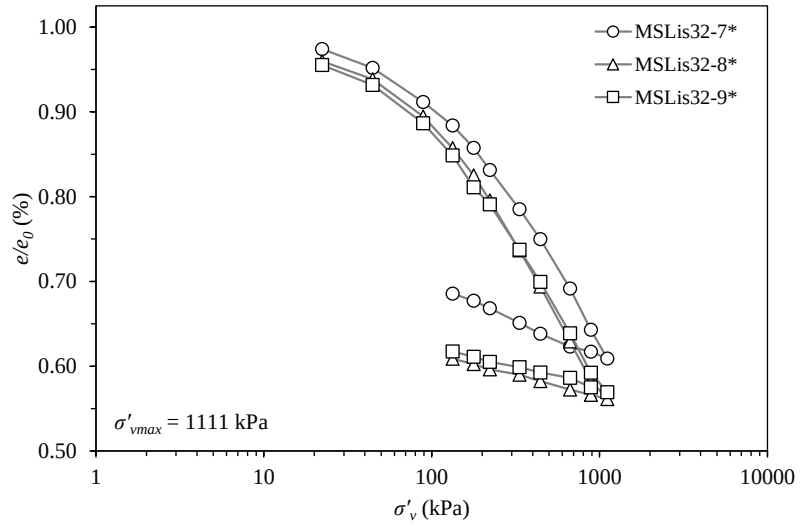


Figure 5.8 Compression curves for low-quality undisturbed Sheppey London Clay

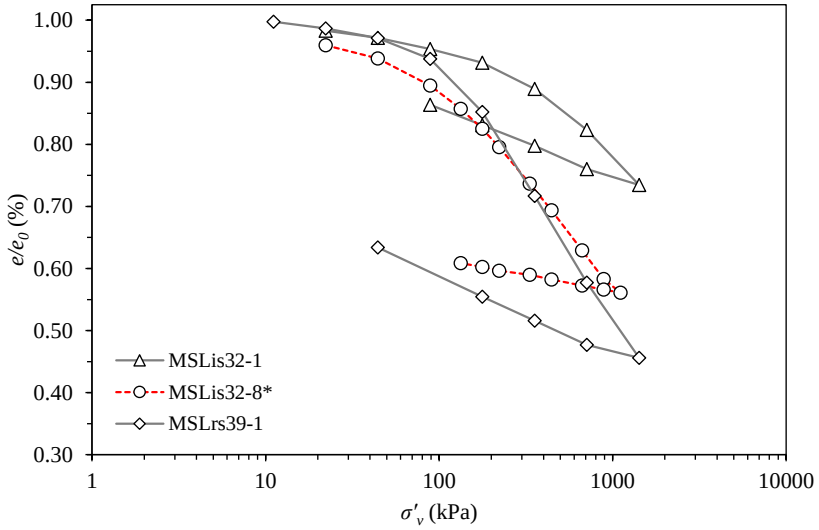


Figure 5.9 Comparison of the compression curves for saturated intact, reconstituted, and low-quality undisturbed Sheppey London Clay

5.4.2.1 Stress-Dependency of the Slope of Compression Curve

Compressibility of intact and reconstituted clays can be evaluated from the variation of the slope of compression curve with vertical effective stress (σ'_v). The slope of compression curve (m_c) at each loading increment is calculated as $\Delta e/\Delta \log \sigma'_v$. For $\sigma'_v < \sigma'_{p,}$ the calculated values represent the slope of the reloading line (C_r), and for $\sigma'_v > \sigma'_p$, the calculated values represent the slope of normal compression line (C_c). Figure 5.10 presents the relationship between m_c and normalised stress σ'_v/σ'_p for intact

specimens. As can be seen, change in loading pattern (dotted lines) does not have a significant influence on the C_r and C_c values. Prior to the preconsolidation pressure, the C_r values increase slightly. Following σ'_p, the values of C_c increase gradually until reaching a peak value around (8-10) σ'_p, after which, a gradual decrease in compressibility is observed. Unlike soft clays that exhibit a sudden increase of C_c in post yield region due to structural collapse (see for example Mataic et al. 2015), the process of destructuration in stiff clays appears to be continuous and follow an almost linear trend until reaching the peak value. In soft clays the peak value falls in a range of (2-3) σ'_p (e.g. Karstunen and Yin, 2010, Mataic et al., 2015), whereas in stiff clays, such as London Clay, this range is extended to (8-10) σ'_p.

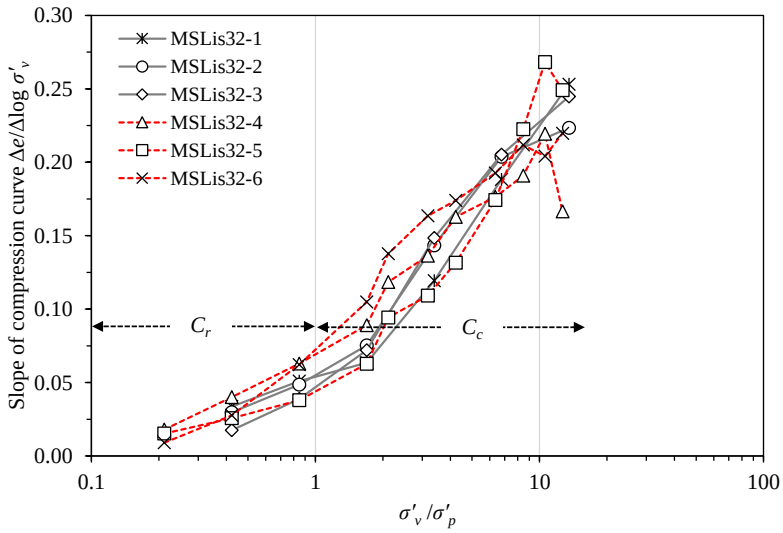


Figure 5.10 Stress-dependency of the slope of compression curve for intact Sheppey London Clay

Figure 5.11 presents the relationship between m_c and normalised stress σ'_v/σ'_p for reconstituted specimens. Similar to intact specimens, the slope of reloading line increases slightly prior to σ'_p. Increase in slope of reloading line for specimens with w_0 = 0.43 is reasonably higher than the specimens with w_0 = 0.39 given the higher water content that results in higher compressibility. The slope of compression curve in normal consolidation region increases dramatically to a peak value at stress levels between (3-4) σ'_p, at which it starts to decrease slowly.

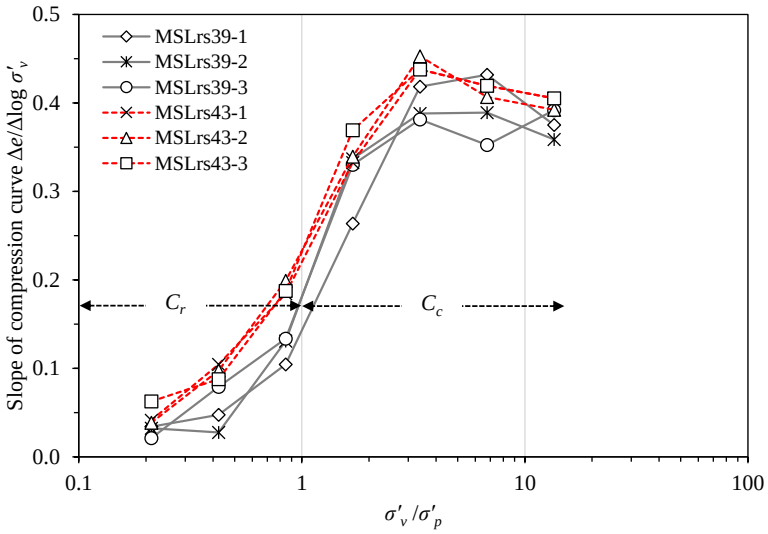


Figure 5.11 Stress-dependency of the slope of compression curve for reconstituted Sheppey London Clay

In soft clays, higher m_c values for intact specimens is typically observed in comparison with the reconstituted specimens, mainly due to the destructuration phenomenon that results in dramatic increase of C_c values in post yield region. However, as explained earlier, in stiff clays such as London Clay, degradation of inter-particle bonds (destructuration) does not occur suddenly and typically takes place gradually with increase in stress level.

Figure 5.12 presents a comparison of the variation of m_c with stress level for intact, reconstituted, and low-quality undisturbed specimens. In the overconsolidation region, the C_r values for low-quality undisturbed specimens increase at the same rate as the reconstituted specimens. However, in the post yield region, the rate of increase in C_c for low-quality undisturbed specimens is lower than that of reconstituted specimens, this being, in part, due to the lower initial water content and presence of inter-particle bonds that result in reduction of compressibility. The maximum value of C_c for low-quality undisturbed specimens occurs in a range of (6-8) σ'_p.

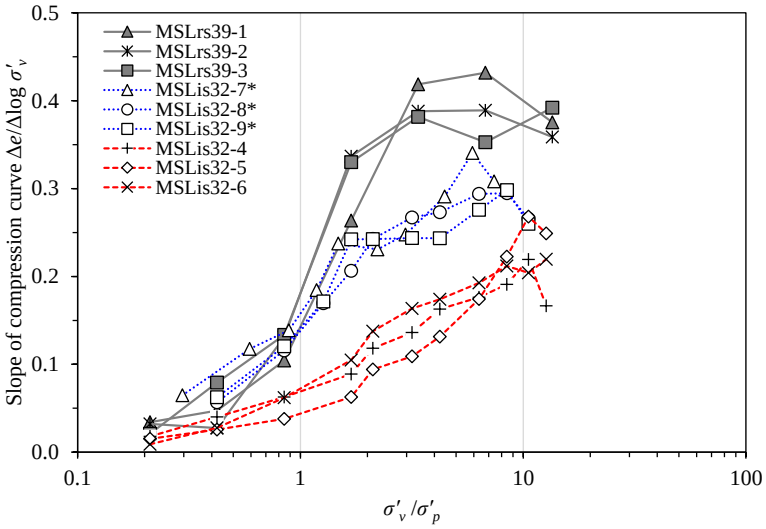


Figure 5.12 Comparison of the stress-dependency of the slope of compression curve for intact, reconstituted, and low-quality undisturbed Sheppey London Clay

5.4.2.2 Stress-Dependency of the Secondary Consolidation Index ($C_{\alpha e}$)

Figure 5.13 presents variation of the secondary consolidation index ($C_{\alpha e}$) with normalised stress σ'_v/σ'_p for intact specimens. It was observed that for doubling vertical stress method (continuous lines), $C_{\alpha e}$ increases gradually with stress level up to (3-4) σ'_p, at which it starts to increase dramatically to a peak value at stress levels in a range of (6-7) σ'_p. This behaviour can be attributed to the structural damage to the specimen during sudden loading at high stress levels. After the peak value, $C_{\alpha e}$ decreases dramatically. For MSLis32-4 to 6 (dotted lines) where the vertical stresses were applied in an unconventional way following the pattern described in Table 5.1, it was observed that $C_{\alpha e}$ increases gradually with stress level up to (8-11) σ'_p, at which it starts to decrease. This unconventional loading method appears, therefore, to produce more reliable results although it involves more loading stages and hence requires more time to complete. The maximum value of $C_{\alpha e}$ falls approximately in the range of 0.007 – 0.008 and 0.005 – 0.006 respectively for conventionally and unconventionally loaded intact specimens.

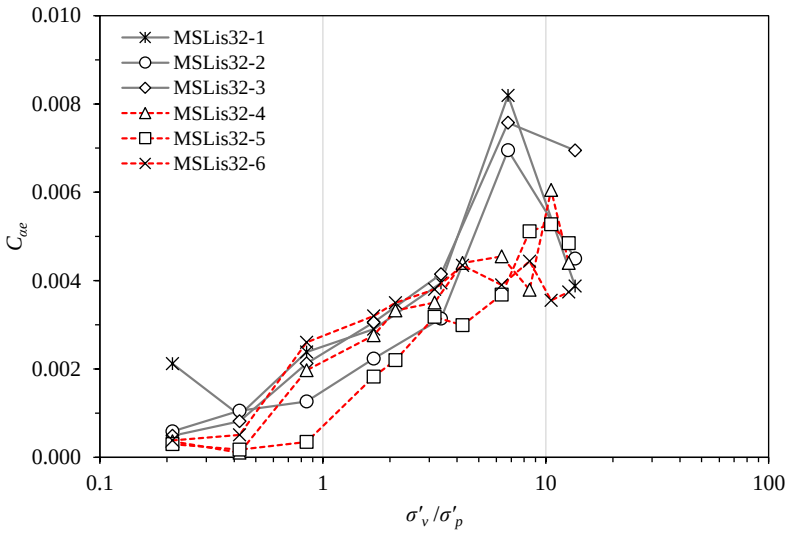


Figure 5.13 Stress-dependency of the secondary consolidation index ($C_{\alpha e}$) for intact Sheppey London Clay

Variation of $C_{\alpha e}$ with normalised stress σ'_v/σ'_p for reconstituted specimens is shown in Figure 5.14. For stress levels prior to preconsolidation pressure, $C_{\alpha e}$ increases slowly for specimens with w_0 = 0.39. For stresses beyond yield stress, $C_{\alpha e}$ increases at a higher rate until reaching a peak value at stress levels in a range of (6-7) σ'_p at which, it starts to decrease. For specimens with higher initial water content (w_0 = 0.43), variation of $C_{\alpha e}$ with normalised stress is slightly different, with $C_{\alpha e}$ increasing dramatically in overconsolidation region and then increasing gradually in normally consolidation region to a peak value at stress levels in a range of (3-4) σ'_p at which, a gradual reduction of $C_{\alpha e}$ values is observed. The maximum value of $C_{\alpha e}$ falls approximately in the range of 0.012 – 0.013 for all tested reconstituted specimens. An average value of $C_{\alpha e}$ = 0.016 was reported by Sorensen (2006) for reconstituted T5 London Clay.

Unlike natural soft clays which typically exhibit higher creep than their corresponding reconstituted specimens, stiff clays such as London Clay, exhibit significantly less creep in comparison with their corresponding reconstituted specimens. This, on the one hand, can be attributed to the more compact nature of stiff clays (low initial void ratio) that results in reduced particles freedom for rearrangement under sustained vertical effective stress, and on the another hand, to the low initial water content of the intact specimens and presence of localised unsaturated pockets with sustainable water menisci developed at inter-particle contacts preventing orientation and rearrangement of particles into a more packed state.

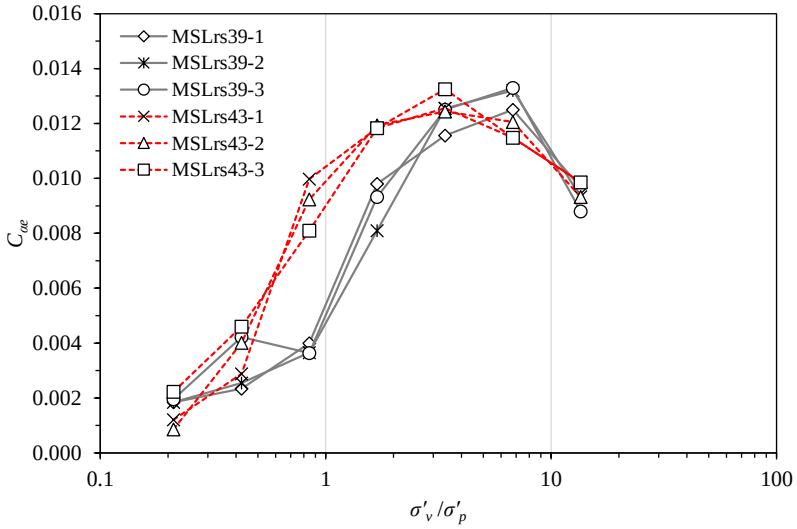


Figure 5.14 Stress-dependency of the secondary consolidation index ($C_{\alpha e}$) for reconstituted Sheppey London Clay

Figure 5.15 presents a comparison of the variation of $C_{\alpha e}$ with stress level for intact, reconstituted, and low-quality undisturbed specimens. In soft clays, the $C_{\alpha e}$ values for intact specimens essentially converge with intrinsic $C_{\alpha e}$ of the reconstituted specimens at high stress levels associated with the completely destroyed inter-particle bonds and rearranged fabric (Mataic, 2016). Indeed, much higher stress levels are required to observe such behaviour for stiff clays, if any. For low-quality undisturbed specimens, it is observed that $C_{\alpha e}$ increases gradually with stress level up to (4-5) σ'_p, at which it starts to decrease. The response of low-quality undisturbed specimens is more similar to that of reconstituted ones, highlighting the effect of soil structure on creep strains.

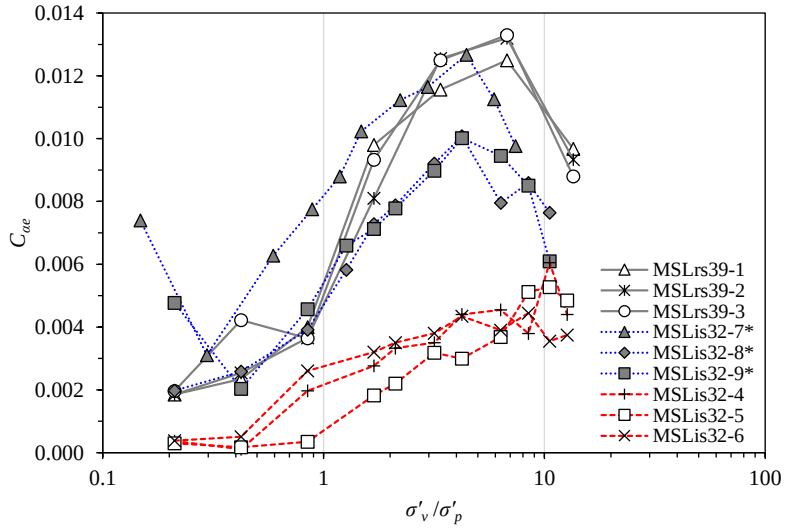


Figure 5.15 Comparison of the stress dependency of $C_{\alpha e}$ for intact, reconstituted, and low-quality undisturbed Sheppey London Clay

5.4.2.3 $C_{\alpha e}/C_c$ Ratio

As discussed in Chapter 2, the ratio of $\alpha = C_{\alpha e}/C_c$ in soft clays has been the subject of numerous studies in the past. Although early researchers such as Mesri and Godlewski (1977) and Mesri and Castro (1987) proposed constant values for α, recent studies (e.g. Yin et al., 2011, Mataic et al., 2015) have demonstrated the inaccuracy of this hypothesis and experimentally evidenced stress-dependency of α. The ratio α for stiff Sheppey London Clay was therefore investigated to examine the applicability of either of these two hypotheses for stiff clays.

Figure 5.16 presents variation of $C_{\alpha e}/m_c$ ratio with normalised stress σ'_v/σ'_p for intact specimens. Unlike natural soft clays that exhibit a sudden increase to a peak value in post yield region due to destructuration phenomenon (Mesri and Castro, 1987, Karstunen and Yin, 2010, Mataic et al., 2015), variation of $C_{\alpha e}/m_c$ ratio with normalised stress for stiff London Clay does not present such trends. At lower stress levels (i.e. overconsolidation region), the $C_{\alpha e}/C_r$ ratio is considerably scattered. This is probably because of the experimental errors in measurement of very small deformations at low stress levels comprising a significant imprecision in calculation of the $C_{\alpha e}/C_r$ ratio. In the normally consolidation region, the $C_{\alpha e}/C_c$ ratio decreases gradually with stress level. The values of α fall approximately in a range of 0.015 – 0.045. Moreover, the values of α for conventionally loaded specimens are generally greater than those of unconventionally loaded specimens (dotted lines). The less scattered values of α for unconventionally loaded specimens in post yield region can further confirm the suitability of this loading method for investigating interrelation of compression and creep indices in stiff clays.

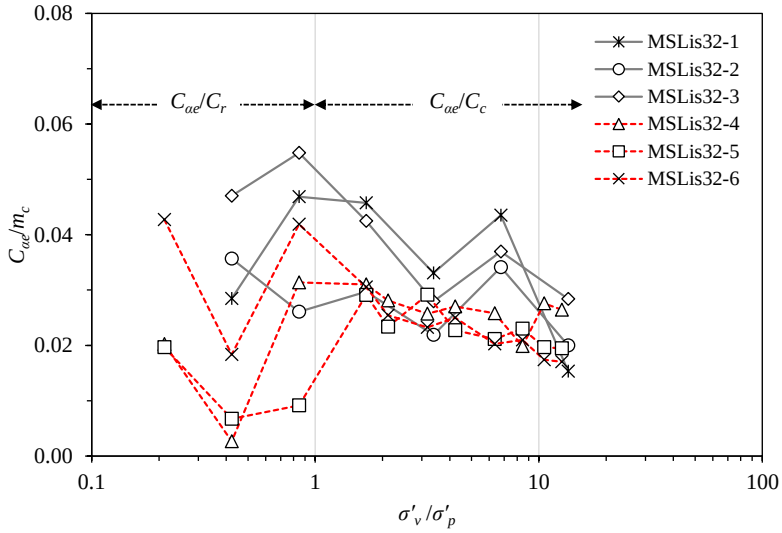


Figure 5.16 Stress-dependency of the α ratio for intact Sheppey London Clay

Figure 5.17 presents variation of $C_{\alpha e}/m_c$ ratio with normalised stress σ'_v/σ'_p for reconstituted specimens. Similar to intact specimens, the $C_{\alpha e}/C_r$ ratio is considerably scattered at lower stress levels (i.e. overconsolidation region) probably due to the experimental measurement errors. However, in the normally consolidation region, the $C_{\alpha e}/C_c$ values are less scattered and decrease gradually to finally converge at the constant average value of 0.024. It is clear that the $C_{\alpha e}/C_c$ ratio is stress-dependent and varies with effective stress. Therefore, the hypothesis of constant $C_{\alpha e}/C_c$ ratio is rejected for stiff clays.

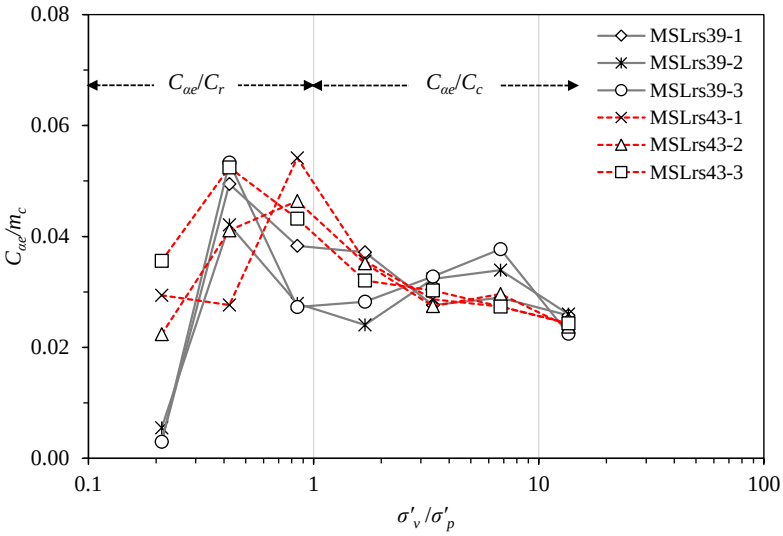


Figure 5.17 Stress-dependency of the α ratio for reconstituted Sheppey London Clay

Figure 5.18 presents a comparison of the variation of $C_{\alpha e}/m_c$ ratio with stress level for both intact and reconstituted specimens. The values of α in the post yield region are in

general smaller for intact specimens than reconstituted ones given lower C_c and $C_{\alpha e}$ values observed for intact specimens (see Figures 5.12 and 5.15). In soft clays, the $C_{\alpha e}/C_c$ values essentially converge at a constant value corresponding to that of the reconstituted specimens. This is justified based on the principle that at high stress levels, all inter-particle bonds are destroyed and the post yield compression curve of a natural clay merges with the intrinsic compression line associated with the corresponding reconstituted specimen. In soft clays, convergence of $C_{\alpha e}/C_c$ values for intact and reconstituted specimens may occur at stress levels in a range of (10-20) σ'_p due to the soft nature and high degree of destructuration in these materials. However, a much higher stress level may require for degradation of inter-particle bonds in stiff clays such as London Clay. Applying such high stresses may not be typically possible using the conventional dead-weight loading method in oedometer apparatuses.

Figure 5.19 presents a comparison of the variation of $C_{\alpha e}/m_c$ ratio with stress level for intact, reconstituted, and low-quality undisturbed specimens. Except MSLis32-7* specimen, the ratio of α for low quality undisturbed specimens exhibits a peak value at stress levels in a range of (4-5) σ'_p, at which it starts to decrease towards the values of α ratio of the reconstituted specimens.

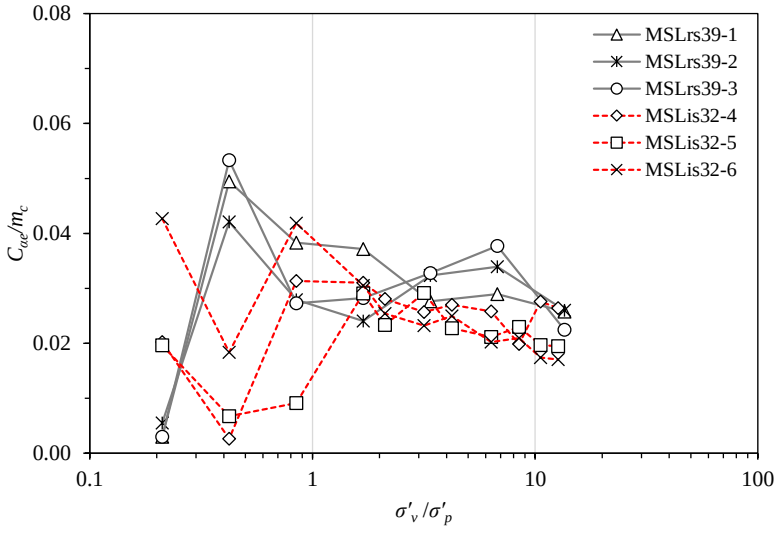


Figure 5.18 Comparison of the stress-dependency of the α ratio for reconstituted and intact Sheppey London Clay

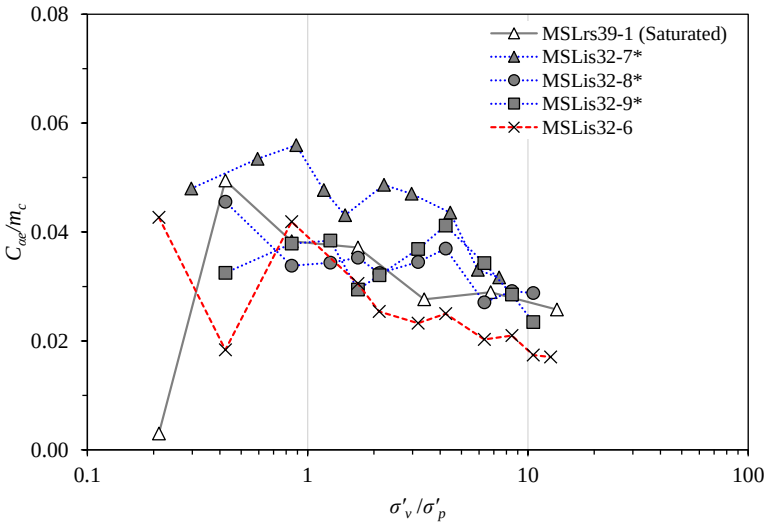


Figure 5.19 Comparison of the stress-dependency of the α ratio for intact, reconstituted, and low quality undisturbed Sheppey London Clay

5.5 Unsaturated MSL Oedometer Tests

5.5.1 Test Procedure and Apparatus

In order to evaluate the effect of soil suction on 1D compressibility of the Sheppey London Clay, MSL oedometer tests with 24 hours loading periods were performed on unsaturated specimens prepared at different initial water contents. The three suction-monitored oedometer cells, described in Chapter 4, were used to perform this set of experiments. The suction-monitored apparatus allows for characterisation of unsaturated soils more slowly than do the suction-controlled apparatuses (Jotisankasa et al., 2007, Caicedo et al., 2008). In order to avoid the complexities associated with the soil structure (mainly inter-particle bonding), this set of experiments were carried out only on reconstituted specimens prepared based on the method described in Chapter 3. The test procedure is similar to that explained earlier for saturated soils (Section 5.4.1). After setting up the specimen in the cell, the two HCTs were installed on the loading cap. The ceramic disks of the tensiometers were covered with some soil paste (see Chapter 4, Section 4.9.5), and a small vertical stress was also applied to the specimen to further ensure the ultimate contact with the tensiometers. The specimen was then allowed to reach moisture equilibrium overnight under an equivalent vertical stress of 8 kPa due to the weight of the hanger and the loading cap. Any possible swelling was also recorded. Prior to each experiment, the HCTs were saturated and preconditioned following the procedure explained by Tarantino (2004) and described in detail in Chapter 4. The average suction recorded by the two HCTs prior to the start of loading

was considered as the initial suction (s_0) of the specimen. In all experiments, the pressure difference recorded by the two HCTs did not exceed 5 kPa. The HCTs were also periodically calibrated in order to account for any possible changes in their performance. Vertical deformations during compression and swelling were measured by an LVDT with travel length of 25 mm and accuracy of 0.001 mm. Table 5.2 presents the details of experiments including the sequence of loading and unloading stages, the initial suction of the specimen, and the HCTs used for monitoring soil suction evolutions. Selection of the initial water contents of the specimens was based on the information obtained from the developed SWRC for reconstituted samples and to examine compressibility of specimens with a wide range of suctions on the transition effect zone (partially saturated zone) of the main drying curve. It must be mentioned here that the suction value corresponding to water content of 15% was much higher than the maximum attainable suction by the developed HCTs. Therefore, the corresponding suction for the MSLru15 specimen was found from the curve fitting of the experimental SWRC data obtained using WT11 tensiometer and CD(er) method as discussed in Chapter 4. The oedometer apparatuses used at The University of Warwick were the imperial type with back loading hangers, which had been secured on a table. The maximum applied vertical stress was, therefore, limited to the amount of dead weights that could be simultaneously applied to the hangers of the three oedometer apparatuses without the risk of overturning. The testing system was later modified in order to carry more loads securely. Some preliminary tests were initially performed on kaolin clay specimens in order to examine the overall performance of the testing system. The results of these experiments were excluded from this thesis.

High performing tensiometers (WT9, WT10, WT11 and WT12) were used for monitoring suction changes during consolidation tests on MSLru28 and MSLru26 specimens due to their high initial suctions. To ensure continuous suction measurements, two HCTs were held on standby in the saturation chamber, to replace the cavitated in-contact HCT. The special design of the oedometer loading cap allows for replacement of the cavitated HCT without any disturbance to the specimen and interruption in measurement of deformations. Replacement of HCTs were performed two times for MSLru28 specimen and the recorded suction measurements were corrected accordingly. For MSLru26 specimen with initial suction of 1907 kPa, the cavitated HCTs had to be replaced several times, and as a result, the continuity of the

suction measurements were significantly interrupted, especially due to occasional cavitation of HCTs overnight. The monitored suction changes for this test are not, therefore, presented here.

Table 5.2 Details of MSL tests on unsaturated specimens

Test ID	Loading/unloading pressures (kPa)	HCT	s_0 (kPa)
MSLru37	22-44-89-178-355-710-1111-710-355-178-89-44-22-11	WT7 & WT8	326
MSLru36	22-44-89-178-355-710-1111-710-355-178-89-44-22-11	WT9 & WT10	433
MSLru35	22-44-89-178-355-710-1111-710-355-178-89-44-22-11	WT11 & WT12	513
MSLru28	25-50-101-202-302-403-504-605-504-403-302-202-101-50-25	WT11 & WT12	1405
MSLru26	25-50-101-202-302-403-504-605-504-403-302-202-101-50-25	WT11 & WT12	1907
MSLru15	25-50-101-202-302-403-504-605-504-403-302-202-101-50-25	NA	21000

5.5.2 Test Results

Figure 5.20 presents the normalised compression curves for unsaturated reconstituted specimens. For comparison, the compression curve of a saturated reconstituted specimen (MSLrs39-1) has also been plotted in Figure 5.20. As can be seen, suction influences the shape and location of the compression curves. Increase in suction level, results in a decrease in overall compressibility of the specimens. Furthermore, increase in suction results in an increase in apparent preconsolidation pressure as shown in Figure 5.21 and supported in the literature (e.g. Wheeler and Sivakumar, 1995, Monroy et al., 2008, Benatti et al., 2010, Haghighi, 2011).

Figure 5.22 presents the variation of pore-water pressure (u_w) during loading and unloading stages for specimens MSLru37, MSLLru36, MSLru35 and MSLru28. Figures 5.22(a) to (d) show an instantaneous increase in u_w (decrease in suction) followed by a gradual pressure equalisation at each loading stage. Moreover, for all loading stages, a suction state was preserved within the specimens, confirming that no water has been expelled from the specimens, and hence, the condition of constant water content was recognised throughout the experiments. Similarly, instantaneous decrease in u_w (increase in suction) followed by a pressure stabilisation was observed at each unloading stage. Unlike the assumption of pore-fluid incompressibility in saturated consolidation theory, the pore-fluid, being formed of air and water, is considered compressible during consolidation of unsaturated clays. Therefore, during the course of compression, with decrease in air volume, the S_r is increased, this being mainly due to

the reduction in void ratio of the specimen; as supported in the literature (e.g. Cuisinier and Laloui, 2004, Koliji, 2008). The decrease in suctions observed at the end of the unsaturated MSL tests can be, therefore, explained by the increase in S_r of the sample.

Figures 5.22(e) to (h) present the variation of suction with vertical stress (ds/dσ), once equilibrium has been reached. As it can be seen on the graphs, suction is decreased during loading and then increased by unloading. For vertical stresses up to 400 kPa (200 kPa for MSLru28), a linear relationship between changes in suction and applied vertical stress was observed. Variation of suction with vertical stresses higher than 400 kPa (200 kPa for MSLru28) appears to be almost constant during both loading and unloading stages. The slopes obtained during loading were very close and varied between -0.30 and -0.34. Except MSLru28 specimen, the slopes obtained during unloading were also very close and varied between -0.02 and -0.08. MSLru28 exhibited a higher slope in unloading (-0.86) than loading (-0.30). For natural clays, the slopes obtained during the unloading stage can be used for estimation of suction changes during sampling and release of stresses (Delage et al., 2007). Although the experiments were performed on reconstituted samples with modified PSD, the obtained results clearly confirmed the importance of suction and suction release, in particular in stiff clays such as London Clay, even though it appears that suction changes during unloading for specimens with low initial suctions (< ~500 kPa) is not significant.

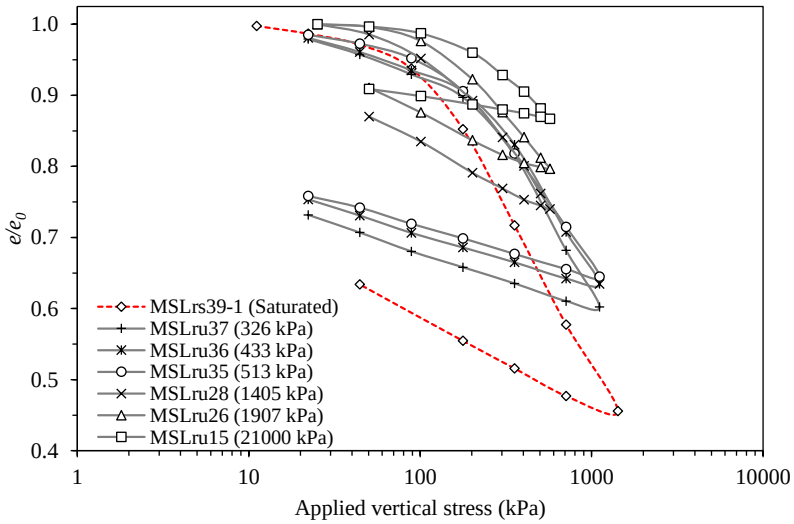


Figure 5.20 Compression curves for unsaturated reconstituted Sheppey London Clay

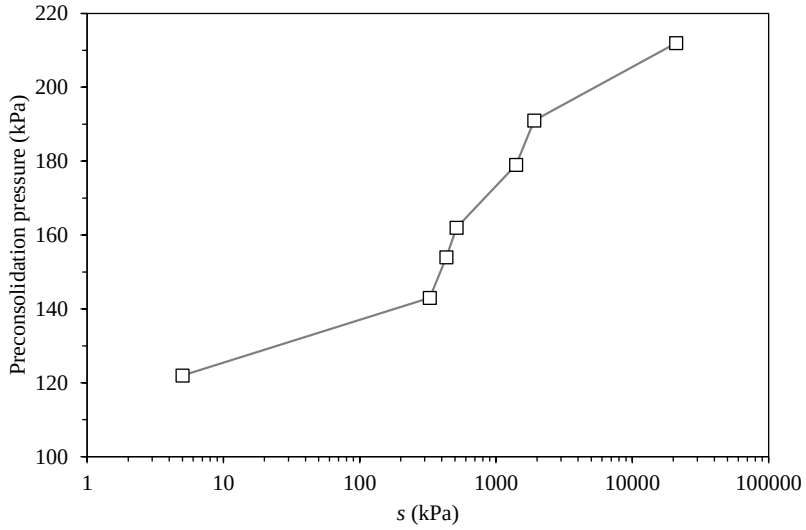


Figure 5.21 Variation of preconsolidation pressure with suction

Figure 5.23 presents the change in pore-water pressure (Δu_w) with each load increment ($\Delta\sigma_v$) immediately after loading and unloading for MSLru37, MSLru36, and MSLru35 specimens. As discussed in Chapter 4, theoretically, for specimens initially consolidated to a known effective stress value, applying a quick unloading under undrained conditions results in development of a negative u_w inside the specimen equal to the unloading increment (Ridley and Burland, 1993). Similar outcomes were expected during quick unloading of the specimens in oedometer tests. However, as can be seen, the tensiometers recorded suctions generally lower than the imposed effective stress. Possible mechanisms controlling this behaviour are:

- Specimen swelling resulted from development of air cavities in pore-water during unloading (Ridley and Burland, 1993).
- Despite very low permeability of the clay specimen, the drained conditions of the unsaturated oedometer test may allow for release of pore-water suction.
- Confinement of the oedometer ring allows only for swelling in the vertical direction, hence development of an immediate impulse to the tip of the HCT during quick unloading, influencing the record of true u_w.

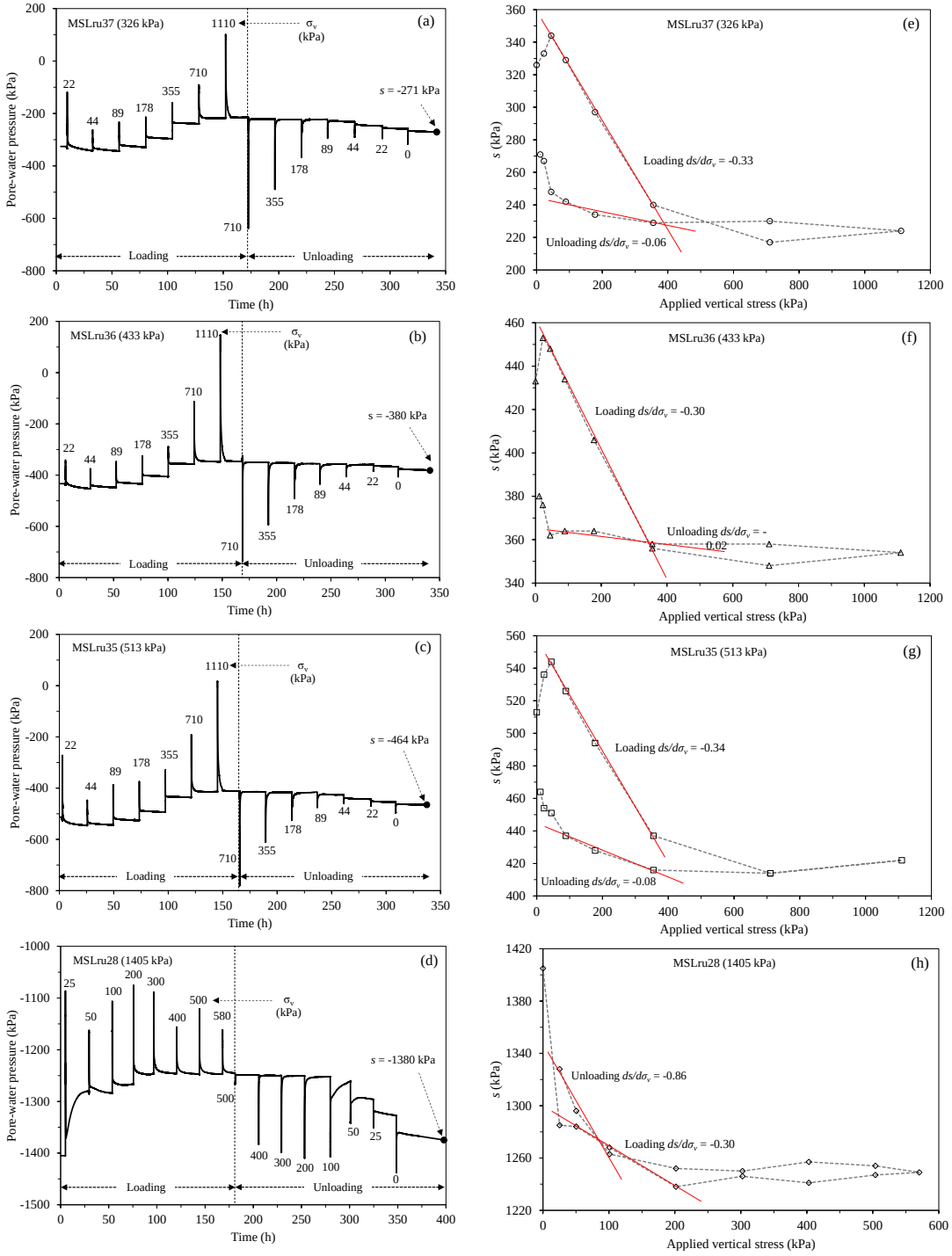


Figure 5.22 Monitoring suction changes during step loading oedometer tests

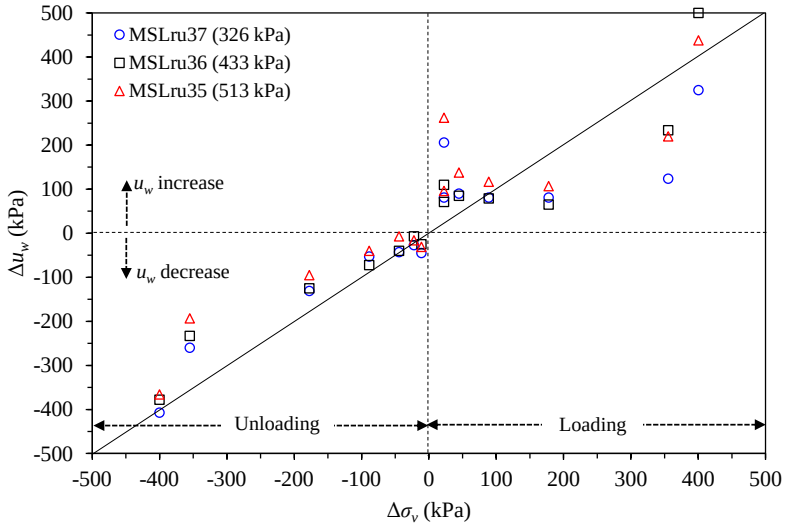


Figure 5.23 Change in pore-water pressure with each load increment

5.5.2.1 Suction-Dependency of the Slope of Compression Curve

Figure 5.24 presents the relationship between the slope of unsaturated compression curve ($m'_c = \Delta e/\Delta \log \sigma_v$) and applied vertical total stress (σ_v) for unsaturated reconstituted specimens. Similar to saturated reconstituted specimens (see Figure 5.11), the slope of compression curves, calculated for each load increment, exhibited stress-dependency and increased with increase in applied vertical stress. However, unlike the saturated specimens, a peak value, after which the m'_c is decreased, was not apparent. Indeed, availability of more data points corresponding to higher stress levels could help in identifying such inflection points, if any. Moreover, it is clearly shown that increase in suction results in decrease of the m'_c values. To further investigate this phenomenon, the values of C_s and C_c for each test were plotted against the initial suction of the specimen (Figure 5.25). Also shown in the figure, is the mathematical prediction (curve fitting) of SWRC for reconstituted samples. It is clearly observed that the C_c values decrease with increase in suction and follow a trend similar to that of SWRC. The C_s values also decrease with increase of suction and follow an approximately linear trend. The later observation contradicts with the statement of Sivakumar (1993) that the gradient of swelling lines are almost independent of suction level. The former observation also contradicts with the results of suction-controlled oedometer tests on compacted London Clay performed by Monroy et al. (2008) who reported a decrease in C_c values with increase in soil suction. The reason behind such contradiction can be attributed to the sample preparation method and the initial conditions of the test specimens. Monroy et al. (2008) prepared the samples by static compaction to an initial

suction of 1000 kPa, and then decreased the suction by hydrating the samples to different equilibrium suctions (zero, 120, and 405 kPa). Therefore, the observed differences in compressibility responses can be explained, in one hand, by the differences in mechanical response of compacted and reconstituted samples, as described in Chapter 3, and in another hand, by the initial hydraulic states of the two samples positioned respectively on the main drying (reconstituted) and main wetting (compacted) curves of the SWRC.

As discussed in Chapter 2, the compression index as a function of suction has been the subject of a long-term dispute among the researchers. Different approaches, as discussed in Zhou et al. (2012), have been proposed to overcome the problems associated with assuming C_c as a function of suction. Among which, the assumption of compression index as a function of S_r appears to be a more logical approach which also produces a better match to the experimental data when used in constitutive models (Zhou et al., 2012). This approach implies that C_c decreases with decrease in S_r. In other words, it is possible to saturate an unsaturated soil by compressing it under constant suction. In fact, in constant suction compression, increase in S_r as a result of reduction in void ratio, can increase the compressibility of the soil due to the stress-induced collapse of macro-pores (Zhou et al., 2012). This approach has been verified based on the experimental results (e.g. Jotisankasa, 2005). Based on this approach, increase of C_c is small at low stresses, and becomes larger at intermediate stress levels until finally equalises the C_c value corresponding to the saturated condition. This behaviour is clearly shown in Figure 5.24. The only difference is that the C_c values of unsaturated specimens do not essentially converge with the values of their saturated condition. Higher applied total stresses might be required to observe such convergences. Moreover, as shown in Figure 5.22, in drained compression tests carried out here, suction evolves throughout the experiment and ends up with a lower value than the initial suction at the start of the test. Therefore, the conditions of constant suction tests, typical of suction-controlled oedometer tests, are not met here. Essentially, for the material tested here, it can be concluded that the slope of compression curve decreases with increase of soil suction.

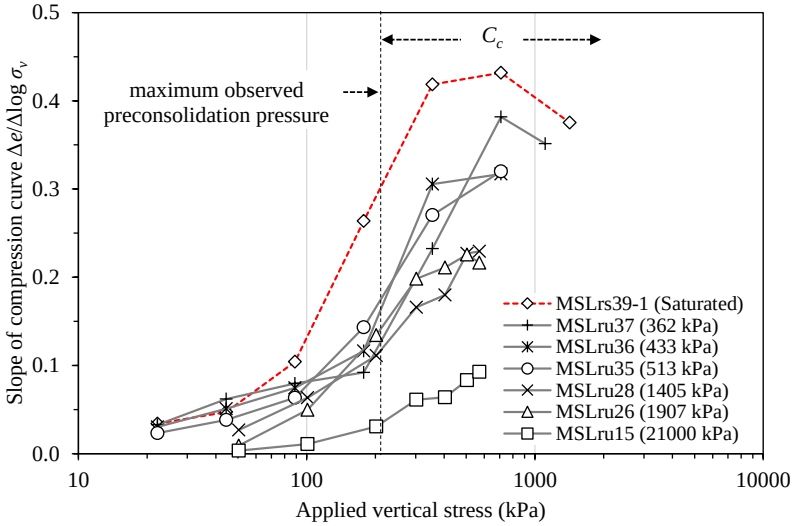


Figure 5.24 Suction- and stress-dependency of the slope of compression curve

In Figure 5.25, variation of C_c with suction follows a trend which is matched closely with the plot of SWRC-*w*. This indicates an interrelation between the compressibility and hydraulic state of the soil on SWRC. In other words, the information of SWRC can be used for qualitative and quantitative estimation of the compression index, at least for drying samples. Formulation of such relationships is beyond the scope of this thesis, and therefore will not be addressed here.

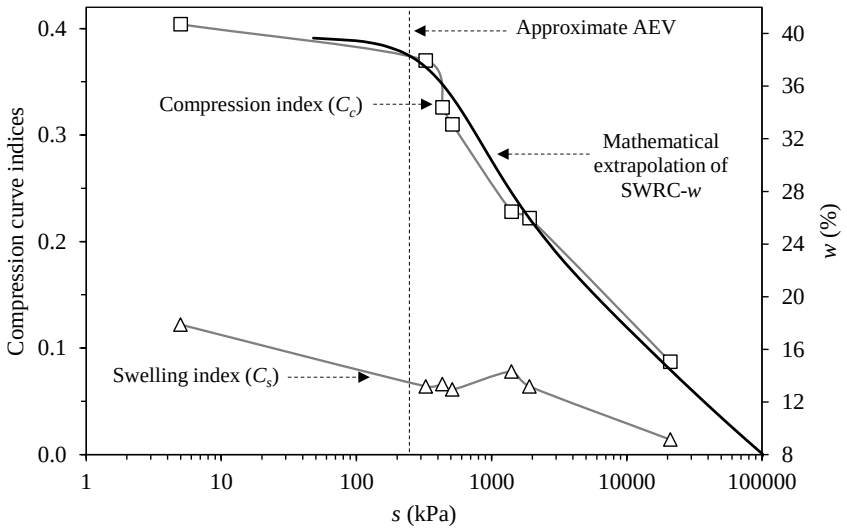


Figure 5.25 Variation of C_c and C_s with suction

5.5.2.2 Suction-Dependency of the Secondary Consolidation Index ($C_{\alpha e}$)

Figure 5.26 presents variation of the secondary consolidation index ($C_{\alpha e}$) with applied vertical total stress (σ_v) for unsaturated reconstituted specimens. Similar to saturated reconstituted specimens (see Figure 5.14), the $C_{\alpha e}$, calculated for each load increment,

exhibited stress-dependency and increased with increase in applied vertical stress. However, unlike the saturated specimens, a peak value, after which the $C_{\alpha e}$ is decreased, was not apparent. In a rough estimation, for specimens with s_0 of 362, 1405, 1907, and 21000 kPa, the maximum value of creep index appears to occur at 710, 504, 504, and 403 kPa vertical total stress respectively. Indeed, availability of more data points corresponding to higher stress levels could help in better identifying such inflection points. Furthermore, increase of $C_{\alpha e}$ is small at low stress levels (< 200 kPa), and becomes larger at higher stress levels. Moreover, it is clearly observed that increase in suction results in decrease of the $C_{\alpha e}$ values. With development of partial saturation state in the specimen during drying, the u_w becomes negative at the back of the generated water menisci at the inter-particle contacts, applying tensile pressure to the soil grains. The additional attractive forces exerted from the water menisci and contractile skin, as discussed in Chapter 2, contribute to the reduction of particles' freedom for rearrangement under sustained vertical effective stress. The rate and magnitude of volumetric creep strains are, therefore, decreased with increase in soil suction.

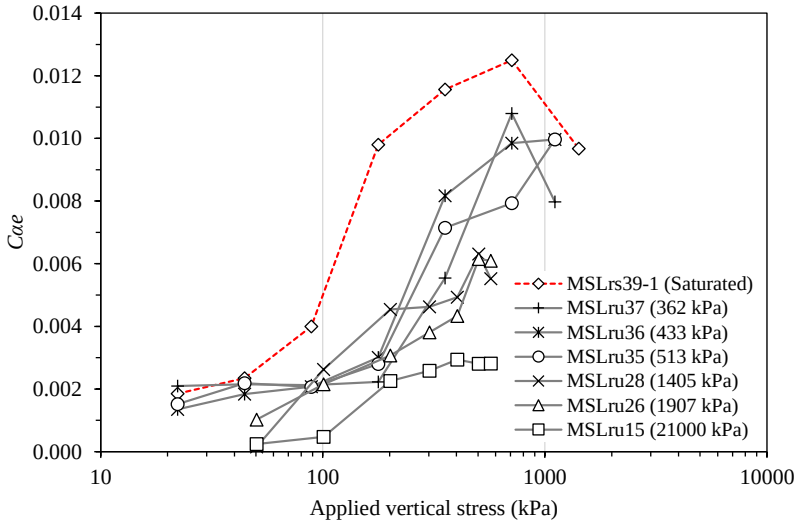


Figure 5.26 Suction- and stress-dependency of the $C_{\alpha e}$ for unsaturated reconstituted Sheppey London Clay

5.5.2.3 $C_{\alpha e}/C_c$ Ratio

Figure 5.27 presents the variation of $C_{\alpha e}/m'_c$ ratio with applied vertical total stress for unsaturated reconstituted specimens. At low stress levels (< 200 kPa), the values of $C_{\alpha e}/m'_c$ decrease with increase in applied total stress. However, at higher stress levels,

the values of $C_{\alpha e}/m'_c$ are scattered and do not follow a clear trend. In a rough estimation, the values of $\alpha = C_{\alpha e}/C_c$ could be said to remain approximately constant with increase in stress level. Excluding the MSLru15 specimen, the values of α obtained for unsaturated conditions appear to fall within a range of 0.023 – 0.030, a similar range as that of obtained for saturated reconstituted specimens (i.e. 0.023 – 0.036). Note that in saturated conditions, the values of α decrease gradually to finally converge at a constant value of 0.024, whereas in unsaturated conditions a clear trend and/or convergence was not observed.

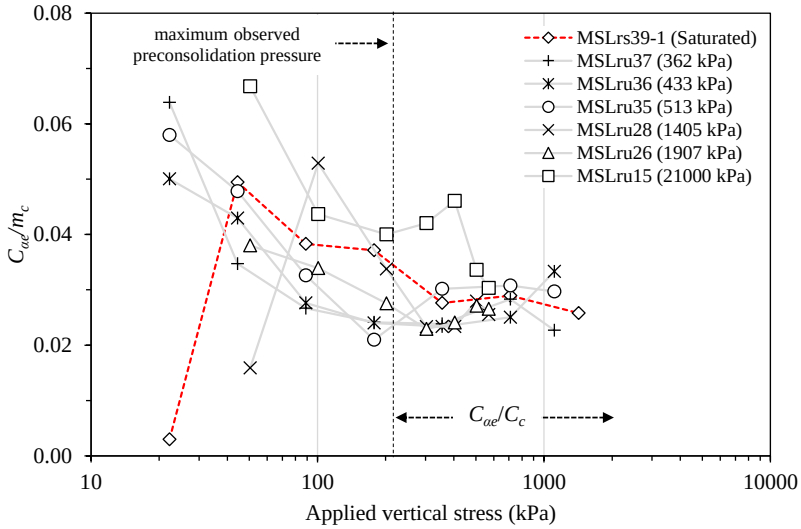


Figure 5.27 Suction- and stress-dependency of the α ratio for unsaturated reconstituted Sheppey London Clay

5.6 Dry MSL Oedometer Tests

5.6.1 Test Procedure and Apparatus

A set of three MSL oedometer tests were carried out on oven-dried Sheppey London Clay samples. These tests were carried out at the University of Warwick using the new unsaturated oedometer cells. Dry samples were obtained by crushing the oven-dried London Clay material to a powder and then grinding the powder in an automatic grinder to further reduce the particles' size. As suggested by Koliji (2008), dry specimens were prepared by direct placement in the oedometer ring followed by slight compaction using a spatula until a relatively flat surface was obtained. Some silica gel was placed inside the fully sealed oedometer cells to prevent moisture absorption from the trapped air inside the cell and development of unsaturated conditions in the specimens. The stages of loading and unloading performed on dry specimens are given in Table 5.3.

Table 5.3 Loading – unloading pattern for MSL tests on dry specimens

Test ID	Loading/unloading pressures (kPa)
MSLd-1	11-22-44-89-178-355-533-710-523-355-178-89-44
MSLd-2	11-22-44-89-178-355-533-710-1066-710-355-178-89-44
MSLd-3	11-22-44-89-178-355-533-710-1421-710-355-178-89-44

5.6.2 Test Results

Figure 5.28 presents the normalised compression curves for dry specimens loaded to maximum vertical total stresses of 710, 1066, and 1420 kPa. The aim of these tests was to allow for better characterisation of the intrinsic behaviour of the Sheppey London Clay in oedometric conditions. It was observed that all specimens showed analogous behaviours with almost equal preconsolidation pressures of approximately 210 kPa. Although, based on the preparation method, the specimens were assumed to be in normal consolidation or lightly overconsolidation state, however, the specimens showed a relatively stiff behaviour followed by a yielding in the compression curve. This response might be due to the moisture absorption and development of unsaturated conditions in the specimens prior and during loading. Similar observations were reported by Koliji (2008) from oedometer tests on dry aggregated Bioley silt. Average C_c and C_s values of respectively 0.197 and 0.009 were obtained from the compression tests. The average compression index for dry specimens is about half of the average compression index obtained for saturated reconstituted specimens. Similar observation was reported by Li et al. (2006) and Li et al. (2009) for Fujinomori Clay where the compression index of the oven-dried specimen was reported to be 35% of that of saturated specimen. Figure 5.29 presents a comparison of the compression curves for saturated reconstituted and dry specimens. The very small swelling index observed for the dry specimen in comparison with the saturated specimen indicates the important role of pore-water in recovery of strains.

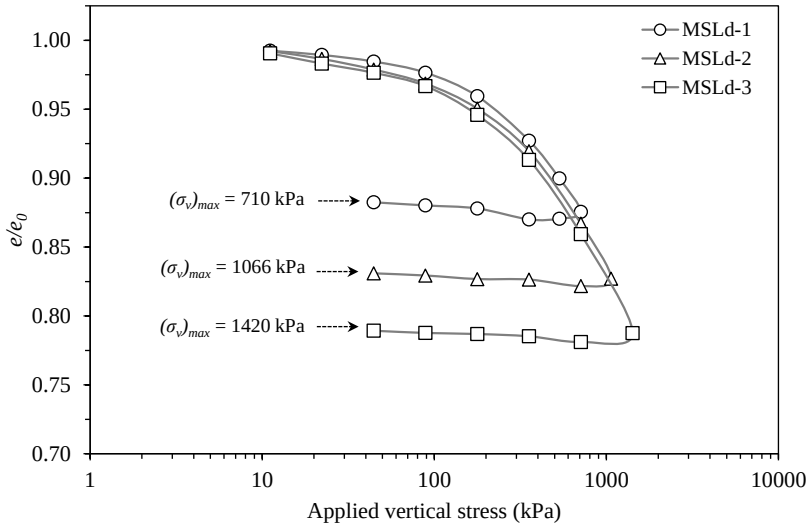


Figure 5.28 Compression curves for oven-dried Sheppey London Clay

5.6.2.1 Stress-Dependency of the Slope of the Compression Curve

Figure 5.30 presents the relationship between m_c and normalised stress σ'_v/σ'_p for dry specimens. In the absence of water, the applied vertical total stress is equal to the vertical effective stress. As it can be seen on the graph, the slope of reloading line increases slightly prior to (0.4-0.5) σ'_p after which, it starts to increase at a higher rate. As discussed earlier and shown on the graph (dotted line), the slope of compression curve for saturated condition in post yield region increases dramatically until it reaches a peak value, at which it starts to decrease. However, the values of C_c for dry specimens do not exhibit such inflection points, at least for the range of applied vertical stresses. Indeed, availability of more data points corresponding to higher stress levels can help in better identifying such inflection points. The maximum C_c for saturated reconstituted specimens, obtained from each load increment, is almost twice the corresponding maximum C_c for dry specimens.

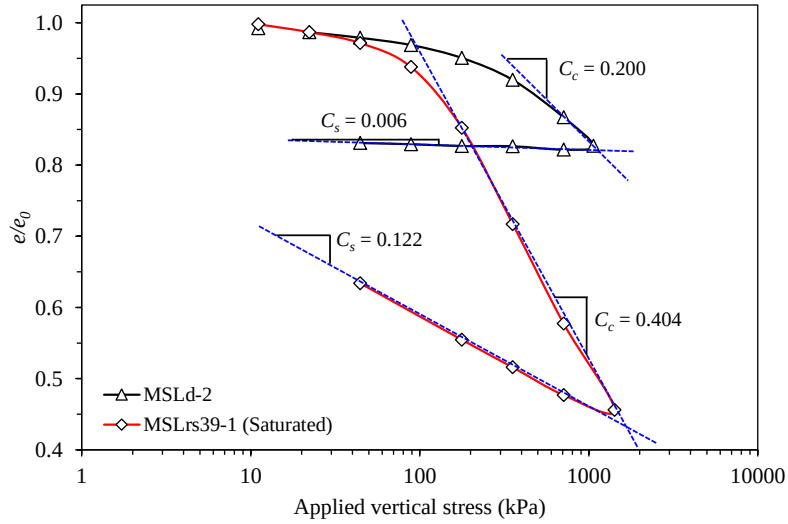


Figure 5.29 Oedometer compression tests of saturated reconstituted and oven-dried Sheppey London Clay

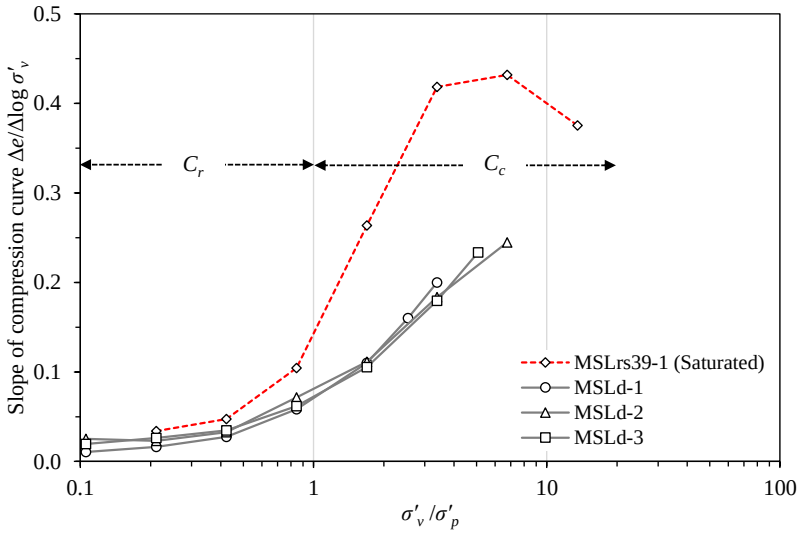


Figure 5.30 Stress-dependency of the slope of compression curve for dry Sheppey London Clay

5.6.2.2 Stress-Dependency of the Secondary Consolidation Index ($C_{\alpha e}$)

Figure 5.31 presents variation of the secondary consolidation index ($C_{\alpha e}$) with normalised stress σ'_v/σ'_p for dry specimens. Prior to preconsolidation pressure, the $C_{\alpha e}$ increases to a peak value at stress levels in range of (0.8-1.0) σ'_p, at which it decreases to essentially reach a constant value of 0.033. The significant differences in $C_{\alpha e}$ values between saturated and dry specimens in normally consolidation region indicates the significant role of pore-water in facilitating creep deformations. In fully saturated condition, pore-water acts as a lubricant to reduce the inter-particle contact forces which consequently enhances particles freedom for rearrangement to a more packed

state. In the absence of water, $C_{\alpha e}$ remains approximately constant with increase in stress level.

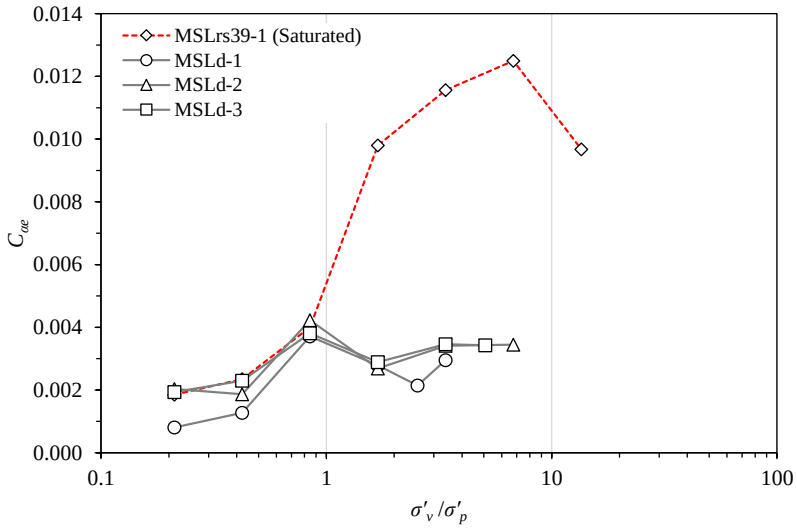


Figure 5.31 Stress-dependency of $C_{\alpha e}$ for dry Sheppey London Clay

5.6.2.3 $C_{\alpha e}/C_c$ Ratio

Figure 5.32 presents variation of $C_{\alpha e}/m_c$ ratio with normalised stress σ'_v/σ'_p for dry specimens. In normal consolidation region, the $C_{\alpha e}/C_r$ ratio decreases with increase in stress level, although the obtained values are scattered. In the post yield region, the values of α for the three tests are converged and continue to decrease with increase in stress level, as observed also for the fully saturated condition.

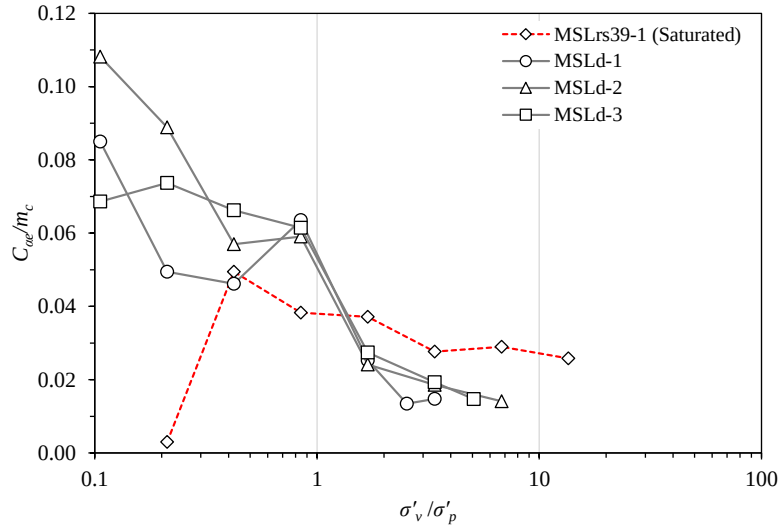


Figure 5.32 Stress-dependency of the α ratio for dry Sheppey London Clay

5.7 MSL Tests Remarks

Table 5.4 summarises the stress ranges at which the maximum values of C_c, $C_{\alpha e}$, and α occur for both intact and reconstituted specimens. The range and average values of α ratio obtained from different sets of experiments are also shown in Table 5.4. The results indicate that for conventionally loaded intact specimens as well as reconstituted specimens with w_0 = 0.39, the maximum values of C_c and $C_{\alpha e}$ do not occur at the same stress level. However, for unconventionally loaded intact specimens as well as reconstituted specimens with w_0 = 0.43, C_c and $C_{\alpha e}$ reach the peak value at the same stress levels synchronously. The latter finding is in contradiction with the observations reported for soft clays (see Mataic et al., 2015). The maximum values of α occur at stress levels in a range of (1-2) σ'_p, for both intact and reconstituted specimens. For unsaturated and dry specimens, a peak value for C_c, $C_{\alpha e}$, and α was not apparent. For saturated intact specimens, the range of α values varies significantly. For conventionally loaded intact specimens, an average α value of 0.03 ± 0.02 can be approximated. However, for unconventionally loaded intact specimens, a lower approximate average α value of 0.02 ± 0.01 is obtained. According to the classification criterion defined by Mesri et al. (1994), Sheppey London Clay lies in the zone of shale or mudstone whose α value ranges from 0.02 to 0.04. For saturated and unsaturated reconstituted specimens, the ratio $C_{\alpha e}/C_c$ lies in a similar range of 0.023 – 0.037. Accordingly, an average value of 0.03 ± 0.01 can be approximated for the α ratio of saturated and unsaturated reconstituted specimens. Finally, this average value is decreased to approximately 0.02 ± 0.01 for dry specimens. The values of α for saturated low-quality undisturbed specimens fall in a range of 0.023 – 0.048, with the lower band value being equal to that of reconstituted specimens, and the upper band value, being similar to that of intact specimens.

Table 5.4 Stress ranges for maximum C_c, $C_{\alpha e}$, and α parameters

Test ID	σ'_v / σ'_p			Range of α values	Average α
	$(C_c)_{max}$	$(C_{\alpha e})_{max}$	$(\alpha)_{max}$		
MSLis32-1 MSLis32-2 MSLis32-3	8 – 10	6 – 7	1 – 2	0.015 – 0.046	0.031 ± 0.016
MSLis32-4 MSLis32-5 MSLis32-6	8 – 10	8 – 11	1 – 2	0.017 – 0.031	0.024 ± 0.007
MSLis32-7* MSLis32-8* MSLis32-9*	6 – 8	4 – 5	4 – 5	0.023 – 0.048	0.036 ± 0.013
MSLrs39-1 MSLrs39-2 MSLrs39-3	3 – 4	6 – 7	1 – 2	0.022 – 0.037	0.03 ± 0.008
MSLrs43-1 MSLrs43-2 MSLrs43-3	3 – 4	3 – 4	1 – 2	0.024 – 0.036	0.03 ± 0.006
MSLru37 MSLru28 MSLru26	3 – 4	2 – 5	NA	0.023 – 0.037	0.03 ± 0.007
MSLru36 MSLru35 MSLru15	NA	NA	NA	0.023 – 0.045	0.034 ± 0.011
MSLd-1 MSLd-2 MSLd-3	NA	NA	NA	0.014 – 0.027	0.021 ± 0.007

5.8 Saturated SSL Oedometer Creep Tests

5.8.1 Test Procedure

In order to have an insight into the creep behaviour of Sheppey London Clay, a set of single-stage loading (SSL) oedometer compression tests were performed on intact and reconstituted specimens. As suggested by Karim (2010), unlike conventional incremental loading tests, the test pressure was applied directly in a single loading stage in order to remove the possible effects of loading and creep history on the measured creep strains. Moreover, in order to avoid the problems associated with sudden loading, the applied pressure was ramped up to the desired vertical stress level at a constant rate of 8-10 kPa per hour. The applied pressure was sustained for a period of up to 2250 hours (94 days). The experiments were carried out at the University of Nottingham using the conventional oedometer apparatuses (Figure 5.1). The test specimens were prepared based on the methods described for MSL oedometer tests (Section 5.4).

Test results in this section are presented in plots of normalised void ratio e/e_p versus logarithm of time, where e_p is the void ratio obtained 24 hours after the end of loading. The decision of considering the results obtained after a period of 24 hours was made so as to ensure full dissipation of u_{exc}, and also to allow for comparison between the results and define a criterion applicable to all experiments. Similar approach was considered by Cui et al. (2009) for investigating time-dependent behaviour of stiff Boom Clay. The values of the maximum applied vertical stresses (σ_{vm}) were chosen so as to be higher than the preconsolidation pressure of the samples and to investigate the creep response in the normal consolidation state. Details of the carried out experiments are summarised in Table 5.5.

Table 5.5 Details of saturated SSL oedometer tests

Test ID	σ_{vm} [kPa]	Duration [hr (day)]
SSLis32-178	178	890 (37)
SSLis32-222	222	860 (36)
SSLis32-355	355	860 (36)
SSLis32-444	444	900 (38)
SSLis32-666	666	900 (38)
SSLrs39-178	178	1440 (60)
SSLrs39-222	222	1620 (68)
SSLrs39-355	355	1620 (68)
SSLrs39-444	444	1110 (46)
SSLrs39-666	666	1110 (46)
SSLrs43-355	355	2256 (94)
SSLrs43-444	444	2256 (94)

5.8.2 Test Results

Figure 5.33(a) presents variation of the normalised void ratio e/e_p with logarithm of time for intact specimens. Higher volume change was observed with increase in σ_{vm}, indicating the stress-dependency of creep strains. The rate of change in void ratio for all specimens was higher during about the first 10 days of sustained loading, after which it started to decrease. The observed behaviour corresponds to primary creep stage characterised as increasing creep strains at a decreasing strain-rate. Similar behaviours were observed for reconstituted specimens [Figure 5.33(b)]. Furthermore, the creep rate and magnitude appears to be, in general, lower for intact specimens than the reconstituted ones (Figure 5.34), this being, in part, due to the low initial water content of the intact specimens (w_0 = 0.32). Soil structure, i.e. fabric anisotropy and inter-particle bonding, also plays a significant role in controlling deformations. The process of destructuration during single-stage loading, and whether the inter-particle bonds

were fully or partly destroyed, is not, however, clearly identified. Moreover, at the same stress level, the rate and magnitude of change in void ratio for reconstituted specimens with higher initial water contents (w_0 = 0.43) were found to be higher. In the absence of inter-particle bonds, the water content of the specimens appears to control the rate and magnitude of creep strains.

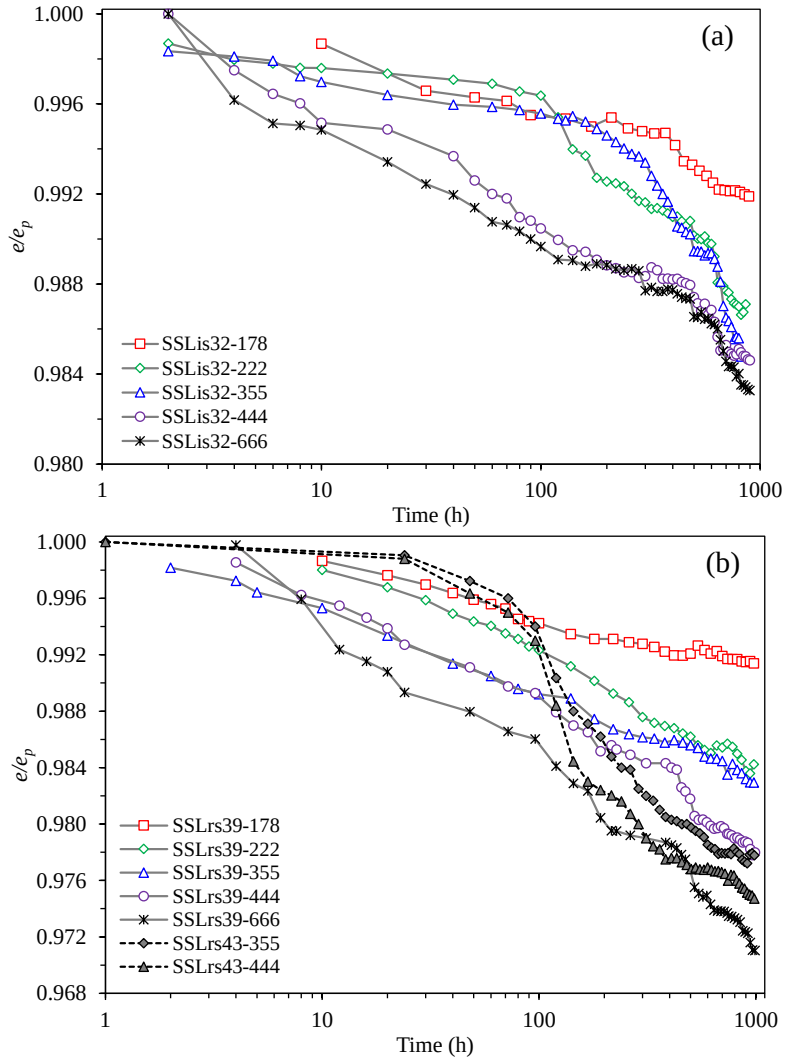


Figure 5.33 SSL oedometer creep tests on saturated Sheppey London Clay: (a) intact specimens; (b) reconstituted specimens

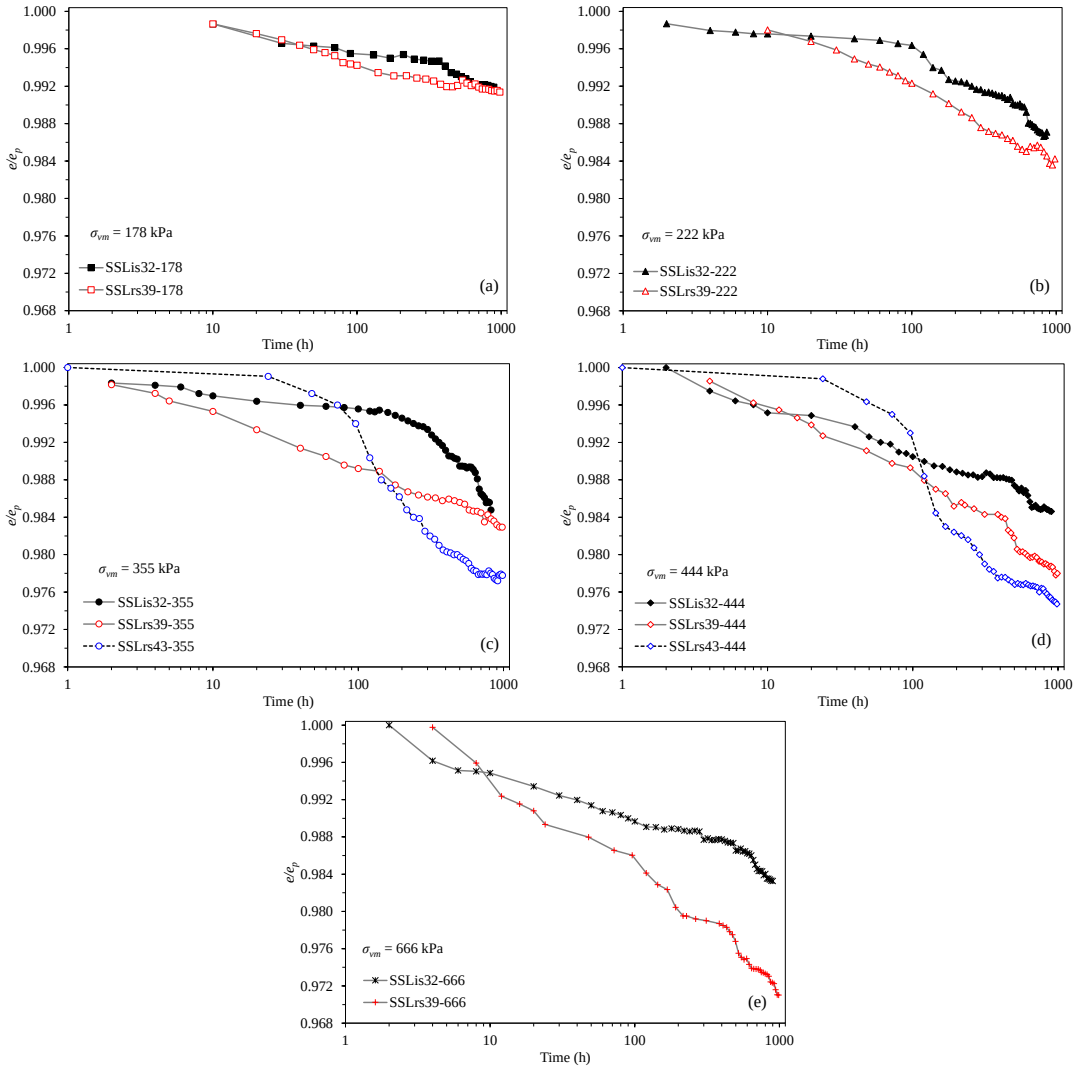


Figure 5.34 Comparison of intact and reconstituted specimens behaviour during SSL oedometer creep tests at different stress levels

In order to study the effect of creep history, two test specimens, named MSLCis32-1332(1) and MSLCis32-1332(2), were loaded with 24 hour load increments to a maximum vertical stress of 1332 kPa, and then allowed to creep for about 55 days. Figure 5.35 presents a comparison of the observed creep behaviour for these two specimens with that of observed from SSL tests on saturated intact specimens. As can be seen, the plots of e/e_p with logarithm of time for these two specimens lie in between the plots of intact specimens, although having a σ_{vm} value of at least two times higher than the single-staged loaded specimens. In fact, the creep strains occurred during each stage of incremental loading brings the specimen into a more packed state, reducing the final creep strains under long-term sustained loading stage. This set of experiments indicates the effect of creep history on the rate and magnitude of creep strains in 1D

oedometer creep tests, and justifies the appropriateness of SSL oedometer tests for investigation of creep response in clays.

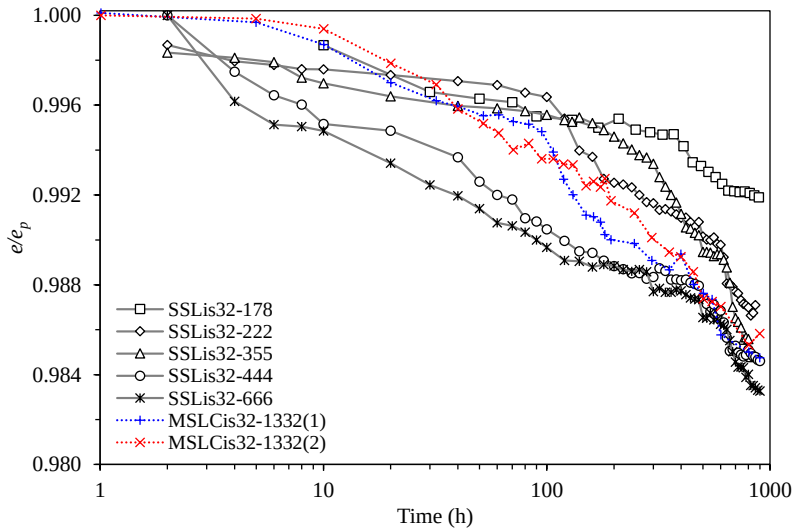


Figure 5.35 Effect of creep history during oedometer creep tests on saturated intact Sheppey London Clay

5.9 Unsaturated SSL Oedometer Tests

5.9.1 Test Procedure

In order to investigate the effect of soil suction on the creep strains, a set of SSL oedometer compression tests were performed on unsaturated reconstituted specimens. Unsaturated specimens were prepared based on the procedure explained in Chapter 3. Experiments were conducted on specimens having initial suction states on the main drying curve of the SWRC in order to eliminate the complexity associated with volumetric deformation due to wetting (wetting-induced deformations or collapse in wetting), and therefore observe the effect of suction on mechanically induced creep deformations. The three suction-monitored oedometer cells, described in Chapter 4, were used to perform this set of experiments. The test specimens were set up in the oedometer cell following the procedure explained for unsaturated MSL oedometer tests (Section 5.5). After reaching equilibrium, axial stress was applied to the specimens in a single loading stage as described in Section 5.8. Details of the carried out experiments are summarised in Table 5.6.

Table 5.6 Details of unsaturated SSL oedometer tests

Test ID	σ_{vm} [kPa]	Average s_0 [kPa]	Duration [hr (day)]	HCTs
SSLru37-666	666	326	670 (28)	WT7 & WT8
SSLru37-444	444	326	700 (29)	WT9 & WT10
SSLru37-355	355	326	860 (36)	WT11 & WT12
SSLru36-666	666	433	670 (28)	WT7 & WT8
SSLru36-444	444	433	500 (21)	WT9 & WT10
SSLru36-355	355	433	820 (34)	WT11 & WT12
SSLru35-355	355	513	820 (34)	WT7 & WT8
SSLru35-222	222	513	820 (34)	WT9 & WT10
SSLru35-178	178	513	640 (27)	WT11 & WT12
SSLru28-666	666	1405	470 (20)	WT11 & WT12
SSLru28-444	444	1405	500 (21)	WT11 & WT12
SSLru28-355	355	1405	670 (28)	WT11 & WT12
SSLru26-222	222	1907	540 (23)	NA
SSLru26-178	178	1907	560 (23)	NA

5.9.2 Test Results

Graphs of Figure 5.36 present the variation of normalised void ratio e/e_p with logarithm of time for specimens having different initial water contents (and therefore different suctions), and subjected to similar vertical stresses. It was clearly observed that at the same vertical stress level, decrease in initial water content (or increase in initial suction) results in a decrease in the rate and magnitude of volumetric creep strains. Unlike saturated soils, the water phase is discontinuous in partially-saturated soils. The generated water menisci between the soil particles hold the grains together. The soil particles are held together by the tensile forces at the solid-water interface. During creep, the under-tension water menisci resist against rearrangement and orientation of the clay particles. Indeed, as discussed in Chapter 2, Section 2.4.4, the observed deformations under prolonged sustained loading, may not be regarded as true creep, as internal stresses change with time is modifying the state of effective stress.

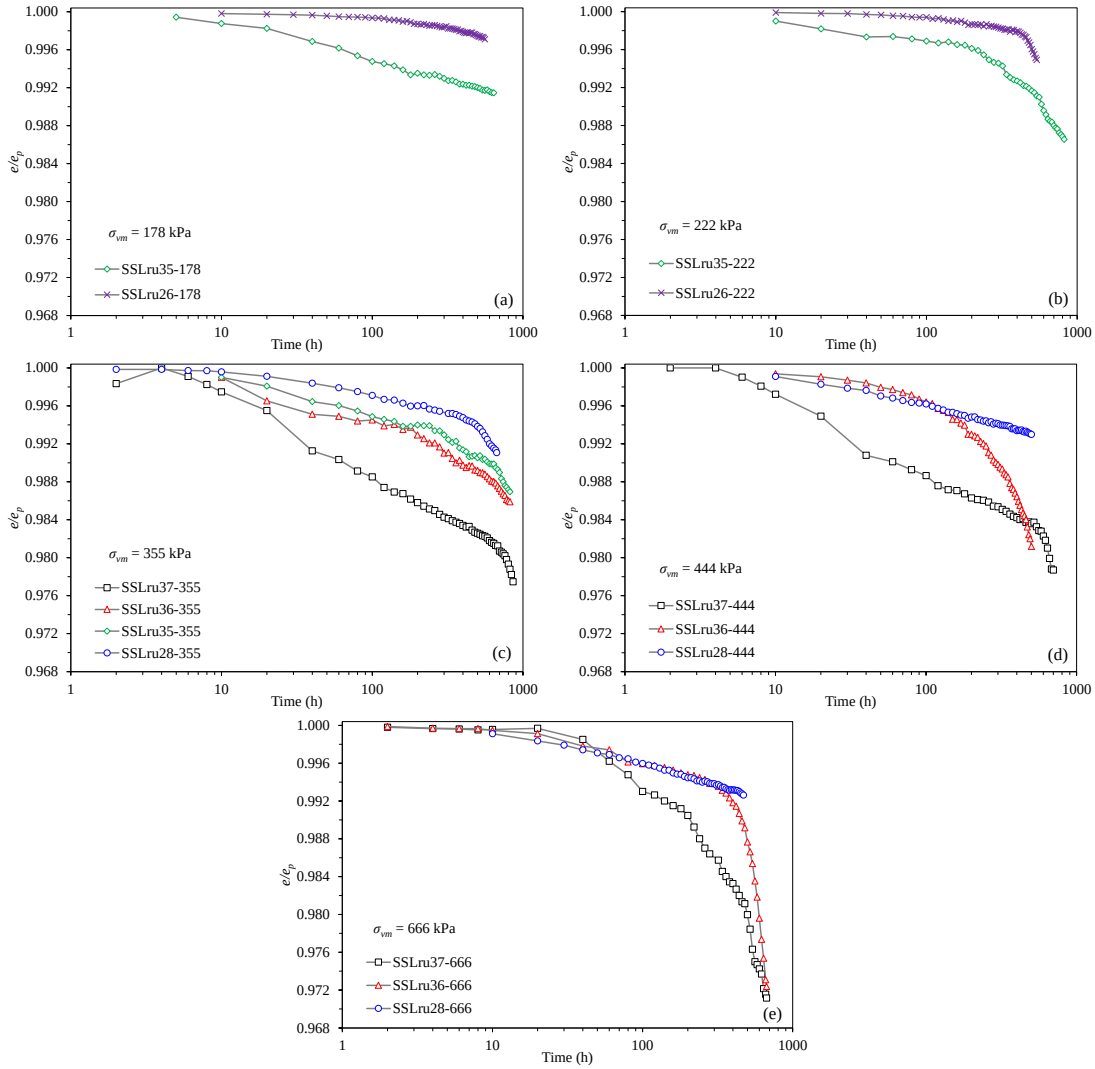


Figure 5.36 Effect of suction during creep tests at different stress levels of: (a) 178 kPa; (b) 222 kPa; (c) 355 kPa; (d) 444 kPa; (e) 666 kPa.

In order to investigate the stress-dependency of creep behaviour in unsaturated conditions, the tests results were plotted in graphs of Figure 5.37 where the variations of e/e_p ratio with logarithm of time have been compared for specimens having similar initial suctions but subjected to different applied vertical stresses. For the specimens with s_0 = 326 kPa [Figure 5.37(a)], the rate of volume change was observed to be smaller for the higher σ_{vm} (i.e. 666 kPa). Similar behaviour was observed for the specimens with s_0 = 433 kPa [Figure 5.37(b)]. However, effect of increase in applied vertical stress was more pronounced during the final hours of the tests. For specimens SLLru28-444 and SLLru28-355 with s_0 = 1405 kPa, the volume change response appeared to be fairly similar, indicating, conceivably, the predominant effect of soil suction in controlling creep deformations. Similar behaviour was also observed for

SLLru26-222 and SLLru26-178 specimens with s_0 = 1907 kPa, further supporting this hypothesis. Indeed, further investigations over a wider range of applied vertical stresses and suctions are required to validate this hypothesis.

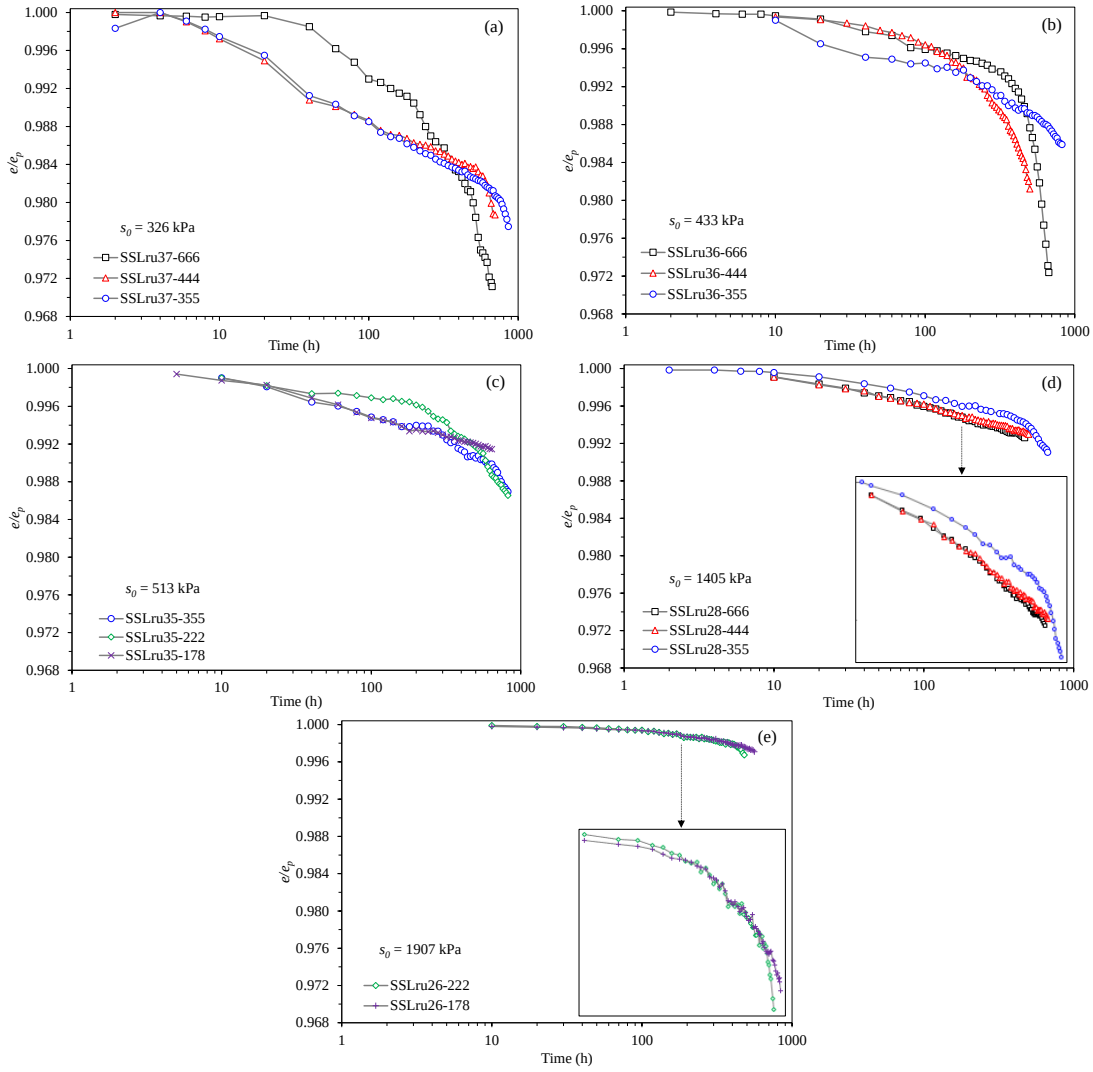


Figure 5.37 Effect of stress level during creep tests on specimens with constant suctions of: (a) 326 kPa; (b) 433 kPa; (c) 513 kPa; (d) 1405 kPa; (e) 1907 kPa.

Figures 5.38(a) and (b) present variation of suction with vertical stress (ds/dσ), during the course of loading for SSLru35-178 and SSLru35-222 specimens. Also shown in the figure, is the volume change of the specimens in the form of variation of e/e_0 ratio with time, where e_0 is the initial void ratio. As it can be seen on the graphs, suction is decreased during loading. Similar to MSL tests (Figure 5.22), an instantaneous increase in u_w (decrease in suction) followed by a gradual pressure equalisation at each loading stage was observed. Moreover, for all loading stages, a suction state was preserved within the specimens, confirming that no water was expelled from the specimens, and

hence, the condition of constant water content was recognised throughout the loading stage. Similar results were obtained for all other test specimens (results not shown here).

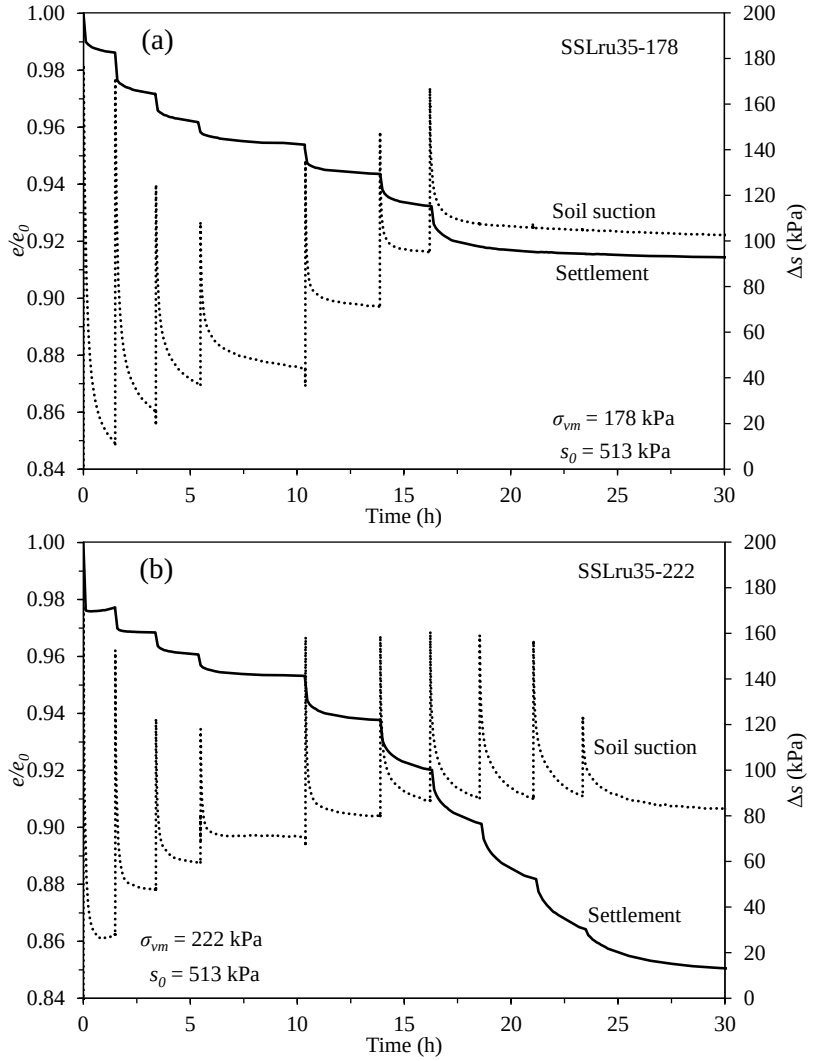


Figure 5.38 Monitoring suction changes during loading stage of SSL oedometer tests

Figure 5.39 presents the results of monitoring suction evolutions during the creep stage of the tests. As no water was expelled from the specimen during the creep straining, observation of a constant suction value was expected. However, it was observed that suction was decreased with time with an almost linear trend for all of the test specimens. In fact, with increase in creep strains at constant water content, total volume is decreased resulting in an increase in the S_r of the sample, which in turn, leads to a decrease in soil suction. This is, however, a possible mechanism, and the observed decrease in suction might be due to the other factors influencing the HCTs measurements, as discussed in Chapter 4. However, if this is the case, keeping the soil suction constant during a constant suction creep test may not be ideal, as this may

require a change (reduction) in S_r of the specimen, and hence, artificially development of creep strains. It must be mentioned here that monitoring suction evolution for specimens with initial suctions of 1405 and 1907 kPa were interrupted several times due to the cavitation of the HCTs. The discontinuity in the obtained results for specimens with s_0 = 1405 kPa were, however, recoverable and, with applied corrections, are presented in Figure 5.39. However, for specimens with s_0 = 1907 kPa, the significant discontinuity in the measurements did not allow for determination of a clear trend in variation of suction with time. These results were, therefore, disregarded and are not presented here.

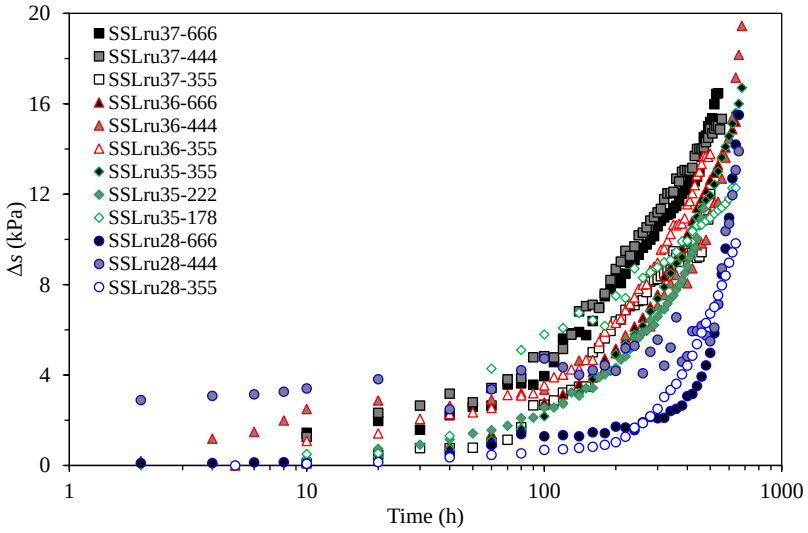


Figure 5.39 Monitoring suction changes during creep stage of SSL oedometer tests

5.10 Dry SSL Oedometer Tests

5.10.1 Test Procedure

A set of three SSL oedometer tests were carried out on oven-dried Sheppey London Clay samples. These tests were carried out at the University of Warwick using the new unsaturated oedometer cells. The test specimens were prepared based on the methods described for MSL oedometer tests (Section 5.6). Details of the carried out experiments are summarised in Table 5.7.

Table 5.7 Details of dry SSL oedometer tests

Test ID	σ_{vm} [kPa]	Test duration [hr(day)]
SSLd-355	355	450 (19)
SSLd-444	444	450 (19)
SSLd-666	666	450 (19)

5.10.2 Test Results

Figure 5.40 presents the variation of normalised void ratio e/e_i with logarithm of time for dry specimens. In the absence of water, consolidation of dry samples is divided into instant compression and secondary consolidation phases. The e_i in this case, equals to the void ratio at the end of instant compression. Increase in applied vertical stress, increases the creep deformations in the initial stages of the tests. However, with elapse of time, the creep rate appears to decrease.

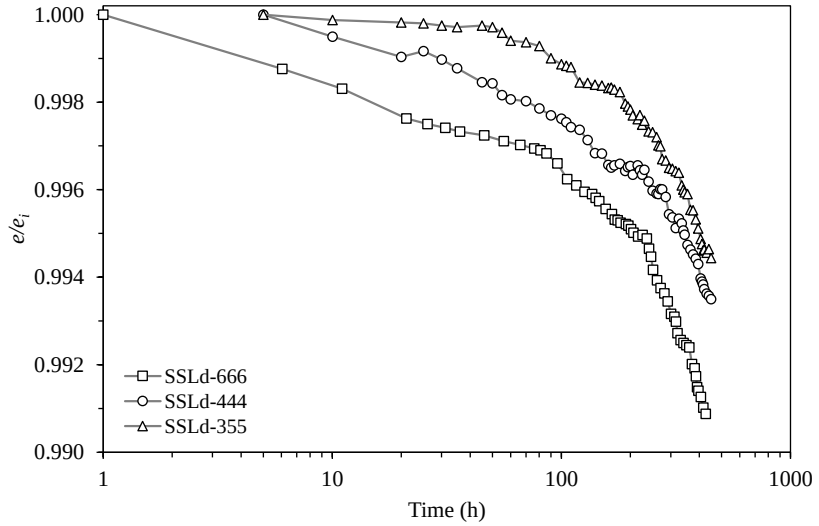


Figure 5.40 SSL oedometer creep tests on dry Sheppey London Clay

Comparing the results of creep tests on dry and saturated reconstituted specimens (Figure 5.41), highlights the important role of water in increase of creep strains as discussed in Section 5.6. At the same stress level, the saturated specimens show significantly higher volume change than the dry specimens, probably mainly due to the friction reduction at the inter-particle contacts in saturated specimens that allows for easier rearrangement of particles into a more packed state.

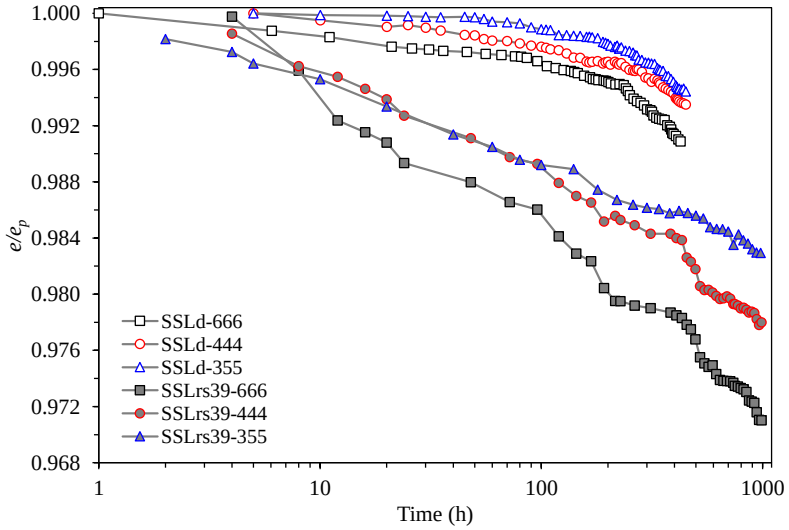


Figure 5.41 Comparison of SSL oedometer creep tests on dry and saturated reconstituted specimens

5.11 A Creep Law

A simple regression analysis was carried out in order to develop an evolution law of the vertical creep strain as a function of the constant loading stage duration. The best-fit curves (or lines) for each test data were determined and the corresponding regression coefficients were recorded. The results of regression analysis are summarised in Table 5.8. It was found that for saturated intact and dry specimens, the linear regression provides better matching results with generally higher R^2 values. However, for the incrementally loaded intact, as well as saturated and unsaturated reconstituted specimens, the power regression appeared to provide better fitting results.

Table 5.8 Regression coefficients for SSL oedometer tests

Test ID	σ_{vm} [kPa]	s_0 [kPa]	Linear regression $y = Ax + B$			Power regression $y = \beta x^{\alpha i}$		
			A	B	R^2	β	α_i	R^2
SSLis32-178	178	0	-5×10^{-6}	0.9961	0.94	1.0069	-0.002	0.90
SSLis32-222	222	0	-1×10^{-5}	0.9953	0.94	1.0149	-0.004	0.94
SSLis32-355	355	0	-1×10^{-5}	0.9975	0.99	1.0227	-0.005	0.91
SSLis32-444	444	0	-8×10^{-6}	0.991	0.94	1.0032	-0.003	0.90
SSLis32-666	666	0	-8×10^{-6}	0.9907	0.97	1.0027	-0.003	0.86
MSLCis32-1332(1)	1332	0	-1×10^{-5}	0.9945	0.84	1.0113	-0.004	0.96
MSLCis32-1332(2)	1332	0	-1×10^{-5}	0.9948	0.93	1.0095	-0.003	0.96
SSLrs39-178	178	0	-2×10^{-6}	0.9936	0.81	0.9989	-0.001	0.91
SSLrs39-222	222	0	-8×10^{-6}	0.9909	0.85	1.0086	-0.004	0.97
SSLrs39-355	355	0	-6×10^{-6}	0.9883	0.93	1.0016	-0.003	0.94
SSLrs39-444	444	0	-1×10^{-5}	0.9884	0.92	1.0110	-0.005	0.97
SSLrs39-666	666	0	-1×10^{-5}	0.9843	0.92	1.0125	-0.006	0.97
SSLrs43-355	355	0	-8×10^{-6}	0.9839	0.83	1.0076	-0.004	0.93
SSLrs43-444	444	0	-6×10^{-6}	0.9809	0.83	1.0080	-0.004	0.91
SSLru37-666	666	326	-4×10^{-5}	0.9978	0.93	1.0549	-0.012	0.94
SSLru37-444	444	326	-1×10^{-5}	0.9893	0.93	1.0083	-0.004	0.84
SSLru37-355	355	326	-1×10^{-5}	0.9882	0.97	1.0088	-0.004	0.94
SSLru36-666	666	433	-4×10^{-5}	1.0035	0.83	1.0532	-0.011	0.75
SSLru36-444	444	433	-4×10^{-5}	1.0003	0.96	1.0418	-0.009	0.96
SSLru36-355	355	433	-1×10^{-5}	0.9946	0.97	1.0187	-0.005	0.98
SSLru35-355	355	513	-1×10^{-5}	0.996	0.94	1.0193	-0.005	0.94
SSLru35-222	222	513	-2×10^{-5}	0.9991	0.93	1.0353	-0.007	0.96
SSLru35-178	178	513	-5×10^{-6}	0.9944	0.93	1.0028	-0.002	0.97
SSLru28-666	666	1405	-8×10^{-6}	0.9963	0.95	1.0055	-0.002	0.99
SSLru28-444	444	1405	-7×10^{-6}	0.9963	0.95	1.0047	-0.002	0.99
SSLru28-355	355	1405	-1×10^{-5}	0.9981	0.95	1.0115	-0.003	0.94
SSLru26-222	222	1907	-8×10^{-6}	1.0004	0.83	1.0092	-0.002	0.70
SSLru26-178	178	1907	-5×10^{-6}	0.9998	0.97	1.0054	-0.001	0.96
SSLd-355	355	NA	-1×10^{-5}	1.0003	0.99	1.0050	-0.001	0.75
SSLd-444	444	NA	-1×10^{-5}	0.9987	0.98	1.0090	-0.002	0.90
SSLd-666	666	NA	-2×10^{-5}	0.9983	0.99	1.0132	-0.004	0.91

Based on the obtained results, a creep law to consider the effect of suction on creep deformations is proposed as;

$$\frac{e}{e_p} = \beta t^{\alpha_i} \qquad 5.6$$

where β is the instantaneous change in void ratio (e_i) normalised with respect to e_p, t represents time, and α_i is the creep coefficient and varies between zero and 0.012 and controls the shape of the curve. Variation of α_i with σ_{vm} and initial water content is shown in Figure 5.42. For certain stress and water content values where data points were not available, extrapolated α_i values were used to plot the 3D surface graph. As

can be seen, the values of α_i increase with increased σ_{vm} and increased water content (decreased suction). For the suction and vertical stress ranges in this study, the values of α_i vary almost linearly with suction and can be calculated for certain σ_{vm} values as;

$$\begin{cases} \alpha_i = -7\times10^{-7}\, s + 0.0024 & \text{For } \sigma_{vm} = 178 \text{ kPa} \\ \alpha_i = -4\times10^{-6}\, s + 0.0088 & \text{For } \sigma_{vm} = 222 \text{ kPa} \\ \alpha_i = -2\times10^{-6}\, s + 0.0060 & \text{For } \sigma_{vm} = 355 \text{ kPa} \\ \alpha_i = -7\times10^{-6}\, s + 0.0121 & \text{For } \sigma_{vm} = 444 \text{ kPa} \\ \alpha_i = -9\times10^{-6}\, s + 0.0150 & \text{For } \sigma_{vm} = 666 \text{ kPa} \end{cases} \quad 5.7$$

The obtained ranges of α_i values agree well with the observed ranges of C_α for MSL tests discussed in Sections 5.4 and 5.5. A similar creep law was also proposed by Priol et al. (2007) based on long-term creep tests on unsaturated chalk specimens. Indeed, more investigations and experimental results are required for validation of the proposed model.

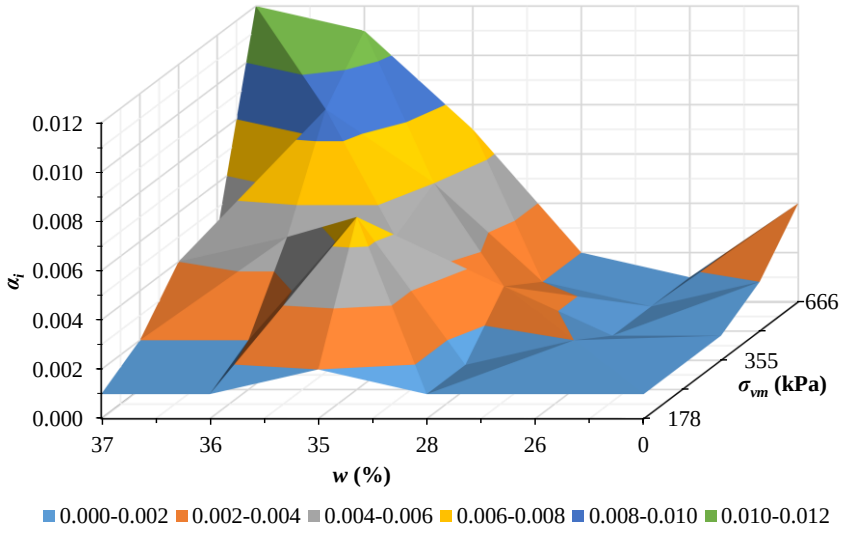


Figure 5.42 Variation of α_i with vertical stress and water content

5.12 Concluding Remarks

Results of a set of MSL and SSL oedometer tests performed on Sheppey London Clay specimens under different conditions of dry, saturated intact, saturated reconstituted, and unsaturated reconstituted were presented. The following conclusions can be drawn;

- The change in loading pattern, which was aimed at reducing the effects of sudden loading and subsequent damages to the soil structure during MSL tests,

does not have a notable influence on the obtained compression curves and the C_s and C_c values for intact specimens; however, it leads to lower $C_{\alpha e}/C_c$ values than the conventionally loaded specimens.

- Unlike soft clays that exhibit a sudden increase of C_c in the post yield region due to structural collapse, the process of destructuration in stiff clays appears to be continuous and follows an almost linear trend until reaching the peak value at stress levels in a range of (8-10) σ'_p.
- Unlike natural soft clays which typically exhibit higher creep than their corresponding reconstituted specimens, stiff clays such as London Clay, exhibit significantly less creep in comparison with their corresponding reconstituted specimens. This, on the one hand, can be attributed to the more compact nature of stiff clays (low initial void ratio), and on the other hand, to the low initial water content of the intact specimens.
- Generally, for Sheppey London Clay, increase in suction results in a decrease in the slope of compression curve (m'_c) and the $C_{\alpha e}$ values, and an increase in apparent preconsolidation pressure (σ'_p).
- According to the classification criterion defined by Mesri et al. (1994), Sheppey London Clay is categorised as shale or mudstone whose α value ranges from 0.02 to 0.04. The $\alpha = C_{\alpha e}/C_c$ ratio for Sheppey London Clay is stress- and suction-dependent, and therefore cannot be considered as a constant value. However, as a rough estimation, an average value of 0.03 ± 0.01 can be approximated for the α ratio of saturated and unsaturated reconstituted specimens.
- During SSL tests, at the same vertical stress level, decrease in initial water content (or increase in initial suction) results in a decrease in the rate and magnitude of volumetric creep strains. Moreover, at the same initial suction, increase in applied vertical stress leads to an increase in the volumetric creep strains.
- The volume change of unsaturated specimens during SSL tests appears to be predominantly controlled by the state of suction stress rather than the applied vertical stress.
- During long-term creep tests at constant water content, a decrease in soil suction monitored by HCTs can be attributed to an increase in S_r of the specimen with decrease in total volume during creep. If this holds true, long-term creep tests

where suction is artificially kept constant may not be ideal and the observed creep strains may not be solely attributed to the applied total vertical stress.

- The volumetric creep deformations of unsaturated stiff clays appear to be relatively simply modelled by a creep law based on a power function; $e/e_p = \beta t^{\alpha i}$.
- Further investigations and more test results over a wider range of soil suction and applied vertical stress levels are required to validate the presented hypotheses.

CHAPTER 6: RATE-DEPENDENCY IN UNSATURATED CONDITIONS

6.1 Introduction

This chapter presents the experimental program conducted for evaluation of rate-dependent behaviour of reconstituted London Clay under unsaturated conditions. Rate-dependency in 1D conditions is assessed based on a series of CRS oedometer tests performed in an innovative suction- and temperature-controlled CRS oedometer cell. A review of the multi-functional CRS oedometer cells reported in the literature, along with their advantages and disadvantages, are provided. Afterwards, the design characteristics of the new cell, its features and improvements, the calibration procedure, and the theoretical frameworks associated with the CRS compression and stress-relaxation tests are presented. Finally, the coupled and independent effects of strain-rate ($\dot{\varepsilon}_v$) and soil suction (s) on 1D stress-strain and stress relaxation behaviours including the effects of pre-relaxation strain, stress, and strain-rate under both saturated and unsaturated conditions are discussed.

6.2 Background of Multi-functional CRS Oedometer Cells

Several apparatuses have been so far devised and constructed for investigating rate-dependent behaviour of geo-materials under non-isothermal and/or unsaturated conditions. A suction- and temperature-controlled oedometer cell was developed by Romero et al. (1995) at the Technical University of Catalonia (UPC), Spain. In this apparatus, axial stress is imposed through an air-pressurised stretchable diaphragm. Temperature is applied and regulated using a thermostatically-controlled heater surrounding the cell, and suction is controlled using axis-translation technique. In order to rectify the drawback associated with the axis-translation technique, as discussed in Chapter 2, auxiliary devices such as vapour traps and diffused air flushing/volume indicator are incorporated into the system (Romero et al., 2003, Romero et al., 2005). Rampino et al. (1999) developed a suction-controlled oedometer cell for unsaturated soils at Università di Napoli Federico II, Italy. Their design was based on the modifications applied to the device initially designed by Wissa and Heiberg (1969). This apparatus allows for running all types of CL tests, i.e. CRS, CRL, and CG tests. Axial stress is applied directly through an air pressurised chamber connected to the

loading cap of the cell. This device, similar to the UPC oedometer, controls matric suction of the specimen using axis-translation technique and therefore is prone to the drawbacks associated with this method of suction control. Another drawback of this apparatus is related to the limitation of maximum air pressure supply in laboratory which restricts application of axial and suction stresses to 1 MPa. Tarantino and De Col (2008) performed static compaction tests on Kaolin clay specimens inside an oedometer cell modified to measure suction variations using two high-capacity tensiometers (HCTs) accommodated on its loading cap. In this oedometer, the axial stress is applied to the sample using a pneumatic actuator, hence allowing for CRL tests to be carried out. CRS test results on undisturbed unsaturated Bapaume loess specimens using a modified oedometer cell were reported by Munoz-Castelblanco et al. (2011). The oedometer cell was equipped with a HCT accommodated at the base of the specimen for direct measurement of soil suction evolutions during constant water content CRS tests carried out at rates of 0.003, 0.010, and 0.059 $\%min^{-1}$. Tarantino and De Col (2008) and Munoz-Castelblanco et al. (2011) concluded that CRS tests are preferred over the conventional IL tests for monitoring suction variations and that the conventional IL tests are better adapted for saturated specimens. Design of a suction- and temperature-controlled oedometer cell at the Ecole Polytechnique Fédérale de Lausanne (EPFL), Switzerland, was also reported by François and Laloui (2010). In this apparatus, the axial stress is applied through a water pressurised membrane made of a stretchable material. Heating is applied through circulating heated water in a ring-shaped chamber surrounding the specimen. Axis-translation is used as the suction control method in this device. The drawbacks of this apparatus can be outlined as; (1) use of stretchable membranes to transmit the vertical pressure to the specimen typically involves difficulties in calibration of membrane friction with the cell wall, (2) errors associated with membrane fatigue influences and modifies the mechanical loading transmitted to the specimen in long-term use, (3) the maximum applicable temperature to the specimen is restricted to the boiling temperature of water (~100º C), (4) the drawbacks of axis-translation technique, as explained above, can further influence the test results. A temperature-controlled CRS oedometer cell was also developed by Tsutsumi and Tanaka (2011) at Hokkaido University, Japan. A high accuracy stepper motor system is utilised in this device for loading the specimen under very small strain-rates. An external load cell placed at the bottom of the cell is used to measure the axial stress. The temperature of the specimen is controlled through circulation of an isothermal

liquid inside a metal pipe spiralled around the specimen. A thermocouple attached to the upper platen of the consolidation cell is used for measurement of temperature variations. The main drawbacks of this device can be expressed as; (1) the use of external load cell involves errors associated with the friction between the loading ram and the guide shaft, and (2) revolutions of the stepper motor were considered as the axial displacement rather than using a dial gauge. Indeed, this can disregard the effect of specimen non-homogeneity on the axial strains. Most recently, a temperature-controlled CRS oedometer cell was developed by Jarad et al. (2017) at Université de Lorraine, France. This cell is installed in a load frame capable of running strain-controlled tests in a range of 0.002 – 0.02 %min^{-1}. A temperature range of 5º C to 70º C could be applied to the specimen through circulation of a thermal liquid in a spiral tube positioned around the cell (similar to cell developed at Hokkaido University). The cell chamber is filled with water to ensure fully saturated conditions throughout the experiments.

6.3 The New CRS Oedometer Cell

The apparatus is a load frame based system where the loading is generally via feedback from a velocity-controlled loading piston. The loading frame has a maximum compressive strength of 50 kN and speed range of 10^{-5} – 10 mm/min for constant rate of displacement. The outer cell body was made of AISI 304 stainless steel whereas the inner cell and the confining ring were made of brass. The cell wall was designed to be thick enough to support the specimen and prevent lateral deformation, and hence satisfy the k_0 conditions. To minimise the disturbance to the specimen, the loading cap was made of a lightweight material i.e. aluminium. The specific design of the CRS oedometer cell enables performance of strain-controlled consolidation tests under both saturated (pore-water pressure control) and unsaturated (suction control) conditions. A 1.5 MPa high AEV porous disk placed at the bottom of the specimen allows for testing soil specimens under suction-controlled conditions. Matric suctions ($u_a - u_w$) of up to 0.7 MPa could be imposed using an axis-translation technique. Pore-air pressure, supplied from an air compressor and regulated by a pressure panel, was applied to the top of the specimen. The porous stone at the top of the specimen helps for uniform distribution of air pressure across the sample area. Pore-water pressure was controlled at the bottom of the specimen and regulated by an air-water interface (bladder) and a

pressure panel. A 3.5 MPa pore-water pressure transducer (PWPT) was used for measurement of positive u_w at the base of the specimen. Water volume exchanges were measured using a semi-automatic volume change apparatus looped with the bladder and the pressure panel. Furthermore, two HCTs accommodated over the periphery and at the mid height of the specimen were used for continuous measurement of matric suction during the experiments. In CRS tests, the generated u_{exc} varies from zero at the top to a maximum value at the base of the specimen. Accommodating HCTs over the periphery and at the mid-height of the specimen allows for measurement of an average u_{exc} during the tests. HCTs could be also used for local measurement of positive u_w inside the specimen. The specific assembly of the tensiometers inserts enables for replacement of the cavitated tensiometers during the experiments without any interruption to the tests and further disturbance of the specimen. A 25 mm travel length linear potentiometric transducer (LPT) placed on the top platen of the cell was used for measurement of axial strain and, therefore, volume change of the specimen. Axial force was measured by an internal 25 kN submersible load cell guided through a ball bearing shaft on the top platen of the cell. The use of internal load cells rectifies the adverse effect of friction on measurements typical of conventional external load cells. This improvement is highlighted during creep and stress-relaxation tests (Fodil et al., 1997). Cylindrical soil specimens of 95 mm diameter and 35 mm height can be tested in this apparatus. These dimensions are compatible with the minimum specimen diameter to thickness ratio of 2.5 recommended by ASTM standard for consolidation testing (ASTM-D4186-06, 2006). Figure 6.1 shows a schematic diagram of the cell structure and its components.

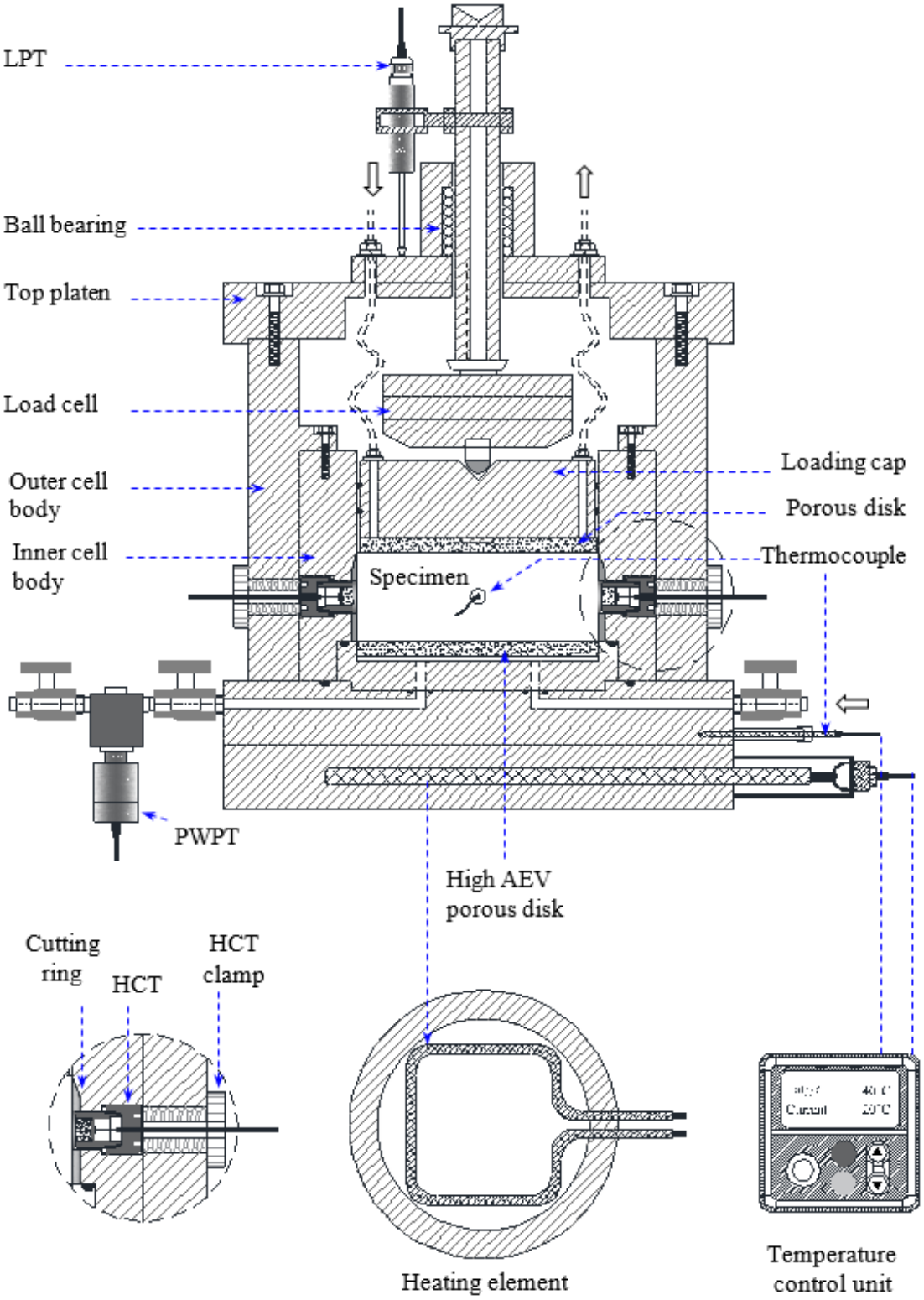


Figure 6.1 Schematic diagram of the CRS cell structure and components

The heating system consisted of a WATROD double-ended tubular heater element (supplied by Watlow Ltd), placed at the base of the cell, and two J-type thermocouples for measurement and monitoring of temperature variations on the cell's body and inside

the specimen. Temperature variations inside the specimen were measured by a thermocouple placed close to the specimen. Another thermocouple located close to the heater was used to record the cell temperature. The signal feedback from this thermocouple was used to keep the temperature constant by acting on the thermostat in the control unit. The heating system enables testing soil specimens over a temperature range of 20° C to 200° C. An isolating ring made of Tufnol material, was placed between the cell base and the loading piston's platen, to prevent any possible damages to the stepper motor as a result of heat transfer.

As explained in Chapter 2, using axis-translation technique for applying suction to the specimen, typically involves evaporation of soil water due to the application of air pressure. Generation of vapour fluxes causes unwanted variation of suction inside the specimen. This effect is further highlighted when testing unsaturated specimens under high temperatures. To restrict the vapour transfer, as suggested by François and Laloui (2010), a vapour trap was installed in the air pressure line to humidify the pressurised air and maintain a high order of relative humidity throughout the experiments. Moreover, as recommended by Romero et al. (2005), to control the air diffusion across the high AEV porous disk, a flushing system was incorporated at the base of the cell, to periodically flush the diffused air bubbles. The spiral circuit machined inside the pedestal and underneath the porous disk further helps in collection of the diffused air bubbles from the system (Rampino et al., 1999).

An 8 channel serial pad (GEODATALOG8 supplied from Controls Testing Equipment) was used for data acquisition from the transducers (load cell, LPT, and PWPT). The built-in data acquisition software enables for offline monitoring and storage of the data. The HCTs' measurements were also monitored using a NI data acquisition system and LabVIEW software as explained in Chapter 4. A LabVIEW code was also developed for monitoring the feedback data from the thermocouples. All the feedback data from the transducers and the temperature control unit were continually stored on a computer. The specific features of this cell enables precise and economical investigation of thermo-hydro-mechanical (THM) properties of soils over suction, temperature, and strain-rate ranges of practical interest. Figure 6.2 presents a layout of the whole testing system set up at the University of Warwick.

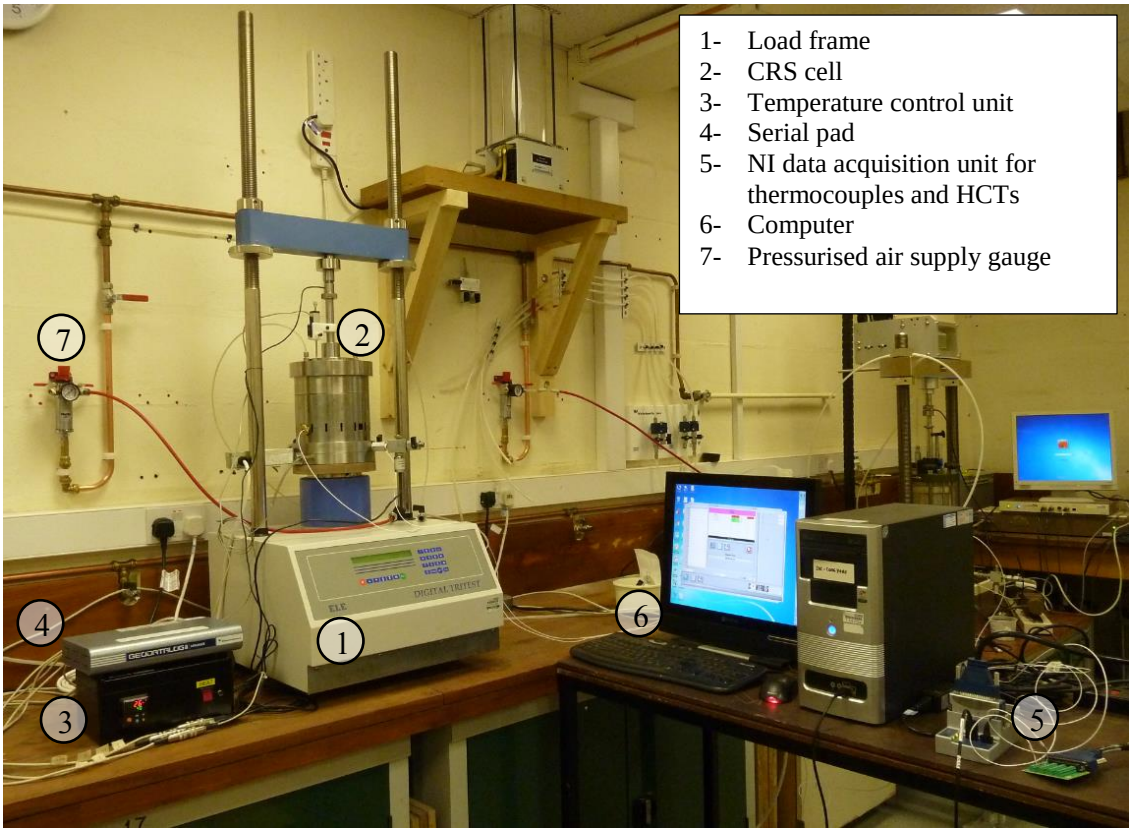


Figure 6.2 CRS system setup and components

6.3.1 Calibrations

6.3.1.1 Inner Wall Friction

Friction between the loading cap's O-ring and the internal wall of the cell as well as between the sample and the inner wall of the cutting ring, are the main sources of possible sidewall friction. In order to minimise the effect of sidewall friction on the measured forces several methodologies can be considered. Lubricating the O-rings on the loading cap as well as the internal cell body and the inner periphery of the cutting ring with a very thin layer of grease can, to some extent, reduce the sidewall friction (Seah and Juirnarongrit, 2003). Attention must be applied not to leave high amount of grease on the cutting ring's inner wall, as grease can influence the inter-particles friction within the soil specimen and modify the consolidation process. A friction correction curve can be obtained from running a set of friction calibration tests without specimens (Sample and Shakelford, 2012). Calibration curves can be used for modification of the compression data to ensure negligible or minimised friction effects. Sample (2007) performed a set of CRS consolidation tests on soil slurries containing bentonite and granular zero valent iron in acrylic columns and reported that increase in strain-rate will increase the induced friction between the top platen O-rings and the inner walls of the

test cells. The side friction from the confining ring has been shown to reduce the average effective stress in a 40 mm high clay specimen by 10-17 % of the applied total vertical stress at the top of the specimen (Lohani et al., 2001). In this study, since the side friction could not be measured, the loading cap's O-rings, the inner cell wall, and the inner wall of the cutting ring were lubricated with a very thin layer of grease in order to minimise this effect on the measurements.

6.3.1.2 Transducers

The external LPT was calibrated against slip gauges in a purpose built mount. The LPT was calibrated over its full range and to a resolution of 0.01 mm. The internal load cell was calibrated using a Testometric loading system with a resolution of 0.001 kN over its full working range (25 kN). Two cycles of loading and unloading were applied to ensure maximum accuracy of the obtained calibration parameters. The PWPT was calibrated in the saturated chamber presented in Chapter 4, and against the digital pressure gauge which was precisely calibrated using a Budenberg hydraulic dead-weight calibration system by the manufacturer. Similar to the load cell, the PWPT was also calibrated over two cycles of loading and unloading in order to obtain accurate calibration factors.

It must be mentioned here that, as the capacity of cell for conduction of temperature-controlled tests was not used in this study, the calibrations associated with non-isothermal conditions are not included in this section.

6.4 Theoretical Framework

6.4.1 Determination of Effective Stress and Void Ratio

The same procedure as described in Chapter 5, was followed for determination of void ratio and effective stress evolutions during the CRS tests. As all the tests were carried out on reconstituted specimens, e_0 was calculated based on Equation 5.2. Change in void ratio was determined based on the measurements of change in the height of the specimen (data from LPT) during 1D loading/unloading. The LPT measurements were also used for calculation of axial strain (ε_a). In saturated tests, the principle of effective stress ($\sigma'_v = \sigma_v - u_w$) was applied and the values of σ'_v were calculated based on the measurements of axial total stress (data from load cell) and pore-water pressure (data

from tensiometers). The experimental results of unsaturated CRS tests were evaluated based on the net normal stress ($\sigma_v - u_a$) to enable comparison of the obtained results with the oedometer tests results presented in Chapter 5. Since the tests were carried out at the atmospheric air pressure, the net normal stress was equal to the applied vertical total stress.

6.4.2 Determination of Compression and Stress-Relaxation Parameters

The compression index (C_c) was calculated as the slope of the normal compression line (NCL) of the compression curve plotted in e/e_0 – log σ'_v (or e/e_0 – log σ_v for unsaturated conditions) space. As suggested by Yin et al. (2014), the coefficient of relaxation (R_α) was defined as the slope of the plot of the vertical effective stress (applied vertical stress for unsaturated specimens) versus time in log σ'_v – log t (or log σ_v – log t for unsaturated conditions) space during relaxation of the stresses;

$$R_\alpha = -\frac{\Delta \log(\sigma'_v)}{\Delta \log(t)} \tag{6.1}$$

The following parameters were introduced by Wang et al. (2017) for interpretation of the stress-relaxation process in triaxial conditions;

$$\xi = \frac{\sigma_s}{\sigma_0} \tag{6.2}$$

where ξ is the residual stress ratio defined as the ratio of the residual deviatoric stress (σ_s) to the deviatoric stress just before the onset of relaxation stage (σ_0). In 1D CRS tests, the σ_s and σ_0 parameters are defined as the residual total vertical stress and the pre-relaxation total vertical stress respectively. The relaxed stress ($\Delta\sigma$) is defined as;

$$\Delta\sigma = \sigma_0 - \sigma_s \tag{6.3}$$

6.5 Experimental Program for CRS Tests

Drained CRS compression tests with continuous pore-water pressure (suction) monitoring were carried out on saturated and unsaturated reconstituted Sheppey London Clay specimens prepared following the procedure described in Chapter 3. All experiments were carried out on reconstituted specimens in order to eliminate the effect

of soil structure (mainly inter-particle bonding) on the test results and to identify only the coupled effects of suction and strain-rate. The new CRS oedometer system made it possible to perform multi-stage tests which included 1D compression tests;

- at a constant rate of strain to investigate the coupled effects of suction and strain-rate.
- with rest periods at intermediate stages with fixed axial strain to investigate the effects of suction, pre-relaxation strain, stress, and strain-rate on the stress-relaxation behaviour.

Based on the discussion presented in Chapter 2, Section 2.5.1.2., two different strain-rates of 4.8×10^{-7} s^{-1} and 2.4×10^{-6} s^{-1} were selected and used for this set of experiments. The values of strain-rates were selected so as to be; (1) compatible with the practical range of strain-rate suggested by Pereira and De Gennaro (2010), (2) fast enough to prevent development of structuration and resistance against loading with time, and (3) fast enough to allow for completion of the experiments within the project's time frame. Two types of tests were carried out; single-staged compression-relaxation tests (SS-CRS), and multi-staged compression-relaxation tests (MS-CRS). In the single-staged tests, the specimen was loaded in a single stage to a pre-specified stress level and then allowed for stress-relaxation, whereas in multi-staged tests, intermediate stress-relaxation stages were considered at pre-determined strain levels. The former set of experiments allow for investigation of suction and strain-rate effects on the compression and stress-relaxation processes, and the latter set of experiments allow for investigation of strain level, stress level, and strain-rate on the stress-relaxation process.

Before commencing each experiment, the preparation of the cell was carried out. The drainage lines and the pressure transducer block were de-aired by means of vacuum and filled with de-aired water. The lower and upper porous discs were also saturated. Functionality of all transducers were checked and the load cell, LPT, and PWPT were zeroed. The HCTs calibrations were checked and where necessary re-calibrated before the start of the tests. The prepared specimen in the cutting ring was then placed inside the cell chamber. The two HCTs, which were preconditioned according to the procedure described by Tarantino (2004), were then installed on the periphery of the specimen and gently clamped. Attention was given not to over-pressurise the HCT during fastening and to prevent the associated clamping errors as discussed in Chapter 4.

Ultimate contact between the HCT and the specimen was ensured by applying soil paste (see Chapter 4, Section 4.9.5) to the HCTs porous disk. The loading cap, with its lubricated O-rings, was then positioned on top of the specimen and the load cell together with the top platen were placed and fastened. The cell was set up on the load frame and an initial vertical stress of 10 kPa was applied to the specimen to eliminate any possible bedding effects. The HCTs were allowed to equilibrate for 2 – 3 hours. Axial load was applied to the specimen from the piston moving upwards at constant rate of displacement, compressing the specimen inside the confining ring.

6.6 CRS Tests Nomenclature

The nomenclature chosen for single-staged CRS oedometer tests is shown in Figure 6.3. The letters "r" represents reconstituted specimens, letters "s" and "u" indicate the saturated or unsaturated states, the number before dash indicates the initial water content, and the letters "A" and "B" after dash represent the applied strain-rates of 4.8×10^{-7} s^{-1} and 2.4×10^{-6} s^{-1} respectively. Note that the strain-rate B is 5 times greater than the strain-rate A. The multi-staged tests were distinguished by a letter "M" before the test ID.

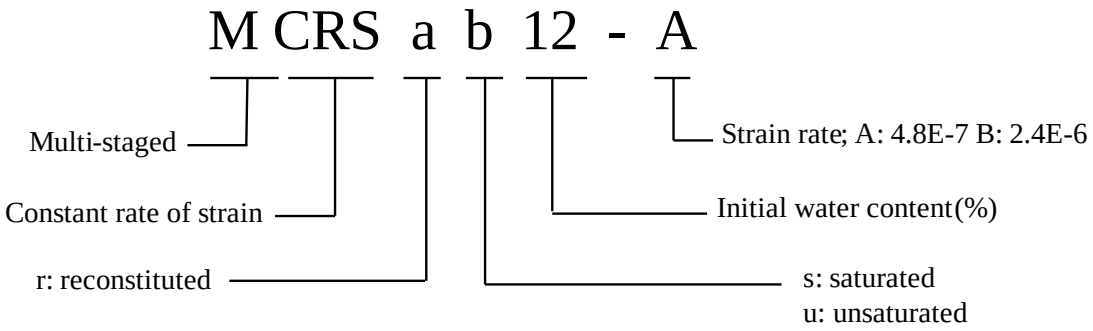


Figure 6.3 Nomenclature of the CRS oedometer tests

6.7 Single-Staged Compression–Relaxation Tests

6.7.1 Test Procedure

A set of 10 drained SS-CRS tests were carried out to investigate the effects of suction and strain-rate on the compression and relaxation responses of reconstituted Sheppey London Clay. Each test comprised of two stages; (1) loading the specimen at constant rate of displacement to the $\sigma_v \cong 3450$ kPa, and (2) stress-relaxation at zero rate of axial displacement for a period of at least 210 hours. The period of stress-relaxation will be

denoted by t_R. All tests were performed in a temperature-controlled laboratory environment to avoid the influence of temperature fluctuations on the output data. The selected strain-rates were both too fast to allow fully drained conditions. Excess pore-water pressure (u_{exc}) was, therefore, built up during the loading stage. Hence, after commencement of the relaxation stage, a combined effect of u_{exc} dissipation and stress relaxation was observed. The values of PPR_{max} were found to be within a range of 1 – 9%, complying well with the suggested PPR_{max} range of 3 – 15% by ASTM-D4186-06 (2006). Table 6.1 summarises the details of the SS-CRS tests.

Table 6.1 Details of the compression stage of the SS-CRS tests

Test ID	w_0 [%]	s_0 [kPa]	$\dot{\varepsilon}_v$ [s^{-1}]	PPR_{max} [%]	σ'_p [kPa]	σ_0 [kPa]	HCTs
CRSrs39-A	39	0	4.8×10^{-7}	4.9	157	3451	WT5 & WT6
CRSru33-A	33	701	4.8×10^{-7}	2.9	436	3080	WT5 & WT6
CRSru32-A	32	802	4.8×10^{-7}	9.0	539	3440	WT5 & WT6
CRSru30-A	30	1045	4.8×10^{-7}	8.0	676	3448	WT5 & WT6
CRSru26-A	26	1905	4.8×10^{-7}	1.1	1493	3459	WT11 & WT12
CRSrs43-B	43	0	2.4×10^{-6}	8.5	108	3435	WT9 & WT10
CRSrs39-B	39	0	2.4×10^{-6}	6.0	227	3450	WT11 & WT12
CRSru36-B	36	433	2.4×10^{-6}	4.9	288	3445	WT11 & WT12
CRSru33-B	33	701	2.4×10^{-6}	3.4	655	3297	WT11 & WT12
CRSru26-B	26	1905	2.4×10^{-6}	1.4	1551	3452	WT11 & WT12

6.7.2 Test Results

Figure 6.4 illustrates the results of CRS tests. The compression curves are shown in terms of axial strain (ε_a) against vertical total stress (σ_v). Also shown in the graphs, are the change in pore-water pressure ($\Delta u = u_w - u_{exc}$) with vertical total stress (dotted lines). It must be mentioned here that the specimens with w_0 = 26% possessed a suction value of about 1905 kPa, a value which was beyond the nominal capacity of the HCTs. The improved HCTs (i.e. WT11 and WT12) were used for monitoring suction evolutions in these specimens. However, due to the time-dependent nature of the experiments, occasional interruptions in continuous suction measurements were occurred due to the cavitation of the HCTs. The discontinuous measurements were, therefore, extrapolated to obtain a complete trend. Moreover, as the pore-water pressure (suction) measurements recorded by the two HCTs installed on each specimen were very similar, only measurements from one of the HCTs are presented in the graphs. For sake of simplicity, the yield stress, also known as "apparent" preconsolidation pressure (σ'_p), was determined as the intersection of the best fitted lines to the pseudo-elastic and

plastic sections of the compression curve. Other graphical methods are also available for determination of the gross yield stress, though it is believed that different methods provide different values (Munoz-Castelblanco et al., 2011).

Inspection of the results reveals the suction-dependency of the stress–strain behaviour during 1D compression. As can be seen, the overall compressibility of the specimens decreases with increase in suction and strain-rate. Moreover, increase in suction resulted in an increase in σ'_p values for both sets of experiments carried out at different strain-rates. The values of σ'_p vary with strain-rates at the strain level of 2 – 3%. Slope of the normal consolidation lines (NCLs) for both sets of tests were found to be suction-dependent and decrease with increase in suction, within the range of applied vertical stresses. This effect was more pronounced for higher strain-rate tests. This finding agrees well with the results from MSL tests on unsaturated reconstituted specimens presented in Chapter 5, Figure 5.24. Furthermore, by extrapolating the compression curves to higher stress levels (>3.5 MPa), it is anticipated that the slope of NCLs will eventually converge at a constant value corresponding to that of saturated specimen, as suggested by Zhou et al. (2012), and discussed in Chapter 5, Section 5.5.2.1. The stress-strain behaviour appears therefore to follow the Isotach concept.

Similar to MSL oedometer tests presented in Chapter 5, a suction state was preserved during the compression stage, confirming that no water has been expelled from the unsaturated specimens, and hence, the condition of constant water content was recognised. Inspecting the variation of u_{exc} with σ'_v reveals that the higher the strain-rate, the higher the generated u_{exc}. The rate of change of Δu was also found to decrease with increase in suction.

As suggested by Head (1992), the break in the curves of excess pore-water pressure versus logarithm of effective stress can be used for estimation of σ'_p. This method, however, appears to be unenforceable for the specific conditions of the carried out experiments in this study (i.e. the unsaturated condition), as generally, an overestimation of the σ'_p values were obtained from the graphs of u_{exc} – log σ'_v.

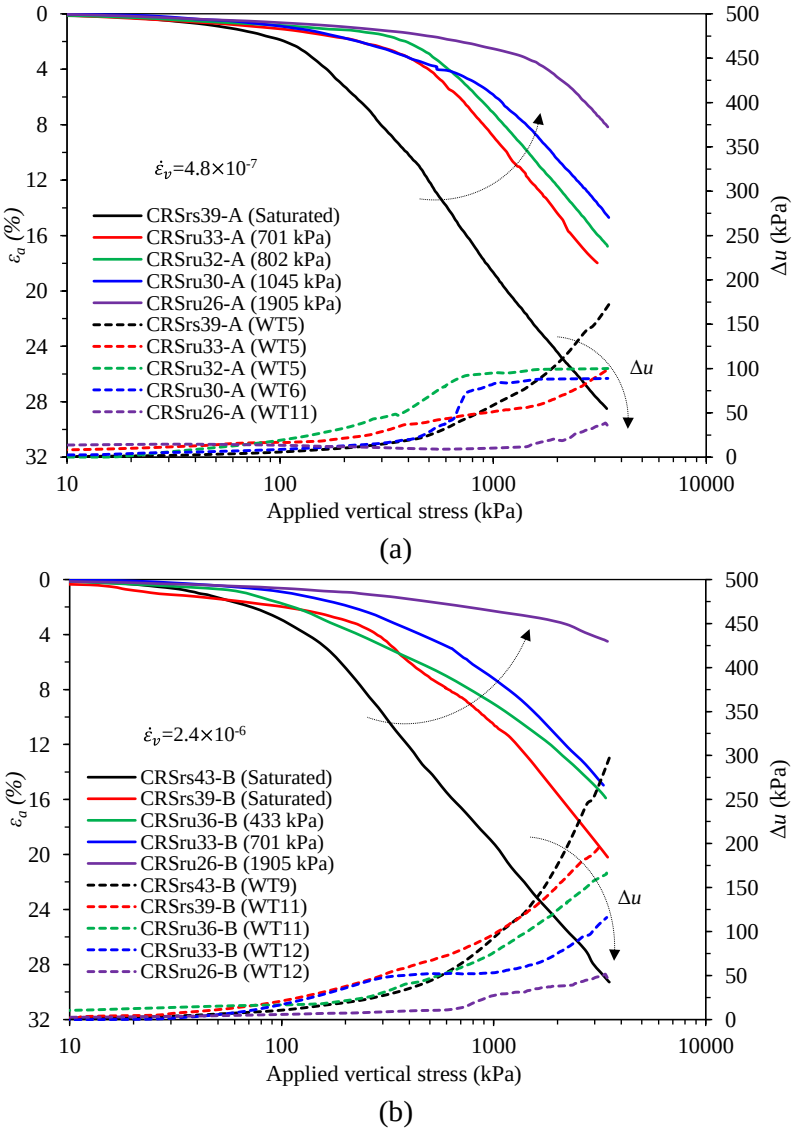
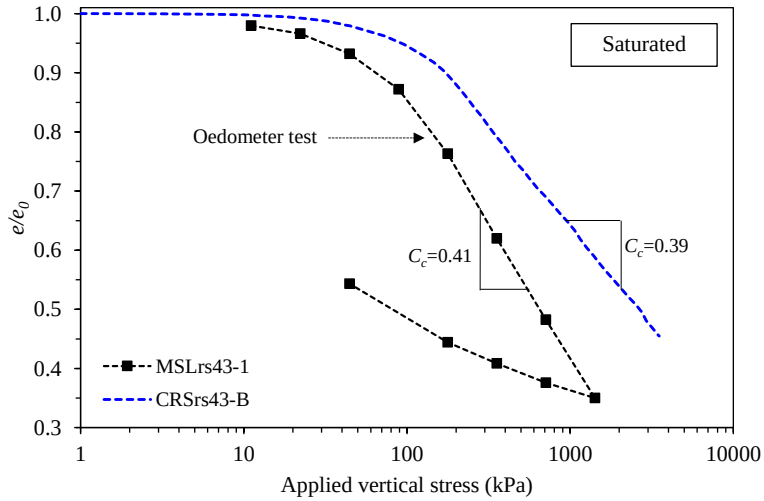


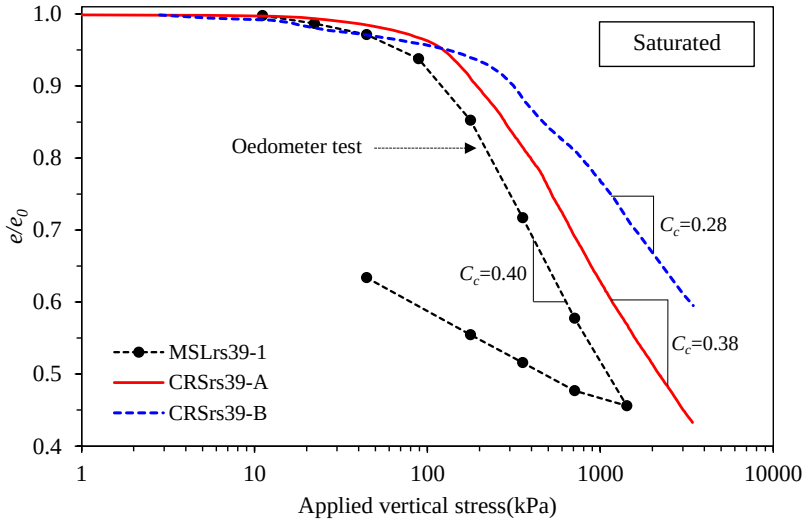
Figure 6.4 CRS compression curves for reconstituted Sheppey London Clay at different suction levels and strain rates of: (a) 4.8×10^{-7} s^{-1}; (b) 2.4×10^{-6} s^{-1}

6.7.2.1 MSL Oedometer Tests vs. CRS Tests

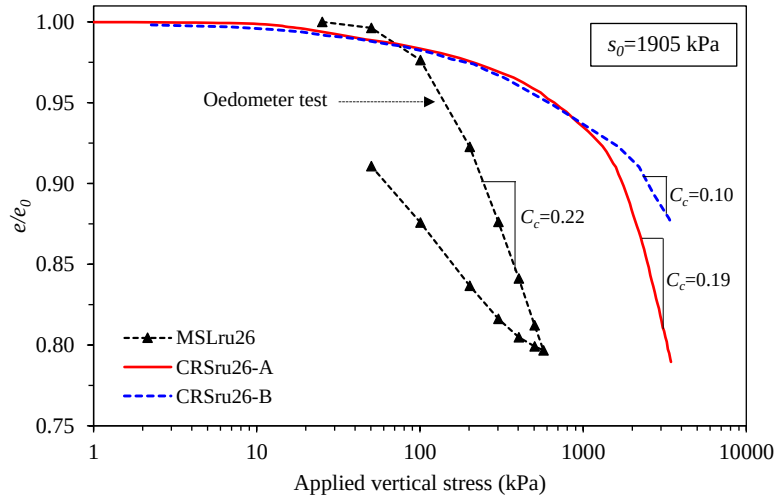
Figure 6.5 presents a comparison of the compression curves obtained from CRS and MSL oedometer tests in e/e_0 – log σ_v space for specimens with w_0 of 43, 39, and 26%. It was observed that the compression curves from CRS tests were shifted to the right, exhibiting higher σ'_p than the MSL tests. Moreover, it was observed that at a given void ratio, the higher the strain-rate the higher the vertical stress. This behaviour was more pronounced for the unsaturated specimen [Figure 6.5(c)], indicating the coupled effects of suction and strain-rate on compression response, with suction playing a more significant role than strain-rate. At a constant suction and within the range of applied vertical stresses, a decrease in the slope of NCL was observed with increase in $\dot{\varepsilon}_v$.



(a)



(b)



(c)

Figure 6.5 Comparison of compression curves obtained from CRS and MSL tests on specimens with initial water contents of: (a) 43%; (b) 39%; (c) 26%.

Figure 6.6 presents the variation of σ'_p with suction for both MSL and CRS tests. It was observed that at a constant suction, the higher the strain-rate, the higher the σ'_p. Similarly, at a constant strain-rate, the higher the suction, the higher the σ'_p. Moreover, increase in σ'_p with suction appears to follow an approximately linear trend for fast, slow, and oedometric strain-rates. An average value of 1.3 has been reported in the literature for the ratio of σ'_p obtained from CRS and MSL tests ($\sigma'_{pCRS}/\sigma'_{pMSL}$) on saturated soft clays for strain-rates in a range of 0.36 to 1.44 %/hr (Leroueil et al., 1983b, Hanzawa et al., 1990, Nash et al., 1992, Cheng and Yin, 2005). The $\sigma'_{pCRS}/\sigma'_{pMSL}$ ratio for specimens with w_0 = 0.39 (saturated) was calculated as 1.29 which is very close to the average value reported for soft clays in abovementioned studies. This ratio might be, therefore, considered as a function of the loading mode rather than the sample type (intact or reconstituted).

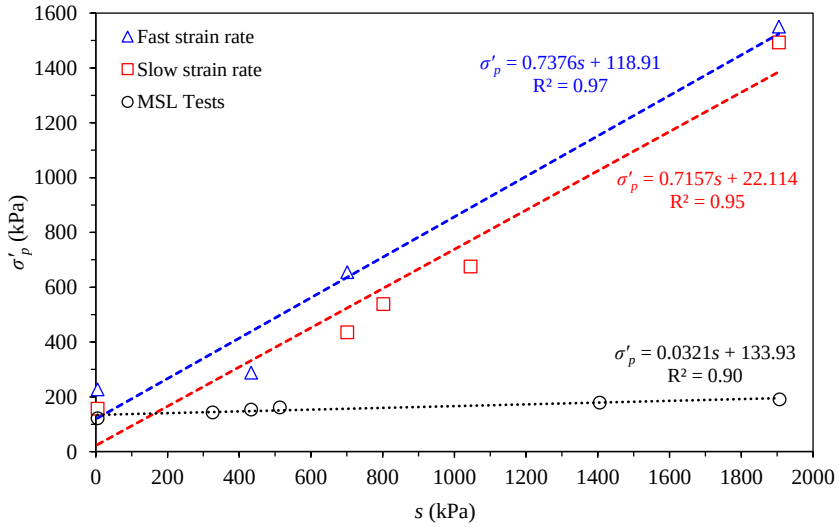


Figure 6.6 Variation of σ'_p with suction for fast, slow, and oedometric strain-rates.

6.7.2.2 Effect of Suction and Strain-Rate on Stress-Relaxation Process

As mentioned earlier, the stress-relaxation process was initiated right after the test specimens, loaded at different strain-rates of A and B = 5A, reached a maximum vertical stress of $\sigma_0 \cong$ 3450 kPa. The gradual decrease of stresses with time were recorded and used for evaluation of the effects of pre-relaxation strain-rate, relaxation time (t_R), and suction state, on the stress-relaxation process. Monitoring pore-water pressure evolutions during the course of stress-relaxation for CRSru26-A and CRSru26-B, having initial suctions of approximately 1905 kPa, was interrupted due to the cavitation of the HCTs. Due to the sensitivity of the stress-relaxation stage, no attempt was made

to replace the cavitated HCTs, and hence, the suction measurements are not available for these two experiments. The final values of soil suction were, however, measured at the end of the tests. Table 6.2 summarises the characterisation parameters. In order to provide a platform for comparison, the values of σ_s corresponding to t_R = 210 hours were used for calculation of the relaxation parameters $\Delta\sigma$, ξ, and R_α.

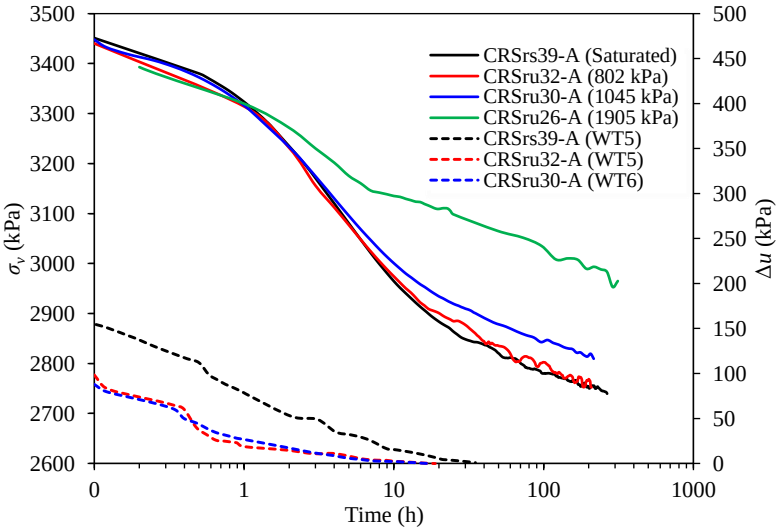
Table 6.2 Characterisation parameters for stress-relaxation stage of the SS-CRS tests

Test ID	s_0 [kPa]	$\dot{\varepsilon}_v$ [s^{-1}]	σ_0 [kPa]	σ_s [kPa]	$\Delta\sigma$ [kPa]	$\Delta\sigma/\sigma_0$ [%]	ξ	R_α	t_R [h]
CRSrs39-A	0	4.8×10^{-7}	3451	2743	711	21	0.79	0.019	266
CRSru32-A	802	4.8×10^{-7}	3440	2752	688	20	0.80	0.019	210
CRSru30-A	1045	4.8×10^{-7}	3448	2809	639	19	0.81	0.018	216
CRSru26-A	1905	4.8×10^{-7}	3459	2989	494	14	0.86	0.011	313
CRSrs43-B	0	2.4×10^{-6}	3435	2630	805	23	0.77	0.029	215
CRSru36-B	433	2.4×10^{-6}	3445	2674	771	22	0.78	0.017	215
CRSru26-B	1905	2.4×10^{-6}	3452	2823	629	18	0.82	0.017	213

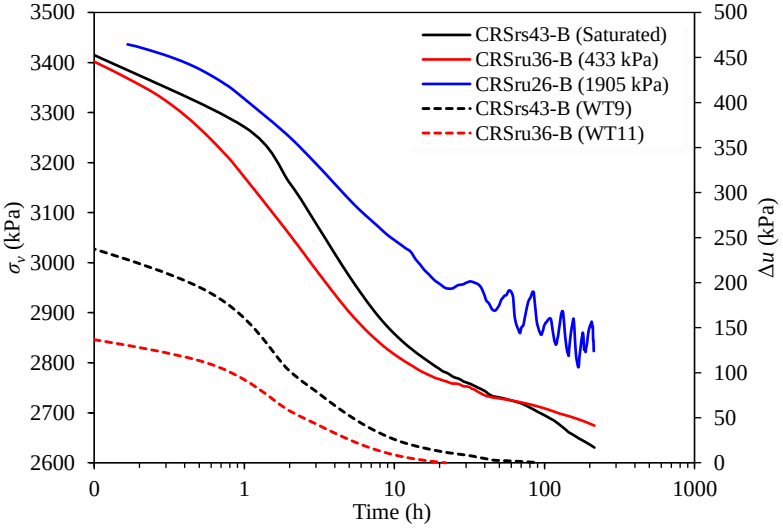
Considering the values of relaxation parameters given in Table 6.2, it was found that, at constant pre-relaxation stress (σ_0), increase in suction resulted in a decrease in the relaxed stresses ($\Delta\sigma$) and consequently an increase in stress-relaxation ratio (ξ). In other words, with increase in suction from 0 to 1905 kPa, the ratio $\Delta\sigma/\sigma_0$ was reduced from 21 to 14% for specimens loaded at the slow strain-rate (A), and from 23 to 18% for specimens loaded at the fast strain-rate (B). Effect of suction in reduction of relaxed stresses appears to be reasonable, considering the stress-relaxation mechanism as a time-dependent process of particles re-adjustment and gradual change in the structural configuration of grains, as discussed in Chapter 2, Section 2.6.1. In essence, the additional bonding forces exerted by the under-tension water menisci developed at the inter-particle contacts, can prevent re-arrangement of particles, and hence, release of stresses accumulated during the loading stage.

Figure 6.7 presents the relaxation of vertical stress with time in a semi-log plot. Also shown in the graphs, are the plots of dissipation of u_{exc} with time during the stress-relaxation stage. The process of stress-relaxation appears to involve three phases of; (1) fast relaxation, (2) decelerating relaxation, and (3) residual relaxation as schematically shown in Figure 6.8. The fast relaxation phase is associated with a quick release of the main accumulated energy inside the specimen, whereas the deceleration and residual phases correspond to the time-dependent particles re-arrangement which involve further dissipation of energy with time. At a constant strain-rate, suction appears to have

more influence on the stress-relaxation process during fast and deceleration phases. In fact, the higher the suction, the lower would be the rate of relaxation during fast and decelerating relaxation phases. Similarly, at a constant suction, the higher the pre-relaxation strain-rate, the higher would be the rate and magnitude of the relaxed stresses as shown in Figure 6.9 for CRSru26-A and CRSru26-B specimens (see also Table 6.2 for corresponding relaxation parameters). Similar observations were reported by Wang et al. (2017) from the results of triaxial stress-relaxation tests on unsaturated lime-treated expansive clay specimens. Indeed, more test results over a wider range of suctions and strain-rates are required for adequately characterisation of the pre-relaxation strain-rate effect on the stress relaxation process in unsaturated stiff clays such as London Clay.



(a)



(b)

Figure 6.7 Stress-relaxation and associated pore-water pressure dissipation in 1D CRS oedometer tests on reconstituted Sheppey London Clay at: (a) 4.8×10^{-7} s^{-1}; (b) 2.4×10^{-6} s^{-1}

It must be noted that, except for the saturated specimens where a slight drainage of water was observed, the processes of u_{exc} dissipation did not involve any significant volume change, given the preservation of suction state in the unsaturated specimens. Effect of pore-water dissipation during relaxation stage of 1D CRS tests on saturated reconstituted London Clay was also reported by Sorensen (2006). Moreover, the fluctuation of results for the residual relaxation phase of some of the tests were due to the occasional failure in the temperature control unit of the laboratory.

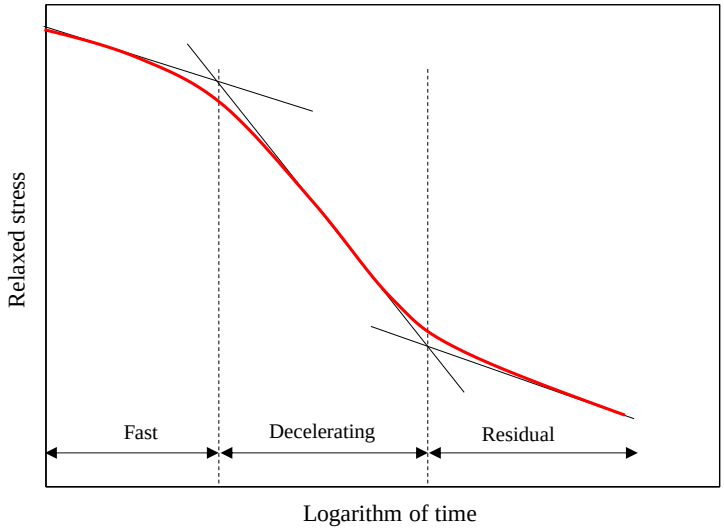


Figure 6.8 Stress-relaxation phases

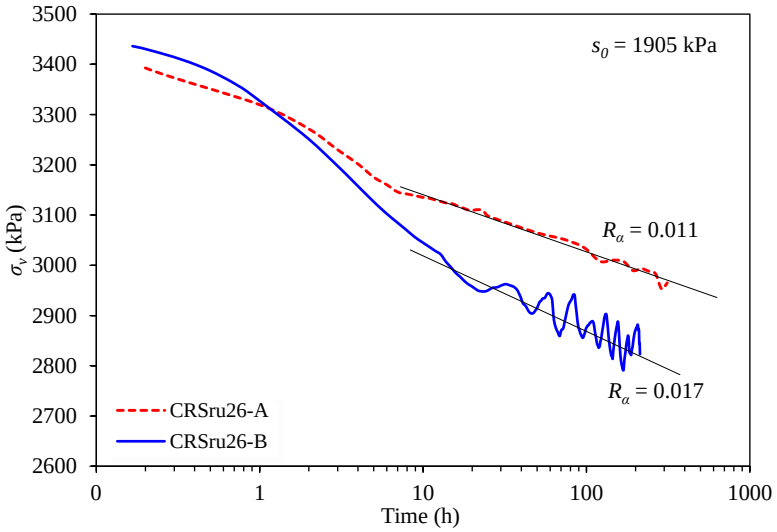


Figure 6.9 Effect of strain-rate on the stress-relaxation response

Figure 6.10 presents the variation of relaxation coefficient (R_α) with suction for fast and slow strain-rates. Although there is a clear difference between the R_α values corresponding to saturated (s = 0) and unsaturated (e.g. s = 1905 kPa) states, with the

limited number of data points it is hard to comment on the relationship between R_α and suction. For the slow and fast strain-rates, the values of R_α fall within a range of 0.011 – 0.019 and 0.017 – 0.029 respectively. As suggested by Yin et al. (2014), and noted in Chapter 2, Section 2.6.1.2, the values of R_α are equal to the values of $\alpha = C_{\alpha e}/C_c$ ratio and can be used for estimation of creep and compression indices. As it was shown in Chapter 5, the values of α were also suction- and stress-dependent (see Figure 5.27) and found to fall within a range of 0.023 – 0.030 for MSL tests on unsaturated reconstituted specimens. This range, with a good approximation, complies with the R_α range of 0.017 – 0.029 obtained from fast strain-rate tests, hence, validating the applicability of $R_\alpha = \alpha$ for saturated and unsaturated reconstituted London Clay specimens tested in this study.

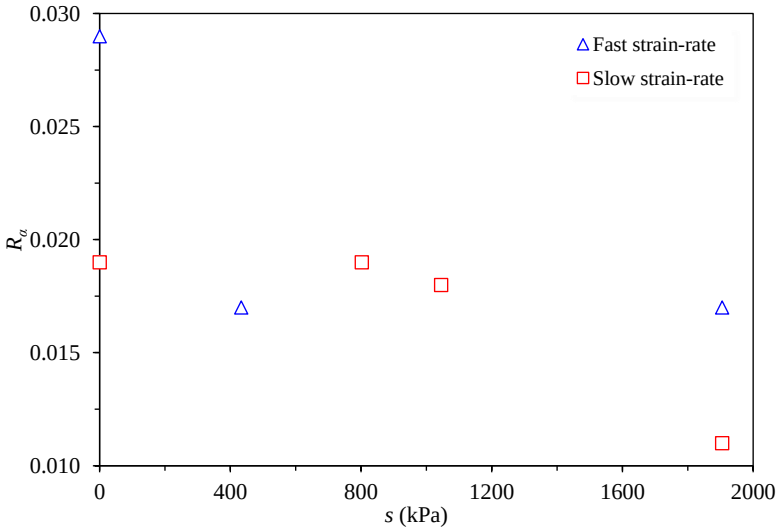


Figure 6.10 Variation of relaxation coefficient (R_α) with suction

6.8 Multi-Staged Compression–Relaxation Tests

6.8.1 Test Procedure

In order to investigate the effect of pre-relaxation strain level (ε_R), a set of two MS-CRS tests were carried out on unsaturated reconstituted specimens, having an initial suction of ~701 kPa (w_0 = 33%). The test procedure involved loading the specimens at a constant rate of displacement with stress-relaxation stages of 24 hours duration set at different strain levels as summarised in Table 6.3.

Table 6.3 Details of MCRS tests

Test ID	w_0 [%]	s_0 [kPa]	$\dot{\varepsilon}_v$ [s^{-1}]	ε_R [%]	HCTs
MCRSru33-A	33	701	4.8×10^{-7}	5, 10, 15, 18	WT9 & WT10
MCRSru33-B	33	701	2.4×10^{-6}	5, 10, 15, 17	WT9 & WT10

6.8.2 Test Results

Figure 6.11 illustrates the variations of σ_v with time during MS-CRS tests. Also shown in the graphs, are the change in pore-water pressure ($\Delta u = u_w - u_{exc}$) with time (dotted lines). The developed u_{exc} during the loading stages were generally dissipated during the first 6 – 8 hours of the consequent stress-relaxation stages. The characterisation parameters for stress-relaxation stages are summarised in Table 6.4. In order to provide a platform for comparison, the values of σ_s corresponding to t_R = 24 hours were used for calculation of the relaxation parameters $\Delta\sigma$, ξ, and R_α.

Table 6.4 Characterisation parameters for stress-relaxation stage of the MS-CRS tests

Test ID	ε_R [%]	σ_0 [kPa]	σ_s [kPa]	$\Delta\sigma$ [kPa]	$\Delta\sigma/\sigma_0$ [%]	ξ	R_α	t_R [h]
MCRSru33-A	5	581	459	122	21	0.79	0.011	24
	10	1192	910	282	24	0.76	0.022	24
	15	2172	1705	467	22	0.78	0.025	24
	18	3213	2574 (2510)	639 (703)	20 (22)	0.80	0.027	24 (78)
MCRSru33-B	5	630	359	271	43	0.57	0.025	19
	10	1639	688 (682)	951 (957)	58 (58)	0.42	0.026	24 (33)
	15	3047	1381	1666	55	0.45	0.028	24
	17	3248	1833 (1731)	1415 (1517)	44 (47)	0.56	0.035	24 (452)

The values of relaxed stresses ($\Delta\sigma$) were found to increase with increase in the pre-relaxation strain (ε_R) for the specimen loaded at the slow strain-rate. However, the values of $\Delta\sigma/\sigma_0$ ratio increased from 21 to 24% for an increase in ε_R from 5 to 10%, then decreased to 22 and 20% respectively for pre-relaxation strains of 15 and 18%. Similarly, for the specimen loaded at the fast strain-rate, the values of $\Delta\sigma$ were found to increase with increase in the pre-relaxation strain up to 15% at which it was decreased to a lower value at ε_R = 17%. The values of $\Delta\sigma/\sigma_0$ ratio increased from 43 to 58% for an increase in ε_R from 5 to 10%, then decreased to 55 and 44% respectively for pre-relaxation strains of 15 and 17%. Overall, larger relaxed stresses were observed with increase in pre-relaxation strains (and consequently pre-relaxation stresses). Moreover, an increase in the pre-relaxation strain-rate by a factor of 5, was found to significantly affect the magnitude of relaxed stresses at each pre-relaxation strain level, resulting in an increase of the $\Delta\sigma$ values by a factor of 2.2 – 3.6.

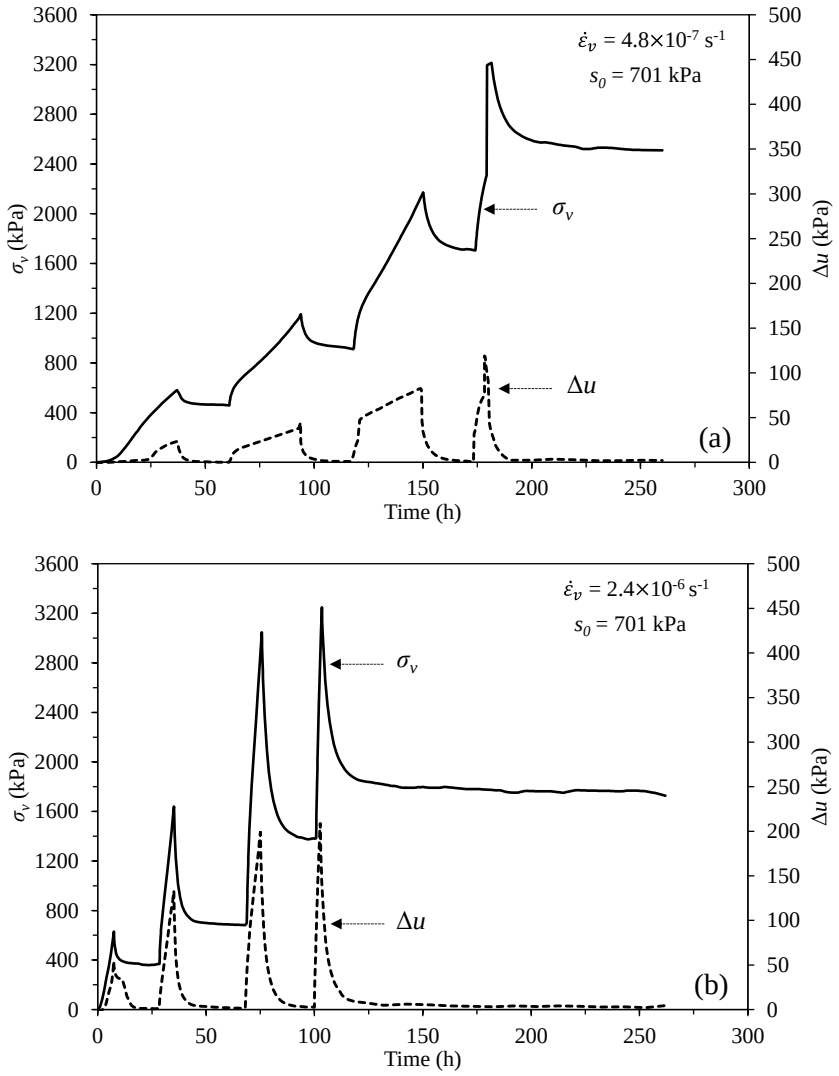
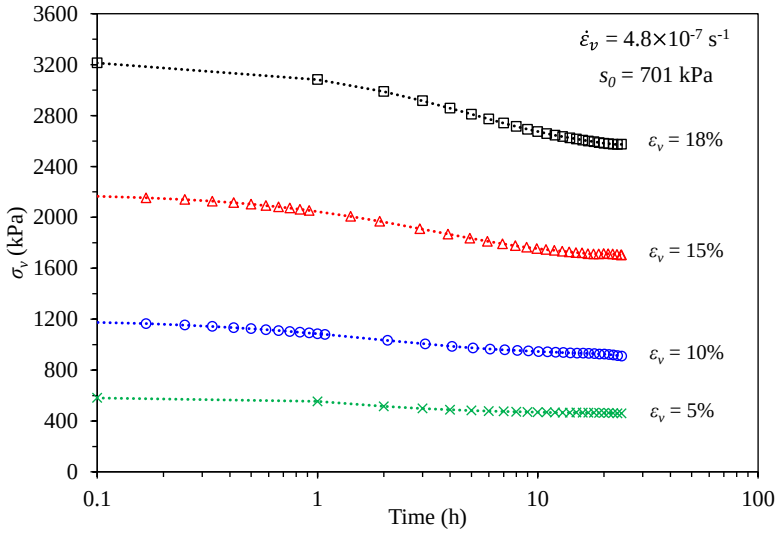
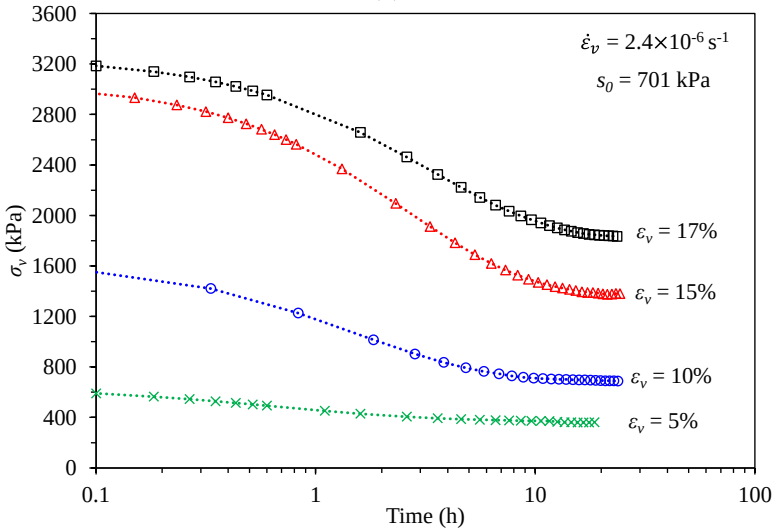


Figure 6.11 Variation of σ_v and Δu with time during multi-staged CRS tests: (a) MCRSru33-A; (b) MCRSru33-B

Figure 6.12 presents the variations of relaxed stresses with time in a semi-log scale. Higher stress-relaxation rates were observed for higher pre-relaxation strains. By plotting the experimental results in a log-log scale, a linear relationship between the vertical total stress and time was observed during relaxation of the stresses and after dissipation of u_{exc} (Figure 6.13). Similar results have been reported in the literature for saturated soft clays (e.g. Yin and Graham, 1989, Kim and Leroueil, 2001, Yin et al., 2014), as discussed in Chapter 2.



(a)



(b)

Figure 6.12 Relaxation of stresses with time at different pre-relaxation strain levels in semi-log scale

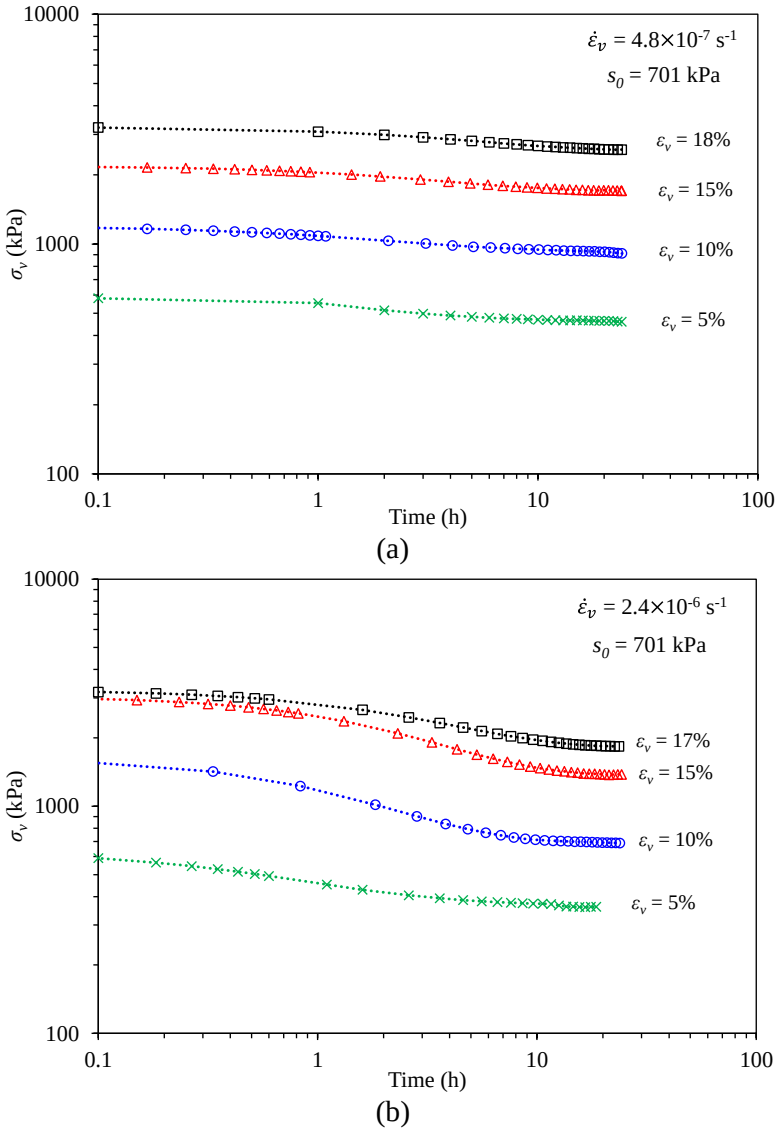


Figure 6.13 Relaxation of stresses with time at different pre-relaxation strain levels in log-log scale

As shown in Table 6.4, with change in ε_R, values of R_α vary within the ranges of 0.011 – 0.027 and 0.025 – 0.035 respectively for slow and fast pre-relaxation strain-rates (Figure 6.14), indicating dependency of the relaxation coefficient to the pre-relaxation strain (or stress) and strain-rate. The observed ranges of R_α for the 24 hours relaxation stages of MS-CRS tests were, however, higher than the ranges obtained from SS-CRS tests with minimum of 210 hours relaxation duration. In essence, the higher calculated R_α values for MS-CRS tests appear to correspond to the decelerating relaxation phase, characterised with higher relaxation rate, whereas the R_α values for SS-CRS tests correspond to the residual relaxation phase, characterised with lower relaxation rate. Larger relaxation periods are, therefore, required for better estimation of relaxation

coefficient, and hence, more accurate determination of time-dependent parameters based on $R_\alpha = C_\alpha/C_c$ relationship.

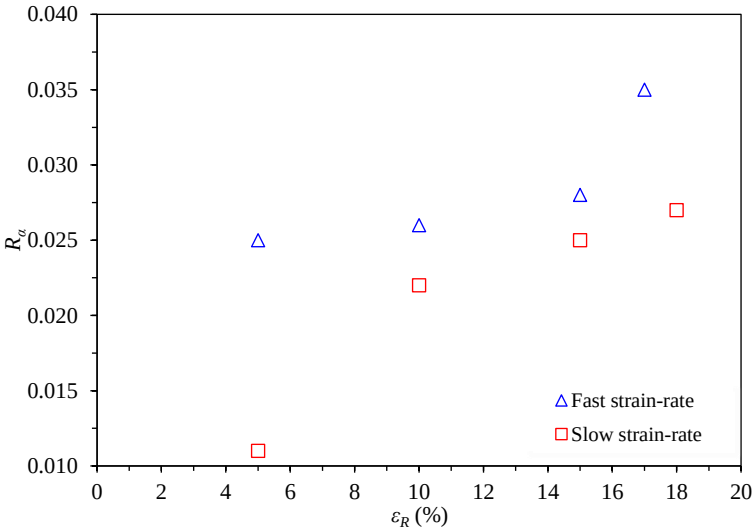


Figure 6.14 Variation of R_α with pre-relaxation strain level and pre-relaxation strain-rate

6.9 Concluding Remarks

In this chapter, design and calibration of a new multi-functional CRS oedometer cell for testing clays under unsaturated and non-isothermal conditions, was presented. Moreover, results of a set of SS-CRS and MS-CRS oedometer performed on reconstituted Sheppey London Clay specimens under saturated and unsaturated conditions and varied strain-rates were presented. The following conclusions can be drawn;

- The rate-dependent behaviour of clays can be conveniently studied from 1D CRS oedometer tests. The selected strain-rates for CRS tests on unsaturated specimens, having a suction range of 433 – 1905 kPa, appear to be appropriate and allow for preservation of a suction state inside the specimen, and hence, conduction of constant water content tests.
- Increase in strain-rate results in an increase in σ'_p and decrease in C_c values. Similar effects were also observed with increase in suction.
- Compression curves from CRS tests exhibit higher σ'_p than the MSL tests. Moreover, at a given void ratio, the higher the strain-rate the higher would be the vertical stress.

- Suction and strain-rate impose a coupled effect on the compression response. At a constant suction, the higher the strain-rate, the higher the σ'_p. Similarly, at a constant strain-rate, the higher the suction, the higher the σ'_p.
- Increase in σ'_p with suction appears to follow an approximately linear trend for fast, slow, and oedometric strain-rates.
- At high stress levels, the unsaturated compression curves become parallel, and the stress-strain behaviour appears to follow the Isotach concept.
- The process of stress-relaxation appears to consist of three phases; (1) fast relaxation, (2) decelerating relaxation, and (3) residual relaxation.
- At a constant pre-relaxation stress (σ_0), increase in suction results in a decrease in the rate of stress-relaxation during fast and decelerating relaxation phases, as well as in the magnitude of the overall relaxed stresses ($\Delta\sigma$).
- At a constant suction, the higher the pre-relaxation strain-rate, the higher would be the rate and magnitude of the relaxed stresses which is in agreement with the observations reported by Wang et al. (2017).
- Although there is a clear difference between the values of relaxation coefficient (R_α) corresponding to saturated ($s = 0$) and unsaturated (e.g. $s = 1905$ kPa) states, it is hard to comment on the relationship between R_α and suction based on the limited available data points.
- The $R_\alpha = C_{\alpha e}/C_c$, suggested by Yin et al. (2014) for saturated soft clays, appears, with an approximation, to be valid for unsaturated reconstituted London Clay in the range of applied vertical stresses and soil suctions in this study.
- A higher rate and magnitude of relaxed stresses were observed with increase in pre-relaxation strains (and consequently pre-relaxation stresses).
- At a constant strain level and suction, an increase in the $\Delta\sigma$ values by a factor of 2.2 – 3.6 was observed with an increase in the pre-relaxation strain-rate by a factor of 5. At the same strain level, increase in pre-relaxation strain-rate also results in an increase in R_α values under constant suction.

CHAPTER 7: CONCLUSIONS AND RECOMMENDATIONS

7.1 Conclusions

The key objectives of the present thesis, as outlined in the introduction chapter, were:

a) To examine the influence of soil suction on the primary and secondary consolidation of natural and reconstituted London Clay.
b) To examine the coupled effects of suction and strain-rate on one-dimensional compression characteristics of the reconstituted London Clay.
c) To characterise the stress-relaxation behaviour of the reconstituted London Clay subjected to suction and strain-rate variations.

Based on the literature review presented in Chapter 2, a significant gap of knowledge with regards to the time- and rate-dependent behaviour of unsaturated clays was identified. The fact that the published experimental programs in this context are scarce may be attributed to the time consuming nature of the experiments, sophisticated sample preparation and test procedures, and the high costs of the required testing equipment. Accordingly, one of the main strategies of this research was to develop advanced and cost-efficient equipment, as well as an optimised experimental plan in order to fulfil the research objectives. To this end, decisions were made to design and construct high-capacity tensiometers with enhanced performance for monitoring soil suction evolutions with time during long-term oedometer tests. Furthermore, a set of three unsaturated oedometer cells were designed and constructed that allow for performing constant water content consolidation tests with monitoring suction evolutions. Moreover, in order to study the coupled effects of suction and strain-rate on the rate-dependent response of unsaturated clays, an advanced suction- and temperature-controlled constant-rate-of-strain oedometer cell was designed and manufactured. Finally, a comprehensive experimental plan was developed for characterisation of the viscous response of natural and reconstituted Sheppey London Clay which mainly consisted of MSL oedometer tests, SSL oedometer creep tests, and CRS compression and relaxation tests. The findings of this research program will be discussed in the following.

7.1.1 Experimental Developments

7.1.1.1 The New HCT

With the aim to improve the performance of the new HCT in terms of maximum attainable suction (s_{max}) and maximum measurement duration (t_{max}) a new approach was considered to minimise the surface roughness of the HCT's water reservoir walls, hence, minimising the number of entrapped gas bubbles and nucleation sites, and therefore elevating the cavitation threshold. This method involved polishing the face-milled (FM) diaphragm surface on the water reservoir side using common methods of SiC abrasive papers (SP) and diamond paste (DP) polishing, and also coating the diaphragm with a micro-layer of a hydrophilic material such as Anti-fog agent (AF), Triton X-100, and TiO_2. The results of this study have been published in the journal of Geotechnical Research (Bagheri et al., 2018) and are outlined herein;

- The mechanism of cavitation in tensiometers is indeed influenced by the surface roughness of the water reservoir. The smoother and the more water-attractive surfaces in water reservoir can significantly reduce the number of entrapped gas bubbles and nucleation sites, hence increasing the cavitation threshold in HCTs.
- While the HCT with FM diaphragm was only capable of measuring suctions up to 65% of its nominal capacity, the surface polishing techniques resulted in an increase of s_{max} values up to 122% of the nominal capacity. Furthermore, AF and Triton coatings and TiO_2 coating increased the s_{max} by 127% and 153% of the nominal capacity, respectively.
- Considering the t_{max} values obtained from the SP polished HCT as an index, the improvements achieved from Triton and TiO_2 coating methods were in the range of 134 – 177%.
- The mechanical surface polishing methods reduce the hydrophilicity of the diaphragms and hence may offset the improvement achieved through reducing the surface roughness. This effect is more evident during long-term measurements of constant high suctions.
- The TiO_2 hydrophilic coating appears to be promising in improving the s_{max} and t_{max} values of the HCTs. Its strong bonding properties to the substrate also

counterbalances potential issues caused by dissolution or detachment of the coating layer, and hence guarantees the long-term functionality of the HCT.

The new HCTs were used for development of SWRC-*w* for the reconstituted London Clay specimens, using continuous drying procedures with (CD(er) tests) and without (CD tests) soil-moisture evaporation-rate control. The experimental program revealed the following findings;

- In contrast with the findings of Cunningham (2000) and Boso et al. (2003) that suggest independency of the tensiometric-based SWRCs to the evaporation-rate, the soil-moisture evaporation-rate was found to influence the measured air-entry value (s_{AEV}) and, slightly, the shape of the curve in transition between saturated and unsaturated states.
- A smooth transition from the saturated to the unsaturated state was observed in CD(er) tests in comparison to the somewhat sharper transition in CD tests.
- The extended SWRCs obtained for CD(er) tests (based on Fredlund and Xing (1994) equation) appear to provide more reliable extrapolation of water retention characteristics corresponding with suctions beyond the capacity of the HCTs. This is not, however, a certain conclusion, and the extrapolated curves need to be checked against the experimental values of soil suction measured using indirect suction measurement methods.

7.1.1.2 The New Suction- and Temperature-Controlled CRS Oedometer

Design of a new multi-functional CRS oedometer cell for testing clays under unsaturated and non-isothermal conditions was presented. Design of the similar systems reported in the literature typically incorporate only one suction control/measurement method that involve limitations mainly in terms of the range of applied/measured suctions. In the design of the new CRS system, for the first time, a combination of two suction control/measurement methods, namely; axis-translation (control) and HCT (measurement) were considered, allowing for more rigorous monitoring of suction evolutions, especially during long-term tests. Also, accommodation of the HCTs on the periphery and mid height of the specimen allows for measurement of average pore-water pressure across the specimen. Furthermore, the range of imposable temperature gradients was extended to 200º C through

integration of a tubular heating element at the base of the specimen, which rectifies the limitations associated with the circulated heated water or isothermal liquids systems, such as leakage and limited temperature gradients. Moreover, the use of an internal submersible load cell for measurement of axial stress in the new system rectifies the problems associated with the pneumatic and water pressurised membranes/chambers (e.g. calibration problems due to the membrane friction with the cell wall, membrane creep and fatigue, and limitation of maximum fluid pressure supply), and external load cells (e.g. friction between the loading ram and the guide shaft). The size of the cutting ring (95 mm diameter and 35 mm high) allows for preparation and testing representative undisturbed specimens directly cored from U100 samplers and block samples of fissured clays such as London Clay. The new CRS oedometer is robust and cost-efficient, and can be used for conducting stress- and strain-controlled compression, stress-relaxation, thermal loading/unloading, cyclic wetting and drying, development of SWRCs, and etc.

7.1.2 1D Primary and Secondary Consolidation in Unsaturated Conditions

A set of MSL and SSL oedometer tests were carried out on dry, saturated intact, saturated reconstituted, and unsaturated reconstituted specimens with the aim to characterise the primary and secondary consolidation response of the Sheppey London Clay. The experimental program revealed the following findings;

- Generally, increase in suction results in a decrease in the slope of compression curve (m'_c) and the $C_{\alpha e}$ values, and an increase in apparent preconsolidation pressure (σ'_p).
- According to the classification criterion defined by Mesri et al. (1994), Sheppey London Clay is categorised as shale or mudstone whose α value ranges from 0.02 to 0.04. The $\alpha = C_{\alpha e}/C_c$ ratio for Sheppey London Clay is stress- and suction-dependent, and therefore cannot be considered as a constant value. However, an average value of 0.03 ± 0.01 can be approximated for the α ratio of saturated and unsaturated reconstituted specimens. It must be noted that small variations of $C_{\alpha e}$ parameter, derived from element level tests, can pose significant impacts on the ground settlement predictions using advanced time-dependent constitutive models (Rezania et al., 2017).

- From the results of SSL creep tests, it was observed that at the same vertical stress level, increase in initial suction results in a decrease in the rate and magnitude of volumetric creep strains. Moreover, at the same initial suction, increase in applied vertical stress leads to an increase in the volumetric creep strains.
- During long-term creep tests at constant water content, a decrease in soil suction monitored by HCTs can be attributed to an increase in degree of saturation of the specimen with decrease in total volume during creep. If this holds true, long-term creep tests where suction is artificially kept constant may not be ideal and the observed creep strains may not be solely attributed to the applied total vertical stress.
- The volumetric creep deformations of unsaturated stiff clays appear to be relatively simply modelled by a creep law based on a power function;

$$\frac{e}{e_p} = \beta t^{\alpha_i}$$

where β is the instantaneous change in void ratio (e_i) normalised with respect to e_p, t represents time, and α_i is the creep coefficient varying between zero and 0.012 and controls the shape of the curve.

7.1.3 1D Rate-Dependent Response in Unsaturated Conditions

Results of a set of SS-CRS and MS-CRS oedometer tests performed on reconstituted Sheppey London Clay specimens under saturated and unsaturated conditions and varied strain-rates were presented. The following conclusions can be drawn;

- The rate-dependent behaviour of clays can be conveniently studied from 1D CRS oedometer tests. However, in the literature, there is no available guideline for determination of a suitable strain-rate for unsaturated CRS tests. The selected strain-rates for CRS tests on unsaturated Sheppey London Clay specimens, having a suction range of 433 – 1905 kPa, appear to be appropriate and allow for preservation of a suction state inside the specimen, and hence, conduction of constant water content tests.
- In the literature, effects of suction and strain-rate on the σ'_p and C_c values have not been clearly identified. The results of CRS tests in this study revealed an

increase in σ'_p and decrease in C_c values with increase in suction and strain-rate. A coupled effect of suction and strain-rate on the compression response was also identified. At a constant suction, the higher the strain-rate, the higher the σ'_p. Similarly, at a constant strain-rate, the higher the suction, the higher the σ'_p.

- Comparing the results of CRS and IL oedometer tests, an approximately linear relationship for variation of σ'_p with suction was obtained for fast ($\dot{\varepsilon}_v$ = 2.4×10^{-6}), slow ($\dot{\varepsilon}_v$ = 4.8×10^{-7}), and oedometric strain-rates.
- At high stress levels, the unsaturated compression curves become parallel, and the stress–strain behaviour appears to follow the Isotach concept.

7.1.4 1D Stress-Relaxation Response in Unsaturated Conditions

As discussed in Chapter 2, a very large number of studies on the stress-relaxation behaviour of saturated clays under oedometric and triaxial conditions can be found in the literature. The reported works are, however, dispersed, and lack a unified framework for characterisation of the stress-relaxation response and the influence of factors such as pre-relaxation strain, stress, and strain-rate. In the unsaturated state, apart from the work of Wang et al. (2017) on unsaturated lime-treated expansive clay specimens, a significant gap currently exists with regard to the stress-relaxation process in unsaturated clays. The results of CRS tests, with stages of stress-relaxation, carried out in this research program on unsaturated Sheppey London Clay provides a basis for further complementary studies. The following conclusions can be drawn;

- The process of stress-relaxation appears to comprise three phases; (1) fast relaxation, (2) decelerating relaxation, and (3) residual relaxation. The fast relaxation phase is associated with a quick release of the main accumulated energy inside the specimen, whereas the decelerating and residual phases correspond to the time-dependent particles' re-arrangement which involve further dissipation of energy with time.
- At a constant pre-relaxation stress (σ_0), increase in suction results in a decrease in the rate of stress-relaxation during fast and decelerating relaxation phases, as well as in the magnitude of the overall relaxed stresses ($\Delta\sigma$).

- At a constant suction, the higher the pre-relaxation strain-rate, the higher would be the rate and magnitude of the relaxed stresses, as also reported by Wang et al. (2017).
- The values of relaxation coefficient (R_α), being the slope of the plot of applied vertical stress versus time in log σ_v – log t space during relaxation of the stresses, vary for saturated (s = 0) and unsaturated (e.g. s = 1905 kPa) states. However, it is difficult to comment on the relationship between the R_α and suction based on the limited available data points.
- The $R_\alpha = C_{\alpha e}/C_c$ relationship, suggested by Yin et al. (2014) for saturated soft clays, appears, with an approximation, to be valid for unsaturated reconstituted London Clay in the range of applied vertical stresses and soil suctions in this study.
- At a constant suction and strain-rate, increase in pre-relaxation strain (and consequently pre-relaxation stress) generally results in an increase in the rate and magnitude of the relaxed stresses.
- At a constant strain level and suction, an increase in $\Delta\sigma$ values by a factor of 2.2 – 3.6 was observed with an increase in the pre-relaxation strain-rate by a factor of 5. At the same strain level, increase in pre-relaxation strain-rate also results in an increase in R_α values under constant suction.

7.2 Recommendations for Future Works

The experimental work in this study, in addition to developing advanced and cost-efficient tools for experimental investigation of unsaturated soils properties, added significant data to the existing data-base on time- and rate-dependent behaviour of clays, and provided a foundation for the future works on the viscous response of unsaturated clays. Accordingly, the following recommendations for future studies are made:

- The new approach for expanding the range and duration of suction measurements for a newly designed HCT, based on hydrophilic coating of the reservoir walls, sounds promising. However, further works are to be done for evaluation of the long-term stability and adhesion of hydrophilic coatings to the diaphragms of the HCTs.

- Further investigations and more test results over a wider range of soil suction and applied vertical stress levels are required to validate the proposed creep law for unsaturated stiff clays.
- Further investigations and more test results over a wider range of soil suction and strain-rate are required to support the findings of this research program with regard to the influence of pre-relaxation strain, stress, and strain-rate on the overall stress-relaxation process in unsaturated conditions.
- The presented experimental testing systems facilitates the conduction of further research programs for investigations of more complex test conditions, e.g. coupling the effects of soil structure and temperature with the strain-rate- and suction-dependent response studied in the present work.

REFERENCES

Acikel, A. S. & Mancuso, C. (2010). Use of CO_2 gas to improve saturation of High Capacity Tensiometer (HCT). 4th Asia-Pacific Conference on Unsaturated Soils, Newcastle, Australia London: Taylor & Francis Group, Buzzi, Fityus & Sheng (eds), 205-208.

Aitchison, G. D. (1961). Relationship of moisture stress and effective stress functions in unsaturated soils. Proceedings of the Conference on Pore Pressure and Suction in Soils, British National Society of the International Society of Soil Mechanics and Foundation Engineering, London. Butterworths, 47-52.

Aldiss, D. T. (2014). The stratigraphical framework for the Palaeogene successions of the London Basin, UK. British Geological Survey Open Report OR/14/008.

Almeida, M. S. S., Martins, I. S. & Carvalho, S. R. L. (1995). Constant rate of strain consolidation of Singapore marine clay - Discussion to paper (ed. K. Lee et al.). *Géotechnique,* 45, 333-336.

Alonso, E. E. & Pinyol, N. M. (2008). Unsaturated soil mechanics in earth and rockfill dam engineering. In: Toll, D. G., Augarde, C. E., Gallipoli, D. & Wheeler, S. J., eds. First European Conference on Unsaturated Soils, E-UNSAT 2008, Durham, UK. London: CRC Press, 3-32.

Alonso, E. E., Gens, A. & Josa, A. (1990). A constitutive model for partially saturated soils. *Géotechnique,* 40, 405-430.

Alonso, E. E., Lloret, A., Gens, A. & Yang, D. Q. (1995). Experimental behaviour of highly expansive double-structure clay. Proceedings of the 1st International Conference on Unsaturated Soils, Paris, France, E.E. Alonso and P. Delage (eds), Rotterdam: Balkema, 1, 11-16.

Alonso, E. E., Olivella, S. & Pinyol, N. M. (2005). A review of Beliche Dam. *Géotechnique,* 55, 267-283.

Alonso, E. E., Pereira, J. M., Vaunat, J. & Olivella, S. (2010). A microstructurally based effective stress for unsaturated soils. *Géotechnique,* 60, 913–925.

Alonso, E., E., Gens, A. & Hight, D. W. (1987). Special problem soils. General report. Proceedings of the 9th European Conference on Soil Mechanics and Foundation Engineering, Dublin, Irland, E.T. Hanrahan, T.L.L. Orr, and T.F. Widds (eds), 1087-1146.

Alsharrad, M. A. (2013). Evolving anisotropy in unsaturated soils: experimental investigation and constitutive modelling, PhD Thesis, University of Glasgow, UK.

Arai, K. (1985). Representation of soft clay behavior based on minimization of dissipated energy. Proceedings of the 5th International Conference on Numerical Modelling in Geomechanics, Nagoya, Japan, 1, 277-284.

ASTM-D1452-09 (2009). Standard Practice for Soil Exploration and Sampling by Auger Borings. ASTM International.

ASTM-D1587-00 (2000). Standard Practice for Thin-Walled Tube Sampling of Soils for Geotechnical Purposes. West Conshohocken: ASTM International.

ASTM-D4186-06 (2006). Standard test method for one-dimensional consolidation properties of saturated cohesive soils using controlled-strain loading. West Conshohoken, PA: ASTM International.

Augustesen, A., Liingaard, M. & Lade, P. V. (2004). Evaluation of time-dependent behavior of soils. *International Journal of Geomechanics, ASCE,* 4, 137-156.

Bagheri, M., Rezania, M. & Mousavi-nezhad, M. (2018). Cavitation in high-capacity tensiometers: effect of water reservoir surface roughness. *Geotechnical Research*, 5(2), 81-95.

Bagheri, M., Rezania, M. & Mousavi-nezhad, M. (2015). An Experimental study of the initial volumetric strain rate effect on the creep behaviour of reconstituted clays. International Symposium on Geohazards and Geomechanics (ISGG2015). IOP Conference Series: Earth and Environmental Science, 26(1), 012034.

Bayesteh, H. & Mirghasemi, A. A. (2015). Numerical simulation of porosity and tortuosity effect on the permeability in clay: Microstructural approach. *Soils and Foundations*, 55, 1158-1170.

Benatti, J. B., Miguel, M. G., Rodrigues, R. A. & Vilar, O. M. (2010). Collapsibility study for tropical soil profile using oedometric tests with controlled suction. *Unsaturated Soils.* E.E. Alonso and A. Gens (eds), CRC Press, 1, 197-198.

Beri, N., Maheshwari, S., Sharma, C. & Kumar, A. (2008). Performance evaluation of powder metallurgy electrode in electrical discharge machining of AISI D2 steel using Taguchi method. *International Journal of Mechanical, Aerospace, Industrial, Mechatronic and Manufacturing Engineering*, 2, 225-229.

Berthelot, M. (1850). Sur quelques phenomenes de dilatation forcee des liquids. *Annale de Chimie et de Physique*, 30, 232-237.

Bilotta, E., Foresta, V. & Migliaro, G. (2008). The influence of suction on stiffness, viscosity and collapse of some volcanic ashy soils. *In:* Toll, D. G., Augarde, C. E., Gallipoli, D. & Wheeler, S. J., eds. 1st European Conference on Unsaturated Soils, E-UNSAT 2008, Durham, UK. London: CRC Press, 349-354.

Biot, M. A. (1955). Theory of elasticity and consolidation for a porous anisotropic soil. *Journal of Applied Physics*, 28, 182-185.

Bishop, A. W. (1959). The principle of effective stress. *Teknisk Ukeblad*, 39, 859-863.

Bishop, A. W., Kumapley, N. K. & El Ruwayih, A. (1975). The influence of pore water tension on the strength of a clay. *Philosophical Transactions of the Royal Society*, 278, 511-554.

Bishop, A. W., Webb, D. L. & Lewin, P. I. (1965). Undisturbed samples of London Clay from the Ashford Common shaft: strength-effective stress relationships. *Géotechnique*, 15, 1-31.

Bjerrum, L. (1967). Engineering geology of norwegian normally-consolidated marine clays as related to settlements of buildings. *Géotechnique*, 17, 81-118.

Blake, T. D. (2006). The physics of moving wetting lines. *Journal of Colloid Interface Science*, 299, 1-13.

Blatz, J., Cui, Y. J. & Oldecop, L. (2008). Vapour equilibrium and osmotic technique for suction control. *Geotechnical and Geological Engineering*, 26(6), 661-673.

Boso, M., Romero, E. & Tarantino, A. (2003). The use of different suction measurement techniques to determine water retention curves. In: Schanz, T., ed. International Conference "From Experimental Evidence towards Numerical Modeling of Unsaturated Soils", Weimar, Germany. Springer, 171-181.

Bouch, J. E. (2006). Petrography of samples of the London Clay of southern England. British Geological Survey Internal Report.

Bremond, N., Arora, M., Ohl, C.-D. & Lohse, D. (2005). Cavitation on surfaces. *Journal of Physics: Condensed Matter*, 17, S3603–S3608.

BS1377 (1990). Methods of test for soils for engineering purposes, Part 2: Classification tests.

BS-EN-1997:2 (2007). Eurocode 7 - Geotechnical design - Part 2: Ground investigation and testing. London: British Standards Instituition.

Bulut, R., and Leong, E. C. (2008). Indirect measurement of suction. *Journal of Geotechnical and Geological Engineering*, 26, 633-644.

Burghignoli, A., Desideri, A. & Milizia NO, S. (2000). A laboratory study on the thermomechanical behaviour of clayey soils. *Canadian Geotechnical Journal,* 37, 764-780.

Burland, J. B. (1990). On the compressibility and shear strength of natural clays. *Géotechnique,* 40, 329-378.

Burland, J. B., Rampello, S., Georgiannou, V. N. & Calabresi, G. (1996). A laboratory study of the strength of four stiff clays. *Géotechnique,* 46, 491-514.

Burnett, A. D. & Fookes, P. O. (1974). A regional engineering geological study of London Clay in the London and Hampshire basins. *Quarterly Journal of Engineering Geology and Hydrogeology*, 17, 257-295.

Caicedo, B., Ulloa, J. C. & Murillo, C. (2008). Preparation of unsaturated soils by oedometric compression. In: Toll, D. G., Augarde, C. E., Gallipoli, D. & Wheeler, S. J., eds. 1st European Conference on Unsaturated Soils, E-UNSAT 2008, Durham, UK, 135-140.

Chapman, P. J., Richards, B. E. & Trevena, D. H. (1975). Monitoring the growth of tension in a liquid contained in Berthelot tube. *Journal of Physics E: Scientific Instruments*, 8, 731-735.

Chau, T. T., Bruckard, W. J., Koh, P. T. L. & Nguyen, A. V. (2009). A review of factors that affect contact angle and implications for flotation practice. *Advances in Colloid and Interface Science,* 150, 106-115.

Cheng, C.-M. & Yin, J.-H. (2005). Strain-rate dependent stress-strain behavior of undisturbed Hong Kong marine deposits under oedometric and triaxial stress states. *Marine Georesources & Geotechnology,* 23, 61-92.

Chevallier, P., Turgeon, S., Sarra-Bournet, C., Turcotte, R. & Laroche, G. (2011). Characterization of multilayer anti-fog coatings. *Applied Materials & Interfaces*, 3, 750-758.

Chiu, C. F., Cui, Y. F., Delage, P., De Laure, E. & Haza, E. (2005). Lessons learnt from suction monitoring during centrifuge modelling. Advanced Experimental Unsaturated Soil Mechanics, Proceedings of an International Symposium on Advanced Experimental Unsaturated Soil Mechanics, Trento, Italy, A. Tarantino, E. Romero, and Y.J. Cui (eds.), 3-8.

Clayton, C. R. I., Matthews, M. C. & Simons, N. E. (1982). Site investigation, New York, Halsted Press.

Collin, F., Cui, Y. J., Schroeder, C. & Charlier, R. (2002). Mechanical behaviour of Lixhe chalk partly saturated by oil and water: experiment and modelling. *International Journal for Numerical and Analytical Methods in Geomechanics,* 26, 897-924.

Collin, F., De Gennaro, V., Delage, P. & Priol, G. (2008). An elasto-viscoplastic model for chalk including suction effects. *In:* Toll, D. G., Augarde, C. E., Gallipoli, D. & Wheeler, S. J., eds. 1st European Conference on Unsaturated Soils, E-UNSAT 2008, Durham, UK. London: CRC Press, 633-639.

Conradi, M. & Kocijan, A. (2016). Surface and anticorrosion properties of hydrophobic and hydrophilic TiO_2 coatings on a stainless-steel substrate. *Materials and Technology*, 50, 967-970.

Craig, R. F. (2004). Soil mechanics, London, Spon Press.

Crawford, C. (1964). Interpretation of the consolidation test. *Journal of Soil Mechanics and Foundation Division,* 90, 87-102.

Croney, D., Coleman, J. D. & Black, W. P. M. (1958). The movement and distribution of water in relation to highway design and performance. *In:* Water and its Conduction in Soils, Highway Research Board, Special Report No. 40, Washington, D.C, 226-252.

Cui, K., Defossez, P., Cui, Y. J. & Richard, G. (2010). Soil compaction by wheeling: change in soil suction due to compression. *European Journal of Soil Science*, 61, 599-608.

Cui, Y. J., Tang, A. M., Mantho, A. T. & De Laure, E. (2008). Monitoring field soil suction using a miniature tensiometer. *Geotechnical Testing Journal* (ASTM), 31(1), 95-100.

Cui, Y.-J., Le, T. T., Tang, A. M., Delage, P. & Li, X. L. (2009). Investigating the time-dependent behaviour of Boom clay under thermomechanical loading. *Géotechnique,* 59, 319-329.

Cuisinier, O. & Laloui, L. (2004). Fabric evolution during hydromechanical loading of a compacted silt. *International Journal for Numerical and Analytical Methods in Geomechanics*, 28, 483-499.

Cunningham, M. R. (2000). The mechanical behaviour of a reconstituted unsaturated soil. Ph.D. Thesis, Imperial College University.

Cunningham, M. R., Ridley, A. M., Dineen, K. & Burland, J. B. (2003). The mechanical behaviour of a reconstituted unsaturated silty clay. *Géotechnique*, 53, 183-194.

Curodeau, A., Richard, M. & Frohn-Villeneuve, L. 2004. Molds surface finishing with new EDM process in air with thermoplastic composite electrodes. *Journal of Materials Processing Technology* 149, 278-283.

De Gennaro, V., Delage, P., Cui, Y. J., Schroeder, C. & Collin, F. (2003). Time-dependent behavior of oil reservoir chalk: a multiphase approach. *Soils and Foundations*, 43, 131-147.

De Gennaro, V., Sorgi, C. & Delage, P. (2005). Air-water interaction and time dependent compressibility of a subterranean quarry chalk. *Symposium Post mining 2005*, Nancy, France, pp.NC.

Degago, S. A. (2011). On creep during primary consolidation of clays. Ph.D. Thesis, Norwegian University of Science and Technology.

Degago, S. A., Grimstad, G., Jostad, H. P. & Nordal, S. (2013). Misconceptions about experimental substantiation of creep hypothesis A. Proceedings of the 18th International Conference on Soil Mechanics and Geotechnical Engineering, Paris, France. 215-218.

Degago, S. A., Grimstad, G., Jostad, H. P., Nordal, S. & Olsson, M. (2011). Use and misuse of the isotache concept with respect to creep hypotheses A and B. *Géotechnique,* 61, 897-908.

Delage, P., and Cui, Y. J. (2008). An evolution of osmotic method of controlling suction. *Geomechanics and Geoengineering*, 3(1), 1-11.

Delage, P., Le, T. T., Tang, A. M., Cui, Y. J. & Li, X. L. (2007). Suction effects in deep Boom Clay block samples. *Géotechnique*, 57, 239-244.

Delage, P., Romero, E. & Tarantino, A. (2008). Recent developments in the techniques of controlling and measuring suction in unsaturated soils. Unsaturated Soils: Advances in Geo-Engineering: Proceedings of the 1st European Conference on Unsaturated Soils, D.G. Toll, C.E. Augarde, D. Gallipoli, S.J. Wheeler (eds.), Durham, CRC Press, 32-52.

Delage, P., Schroeder, C. & Cui, Y. J. (1996). Subsidence and capillary effects in chalks. Prediction and performance on rock mechanics and rock engineering - ISRM International symposium, EUROCK96, G. Barla (ed), Torino, Italy. 1291-1298.

Delage, P., Sultan, N., Cui, Y. & Li, X. (2009). Permeability changes in Boom clay with temperature. International Conference and Workshop "Impact of Thermo

Hydro-Mechanical-Chemical (THMC) Processes on the Safety of Underground Radioactive Waste Repositories", Luxembourg.

Den Hann, E. J. & Van Den Berg, P. (2001). Evaluation of creep models for soft soils (under axially symmetric conditions), Report No. CO-710203/21, Department of Strategic Research, GeoDelft, pp.39.

Deng, Y. F., Cui, Y. J., Tang, A. M., Li, X. L. & Sillen, X. (2012). An experimental study on the secondary deformation of Boom clay. *Applied Clay Science*, 59-60, 19-25.

Dineen, K. & Burland, J. B. (1995). A new approach to osmotically controlled oedometer testing. 1st International Conference on Unsaturated Soils, E.E. Alonso & P. Delage (eds), Paris, 459-465.

Dineen, K. (1997). The influence of soil suction on compressibility and swelling. Ph.D. Thesis, Imperial College London.

Dobak, P. (2003). Loading velocity in consolidation analysis. *Geological Quarterly*, 47, 13-20.

Doran, I. G., Sivakumar, V., Graham, J. & Johnson, A. (2000). Estimation of in situ stresses using anisotropic elasticity and suction measurements. *Géotechnique*, 50, 189-196.

Drelich, J. (1997). The effect of drop (bubble) size on contact angle at solid surfaces. *Journal of Adhesion*, 63, 31-51.

Drelich, J., Chibowski, E., Meng, D. D. & Terpilowski, K. (2011). Hydrophilic and superhydrophilic surfaces and materials. *Soft Matter*, 7, 9804-9828.

Ellison, R. A., Woods, M. A., Allen, D. J., Forster, A., Pharaoh, T. C. & King, C. (2004). Geology of London. Memoir of the British Geological Survey, Sheets 256 (North London), 257 (Romford), 270 (South London) and 271 (Dartford) (England and Wales).

EN-ISO-22475:1 (2006). Geotechnical investigation and testing - Sampling methods and groundwater measurements - Part1: Technical principles for execution.

Estabragh, A. R. & Javadi, A. A. (2008). Critical state for overconsolidated unsaturated silty soil. *Canadian Geotechnical Journal*, 45, 408-420.

Feng, T.-W. (1991). Compressibility and permeability of natural soft clays, and surcharging to reduce settlements. Ph.D. Thesis, University of Illinois at Urbana-Champaign.

Field, M., Koster, W. P. & Kohls, J. B. (1970). Machining of high strength steels with emphasis on surface integrity. Technical Report AFML-TR-70-11, Air Force Material Laboratory, MATF, Wright-Patterson Air Force Base, Ohio, U.S.A.

Fisher, J. C. (1948). The fracture of liquids. *Journal of Applied Physics*, 19, 1062-1067.

Fodil, A., Aloulou, W. & Hicher, P. Y. (1997). Viscoplastic behaviour of soft clay. *Géotechnique*, 47, 581-591.

François, B. & Laloui, L. (2010). An oedometer for studying combined effects of temperature and suction on soils. *Geotechnical Testing Journal*, 33, 1-11.

Fredlund, D. G. & Houston, S. L. (2013). Interpretation of soil-water characteristic curves when volume change occurs as soil suction is changed. *In:* Advances in Unsaturated Soils: Proceedings of the 1st Pan-American Conference on Unsaturated Soils, PanAmUNSAT 2013, Taylor & Francis Group, London, ISBN: 978-041562095-6, Volume: 1, 15-31.

Fredlund, D. G. & Morgenstern, N. R. (1976). Constitutive relations for volume change in unsaturated soils. *Canadian Geotechnical Journal*, 13, 261-276.

Fredlund, D. G. & Morgenstern, N. R. (1977). Stress state variables for unsaturated soils. *Journal of the Geotechnical Engineering Division, ASCE*, 103, 447-466.

Fredlund, D. G. & Rahardjo, H. (1993). Soil mechanics for unsaturated soils, New York, John Wiley & Sons.

Fredlund, D. G. & Xing, A. (1994). Equations for the soil-water characteristic curve. *Canadian Geotechnical Journal*, 31, 521-532.

Fredlund, D. G. (2000). The 1999 R.M. Hardy Lecture: The implementation of unsaturated soil mechanics into geotechnical engineering. *Canadian Geotechnical Journal*, 37, 936-986.

Fredlund, D. G. (2006). Unsaturated soil mechanics in Engineering Practice. *Journal of Geotechnical and Geoenvironmental Engineering*, 132, 286-321.

Fredlund, D. G., Gan, J. K. M., Guan, Y. & Richardon, N. (1997). Suction measurements on a Saskatchewan soil using a direct measurement, high suction sensor. Transportation Research Board, 76th Annual Meeting. Washington DC.

Fredlund, D. G., Vanapalli, S. K., Xing, A. & Pufahl, D. E. (1995). Predicting the shear strength function for unsaturated soils using the soil-water characteristic curve. *In:* E.E. Alonso & P. Delage. (eds), 1st International Conference on Arid Soils, Paris, 63-69.

Fredlund, D. G., Xing, A. & Huang, S. (1994). Predicting the permeability functions for unsaturated soils using the soil-water characteristic curve. *Canadian Geotechnical Journal,* 31, 533-546.

Freeborough, F., Kirkahm, M. & Jones, L. D. (2006). Determination of the shrinking and swelling properties of the London Clay Formation: Laboratory Report. Keyworth, Nottingham: British Geological Survey Internal Report.

Gallipoli, D., Gens, A., Sharma, R. & Vaunat, J. (2003a). An elasto-plastic model for unsaturated soil incorporating the effects of suction and degree of saturation on mechanical behavior. *Géotechnique,* 53, 123-135.

Gallipoli, D., Wheeler, S. J. & Karstunen, M. (2003b). Modelling the variation of degree of saturation in a deformable unsaturated soil. *Géotechnique,* 53, 105-112.

Gasparre, A. (2005). Advanced labortory characterisation of London Clay. Ph.D. Thesis, University of London.

Gasparre, A., Nishimura, S., Coop, M. & Jardine, R. J. (2007). The influence of structure on the behaviour of London Clay. *Géotechnique,* 57, 19-31.

Gens, A. & Alonso, E. E. (1992). A framework for the behaviour of unsaturated expansive clays. *Canadian Geotechnical Journal,* 29, 761-773.

Georgiannou, V. N. & Hight, D. W. (1994). The effects of centreline tube sampling strains on the undrained behaviour of two stiff overconsolidated clays. *Geotechnical Testing Journal,* 17, 475-487.

Gilkers, R. J. (1968). Clay mineral provinces in the Tertiary sediments of the Hampshire Basin. *Clay Minerals,* 7, 351-361.

Good, R. J. (1992). Contact-angle, wetting, and adhesion - a critical-review. *Journal of Adhesion Science and Technology,* 6, 1269-1302.

Gorman, C., Hopkins, T., Deen, R. & Drnevich, V. (1978). Constant-rate-of-strain and controlled-gradient consolidation testing. *Geotechnical Testing Journal,* 1, 3-15.

Graham, J., Crooks, J. H. A. & Bell, A. L. (1983). Time effects on the stress strain behavior of natural soft clays. *Géotechnique,* 33, 327-340.

Grant, S. & Salehzade, A. (1996). Calculation of temperature effects on wetting coefficients of porous solids and their capillary pressure functions. *Water Resources Research,* 32, 261-270.

Guan, Y. & Fredlund, D. G. (1997). Use of tensile strength of water for the direct measurement of high soil suction. *Canadian Geotechnical Journal*, 34, 604-614.

Guan, Y. (1996). The measurement of soil suction. Ph.D. thesis, University of Saskatchewan.

Hamilton, J. J. & Crawford, C. B. (1959). Improved determination of preconsolidation pressure of a sensitive clay. American Society for Testing and Materials, SPT254.

Hanzawa, H. (1989). Evaluation of design parameters for soft clays as related to geological stress history. *Soils and Foundations*, 29, 99-111.

Hanzawa, H., Fukaya, T. & Suzuki, K. (1990). Evaluation of engineering properties for an Ariake clay. *Soils and Foundations*, 30, 11-24.

Harvey, E. N., Barnes, D. K., Mcelroy, W. D., Whiteley, A. H., Pease, D. C. & Cooper, K. W. (1944). Bubble formations in animal, 1-Physical factor. *Journal of Cellular and Comparative Physiology*, 24, 1-22.

Harvey, E. N., Mcelroy, W. D. & Whiteley, A. H. (1947). On cavity formation in water. *Journal of Applied Physics*, 18, 162-172.

Hasegawa, M., Seireg, A. & Lindberg, R. A. (1976). Surface roughness model for turning. *Tribology International*, 9(6), 285-289.

He, L., Leong, E. C. & Algamal, A. (2006). A miniature tensiometer for measurement of high matric suction, In: Proceedings of 4th International Conference on Unsaturated Soils, G.A. Miller, C.E. Zapata, S.L. Houston, and D.G. Fredlund (eds), Carefree, Arizona, US, ASCE, 2, 1897-1907.

Head, K. (1992). Manual of soil laboratory testing, London, Pentech press.

Henderson, S. J. & Speedy, R. J. (1980). A Berthelot-Bourdoon tube method for studying water under tension. *Journal of Physics E: Scientific Instrumentation*, 13, 778-782.

Hicher, P. Y. (1985). Comportement mecanique des argiles saturees sur divers chemins de sollicitations monotones et cycliques. Application a une modelisation elastoplastique et viscoplastique.: PhD Thesis, Universite Paris VI.

Hight, D. W. & Jardine, R. J. (1993). Small strain stiffness and strength characteristics of hard London Clay Tertiary clays. International Symposium on Hard Soils-Soft Rocks, Anagnostopoulos et al. (eds), Athens, Greece. Rotterdam: Balkema, 522-533.

Hight, D. W., Gasparre, A., Nishimura, S., Minh, N. A., Jardine, R. J. & Coop, M. R. (2007). Characteristics of the London Clay from the Terminal 5 site at Heathrow Airport. *Géotechnique*, 57, 3-18.

Hight, D. W., Higgins, K. G., Jardine, R. J., Potts, D. M., Pickles, A. R., De Moor, E. K. D. & Nyirenda, Z. M. (1993). Predicted and measured tunnel distortions associated with construction of Waterloo International Terminal. Predictive Soil Mechanics: Proceedings of the Worth Memorial Symposium, St Catherine's College, Oxford, G.T. Houlsby and A.N. Schofield (eds), Thomas Telford, London, 317-338.

Hight, D. W., Mcmillan, F., Powell, J. J. M., Jardine, R. J. & Allenou, C. P. (2003). Some characteristics of London Clay. *In:* Proceedings of the 1st International Workshop on Characterisation and Engineering Properties of Natural Soils, Singapore, T. S. Tan, K. K. Phoon, D. W. Hight, and S. Leroueil (eds), A.A. Balkema, 851-907.

Hu, P., Yang, Q. & Li, P.-Y. (2010). Direct and indirect measurement of soil suction in the laboratory. *Electronic Journal of Geotechnical Engineering*, 15, 1-10.

Hueckel, T. A. (1992). Water-mineral interaction in hygromechanics of clays exposed to environmental loads: a mixture-theory approach. *Canadian Geotechnical Journal*, 29, 1071-1086.

Huggett, J. M. (1994). Diagenesis of mudrocks and concretions from the London clay formation in the London basin. *Clay Minerals*, 29, 693-707.

Ishida, N., Inoue, T., Miyahara, M. & Higashitani, K. (2000). Nano bubbles on a hydrophobic surface in water observed by tapping-mode atomic force microscopy. *Langmuir*, 16, 6377-6380.

ISO/DIS4287/1 (1987). Surface Roughness Terminology Part 1: Surface and its parameters. International Organization for Standardization.

Jarad, N. (2016). Temperature impact on the consolidation and creep behaviour of compacted clayey soils. Ph.D. Thesis, Université de Lorraine.

Jarad, N., Cuisinier, O. & Masrouri, F. (2017). Effect of temperature and strain rate on the consolidation behaviour of compacted clayey soils. *European Journal of Environmental and Civil Engineering*, 21, 1-18.

Jardine, R. J., Gens, A., Hight, D. W. & Coop, M. R. (2004). Developments in understanding soil behavior. Advances in Geotechnical Engineering: The Skempton Conference: Proceedings of a Conference on Advances in

Geotechnical Engineering, London, R.J. Jardine, D.M. Potts, and K.G. Higgins (eds), Thomas Telford, London, 1, 103-206.

Jardine, R. J., Smith, P. R. & Nicholson, D. P. (2003). Properties of the soft Holocene Thames Estuary Clay from Queenborough, Kent. *In:* Proceedings of the 1st International Workshop on Characterisation and Engineering Properties of Natural Soils, Paris, T. S. Tan, K. K. Phoon, D. W. Hight, & S. Leroueil (eds), A. A. Balkema, 599-643.

Jennings, J. E. (1960). A revised effective stress law for use in the prediction of the behavior of unsaturated soils. Proceedings of the Conference on Pore Pressure and Suction in Soils, London. Butterworths, 26-30.

Jennings, J. E. B. & Burland, J. B. (1962). Limitations to the use of effective stresses in unsaturated soils. *Géotechnique*, 12, 125-144.

Jones, S. F., Evans, G. M. & Galvin, K. P. (1999). Bubble nucleation from gas cavities - a review. *Advances in Colloid and Interface Science*, 80, 27-50.

Jotisankasa, A. (2005). Collapse behaviour of a compacted silty clay. Ph.D. Thesis, University of London.

Jotisankasa, A., Coop, M. & Ridley, A. (2007a). The development of a suction control system for a triaxial apparatus. *Geotechnical Testing Journal*, 30, 1-7.

Jotisankasa, A., Porlila, W., Soralump, S. & Mairiang, W. (2007b). Development of a low-cost miniature tensiometer and its applications. In: Proceedings of 3rd Asian Conference on Unsaturated Soils UNSAT-ASIA 2007, Nanjing, China, Z.Z. Yin, Y.P. Yuan and A.C.F. Chiu (eds), Beijing: Science Press, ISBN: 7-03-018739-0, 475-480.

Kamao, S. (2016). Creep and relaxation behavior of highly organic soil. *International Journal of GEOMATE*, 11, 2506-2511.

Karim, M. R. (2010). Modelling the long term behaviour of soft soils. Ph.D. Thesis, University of New South Wales, Australia.

Karstunen, M. & Koskinen, M. (2008). Plastic anisotropy of soft reconstituted clays. *Canadian Geotechnical Journal*, 45, 314-328.

Karstunen, M. & Yin, Z.-Y. (2010). Modelling time-dependent behaviour of Murro test embankment. *Géotechnique*, 60, 735-749.

Karstunen, M., Krenn, H., Wheeler, S. J., Koskinen, M. & Zentar, R. (2005). Effect of anisotropy and destructuration on the behaviour of Murro test embankment. *International Journal of Geomechanics*, 5, 87-97.

Karube, D. & Kato, S. (1994). An ideal unsaturated soil and the Bishop's soil. Proceedings of the 13th International Conference on Soil Mechanics and Foundation Engineering, New Delhi, 43-46.

Kim, Y. T. & Leroueil, S. (2001). Modeling the viscousplastic behavior of clays during consolidation: application to Berthierville clay in both laboratory and field conditions. *Canadian Geotechnical Journal*, 38, 484-497.

King, C. (1981). The stratigraphy of the London Clay and associated deposits. Backhuys, Rotterdam: Tertiary Research Special Paper.

Koliji, A. (2008). Mechanical Behaviour of Unsaturated Aggregated Soils. Ph.D. Thesis, École Polytechnique Fédérale de Lausanne.

Komoto, N., Tatsuoka, F. & Nishi, T. (2003). Viscous stress-strain properties of undisturbed Pleistocene clay and its constitutive modelling. Proceedings of 3rd International Symposium on Deformation Characteristics of Geomaterials, Lyon, France, H. Di Benedetto, T. Doanh, H. Geoffroy, and C. Sauzeat (eds), 579-587.

Lacasse, S., Berre, T. & Lefebvre, G. Block (1985). Sampling of sensitive clays. Proceeding of 11th International Conference on Soil Mechanics and Foundation Engineering, San Francisco, Publications Committee of XI ICSMFF (ed), 887-892.

Lacerda, W. & Houston, W. (1973). Stress relaxation in soils. Proceedings of the 8th International Conference on Soil Mechanics and Foundation Engineering, Moscow, 3, 221-227.

Ladanyi, B. & Benyamina, M. B. (1995). Triaxial relaxation testing of a frozen sand. *Canadian Geotechnical Journal*, 32, 496-511.

Ladd, C. C., Foott, R., Ishihara, K., Schlosser, F. & Poulos, H. G. (1977). Stress deformation and strength characteristic SOA report. Proceedings of the 9th International Conference of Soil Mechanics and Foundation Engineering, Tokyo, 421-494.

Ladd, R. S. (1978). Preparing test specimens using undercompaction. *Geotechnical Testing Journal*, 1, 16-23.

Lade, P. V., Liggio, C. D. & Nam, J. (2009). Strain rate, creep, and stress drop-creep experiments on crushed coral sand. *Journal of Geotechnical and Geoenvironmental Engineering,* 135, 941-953.

Lai, X., Wang, S., Qin, H. & Liu, X. (2010). Unsaturated creep tests and empirical models for sliding zone soils of Qianjiangping landslide in the Three Gorges. *Journal of Rock Mechanics and Geotechnical Engineering*, 2, 149-154.

Laloui, L. (2010). New trends in mechanics of unsaturated geomaterials, ISTE, John Wiley & Sons.

Larsson, R. & Sällfors, G. (1986). Automatic Continuous Consolidation Testing in Sweden. *Consolidation of Soils, STP 892, ASTM*, 299-328.

Le, T. M., Fatahi, B. & Khabbaz, H. (2012). Viscous behavior of soft clay and inducing factor. *Geotechnical and Geological Engineering*, 30, 1069-1083.

Leong, E. C., Zhang, X.-H. & Rahardjo, H. (2012). Calibration of a thermal conductivity sensor for field measurement of matric suction. *Géotechnique*, 62, 81-85.

Leoni, M., Karstunen, M. & Vermeer, P. A. (2008). Anisotropic creep model for soft soils. *Géotechnique*, 58, 215-226.

Leroueil, S. & Marques, M. E. S. (1996). Importance of strain rate and temperature effects in geotechnical engineering. *ASCE Geotechnical Special Publication*, New York, 61, 1-60.

Leroueil, S. & Vaughan, P. R. (1990). The general and congruent effects of structure in soils and weak rocks. *Géotechnique,* 40, 467-488.

Leroueil, S. (1988). Recent developments in consolidation of natural clays. *Canadian Geotechnical Journal,* 25, 85-107.

Leroueil, S. (1996). Compressibility of clays: fundamental and practical aspects. *Journal of Geotechnical Engineering,* 122, 534-543.

Leroueil, S. (2006). Suklje's Memorial Lecture: The isotach approach: Where are we 50 years after its development by Professor Suklje?, Proceeding of the 13th European-Danube Conference on Geotechnical Engineering, Ljubljana, Slovenia, 1, 55-88.

Leroueil, S., Kabbaj, M., Tavenas, F. & Bouchard, R. (1985). Stress-strain-strain rate relation for the compressibility of sensitive natural clays. *Géotechnique,* 35, 159-180.

Leroueil, S., Perret, D. & Locat, J. (1996). Strain rate and structuring effects on compressibility of a young clay. *In:* Proceeding of Measuring and Modelling of Time Dependent Soil Behavior, Geotechnical Special Publication, Sheahan, T. C. & Kaliakin, V. N. (eds), Reston 137-150.

Leroueil, S., Samson, L. & Bozozuk, M. (1983a). Laboratory and field determination of preconsolidation pressure at Geloucester. *Canadian Geotechnical Journal,* 20, 446-453.

Leroueil, S., Tavenas, F., Samson, L. & Morin, P. (1983b). Preconsolidation pressure of Champlain clays, Part II, Laboratory determination. *Canadian Geotechnical Journal,* 20, 803-816.

Lewis, G. M. (1961). The tensile strength of liquids in Berthelot tubes. IOP Sciences: Proceedings of the Physical Society of London, 78(1), 133-144.

Li, J. Z., Peng, F. L. & Xu, L. S. (2009). One-dimensional viscous behavior of clay and its constitutive modeling. *International Journal of Geomechanics,* 9, 43-51.

Li, J. Z., Peng, F. L., Xu, L. S. & Tatsuoka, F. (2006). Viscous properties of clay with different water content. *Soil and rock behavior and modeling* (GSP 150), ASCE, 194, 55-61.

Li, J.-Z., Tatsuoka, F., Nishi, T. & Komoto, N. (2003). Viscous stress-strain behaviour of clay under unloaded conditions. Proceedings of the 3rd International Symposium on Deformation Characteristics of Geomaterials: IS Lyon 03, Lyon, France, Di Benedetto et al. (eds), Balkema, 617-625.

Li, L. & Zhang, X. (2014). Development of a new high-suction tensiometer. In: Wenqi, D., Lianyang, Z., Xiaojun, L. & Xiong, Z., eds. Geo-Shanghai2014, International Conference on Soil Behavior and Geomechanics, Shanghai, China, 416-425.

Li, X. S. (2003). Effective stress in unsaturated soil: a microstructural analysis. *Géotechnique,* 53(2), 273-277.

Liingaard, M., Augustesen, A. & Lade, P. V. (2004). Characterization of models for time-dependent behavior of soils. *International Journal of Geomechanics,* 4, 157-177.

Liu, H., Ju, Z., Bachmann, J., Horton, R. & Ren, T. (2012). Moisture-dependent wettability of artificial hydrophobic soils and its relevance for soil water desorption curves. *Soil Science Society of America Journal,* 76, 342-349.

Lohani, T. N., Imai, G., Tani, K. & Shibuya, S. (2001). Gmax of fine-grained soils at wide void ratio range, focussing on the time-dependent behavior. *Soils and Foundations,* 41, 87-102.

Lourenço, S. D. N. (2008). Suction measurement and water retention in unsaturated soils. Ph.D. Thesis, Durham University.

Lourenço, S. D. N., Gallipoli, D., Augarde, C. E., Toll, D. G., Fisher, P. C. & Congreve, A. (2012). Formation and Evolution of Water Menisci in Unsaturated Granular Media. *Géotechnique*, 193-199.

Lourenço, S. D. N., Gallipoli, D., Toll, D. G. & Evans, F. D. (2006). Development of a commercial tensiometer for triaxial testing of unsaturated soils. Unsaturated Soils: Proceedings of the 4th International Conference on Unsaturated Soils, Carefree, Arizona, USA, G. A. Miller, C. E. Zapata, S. L. Houston, and D. G. Fredlund (eds), Geotechnical Special Publications 147, Reston, VA: American Society of Civil Engineers, 1875-1886.

Lourenço, S. D. N., Gallipoli, D., Toll, D. G., Augarde, C. E. & Evans, F. D. (2011). A new procedure for the determination of the soil water retention curves by continuous drying using high suction tensiometers. *Canadian Geotechnical Journal*, 48, 327-335.

Lourenço, S. D. N., Gallipoli, D., Toll, D. G., Augarde, C. E., Evans, F. D. & Medero, G. M. (2008). Calibrations of a high suction tensiometer. *Géotechnique*, 58, 659-668.

Lourenço, S. D. N., Jones, N., Morley, C., Doerr, S. H. & Bryant, R. (2015). Hysteresis in the soil water retention of a sand–clay mixture with contact angles lower than ninety degrees. *Vadose Zone Journal*, 1-8.

Lu, N. & Griffiths, D. V. (2004). Profiles of steady-state suction stress in unsaturated soils. *Journal of Geotechnical and Geoenvironmental Engineering*, 130, 1063-1076.

Mahler, C. F. & Diene, A. A. (2007). Tensiometer development for high suction analysis in laboratory lysimeters. In: Schanz, T. (ed.) Experimental Unsaturated Soil Mechanics. Springer Proceedings in Physics, vol 112. Springer, Berlin, Heidelberg, 103-115.

Mahler, C. F., Pacheco, A. C. & Souza, H. G. (2002). Development of an automatic tensiometer in laboratory using a Mini-Lysimeter. In: Juca, J. F. T., De Campos, T. M. P. & Marinho, F. A. M., eds. Proceedings of the 3rd International Conference on Unsaturated Soils, Recife, Brazil, 1021-1027.

Mancuso, C. & Papa, R. (2014). A high capacity tensiometer to measure soil suction. Proceedings of the 20th IMEKO TC4 International Symposium; Measurement of Electrical Quantities, Benevento, Italy, 1, 212-215.

Mantho, A. T. (2005). Soil-atmosphere transfers - application to drought. Ph.D. Thesis, Ecole National des Ponts et Chaussrees.

Marinho, F. A. M. & Chandler, R. J. (1994). Discussion: A new instrument for the measurement of soil moisture suction. *Géotechnique,* 44, 551-556.

Marinho, F. A. M. & Chandler, R. J. (1995). Cavitation and the direct measurement of soil suction. In: Alonso, E. E. & Delage, P., eds. 1st International Conference on Unsaturated Soils (UNSAT95), Paris, France. Rotterdam: AA Balkema, 623-630.

Marinho, F. A. M. & Pinto, C. S. (1997). Soil suction measurement using a tensiometer. Symposium on recent development in soil and pavement mechanics. Rio de Janeiro, Brazil, A A Balkema, 249-254.

Marinho, F. A. M. & Teixeira, P. F. (2009). The use of high capacity tensiometer for determining the soil water retention curve. *Soil and Rocks Journal*, 32, 91-96.

Marinho, F. A. M., Take, W. A. & Tarantino, A. (2008). Measurement of matric suction using tensiometric and axis translation techniques. *Geotechnical and Geological Engineering,* 26, 615-631.

Masin, D., Stallebrass, S. E. & Atkinson, J. H. (2003). Laboratory modelling of natural structured clays. Proceedings of the International workshop on geotechnics of soft soils: theory and practice, Vermeer, Schweiger, Karstunen & Cudny (Eds.), Noordwijkerhout, The Netherlands, 491-496.

Mataic, I. (2016). On structure and rate dependence of Pernio clay. Ph.D. Thesis, Aalto University.

Mataic, I., Wang, D. & Korkiala-Tanttu, L. (2015). Effect of destructuration on the compressibility of Pernio clay in incremental loading oedometer tests. *International Journal of Geomechanics ASCE,* 16(1), 04015016.

Matsumoto, M. & Kataoka, Y. (1988). Study on liquid-vapour interface of water. I. Simulational results of thermodynamic properties and orientational structure. *Journal of Chemical Physics,* 88, 3233-3245.

Matyas, E. L. & Radhakrishna, H. S. (1968). Volume change characteristics of partially saturated soils. *Géotechnique,* 18, 432-448.

Mavroulidou, M., Xiwei, Z., Gunn, M. J. & Cabarkapa, Z. (2013). Water retention and compressibility of a lime-treated high plasticity clay. *Geotechnical and Geological Engineering,* 31, 1171-1185.

McGinty, K. (2006). Bothkennar clay: experimental analysis of anisotropy and destructuration. PhD Thesis, University of Glasgow.

Meilani, I., Rahardjo, H., Leong, E. C. & Fredlund, D. G. (2002). Mini suction probe for matric suction measurements. *Canadian Geotechnical Journal*, 39, 1427-1432.

Mendes, J. & Buzzi, O. (2013). New insight into cavitation mechanisms in high-capacity tensiometers based on highspeed photography. *Canadian Geotechnical Journal*, 50, 550-556.

Mendes, J. & Buzzi, O. (2014). Performance of the University of Newcastle high capacity tensiometers. *In:* Unsaturated Soils: Research and Applications - Proceedings of the 6th International Conference on Unsaturated Soils, UNSAT 2014. Taylor & Francis, 1611-1616.

Mendes, J., Gallipoli, D., Toll, D., Augarde, C. E. & Evans, F. D. (2008). A system for field measurement of suctions using high capacity tensiometers. In: 1st European Conference on Unsaturated Soils, Durham, England, D.G. Toll, C.E. Augarde, D. Gallipoli, S.J. Wheeler (eds), Taylor and Francis, London, 219-225.

Mesri, G. & Castro, A. (1987). Ca/Cc concept and K0 during secondary compression. *Journal of Geotechnical Engineering*, 113, 230-247.

Mesri, G. & Choi, Y. K. (1985). The uniqueness of the End-Of-Primary (EOP) void ratio-effective stress relationship. Proceedings of the 11th International Conference on Soil Mechanics and Foundation Engineering, San Francisco, 587-590.

Mesri, G. & Feng, T.-W. (1986). Discussion: "Stress-strain-strain rate relation for the compressibility of sensitive natural clays." by Leroueil et al. *Géotechnique*, 36, 283-290.

Mesri, G. & Godlewski, P. M. (1977). Time and stress-compressibility interrelationship. *Journal of Geotechnical Engineering Division, ASCE*, 103, 417-430.

Mesri, G. & Olson, R. E. (1971). Mechanism controlling the permeability of clays. *Clays and Clay Minerals*, 19, 151-158.

Mesri, G. & Vardhanabhuti, B. (2006). Closure of 'Secondary compression' by Mesri & Vardhanabhuti (2005). *Journal of Geotechnical and Geoenvironmental Engineering*, 132, 817-818.

Mesri, G. (1973). Coefficient of secondary compression. *Journal of Soil Mechanics Division. ASCE*, 99, 123-137.

Mesri, G. (2001). Primary compression and secondary compression. *Soil Behavior and Soft Ground Construction.* J.T. Germaine, T.C. Sheahan, & R.V. Whitman (eds), ASCE Special Geotechnical Publication No. 119, 122-166.

Mesri, G. (2009). Discussion of 'Effects of friction and thickness on long-term consolidation behavior of Osaka Bay clays' by Watabe, Udaka, Kobayashi, Tabata & Emura (2008). *Soils and Foundations*, 49, 823-824.

Mesri, G., Rebres-Cordero, E. & Shields, D. R. (1981). Shear stress−strain−time behavior of clays. *Géotechnique*, 31, 537-552.

Micro-Measurements (2010). Technical Note: Design considerations for diaphragm pressure transducers. Strain gages and instruments. Raleigh, USA.

Mitchell, J. K. (1956). The fabric of natural clays and its relation to engineering properties. *Highways Research Board*, 35, 693-713.

Mitchell, J. K. (1993). Fundamentals of Soil Behaviour, New Jersey, John Wiley & Sons.

Mitchell, J. K., Baxter, C. D. P. & Soga, K. (1997). Time effects on the stress-deformation behaviour of soils. Proceedings of Professor Sakuro Murayama Memorial Symposium, Kyoto, Japan, 1-64.

Monroy, R. (2005). The influence of load and suction changes on the volumetric behaviour of compacted London Clay. Ph.D. Thesis, Imperial College London.

Monroy, R., Zdravkovic, L. & Ridley, A. M. (2010). Evolution of microstructure in compacted London Clay during wetting and loading. *Géotechnique*, 60, 105-119.

Monroy, R., Zdravkovic, L. & Ridley, A. M. (2008). Volumetric behaviour of compacted London Clay during wetting and loading. *In:* Toll, D. G., Augarde, C. E., Gallipoli, D. & Wheeler, S. J., eds. First European Conference on Unsaturated Soils, E-UNSAT 2008, Durham, UK, 315-320.

Muñoz-castelblanco, J., Delage, P., Pereira, J. M. & Cui, Y. J. (2011). Some aspects of the compression and collapse behaviour of an unsaturated natural loess. *Géotechnique Letters*, 1, 17-22.

Murray, E. J. & Sivakumar, V. (2010). Unsaturated soils: a fundamental interpretation of soil behaviour, Oxford, Wiley-Blackwell.

Näätänen, A., Vepsalainen, P. & Lojander, M. (1998). Finite element calculations on Haarajoki test embankment. 4th European Conference on Numerical Methods in Geotechnical Engineering (NUMGE), Udine, Italy, A. Cividini (ed), New York: Springer, 151-160.

Nash, D. F. T., Sills, G. C. & Davison, L. R. (1992). One-dimensional consolidation testing of soft clay from Bothkennar. *Géotechnique*, 42, 241-256.

Navarro, V. & Alonso, E. E. (2001). Secondary compression of clays as a local dehydration process. *Géotechnique*, 51, 859-869.

Ng, C. W. W. & Menzies, B. (2007). Advanced unsaturated soil mechanics and engineering, London: Taylor and Francis, 712pp.

Ng, C. W. W. & Pang, Y. W. (2000a). Experimental investigation of soil-water characteristics of a volcanic soil. *Canadian Geotechnical Journal*, 37, 1252-1264.

Ng, C. W. W. & Pang, Y. W. (2000b). Influence of stress state on soil-water characteristics and slope stability. *Journal of Geotechnical and Geoenvironmental Engineering*, 126, 157-166.

Ng, C. W. W., Xu, J. & Yung, S. Y. (2009). Effects of wetting-drying and stress ratio on anisotropic stiffness of an unsaturated soil at very small strains. *Canadian Geotechnical Journal*, 46, 10062-1076.

Nishimura, S. (2005). Laboratory study on anisotropy of natural London Clay. Ph.D. Thesis. Imperial College London.

Nur, A. & Byerlee, J. (1971). Exact effective stress law for elastic deformation of rocks with fluids. *Journal of Geophysical Research*, 76, 6414-6419.

Nuth, M. & Laloui, L. (2008). Effective stress concept in unsaturated soils: Clarification and validation of a unified framework. *International Journal for Numerical and Analytical Methods in Geomechanics*, 32, 771-801.

Oda, Y. & Mitachi, T. (1988). Stress relaxation characteristics of saturated clays. *Soils and Foundations*, 28, 69-80.

Ohkoa, Y., Saitohb, S., Tatsumaa, T. & Fujishimaa, A. (2001). Photoelectrochemical anticorrosion and self-cleaning effects of a TiO2 coating for type 304 stainless steel. *Journal of the Electrochemical Society*, 148, B24-B28.

Oldecop, L. A. & Alonso, E. E. (2002). Fundamentals of rockfill time-dependent behaviour. *In:* Unsaturated Soils: Proceedings of the 3rd International

Conference on Unsaturated Soils, Recife, Brazil, Juca, De Campus, and Marinho (eds), 793-798.

Oliveira, O. M. & Marinho, F. A. M. (2008). Suction equilibrium time for a high capacity tensiometer. *Geotechnical Testing Journal*, 31, 1-5.

Pan, H., Qing, Y., and Pei-young, L. (2010). Direct and indirect measurement of soil suction in laboratory. *Electronic Journal of Geotechnical Engineering*, 15, 1-14.

Pasha, A. Y., Khoshghalb, A. & Khalili, N. (2016). Pitfalls in interpretation of gravimetric water content–based soil-water characteristic curve for deformable porous media. *International Journal of Geomechanics*, 16(6), D4015004-1.

Pedrotti, M., Tarantino, A. & Boeck, F. (2014). Experience gained from the conditioning of high-capacity tensiometers. *In:* Khalili, N., Russell, A. R. & Khoshghalb, A. (eds.) E-UNSAT 2014, Unsaturated Soils: Research and Applications. Sydney, Australia: CRC Press, 1651-1658.

Pereira, J. M. & De Gennaro, V. (2010). On the time-dependent behaviour of unsaturated geomaterials. 5th international conference on unsaturated soils, Barcelona, Spain, E.E. Alonso and A. Gens (eds), 1-6.

Perzyna, P. (1964). The constitutive equations for rate sensitive plastic materials. *Quarterly of Applied Mathematics*, 20, 231-332.

Pillai, R. J., Robinson, R. G. & Boominathan, A. (2012). Closure to "Effect of microfabric on undrained static and cyclic behavior of kaolin clay" by Rakesh J. Pillai, R. G. Robinson, and A. Boominathan. *Journal of Geotechnical and Geoenvironmental Engineering*, 138, 771-772.

Poirier, S. E., Degroot, D. J. & Sheahan, T. C. (2005). Measurement of suction in a marine clay as an indicator of sample disturbance. In: Mayne, P. W., Rathje, E., Dejong, J., Rechenmacher, A., Yamamuro, J., Sharma, S. & Willson, C., eds. Geo-Frontiers Congress - Site Characterization and Modelling, Austin, Texas, USA. 1-10.

Premchitt, J., Ho, K. S. & Evans, N. C. (1996). Conventional and CRS Rowe cell consolidation test on some Hong Kong clays. *GEO Technical Note No. TN 4/95*. Geotechnical Engineering Office, Civil Engineering Department, Hong Kong.

Priol, G. (2005). Comportement mécanique d'une craie pétrolifère—comportement différé et mouillabilité. Ph.D. Thesis, Ecole des ponts, ParisTech, France.

Priol, G., De Gennaro, V., Delage, P. & Servant, T. (2007). Experimental investigation on the time dependent behavior of a multiphase chalk. *In:* Schanz, T., ed. Experimental unsaturated soil mechanics,. Springer Proceedings Physics 112, 161-167.

Rahardjo, H. & Leong, E. C. (2006). Suction measurements. *Geotechnical Special Publication* (ASCE), 147, 81-104.

Rampino, C., Mancuso, C. & Vinale, F. (1999). Laboratory testing on an unsaturated soil: equipment, procedures, and first experimental results. *Canadian Geotechnical Journal*, 36, 1-12.

Raveendiraraj, A. (2009). Coupling of mechanical behavior and water retention behavior in unsaturated soils. Ph.D. Thesis, University of Glasgow.

Rees, E. P. & Trevena, D. H. (1964). The behavior of liquids in steel berthelot tubes. *British Journal of Applied Physics*, 15, 337-339.

Rees, E. P. & Trevena, D. H. (1966). A study of the Berthelot method of measuring tensions in liquids. *British Journal of Applied Physics*, 17, 671-674.

Rezania, M., Bagheri, M., Mousavi-nezhad, M. & Sivasithamparam, N. (2017). Creep analysis of an earth embankment on soft soil deposit with and without PVD improvement. *Geotextiles and Geomembranes*, 45(5), 537-547.

Richards, B. E. & Trevena, D. H. (1976). The measurement of positive and negative pressures in a liquid contained in a Berthelot tube. J*ournal of Physics D: Applied Physics*, 9, L123-L126.

Richards, B. G. (1966). The significance of moisture flow and equilibria in unsaturated soils in relation to the design of engineering structures built on shallow foundations in Australia. Symposium on Permeability and Capillarity, American Society for Testing and Materials, Atlantic City, NJ, 39-46.

Richardson, A. M. & Whitman, R. V. (1963). Effect of strain rate upon undrained shear resistance of a saturated remoulded fat clay. *Géotechnique*, 13, 310-324.

Ridley, A. M. & Burland, J. B. (1993). A new instrument for the measurement of soil moisture suction. *Géotechnique*, 43, 321-324.

Ridley, A. M. & Burland, J. B. (1995). Measurement of suction in materials which swell. *Applied Mechanics Reviews*, 48, 727-732.

Ridley, A. M. & Burland, J. B. (1999). Discussion: Use of tensile strength of water for the direct measurement of high soil suction. *Canadian Geotechnical Journal*, 36, 178-180.

Ridley, A. M. & Burland, J. B. (1996). A pore pressure probe for the in situ measurement of soil suction. International Conference on Advances in Site Investigation Practice, London, C. Craig (ed), Thomas Telford, London, 510-520.

Ridley, A. M. (1993). The measurement of soil moisture suction. Ph.D. Thesis, University of London.

Ridley, A. M., Dineen, K., Burland, J. B. & Vaughan, P. R. (2003). Soil matrix suction: some examples of its measurement and application in geotechnical engineering. *Géotechnique*, 53, 241-253.

Rojas, J. C., Pagano, L., Zingariello, C., Mancuso, C., Giordano, G. & Passeggio, G. (2008). A new high capacity tensiometer: first results. 1st European Conference on Unsaturated Soils. Durham, UK, D.G. Toll, C.E. Augarde, D. Gallipoli, S.J. Wheeler (eds), 205-211.

Romero, E., Gens, A. & Lloret, A. (1999). Water permeability, water retention and microstructure of unsaturated compacted Boom clay. *Engineering Geology*, 54, 117-127.

Romero, E., Gens, A. & Lloret, A. (2003). Suction effects on a compacted clay under non-isothermal conditions. *Géotechnique*, 53, 65-81.

Romero, E., Lloret, A. & Gens, A. (1995). Development of a new suction and temperature controlled oedometer cell. In: Alonso, E. E. & Delage, P., eds. 1st International Conference on Unsaturated Soils, Paris, A.A. Balkema/Presses des Ponts et Chaussees, Paris, 553-559.

Romero, E., Villar, M. V. & Lloret, A. (2005). Thermo-hydro-mechanical behavior of two heavily overconsolidated clays. *Engineering Geology Journal*, 81, 255-268.

Rosen, M. J. & Kunjappu, J. T. (2012). Surfactants and interfacial phenomena, Hoboken, New Jersey, John Wiely and Sons.

Rowe, P. W. & Barden, L. (1966). A new consolidation cell. *Géotechnique*, 16, 162-170.

Royse, K. R., De Freitas, M., Burgess, W. G., Cosgrove, J., Ghail, R. C., Gibbard, P., King, C., Lawrence, U., Mortimore, R. N., Owen, H. & Skipper, J. (2012). Geology of London, UK. Proceedings of the Geologists' Association, 123, 22-45.

Russell, A. R. & Khalili, N. (2006). A unified bounding surface plasticity model for unsaturated soils. *International Journal of Geomechanics*, 30, 181-212.

Saihi, F., Leroueil, S., La Rochelle, P. & French, I. (2002). Behaviour of the stiff and sensitive Saint-Jean-Vianney clay in intact, destructured, and remoulded conditions. *Canadian Geotechnic*, 39, 1075-1087.

Salimzadeh, S. & Khalili, N. (2014). Consolidation of unsaturated lumpy clays. *Journal of Geo-engineering Sciences*, 2, 67-82.

Sällfors, G. (1975). Preconsolidation pressure of soft high plastic clays. Ph.D. Thesis, Chalmers University of Technology.

Sample, K. M. & Shakelford, C. D. (2012). Apparatus for constant rate-of-strain consolidation of slurry mixed soils. *Geotechnical Testing Journal*, 35, 409-419.

Seah, T. H. & Juirnarongrit, T. (2003). Constant rate of strain consolidation with radial drainage. *Geotechnical Testing Journal*, 26, 1-12.

Sharma, R. S. & Wheeler, S. J. (2000). Behaviour of an unsaturated highly expansive clay during cycles of wetting and drying. Asian Conference on Unsaturated Soils, UNSAT-ASIA2000, Singapore, H. Rahardjo, D. G. Toll, and E. C. Leong (eds), 721-726.

She, H. Y. & Sleep, B. E. (1998). The effect of temperature on capillary pressure-saturation relationships for air-water and perchloroethylene-water systems. *Water Resources Research*, 34, 2587-2597.

Sheahan, T. C., Ladd, C. C. & Germaine, J. T. (1994). Time-dependent triaxial relaxation behavior of a resedimented clay. *Geotechnical Testing Journal*, 17, 444-452.

Shuter, E. & Teasdale, W. E. (1989). Techniques of Water-Resource Investigations of the United States Geological Survey - Chapter F1; Application of drilling, coring, and sampling techniques to test holes and wells. U.S. Geological Survey.

Singh, A. & Mitchell, J. K. (1969). Creep potential and rupture of soils. Proceedings of the 7th International Conference on Soil Mechanics and Foundation Engineering, Mexico, Sociedad Mexicana de Mecanica, 379-384.

Singh, D. N. & Kuriyan, S. J. (2003). Estimation of unsaturated hydraulic conductivity using soil suction measurements obtained by an insertion tensiometer. *Canadian Geotechnical Journal*, 40, 476-483.

Sivakumar, V. & Wheeler, S. J. (2000). Influence of compaction procedure on the mechanical behaviour of an unsaturated compacted clay. Part 1: Wetting and isotropic compression. *Géotechnique*, 50, 359-368.

Sivakumar, V. (1993). A critical state framework for unsaturated soil. Ph.D. Thesis, University of Sheffield, UK.

Sjoblom, K. J. (2000). The mechanics involved during the desaturation process of a porous matrix. Ph.D. Thesis, Massachusetts Institute of Technology.

Skempton, A. W. & Sowa, V. A. (1963). The behavior of saturated clays during sampling and testing. *Géotechnique*, 13, 269-290.

Skempton, A. W. (1960). Effective stress in soils, concrete and rocks. *Pore Pressure and Suction in Soils.* London: Butterworths.

Skempton, A. W. (1964). Long-term stability of clay slopes. *Géotechnique*, 14, 77-101.

Skempton, A. W. (1961). Horizontal stresses in an overconsolidated Eocene clay. Proceedings of the 5th International Conference on Soil Mechanics and Foundation Engineering, Paris, France, Dunod, 351-357.

Skempton, A. W., Schuster, F. R. S. & Petley, D. J. (1969). Joints and fissures in the London Clay at Wraysbury and Edgware. *Géotechnique*, 19, 205-217.

Smith, R. E. & Wahls, H. E. (1969). Consolidation under constant rate of strain. *Journal of Soil Mechanics and Foundations, Division of American Society of Civil Engineers*, 95, 519-539.

Soga, K. & Mitchell, J. K. (1996). Rate-dependent deformation of structured natural clays. Session on Measuring and Modeling Time Dependent Soil Behaviour, ASCE Convention, Washington, *ASCE Geotechnical Special Publication*, 61, 243-257.

Sorensen, K. K. (2006). Influence of viscosity and ageing on the behaviour of clays. Ph.D. Thesis, University College London.

Sorensen, K. K., Baudet, B. A. & Simpson, B. (2010). Influence of strain rate and acceleration on the behaviour of reconstituted clays at small strains. *Géotechnique*, 60, 751-761.

Stallebrass, S. E., Atkinson, J. H. & Masin, D. (2007). Manufacture of samples of overconsolidated clay by laboratory sedimentation. *Géotechnique*, 57, 249-253.

Stannard, D. I. (1992). Tensiometers-theory, construction and use. *Geotechnical Testing Journal*, 15, 48-58.

Starov, V. M., Velarde, M. G. & Radke, C. J. (2007). Wetting and spreading dynamics, Boca Raton, CRC Press.

Suklje, L. (1969). Rheological aspects of soil mechanics, New York, Wiley.

Suklje, L. (1957). The analysis of the consolidation process by the iso-taches method. Proceedings of the 4th International Conference on Soil Mechanics and Foundation Engineering, London, Butterworths, 1, 200-206.

Sun, D., Chen, B. & Wei, C. (2014). Effect of fabric on mechanical behavior of marine clays. *Marine Georesources & Geotechnology*, 32, 1-17.

Sun, J. (1999). Rheology of geotechnical materials and its application to engineering. China Architecture and Building Press, Beijing, China.

Tabor, D. (1969). Gases, liquids and solids, Penguin Books.

Take, W. A. & Bolton, M. D. (2003). Tensiometer saturation and the reliable measurement of soil suction. *Géotechnique*, 53, 159-172.

Take, W. A. & Bolton, M. D. (2004). Discussion: Tensiometer saturation and the reliable measurement of soil suction. *Géotechnique*, 54, 229-232.

Take, W. A. (2003). The influence of seasonal moisture cycles on clay slopes. Ph.D. Thesis, Cambridge University.

Takino, H., Ichinohe, T., Tanimoto, K., Yamaguchi, Y., Nomura, K. & Kunieda, M. (2005). High-quality cutting of polished single-crystal silicon by wire electrical discharge machining. *Article Precision Engineering*, 29, 423-430.

Tanaka, H. (2005). Consolidation behavior of natural soils around pc value—inter-connected oedometer test. *Soils and Foundations*, 45, 97-105.

Tarantino, A. & De Col, E. (2008). Compaction behavior of clay. *Géotecnique*, 58, 199-213.

Tarantino, A. & Mongiovi, L. (2000). Experimental investigations on the stress variables governing unsaturated soil behaviour at medium to high degree of saturation. In: Tarantino, A. & Mancuso, C. (eds.) Experimental evidence and theoretical approaches in unsaturated soils. Rotterdam Balkema, 3-19.

Tarantino, A. & Mongiovi, L. (2001). Experimental procedures and cavitation mechanisms in tensiometer measurements. *Geotechnical and Geological Engineering Journal*, 19, 189-210.

Tarantino, A. & Mongiovi, L. (2002). Design and construction of a tensiometer for direct measurement of matric suction. In: Juca, J. F. T., De Campos, T. M. P. & Marinho, F. A. M., eds. 3rd International Conference on Unsaturated Soils. UNSAT2002, Recife, Brazil. Netherlands: A.A. Balkema Publishers, 319-324.

Tarantino, A. & Mongiovi, L. (2003). Calibration of tensiometer for direct measurement of matric suction. *Géotechnique*, 53, 137-141.

Tarantino, A. & Tombolato, S. (2005). Coupling of hydraulic and mechanical behavior in unsaturated compacted clay. *Géotechnique*, 55, 307-317.

Tarantino, A. (2017). Personal communication.

Tarantino, A. (2004). Panel Lecture: Direct measurement of soil water tension. In: Juca, J. F. T., De Campos, T. M. P. & Marinho, F. A. M., eds. 3rd International Conference on Unsaturated Soils, Recife, Brazil. A.A. Balkema, 1005-1017.

Tarantino, A., Gallipoli, D., Augarde, C. E., De Gennaro, V., Gomez , R., Laloui, L., Mancuso, C., El Mountassir, G., Munoz, J. J., Pereira, J.-M., Peron, H., Pisoni, G., Romero, E., Raveendiraraj, A., Rojas, J. C., Toll, D. G., Tombolato, S. & Wheeler, S. J. (2011). Benchmark of experimental techniques for measuring and controlling suction. *Géotechnique*, 61, 303–312.

Tarantino, A., Gallipoli, D., Jommi, C., Mendes, J., Capotosto, A., Amabile, A., Pedrotti, M., Pozzato, A., Benes, V., Bottaro, F., Denzer, H. & Boeck, F. (2016). Advances in the monitoring of geo-structure subjected to climate loading. E-UNSAT 2016. Paris, France, P. Delage, Y.-J. Cui, S. Ghabezloo, J.-M. Pereira, A.-M. Tang (eds), 71-81.

Tatsuoka, F., Di Benedetto, W., Enomoto, T., Kawabe, S. & Kongkitkul, W. (2008). Various viscosity types of geomaterials in shear and their mathematical expression. *Soils and Foundations*, 48, 41-60.

Tavenas, M., Leroueil, F., La Rochelle, P. & Roy, M. (1978). Creep behaviour of an undisturbed lightly overconsolidated clay. *Canadian Geotechnical Journal*, 15, 402-423.

Temperly, H. N. V. (1946). The behavior of water under hydrostatic tension: II. *Proceedings of the Physical Society of London*, 58, 436-443.

Temperly, H. N. V. (1947). The behavior of water under hydrostatic tension: III. *Proceedings of the Physical Society of London*, 59, 199-208.

Toker, N. K., Germaine, J. T., Sjoblom, K. J. & Culligan, P. J. (2004). A new technique for rapid measurement of continuous soil moisture characteristic curves. *Géotechnique*, 54, 179-186.

Toll, D. G. & Ong, B. H. (2003). Critical state parameters for an unsaturated residual sandy clay. *Géotechnique*, 53, 93-103.

Toll, D. G. (1990). A framework for unsaturated soil behaviour. *Géotechnique*, 40, 31-44.

Toll, D. G., Lourenço, S. D. N., Mendes, J., Gallipoli, D., Evans, F. D., Augarde, C. E., Cui, Y. J., Tang, A. M., Rojas, J. C., Pagano, L., Mancuso, C., Zingariello, C. & Tarantino, A. (2011). Soil suction monitoring for landslides and slopes. *Quarterly Journal of Engineering Geology and Hydrogeology*, 44, 23-33.

Tompsett, G. A., Krogh, L., Griffin, D. W. & Conner, W. C. (2005). Hysteresis and scanning behavior of mesoporous molecular sieves. *Langmuir*, 21, 8214-8225.

Tong, F. & Yin, J. H. (2013). Experimental and constitutive modeling of relaxation behaviors of three clayey soils. *Journal of Geotechnical and Geoenvironmental Engineering*, 139, 1973-1981.

Towhata, I., Kuntiwattanaku, P., Seko, I. & Ohishi, K. (1993). Volume change of clays induced by heating as observed in consolidation tests. *Soils and Foundations*, 33, 170-183.

Tsai, F. C., Yan, B. H., Kuan, C. Y. & Huang, F. Y. (2008). A Taguchi and experimental investigation into the optimal processing conditions for the abrasive jet polishing of SKD61 mold steel. *International Journal of Machine Tools & Manufacture*, 48, 932-945.

Tse, E. Y. M. & Ng, C. W. W. (2008). Effects of drying and wetting cycles on unsaturated shear strength. *In:* Toll, D. G., Augarde, C. E., Gallipoli, D. & Wheeler, S. J. (eds.) *Unsaturated Soils: Advances in Geo-Engineering*, 481-486.

Tsuchida, T., Kobayashi, M. & Mizukami, J. (1991). Effect of aging of marine clay and its duplication by high temperature consolidation. *Soils and Foundations*, 31, 133-147.

Tsutsumi, A. & Tanaka, H. (2011). Compressive behavior during the transition of strain rate. *Soils and Foundations*, 51, 813-822.

Tsutsumi, A. & Tanaka, H. (2012). Combined effects of strain rate and temperature on consolidation behavior of clayey soils. *Soils and Foundations*, 52, 207-215.

Vaid, Y. & Campanella, R. G. (1977). Time-dependent behaviour of undisturbed clay. *ASCE Journal of the Geotechnical Engineering Division*, 103, 693-709.

Van Genuchten, M. T. (1980). A closed-form equation for predicting the hydraulic conductivity of unsaturated soils. *Soil Science Society of America Journal*, 44, 892-898.

Vanapalli, S. K., Fredlund, D. G. & Pufahl, D. E. (1999). The influence of soil structure and stress history on the soil-water characteristics of a compacted till. *Géotechnique*, 49, 143-159.

Vanapalli, S. K., Fredlund, D. G., Pufahl, D. E. & Clifton, A. W. (1996). Model for prediction of shear strength with respect to soil suction. *Canadian Geotechnical Journal*, 33, 379-392.

Villar, M. V. & Gómez-espina, R. (2008). Effect of temperature on the water retention capacity of FEBEX and MX-80 bentonites. *In:* Toll, D. G., Augarde, C. E., Gallipoli, D. & Wheeler, S. J., eds. 1st European Conference on Unsaturated Soils, E-UNSAT 2008, Durham, UK. CRC Press, 257-262.

Vincent, R. S. (1941). Measurement of tension in liquids by means of a metal bellows. *Proceedings of the Physical Society of London*, 53, 126-140.

Vincent, R. S. & Simmonds, G. H. (1943). Examination of the Berthelot method of measuring tension in liquids. *Proceedings of the Physical Society of London*, 55, 376-382.

Wang, M., Xu, X., Li, J., Shen, F. & Li, Y. (2017). An experiment study on stress relaxation of unsaturated lime-treated expansive clay. *Environmental Earth Sciences*, 76, 241.

Wang, Y. H. & Fredlund, D. G. (2003). Towards a Better Understanding of the Role of the Contractile Skin. Proceedings of the 2nd Asian Conference on Unsaturated Soils, Osaka, 419-424.

Wang, Z., Luan, Y., Pang, T. & Liu, W. (1998). Elastic and electrolytic ultraprecision polishing. *Metal finishing*, 96(7), 22-24.

Ward, W. H., Marsland, A. & Samuels, S. G. (1965). Proprieties of the London Clay at the Ashford Common shaft: in-situ and undrained strength tests. *Géotechnique*, 15, 321-344.

Wheeler, S. J. & Karube, D. (1995). State of the art report-constitutive modeling. Proceedings of 1st International Conference on Unsaturated Soils, Paris, E.E. Alonso and P. Delage (eds), 1323-1356.

Wheeler, S. J. & Sivakumar, V. (1995). An elasto-plastic critical state framework for unsaturated soil. *Géotechnique*, 45, 35-53.

Wheeler, S. J., Cundy, M., Neher, H. P. & Wiltafsky, C. (2003b). Some developments in constitutive modelling of soft clays. International Workshop on Geotechnics

of Soft Soils - Theory and Practice. Vermeer, Schweiger, Karstunen & Cundy (eds), 3-22.

Wheeler, S. J., Sharma, R. S. & Buison, M. S. R. (2003c). Coupling of hydraulic hysteresis and stress-strain behaviour in unsaturated soils. *Géotechnique,* 53, 41-54.

Wijaya, M. & Leong, E. C. (2016). Performance of high‐capacity tensiometer in constant water content oedometer test. *International Journal of Geo-Engineering*, 7, 1-15.

Wijaya, M., Leong, E. C. & Rahardjo, H. (2014). CRS compression tests of an unsaturated kaolin with pore-water pressure measurement. *Unsaturated Soils: Research & Applications.* CRC Press, Khalili, Russel & Khoshghalb (eds), 1639-1644.

Wijaya, M., Leong, E. C. & Rahardjo, H. (2015). Effect of shrinkage on air-entry value of soils. *Soils and Foundations*, 55, 166-180.

Williams, J., Prebble, R. E., Williams, W. T. & Hignett, C. T. (1983). The influence of texture, structure and clay mineralogy on the soil moisture characteristic. *Australian Journal of Soil Research,* 21, 15-32.

Wissa, A. E. Z. & Heiberg, S. (1969). A new one-dimensional consolidation test. Department of Civil Engineering Research Report 69-9. Massachusetts Institute of Technology.

Wissa, A., Christain, J., Davis, H. & Heiberg, S. (1971). Consolidation at constant rate of strain. *Journal of Soil Mechanics and Foundation Division*, 97, 1391-1413.

Wulfsohn, D., Adams, B. A. & Fredlund, D. G. (1996). Application of Unsaturated Soil Mechanics for Agricultural Conditions. *Canadian Agricultural Engineering,* 38, 173-181.

Yin, J. & Miao, Y. (2013). Intrinsic compression behavior of remolded and reconstituted clays - reappraisal. *Open Journal of Civil Engineering,* 3, 8-12.

Yin, J. H. & Graham, J. (1989). Viscous elastic plastic modelling of one-dimensional time dependent behaviour of clays. *Canadian Geotechnical Journal*, 26, 199-209.

Yin, J. H. & Tong, F. (2011). Constitutive modeling of the timedependent stress-strain behaviour of saturated soils exhibiting both creep and swelling. *Canadian Geotechnical Journal,* 48, 1870-1885.

Yin, J. H. (1999). Non-linear creep of soils in oedometer tests. *Géotechnique*, 49, 699-707.

Yin, S. & Shinmura, T. (2004). Vertical vibration-assisted magnetic abrasive finishing and deburring for magnesium alloy. *International Journal of Machine Tools & Manufacture*, 44, 1297-1303.

Yin, Z. Y. & Hicher, P. Y. (2008). Identifying parameters controlling soil delayed behaviour from laboratory and in situ pressuremeter testing. *International Journal for Numerical and Analytical Methods in Geomechanics*, 32, 1515-1535.

Yin, Z.-Y., Chang, C. S., Karstunen, M. & Hicher, P.-Y. (2010). An anisotropic elastic–viscoplastic model for soft clays. *International Journal of Solids and Structures*, 47, 665-677.

Yin, Z.-Y., Karstunen, M., Chang, C. S., Koskinen, M. & Lojander, M. (2011). Modeling Time-Dependent Behavior of Soft Sensitive Clay. *Journal of Geotechnical and Geoenvironmental Engineering*, 137, 1103-1113.

Yin, Z.-Y., Zhu, Q.-Y., Yin, J.-H. & Ni, Q. (2014). Stress relaxation coefficient and formulation for soft soils. *Géotechnique Letters*, 4, 45-51.

Young, C. (2014). The geology and landscape of the Isle of Sheppey. In: Badmin, J. (ed.) The natural history of Isle of Sheppey. Kent Field Club, 47-66.

Yu, B. M. & Li, J. H. (2004). Geometry model for tortuosity of flowpath in porous media. *Chinese Physics Letters*, 21, 1569–1571.

Yu, J. C., Ho, W., Lin, J., Yip, H. & Wong, P. K. (2003). Photocatalytic activity, antibacterial effect, and photoinduced hydrophilicity of TiO2 films coated on a stainless steel substrate. *Environmental Science and Technology*, 37, 2296–2301.

Yu, Y. & Axelsson, K. (1994). Constitutive modelling of Swedish cohesive soils accounting for anisotropy. Proceedings of 8th International Conference on Computer Methods and Advances in Geomechanics, Morgantown, W. Va, USA, H. J. Siriwardane and M. M. Zaman. (eds), A.A. Balkema, Rotterdam, 737-743.

Zheng, Q., Durben, D. J., Wolf, G. H. & Angell, C. A. (1991). Liquids at large negative pressures: water at the homogenous nucleation limit. *Science*, 254, 829-832.

Zhou, A. N., Sheng, D., Sloan, S. W. & Gens, A. (2012). Interpretation of unsaturated soil behaviour in the stress – saturation space, I: Volume change and water retention behaviour. *Computers and Geotechnics*, 43, 178-187.

Zhou, R. Z. B., Take, A. & Ng, C. W. W. (2006). A case study in tensiometer interpretation: centrifuge modelling of unsaturated slope behavior. 4th International Conference on Unsaturated Soils, Carefree, Arizona. G. A. Miller, C. E. Zapata, S. L. Houston, and D. G. Fredlund (eds), ASCE, 2300-2311.

Zhu, J. G., Yin, J. H. & Luk, S. T. (1999). Time-dependent stress-strain behavior of soft Hong Kong marine deposits. *Geotechnical Testing Journal*, 22, 112-120.

Zhu, Y.-B. & Yu, H.-M. (2014). An improved Mesri creep model for unsaturated weak intercalated soils. *Journal of Central South University*, 21, 4677-4681.

Zou, L., Wang, S. & Lai, X. (2013). Creep model for unsaturated soils in sliding zone of Qianjiangping landslide. *Journal of Rock Mechanics and Geotechnical Engineering*, 5, 162-167.